UV-Resonance Raman Studies of Small Peptides and Proteins

by

Zeeshan Ahmed

B. Sc. in Chemistry, George Mason University, 2001

Submitted to the Graduate Faculty of

University of Pittsburgh in partial fulfillment

of the requirements for the degree of

Doctor of Philosophy

University of Pittsburgh

2008

UNIVERSITY OF PITTSBURGH

FACULTY OF ARTS AND SCIENCES

This dissertation was presented

by

Zeeshan Ahmed

It was defended on

October 13, 2008

and approved by

Prof. Sunil Saxena, Department of Chemistry

Prof. David Earl, Department of Chemistry

Prof. Ronald Wetzel, Department of Structural Biology

Dissertation Advisor: Prof. Sanford A. Asher, Distinguished Professor, Chemistry

UV-Resonance Raman Studies of Small Peptides and Proteins

Zeeshan Ahmed, PhD

University of Pittsburgh, 2008

An understanding of protein folding and how it impacts the structure and function of proteins will have a major impact on our understanding of the molecular underpinings of life. In particular, a robust understanding of protein folding will provide a molecular insight into misfolded protein diseases such as Alzheimer's disease. Currently, our understanding of protein folding is limited by the available tool-set, necessitating the development of novel spectroscopic tools for protein structure elucidation. This work is a continuation of our ongoing efforts to develop UV-resonance Raman spectroscopy (UVRR) as a powerful tool for protein structure determination.

We utilize UVRR to determine changes in the conformation distribution of various model systems, such as the mini-protein Trp-cage and the therapeutically relevant $gp41_{659-671}$ peptide. Utilizing deep UV-excitation we quantitatively track temperature induced conformation changes in these peptides. Similarly we utilized UVRR and circular dichroism to determine the conformation distribution of elastin-like peptides and demarcated the role of val, pro and gly peptide bonds in the elastin's hydrophobic collapse peptides. Our results indicate that conformation changes leading to elastin's inverse temperature transition are localized at the gly and pro peptide bonds.

We utilized UVRR and DFT calculations to demonstrate that the AmII'p frequency is sensitive to Ψ-conformation changes. We correlate a 7 cm^{-1} downshift in the AmII'p frequency of polyproline to temperature-induced conformation changes from $\Psi = 145^{o}$ to $\Psi = 100^{o}$. The latter high temperature compact conformation shows a ~26% decrease in its solvent accessible surface area, indicating a temperature induced hydrophobic collapse.

We utilized steady-state and time-resolved UVRR spectroscopy to determine the molecular mechanism of poly-(*N*-isopropylacrylamide)'s (PNIPAM) temperature-induced hydrophobic collapse. Our results indicate that the hydrophobic collapse results in the loss of a C=O-water hydrogen bond at the carbonyl site. The N-H-water remains unperturbed by PNIPAM's collapse. The collapse rate (10^6 s^{-1}) indicates a persistence length of n~10. We postulate that at elevated temperature PNIPAM forms hydrophobic nano-pockets when the (*i*, *i* +3) groups make hydrophobic contacts. A persistence length of n~10 suggests a cooperative collapse where hydrophobic interactions between adjacent hydrophobic pockets stabilize the collapsed PNIPAM.

TABLE OF CONTENTS

PREFACE XIX

1.0 PROTEIN FOLDING 1

1.1 NATIVE STATE INTERACTIONS 2

1.1.1 Disulfide bridges 3

1.1.2 Electrostatic interactions 3

1.1.3 Hydrogen bonding 4

1.1.4 Van der Waals interactions 4

1.1.5 Hydrophobic Effect 5

1.2 EARLY HISTORY OF PROTEIN FOLDING 7

1.3 THEORETICAL MODELING 8

1.4 EXPERIMENTAL APPROACH 10

1.4.1 Kinetic studies of protein folding 11

1.5 CONCLUSION 12

1.6 REFERENCES 13

2.0 RAMAN SCATTERING 18

2.1.1 Classical Treatment 18

2.1.2 Quantum Mechanical Treatment 21

2.1.3 Frequency Denominators 23

2.1.4 Utility of Resonance Raman in the study of protein folding 25
2.2 REFRENCES 26
3.0 UV-RESONANCE RAMAN THERMAL UNFOLDING STUDY OF TRP-CAGE SHOWS THAT IT IS NOT A SIMPLE TWO-STATE MINIPROTEIN 28
3.1 INTRODUCTION 29
3.2 EXPERIMENTAL 32
3.3 RESULTS AND DISCUSSION 33
3.3.1 204-nm Excitation Temperature Dependence 33
3.3.2 Proline-Trp Excitonic Interactions 39
3.3.3 α-Helix Melting 42
3.3.4 Trp and Tyr water exposure 46
3.4 CONCLUSIONS 50
3.5 REFERENCES 55
4.0 UV-RESONANCE RAMAN INVESTIGATION OF A 3_{10} HELICAL PEPTIDE REVEALS A ROUGH ENERGY LANDSCAPE 59
4.1 INTRODUCTION 60
4.2 EXPERIMENTAL 62
4.3 RESULTS AND DISCUSSION 63
4.3.1 204 nm excitation temperature dependence 63
4.4 CONFORMATION ANALYSIS 70
4.5 CONCLUSIONS 74
4.6 REFERENCES 75

5.0 CIRCULAR DICHROISM AND UV-RESONANCE RAMAN INVESTIGATION OF THE TEMPERATURE DEPENDENCE OF THE CONFORMATIONS OF LINEAR AND CYCLIC ELASTIN 79

5.1 INTRODUCTION 80

5.2 EXPERIMENTAL 83

5.3 RESULTS AND DISCUSSION 85

5.3.1 Cyclic Elastin 85

5.3.2 Linear Elastin 96

5.4 CONCLUSION 101

5.5 REFERENCES 104

6.0 UV-RESONANCE RAMAN REVEALS TEMPERATURE-INDUCED HYDROPHOBIC COLLAPSE IN POLYPROLINE PEPTIDE 109

6.1 INTRODUCTION 110

6.2 EXPERIMENTAL 114

6.2.1 Computational details 114

6.3 RESULTS AND DISCUSSION 116

6.3.1 Impact of *cis-trans* isomerization 116

6.3.2 The impact of hydrogen bonding 118

6.3.3 Ψ-angle dependence 124

6.3.4 Φ-angle dependence 131

6.3.5 Temperature Dependent Spectra of Polyproline 135

6.4 CONCLUSIONS 139

6.5 REFERENCES 141

7.0 UV-RESONANCE RAMAN DETERMINATION OF MOLECULAR MECHANISM OF POLY(*N*-ISOPROPYLACRYLAMIDE) VOLUME PHASE TRANSITION HYDROPHOBIC COLLAPSE 146

7.1 INTRODUCTION 147

7.2 EXPERIMENTAL 150

7.3 RESULTS AND DISCUSSION: 153

7.3.1 DLS measurements 153

7.3.2 UVRR spectral band assignments 154

7.3.3 Temperature dependence of PNIPAM 158

7.3.4 A Model of PNIPAM Collapse 168

7.3.5 Kinetics of PNIPAM's hydrophobic collapse 171

7.4 CONCLUSIONS 175

7.5 REFERENCES 178

8.0 CONCLUSIONS 182

8.1 REFERENCES 187

LIST OF TABLES

Table 3.1: Band assignment of Trp-cage's spectra 36

Table 3.2: Amide cross sections of AP 45

Table 5.1: Conformation Distribution of Linear and Cyclic Elastin 95

Table 6.1: Calculated geometric parameters of *cis*- and *trans*-conformer of Ac-Pro-Me 117

Table 6.2: Temperature dependence of AmII'p frequency 120

Table 6.3: Calculated normal mode composition of ala-pro (Ψ = 145º). 121

Table 6.4: Ala-Pro (Φ = -90º, Ψ = 145º) AmII'p frequency dependence on solvent dielectric effect and hydrogen bonding 123

LIST OF FIGURES

Figure 1.1: Hydrogen bonding between the amide groups stabilizes secondary structures such as the β-sheet or α-helix, respectively. Reproduced from http://www.bio.mtu.edu 4

Figure 1.2: a) Torsion angles phi and psi b) The Ramachandran plot of available phi and psi angles. Reproduced from http://www.cryst.bbk.ac.uk/ 7

Figure 1.3: a) Folding along a smooth energy landscape devoid of any intermediates. b) A rough energy landscape with multiple kinetic intermediates. Reproduced from reference #6 9

Figure 2.1: Different types of Raman scattering processes and their dependence upon the ω_{ri}-ω_1 term. Figure adopted from Long.[2] 23

Figure 3.1: 204-nm UV resonance Raman spectra of Trp-Cage measured between 4º and 70 ºC. Three 5 min spectrum were summed and scaled to the intensity of 932 cm^{-1} perchlorate band. The bands arise mainly from amide vibrations except for a few which derive from aromatic side chain vibrations. 34

Figure 3.2: Spectral deconvolution of 4 ºC 204-nm UVRR Trp-cage spectra with Voight bands. The excellence of the fit is evident from the flat residual displayed underneath. 35

Figure 3.3: 204-nm UV resonance Raman spectra of Trp-cage at 4 and 70 ºC and their difference spectra. The difference spectra show a decrease in the intensity of a triplet in the AmIII

frequency region indicating a loss of α-helix with increasing temperature. The intensity of the AmII' of Proline also decreases with increasing temperature. 38

Figure 3.4: UV absorption spectra of Trp monomer (AcTrpEE), polyproline, and a solution of Trp (W) and polyproline, and the (Polyproline + Trp) – Trp difference spectrum. Insert shows Trp monomer spectra and difference spectra of (Polyproline +Trp) minus 0.91* Polyproline.... 39

Figure 3.5: A) Temperature dependence of 204-nm excited Raman intensity of proline AmII' band. B) Temperature dependence of the C_α-H symmetric bending band intensity and the α-helical AmIII band triplet intensity. The triplet intensity is extracted from temperature difference spectrum. Increasing C_α-H and AmIII triplet intensities indicate loss of α-helicity at higher temperatures. C) Temperature dependence of the relative Raman intensities of different Trp bands: W18 (▼, 765 cm^{-1}), W17 (x, 884 cm^{-1}), W16 (•, 1014 cm^{-1}), W7 (◊, 1365 cm^{-1}), W3 (▲1558 cm^{-1}). D) 229 nm UV resonance Raman spectra of Trp monomers in polyproline solution at different temperatures. The spectra show bands arising form the resonance enhanced Trp along with AmII' of proline which overlaps with W8a band of Trp. Temperature dependence of W6 and W18 bands of Trp is displayed in the insert. 41

Figure 3.6: 204-nm UV resonance Raman spectrum of AP peptide at 60º C. The measured spectra are deconvoluted into a sum of Voight bands. At 60 ˚C AP is 95% PPII. 43

Figure 3.7: 229-nm UV resonance Raman spectra of Trp-Cage at different temperatures. Three spectra accumulated for ten minutes each were summed and normalized to the 932 cm^{-1} perchlorate band intensity. The spectra show bands arising form the resonance enhanced Trp and Tyr ring vibrations. 47

Figure 3.8: A schematic representation of Trp-cage's temperature dependent conformational changes. 51

Figure 4.1: 204- and 194-nm UV resonance Raman spectra of $gp41_{659-671}$ measured at 1 ºC. Also displayed are the 204-nm excitation UVRR spectra of Trp monomer, where the 1483 cm^{-1} carboxylate stretching band overlaps with the W4 and W5 bands of Trp. As compared to 204-nm, the 194-nm excited $gp41_{659-671}$ spectra shows considerably less Trp spectral contribution. The decreased Trp contribution allows us to resolve amide bands from overlapping Trp bands. 65

Figure 4.2: Upper traces are 204-nm UV-resonance Raman spectra of $gp41_{659-671}$ measured between 1 ºC and 30 ºC. In order to facilitate spectral interpretation the Trp contribution was subtracted. The resulting spectra show resonance enhanced amide vibrations. Below, the green trace shows the 204-nm excited pure α-helix spectra of AP peptide (adapted from ref 70) which shows its characteristic narrow $AmIII_3$ band at 1260 cm^{-1}. 66

Figure 4.3: 204-nm UV-resonance Raman spectra of $gp41_{659-671}$ in pure water, 10 % and 30% v/v TFE concentration at 1 ºC. The TFE contribution has been subtracted from the spectra. The resulting spectra show bands arising from amide and Trp vibrations. In 10% TFE the presence of C_α-H_b band indicates ~55% helicity, whereas in 30% TFE the C_α-H_b band shows negligible band intensity indicating a 92% helical content. Insert shows CD spectra of $gp41_{659-671}$ in water, 10% and 30% v/v TFE solutions. As discussed in the text these CD spectra show the peptide's 3_{10}-helix content increases with TFE concentration. 68

Figure 4.4: Spectral deconvolution of 1 ºC 194-nm UVRR $gp41_{659-671}$ spectra with Voight bands. The excellence of the fit is evident from the flat residual displayed underneath 71

Figure 4.5: 194-nm UV resonance Raman spectra of $gp41_{659-671}$ measured between 1 ºC and 60 ºC. Three 10 min spectra were summed and scaled to the intensity of 932 cm^{-1} perchlorate band. The bands arise mainly from amide vibrations except for those that derive from Trp ring vibrations..... 72

Figure 5.1: Temperature dependent CD spectra of cyclic elastin. The insert shows the 20 ºC CD spectra of cyclic elastin during and subsequent to heating. The CD spectrum subsequent to heating (20 ºCb) shows a slight overall decrease in spectral intensity after heating. This change likely derives from temperature induced degassing/bubble formation on cell walls at high temperatures. 86

Figure 5.2: Temperature dependent changes in the mean residue ellipticities of cyclic and linear elastin at 200 nm 87

Figure 5.3: 204-nm UV resonance Raman spectra of cyclic elastin measured at 20 and 60 ºC normalized to the intensity of 932 cm^{-1} perchlorate band. The difference spectrum shows temperature dependent changes in the conformation-sensitive $AmIII_3$ region, as well as intensity changes in the C_α-H_b region. The AmII'p narrows at 60 ˚C suggesting the proline peptide bonds adopt a more well-defined conformation at higher temperatures. The trough in the AmII region is an artifact that derives from over-subtraction of the interfering O_2-stretching vibration at 1560 cm^{-1} when the NMR tube contribution was subtracted from the measured spectrum. 88

Figure 5.4: Spectral deconvolution of 20 ºC 204 nm UV resonance Raman spectra of cyclic elastin with mixed Gaussian and Lorentzian bands. The quality of the fit is evident from the flat residual displayed underneath. 90

Figure 5.5: A) 204-nm UV resonance Raman spectra of linear and cyclic elastin at 20 ºC and their difference spectra. The featureless difference spectrum indicates that the cyclic and linear peptides have similar conformations. B) CD spectra of linear and cyclic elastin at 20 ºC. Cyclic elastin shows a more prominent positive feature at ~207 nm, indicating a greater population of β-type II turns in the cyclic peptide. 96

Figure 5.6: Temperature dependent CD spectra of linear elastin. The insert shows the 20 ºC CD spectra of cyclic elastin during and subsequent (20 ºC) to heating. 97

Figure 5.7: Spectral deconvolution of 20 ºC 204 nm UV resonance Raman spectra of linear elastin with Gaussian and Lorentzian bands. The quality of the fit is evident from the flat residual. 99

Figure 5.8: 204-nm UV resonance Raman spectra of linear elastin measured at 20 and 60 ºC. The difference spectrum shows narrowing of the AmII' band width at 60 ºC which is indicative of a transition to a relatively well-defined conformation. The trough in the AmII region is an artifact that derives from over-subtraction of the interfering O_2 stretching vibration at 1560 cm^{-1} when the NMR tube contribution was subtracted from the measured spectra 101

Figure 6.1: The calculated structures of cis and trans isomers of Ac-Pro-Me. The C-N bond length elongates (0.004 Å) in the cis conformation resulting in an 8 cm^{-1} downshift of the AmII'p vibration. The C=O bond length contracts by 0.003 Å which results in a 13 cm^{-1} upshift of the AmI' vibration. 116

Figure 6.2: The 204-nm excited AmII'p band of Ala-Pro (1mg/ml) shows an insignificant change in frequency ($\Delta\nu$ = 1 cm^{-1}) as the temperature is increased from 4 to 65 ºC. The band intensity however, shows a 22% decrease with increasing temperature. 119

Figure 6.3: Calculated conformational dependence of AmII'p frequency of ala-pro on Ψ-dihedral angle in water, heptane and gas phase (insert)..... 124

Figure 6.4: Calculated Ψ-dependence of the (A) C-N bond length (B) and C=O bond length of ala-pro in water, heptane and gas phase. C) Calculated dependence of ala-pro AmII'p frequency and C-N bond length in water (grey circles) and gas phase (black squares). D) Calculated Ψ-dependence of the peptide bond planarity angle (Θ) in water, heptane and gas phase..... 127

Figure 6.5: The torsional angle ω' of ala-pro is defined as a rotation around C-N bond in the dihedral plane defined by the C-C(O)-N-C^* atoms..... 128

Figure 6.6: Calculated Φ-dependence of ala-pro (A) AmII'p frequency (B) C-N bond length (C) and the Θ planarity angle in water, heptane, acetonitrile and gas phase. (D) The calculated ala-pro AmII'p frequencies and C-N bond lengths in water (grey circles) and gas phase (black squares) are linearly correlated. 134

Figure 6.7: Polyproline shows a 7 cm^{-1} downshift in the AmII'p band frequency as the temperature increases from 5 to 65 ºC. The CD spectra (insert) of polyproline at 5 and 50 ºC shows characteristic features of the PPII conformation, indicating a lack of significant *trans* to *cis* isomerization with increasing temperature..... 136

Figure 6.8: The structure of ideal PPII pro peptide (left) and the proposed structure of collapsed polyproline (right). 138

Figure 7.1: Temperature dependent DLS measurements show that PNIPAM particles collapse between 20 ºC and 40 ºC with a transition temperature of ~33 ºC 153

Figure 7.2: 204 nm excited UV Raman spectra of PNIPAM and d_7-PNIPAM at 5 ºC. Both spectra were normalized to the peak intensity of their AmIII bands. The difference spectrum was obtained by subtracting the PNIPAM spectra from that of d_7-PNIPAM. 155

Figure 7.3: The structure of PNIPAM and its deuterated isotopomers, d_7-PNIPAM. The C_α-hydrogen that gives rise to the resonance enhanced $C_\alpha H_b$ band at ~1387 cm^{-1} is highlighted. The curved arrow highlights the Ψ dihedral angle rotation around the C_α-C(O) bond. The AmIII band frequency is sensitive to the Ramachandran Ψ angle rotation around the C_α-C(O) bond. 156

Figure 7.4: Temperature dependence of the 204 nm excited UVRR spectra of PNIPAM. The AmI band intensity increases and upshifts with temperature, while the AmII band intensity decreases. and downshifts with temperature..... 159

Figure 7.5: 204-nm excited UVRR spectra of PNIPAM at (A) 4 ºC and (B) 45 ºC the spectra were decomposed into a minimum sum of mixed Lorentzian and Gaussian bands. The AmI region was fit to Gaussian bands. The measured and modeled spectra overlap almost completely. The different amide-hydrogen bonding sites are shown in the Fig 5A insert..... 161

Figure 7.6: The intensity ratio of the 1655 cm^{-1}/1624 cm^{-1} AmI bands shows an abrupt increase between 30 ºC and 40 ºC..... 162

Figure 7.7: PNIPAM spectra in water (45 ºC) and in the solid dehydrated state normalized to the peak intensity of the AmIII bands show significant differences in the amide band frequencies. In particular, the AmI vibration upshifts while, the AmII vibration downshifts by 7 cm^{-1} upon PNIPAM dehydration. The insert shows the results of spectral decomposition in the AmI and AmII region of the dry, solid PNIPAM which show increased band intensity for the 1654 cm^{-1} AmI region..... 167

Figure 7.8: A cartoon of collapsed and extended conformation of PNIPAM (side-view) as drawn in Material Studio software. Note that the carbonyl groups are fully exposed in the extended conformation but are located inside the hydrophobic pocket in the collapsed state. The carbonyl oxygens are colored red while, the nitrogens are blue..... 169

Figure 7.9: Single chain PNIPAM shows a ~20 cm^{-1} upshift in the AmI vibrational frequency upon PNIPAM collapse. Spectral decomposition of the AmI and AmII regions at 24 and 42 ºC are shown in inserts..... 170

Figure 7.10: Time resolved 204-nm UVRR (hot – 30 ºC) difference spectra at different delay times. The AmI band shows the largest spectral shift. B) The peak-to-peak AmI band amplitude in the (hot – 30 ºC) transient difference spectra at different delay time is used to model the kinetics of the PNIPAM's hydrophobic collapse. All changes in the AmI region are complete within 1 μs; we do not observe any significant changes in the AmI region at longer timescales (insert). The amide band intensity in the difference spectra shows a small decrease at 100 μs which indicates sample volume cooling due to equilibration. 173

PREFACE

I would like to express the immense gratitude I have for my colleagues and friends who have been of tremendous help and a source of inspiration during the course of my doctoral program. First and foremost, my advisor Prof. Asher to whom I am forever indebted for his wisdom and patience. It was Prof. Asher who introduced me to the fascinating world of UVRR and protein folding. Throughout my graduate career he has provided invaluable guidance and encouragement to overcome the numerous obstacles that occasionally cropped up. From him, I learned the true value of independent work, and critical analysis, values that have allowed me become a better scientist.

I would like to thank Dr. Pratt, for his guidance and support throughout my years in Pittsburgh. I am grateful for his continuing guidance in my pursuit of a better understanding of all things small.

I would like to express special thanks to Dr. John Williams for the privilege of working in the departmental mass-spectrometry facility.

I would like to thank my group mates, past and present for all their support during these years. Special thanks to Dr. Iliar Beta and Mark Sparrow who early in my career provided much needed assistance with laser operations. Without the generous help of Dr. Nataliya Myshakina, the last leg of my graduate career would not have gone so smoothly. Of course, during all these

years at Asher group Sharon Mansfield was always there to smooth things over whenever the need arose.

Dave Hart from Coherent Inc. was an invaluable resource with YAG lasers and our own machine shop, electronic shop and university engineers in general helped keep the lab running.

I would be remiss if I did not acknowledge the people whose company made my time in Pittsburgh a delight. I will always cherish my time with Dr. Marco Banoro, Prof. Abdil Ozdemir, Dr. Mingxiang Lin and Dr. Soraya Pornswan at the oenophile club. I am also grateful for the late Dr. Moorthy, Mr. Fangyong, and Mr. Sylvere for the many cups of tea and stimulating discourse that often followed.

I will always remember dinners at Lidia's with Dr. Taormina and his lovely wife Trisha. I am grateful that I got to meet Curtis Smith, Mark Choy, Nancy Cedric and the rest of the boxing crew at Trees hall. They helped me find and hone in that competitive side of mine that will surely come-in handy in my future endeavors. Of course, this list would be incomplete without Erika Englund to whom I owe much. In her company I grew and found more to myself and ever before.

I am grateful to my undergraduate research advisor Dr. Hussam (GMU) and my high school AP physics teacher Dr. Patel for their encouragement over the years.

Lastly, and most importantly, my family, for their unconditional love and support through all of my days.

1.0 PROTEIN FOLDING

In 1953, a jubilant Francis H. Crick, the co-discoverer of DNA proclaimed to the patrons of The Eagle, "We have discovered the secret of Life!"[1] His enthusiasm was of course justified because it is our genetic code carries the necessary information to create life, generation after generation. However, what Crick forgot to mention was that it's proteins that do all the dirty work.[2]

Proteins are involved in almost every aspect of cellular life: structure building, recognition, catalysis, chemical signaling, transportation, DNA replication and repair etc etc[1]. Due to evolutionary pressure, proteins have evolved into different classes, each to carryout a specific task. In general, a catalytic protein like superoxide dismutase differs in structure and composition from a transport protein such as hemoglobin.[1,3] The function and efficiency of a protein is determined by its structure,[1] which is encoded in it's sequence.[1,2,4] Hence, an understanding of how the sequence influences peptide's conformation will provide us with a molecular understanding of the most fundamental process governing cellular life.

Protein folding is perhaps best understood in terms of the famous Levinthal paradox.[1,2,4,5] Consider a hypothetical a 100 residue protein, where each residue can adopt eight different conformations, the peptide chain has 10^{89} different available

conformations. If the peptide randomly searches for the thermodynamically stable native state at the rate of 10^{13} s^{-1}, it would take the peptide approximately 10^{66} years to search all possible conformations. An unbiased sampling of all possible conformations would thus make the *thermodynamically stable state, kinetically inaccessible*.[2,5,6] The paradoxical disconnect between the kinetics and thermodynamics of protein folding led Leventhal to suggest that proteins must use specific pathways or mechanisms that greatly enhance their folding rate.

1.1 NATIVE STATE INTERACTIONS

An understanding of protein folding requires a firm grasp of the various thermodynamic forces driving a protein's transition from an unordered to a well-ordered state. Folding from unordered state to a well defined state is disfavored by entropy. Thus, successful protein folding requires that the native enthalpic interactions must be sufficiently large so as to overcome the loss of entropy and provide sufficient stability to the native state under physiological conditions.[7,8] In general the native state is stabilized by the following interactions:

1.1.1 Disulfide bridges

A disulfide bridge is a covalent bond between sulflhydrl (–SH) groups of two cysteine residues and is typically found in large tertiary proteins. Disulfide bridges serve to provide extra stability to the tertiary structure.[1,2]

1.1.2 Electrostatic interactions

At physiological pH, the *C*- and *N*-termini of peptide chains along with acidic and basic side chains of amino acids are all charged.[1] In large proteins charged amino acids are typically found at the surface. The burial of an unpaired charged side chain inside the hydrophobic core is energetically unfavorable.

At the surface, charge and dielectric screening dampen inter-residue electrostatic interactions, diminishing their contribution to the stabilization of native conformation.[1,2,7,9] Typically the secondary and tertiary structure of proteins is stabilized by attractive electrostatic interactions e.g. in Trp-cage peptide[10] the Asp-(Arg/Lys) interaction stabilizes the native conformation by ~5.8−7.5 kJ mol^{-1}. In some cases, however, electrostatic repulsions can also help define secondary structures e.g. electrostatic repulsions between successive lysine residues force poly-lysine to predominantly adopt an extended 2.5_1 helix-like conformation.[11]

1.1.3 Hydrogen bonding

Carbonyl to amide N-H hydrogen bonding is primarily responsible for the stability of secondary structures such as the α-helix or β-sheet conformation (Fig 1.1).[2,7-9] While, a single hydrogen bond contributes on average only 12 kJ/mol of stabilization, the large number of hydrogen bonds present in a typical secondary structure such as an α-helix are sufficient to stabilize secondary structures.[1]

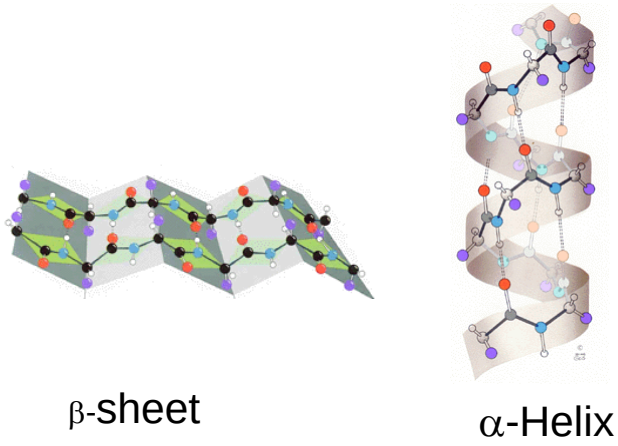

Figure 1.1: Hydrogen bonding between the amide groups stabilizes secondary structures such as the β-sheet or α-helix, respectively. Reproduced from http://www.bio.mtu.edu

1.1.4 Van der Waals interactions

Van der Waals interactions or dispersion forces are the weakest of all interactions involved in protein folding. While a single methyl-methyl interaction is significantly weaker than a hydrogen bond,[12] the sheer number of such interactions in protein's

hydrophobic core is quiet significant. Van der Waals interactions typically contribute 1.2 - 4 kJ/mol towards protein stability.[1,2]

1.1.5 Hydrophobic Effect

The Hydrophobic effect constitutes the most obscure class of interactions in biophysics. Much confusion exists in the literature as to the exact nature and contribution of hydrophobic interactions in protein folding. The problem lies in the fact that hydrophobicity in itself is an abstract concept.[13]

Hydrophobicity was initially used to explain the low solubility of non-polar solutes and the subsequent changes in physical properties of water upon dissolution of non-polar solutes.[12,13] According to this rationalization, introduction of non-polar solute leads to formation of low entropy calthrates or cage-like water structures[14-17] that surround the non-polar solutes.[1,2,13] Consequent reduction in the entropy of water molecules is responsible for the hydrophobic effect.

In their classic paper Frank and Evans developed a coherent framework based on statistical mechanics that correlates entropy changes with changes in molecules free volume (V_f).[17] The authors proposed that the unusual behavior of non-polar solutes in water, namely their abnormally high entropy of vaporization (S_v) and equally striking temperature dependent change in S_v, (S_v/T) could be rationalized by invoking the presence of structured or iceberg-like water around the non-polar solutes. Increased hindrance to internal motions in ice-like configuration decreases the fluctuation or librational entropy of water and is responsible for the unusually high S_v of non-polar

solutes in water. Similar structural making/breaking arguments are applicable to electrolytic solutes.[17]

Many different variations of the iceberg models like the "flickering iceberg model" have been proposed, however, the basic argument has remained the same.[13] Alternative models such as the Scaled Particle Theory (SPT) model[13,18] have suggested that hydrophobicity has its origin in water's high molar volume as opposed to the formation of local structure. The high molar volume of water leads to an unfavorable Gibbs free energy for cavity formation and hence results in an overall reduced/unfavorable free energy of solvation.[19]

While SPT and other advanced models have gained acceptance over the last few years, the Frank and Evans iceberg model remains popular as it allows one to visualize the net effects with relative ease. Regardless of whichever model is adopted the fact remains that solvation of non-polar solutes[20] involves an unfavorable free energy penalty.[21-24] In order to minimize the impact of the unfavorable entropy term, hydrophobic groups cluster together, thus decreasing the number of molecules in the solvation shell surrounding the hydrophobic groups.[25] Increased librational entropy of released water molecules reduces the entropic cost of hydrophobic solvation and compensates for loss of configuration entropy incurred upon cluster formation. Thus, the libration free energy drives the aggregation of non-polar groups/solutes in water.[12,26] This phenomenon is also responsible for the hydrophobic collapse[27,28] of unordered peptide chains which greatly reduces the solvent accessible surface area of non-polar residues. Formation of a compact state hastens protein folding,[29] by greatly reducing the number of available configuration of the peptide chain.

1.2 EARLY HISTORY OF PROTEIN FOLDING

While, the nature of interactions involved in stabilizing the protein conformation has been known for a while, an understanding of protein kinetics has been long lacking. Anfinsen's discovery that denatured proteins can *in vitro* fold to its native conformation jump started the field of protein folding.[4] In 1965, using hard sphere approximation, Ramachadran[30] and coworkers demonstrated that due to steric clashes in the peptide backbone, only a small range of φ and ψ dihedral angles[31,32] are accessible (Fig 1.2). The inaccessibility of a large region of the Ramachandran space indicates that only a finite number of conformations would ever be available to the unfolded state. However, it should be noted that the number of accessible states is still quite large.

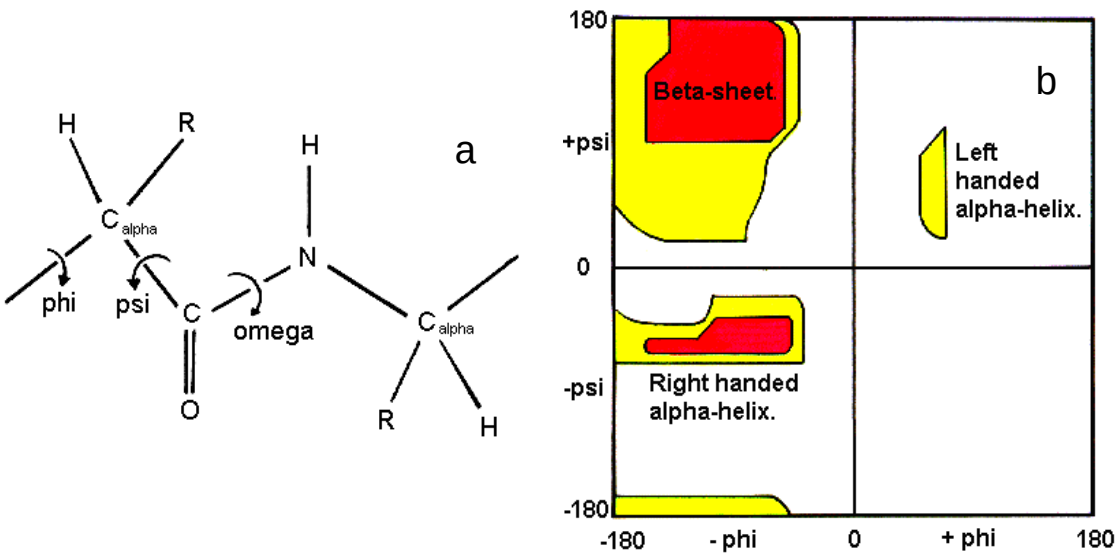

Figure 1.2: a) Torsion angles phi and psi b) The Ramachandran plot of available phi and psi angles. Reproduced from http://www.cryst.bbk.ac.uk/

1.3 THEORETICAL MODELING

Over the last two decades advancements in computational power have permitted increasingly detailed insight into protein folding,[33] although analytical solutions of large systems remain prohibitively expensive. In order to make computation less challenging, potential energy surfaces (PES)[33,34] are used to reduce computation time. Over the years, the use of approximate methods such as lattice bead model[35,36] the HP, and HP+[37] models, along with statistical mechanics[38-40], stochastic dynamics[41], and spin glass mechanics[42] models has allowed theoreticians to gain a better understanding of the driving forces behind protein folding.[29]

Recent advances in computing power combined with efficient algorithms such as the *replica exchange model* [43,44] have allowed researchers to carry out all-atom molecular dynamics (MD) simulations of small peptides and proteins such as Trp-cage[45-49] for as long as a 100 ns. Distributed computing resources such as *Folding@home* can reach the 1 millisecond time regime.[50]

Results from these studies motivated the development of the so-called "new view" of protein folding.[6] The new view holds that folding is an ensemble process, where the unfolded protein has large conformational entropy. The hydrophobic collapse of polypeptide leads to a drastic decrease in the configuration space and hence facilitates fast folding. As folding proceeds, the configurational entropy decreases in a funnel-like manner until the native state is reached (Fig 1.3).[6]

In this scheme the exact folding pathway is not important as there are many different possible combinations through which the peptide could have reduced its total

energy (Fig 1.3a). Intermediates arise due to trapping of peptide chains in basins, from which they have to climb out.[6] This effort requires partial melting of the intermediate and hence slows down the overall folding rate.[6] An excessive out-cropping of basins, hills and valleys would lead to a rough energy landscape, where the protein finds itself mired in a slow, frustrating search for the native state (Fig 1.3b).[6,42,51] This scenario is prevented due to the "principle of minimal frustration".[42]

The principle of minimal frustrations holds that during the folding process the peptide chain avoids such conformations that would hinder formation of native contacts i.e. the primary sequence of peptide is optimized to avoid local minima which ensures fast folding.[42]

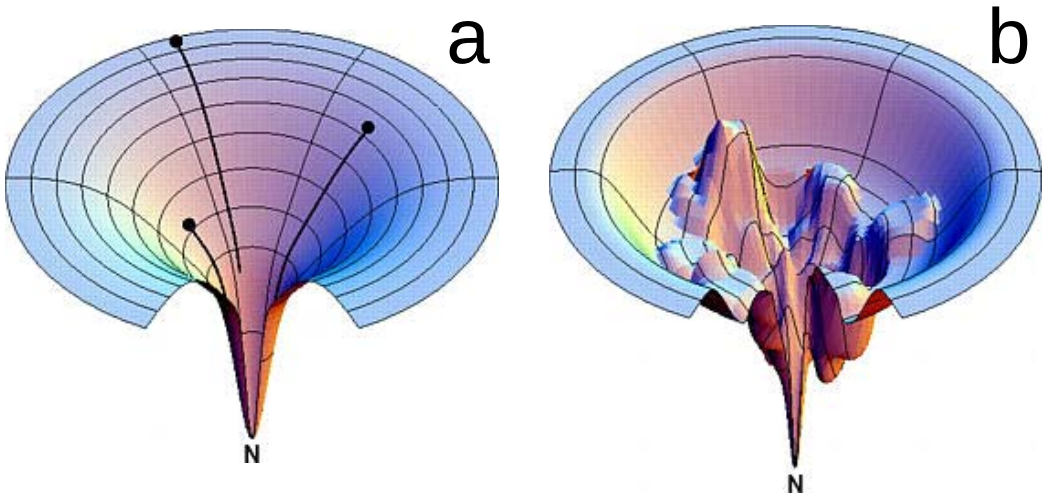

Figure 1.3: a) Folding along a smooth energy landscape devoid of any intermediates. b) A rough energy landscape with multiple kinetic intermediates. Reproduced from reference #6

In a departure from traditional chemical kinetic theories, the "new view" does not hold the transition state as a specific conformation, but rather as a kinetic bottleneck in the folding pathway.[6] The bottleneck limits the rate at which the protein can approach its

native state. Hence any change that affects the characteristics of the bottleneck directly impacts the observed folding time.[6]

The principle advantage of the funnel theory is that it allows scientists to easily visualize and understand the folding landscape.[52] The funnel theory in itself however, does not present a complete description of the folding process. Recent experimental studies have demonstrated that the unfolded state of proteins contain a significant PPII content i.e. the unfolded state is not an ideal random coil, rather it shows considerable local structure.[53-66] These results suggest that protein folding may be initiated from a localized region of the configuration space; furthermore, recent theoretical and experimental work indicates α-helix to PPII transition passes through a turn-like intermediate conformation.[67,68] These results require that the ensemble picture of funnel theory should be modified to incorporate mechanistic details of proteins folding.

1.4 EXPERIMENTAL APPROACH

While, theoreticians were busy trying to reconcile the thermodynamics of protein folding with its kinetics, experimentalist went on to develop an array of new techniques designed to probe the earliest steps in protein folding. In this regard advancements in biotechnology helped usher in a new era in structural biology. With the aid of biotechnology,[1] scientists now wield a powerful new tool, "site directed mutagenesis" which purposefully replaces a native residue with one of experimentalist's choice.[69] Site-directed mutagenesis has afforded an unprecedented opportunity to gain a better

understanding of α-helical propensities,[2,5] sterics,[2] hydrophobicity and Van der Waals interactions in protein folding.[1,2,5] In particular site-directed mutagenesis has been particularly useful in examining the impact of individual amino acids on protein folding.

1.4.1 Kinetic studies of protein folding

Due to the inherently slow mixing time of stop-flow systems early kinetic measurements were limited to millisecond time regime[2] Advances in design and commercial availability of necessary components led to the development of continuous flow systems based on the principles of either hydrodynamic focusing[70] or turbulent mixing[71] with dead times of as little as ~ 45 μs.[27] The principle benefit of using ultrafast continuous flow mixers is low sample consumption which allows one to study poorly expressed or valuable proteins.

Ultrafast mixing can be used to generate a large free energy perturbation in any biochemical system and hence the instrumental setup is generally applicable to a host of interesting problems. However, the relatively large dead times of instruments prohibit examination of fast kinetic events such as folding of single isolated secondary structure units such as the α-helix[70] which fold in the nanosecond time regime.[10,72,73] A better understanding of elementary units would allow us to gain an empirical understanding of the earliest steps in protein folding; furthermore, such small systems are accessible to theoretical techniques and hence provide a convenient meeting point for theory and experiment.[10,74]

In recent years nanosecond kinetics of elementary structures have been examined using either photochemical triggering[75] or laser temperature jump (T-jump) experiments.[76] Laser T-jump experiments came into prominence due to their general applicability to biochemical systems.

T-jump spectrometers based on IR,[9] fluorescence[72,77] and UV resonance Raman (UVRR)[76] spectroscopy have been reported. Time-resolved IR and UVRR measurements indicate single isolated α-helices unfold in ~200 ns while, folding appears to take ~0.6 μs. The α-helix fold considerably faster then β-hairpins (0.76-7 μs)[78-82] and small tertiary proteins (4 μs)[77] of similar length.

These results indicate that isolated α-helix folding is limited by diffusion of peptide chain through the solvent. In peptide conformations boasting tertiary contacts folding rate is limited by internal friction. Recent work by Hagen and coworkers indicate that internal friction limits the protein folding rate at 10^5 s^{-1}.[83]

1.5 CONCLUSION

The past few years have witnessed a tremendous growth in our understanding of protein folding. In early 1990's theoretical calculations highlighted the role of hydrophobic interactions in protein folding. Theses theoretical studies along with sophisticated kinetics measurements led to the development and widespread use of the funnel theory. This new view sought to cast the folding process as a chaotic, ensemble process where the exact nature of a single folding trajectory was de-emphasized along with old notions

of a well-ordered transition state. In their place, the idea of ensembles was put forth. According to this new-view, the diversity of folding-behavior arises due to averaging over many different trajectories. The rate limiting step arises due to a bottleneck in the energy landscape where the peptide chain finds itself with only a few pathways that can converge to the native state. The limited number of conformations a peptide chain can adopt at this stage is primarily responsible for the slow descent to global minima.[6,34]

Recent studies, however, have challenged some of the basic assumptions underlying the funnel theory. These studies indicate that the protein folding appears to follow a general pathway. The unfolded state of proteins contains significant PPII content,[65,67,84] hence, the folding reaction is likely initiated from the PPII region of Ramachandran space. Furthermore, β-turn like conformations likely serves as intermediates in the folding transition.[85] These results argue that the funnel theory must be modified to include mechanistic details in describing the folding process.

1.6 REFERENCES

(1) Garrett, R. H. G., Charles M.; *Biochemistry*, Second ed.; Saunders College Publishing: Philadelphia, Pa, 1999.
(2) Pain, R. H. *Mechanisms of Protein Folding*; Oxford University Press: New York, NY, 1994.
(3) Lippard, S. J. B., Jeremy M. *PRINCIPLES OF Bioinorganic Chemistry*; University Science Books: Mill Vallery, 1994.
(4) Anfinsen, C. B. *Science* **1973**, *181*, 223.
(5) Cleland, J. *Protein folding: in vivo and in vitro*; American Chemical Society: Washington D. C., 1993.
(6) Dill, K. A.; Chan, H. S. *Nat. Struct. Biol.* **1997**, *4*, 10.
(7) Dill, K. A. *Biochemistry* **1990**, *29*, 7133.
(8) Dill, K. A.; Alonso, D. O. V.; Hutchinson, K. *Biochemistry* **1989**, *28*, 5439.

(9) Glaser, R. *Biophysics*; Springer: New York, 2000.
(10) Neidigh, J. W.; Fesinmeyer, R. M.; Andersen, N. H. *Nature Structural Biology* **2002**, *9*, 425.
(11) Mikhonin, A. V.; Myshakina, N. S.; Bykov, S. V.; Asher, S. A. *JACS* **2005**, *127*, 7712.
(12) Tanford, C. *The hydrophobic effect: formation of micelles and biological membranes*; Wiley: New York, 1973.
(13) Blokzijl, W.; Engberts, J. B. F. N. *Angew. Chem. Int. Ed. Engl.* **1993**, *32*, 1545.
(14) Kusalik, P. G.; Svishchev, I. M. *Science* **1994**, *265*, 1219.
(15) Frank, H. S. *Journal of Chemcial Physics* **1945**, *13*, 493.
(16) Frank, H. S. *Journal of Chemcial Physics* **1945**, *13*, 478.
(17) Frank, H. S.; Evans, M. W. *Journal of Chemcial Physics* **1945**, *13*, 507.
(18) Pierotti, R. A. *Chemical Reviews* **1976**, *76*, 717.
(19) Lee, B. *Biopolymers* **1991**, *31*, 993.
(20) Carr, P. W.; Li, J.; Dallas, A. J.; Eikens, D. I.; Tan, L. C. *Journal of Chromatography A* **1993**, *656*, 113.
(21) Searle, M. S.; Williams, D. H. *J. Am. Chem. Soc.* **1992**, *114*, 10690.
(22) Searle, M. S.; Williams, D. H.; Gerhard, U. *J. Am. Chem. Soc.* **1992**, *114*, 10697.
(23) Dunitz, J. D. *Science* **1994**, *264*, 671.
(24) Horvath, C.; Melander, W.; Molnar, I. *Journal of Chromatography* **1976**, *125*, 129.
(25) Ben-Naim, A. *J. Phys. Chem.* **1991**, *95*, 1437.
(26) Ramadan, M. S.; Evan, D. F.; Lumry, R. *J. Phys. Chem.* **1983**, *87*, 4538.
(27) Hagen, S. J.; Eaton, W. A. *J. Mol. Biol.* **2000**, *297*, 781.
(28) Hagen, S. J. *Proteins: Structure, Function, and Genetics* **2003**, *50*, 1.
(29) Wolynes, P. G.; Onuchic, J. N.; Thirumalai, D. *Science* **1995**, *267*, 1619.
(30) Ramakrishnan, C.; Ramachandran, G. N. *Biophys J.* **1965**, *5*, 909.
(31) Nomenclature, I.-I. C. o. B. *Biochemistry* **1970**, *9*, 3471.
(32) Mirkin, N. G.; Krimm, S. *J. Phys. Chem. A* **2002**, *106*, 3391.
(33) Fraga, S.; Parker, J. M. R.; Pocock, J. M. *Computer Simulations of Proteins Structures and Interactions*; Springer: New York, 1995.
(34) Dobson, C. M.; Salij, A.; Karplus, M. *Angew. Chem. Int. Ed. Engl.* **1998**, *37*, 868.
(35) Nakamura, H. K.; Sasaki, T. N.; Sasai, M. *Chemical Physics Letters* **2001**, *347*, 247.
(36) Saven, J. G. *Chemical Reviews* **2001**, *101*, 3113.
(37) Chan, H. S.; Dill, K. A. *Proteins: Struct. Funct. Genet.* **1998**, *30*, 2.
(38) Hao, M.-H.; Scheraga Harold, A. *J. Phys. Chem.* **1994**, *98*, 9882.
(39) Sullivan, D. C.; Kuntz, I. D. *J. Phys. Chem. B* **2002**, *106*, 3255.
(40) Abkevich, V. I.; Gutin, A. M.; Shakhnovich, E. I. *Journal of Chemcial Physics* **1994**, *101*, 6052.
(41) Bryngelson, J. D.; Wolynes, P. G. *J. Phys. Chem.* **1989**, *93*, 6902.
(42) Bryngelson, J. D.; Wolynes, P. G. *Proc. Nat. Acad. Sci. U.S.A.* **1987**, *84*, 7524.
(43) Sugita, Y.; Okamoto, Y. *Chemical Physics Letters* **2000**.
(44) Garcia, A. E.; Sanbonmatsu, K. Y. *Proc. Nat. Acad. Sci. U.S.A.* **2002**, *99*, 2782.
(45) Ding, F.; Buldyrev, S. V.; Dokholyan, N. V. *Biophysical Journal* **2005**, *88*, 147.

(46) Iavarone, A. T.; Parks, J. H. *Journal of the American Chemical Society* **2005**, *127*, 8606.
(47) Pitera, J. W.; Swope, W. *Proceedings of the National Academy of Sciences of the United States of America* **2003**, *100*, 7587.
(48) Zhou, R. *Proceedings of the National Academy of Sciences of the United States of America* **2003**, *100*, 13280.
(49) Simmerling, C.; Strockbine, B.; Roitberg, A. E. *Journal of the American Chemical Society* **2002**, *124*, 11258.
(50) Zagrovic, B.; Snow, C. D.; Khaliq, S.; Shirts, M. R.; Pande, V. S. *Journal of Molecular Biology* **2002**, *323*, 153.
(51) Onuchic, J. N.; Socci, N. D.; Luthey-Schulten, Z.; Wolynes, P. G. *Folding & Design* **1996**, *1*, 441.
(52) Ferguson, N.; Wei, L.; Capaldi, A. P.; Kleanthous, C.; Radford, S. E. *J. Mol. Biol.* **2001**, *307*, 393.
(53) Blanch, E. W.; Morozova-Roche, L. A.; Cochran, D. A. E.; Doig, A. J.; Hecht, L.; Barron, L. D. *Journal of Molecular Biology* **2000**, *301*, 553.
(54) Chen, K.; Liu, Z.; Zhou, C.; Shi, Z.; Kallenbach, N. R. *Journal of the American Chemical Society* **2005**, *127*, 10146.
(55) Creamer, T. P. *Proteins: Structure, Function, and Genetics* **1998**, *33*, 218.
(56) Creamer, T. P.; Campbell, M. N. *Advances in Protein Chemistry* **2002**, *62*, 263.
(57) Ferreon, J. C.; Hilser, V. J. *Protein Sci.* **2003**, *12*, 447.
(58) Kelly, M. A.; Chellgren, B. W.; Rucker, A. L.; Troutman, J. M.; Fried, M. G.; Miller, A.-F.; Creamer, T. P. *Biochemistry* **2001**, *40*, 14376.
(59) Rath, A.; Davidson, A. R.; Deber, C. M. *Biopolymers* **2005**, *80*, 179.
(60) Rucker, A. L.; Creamer, T. P. *Protein Sci.* **2002**, *11*, 980.
(61) Rucker, A. L.; Pager, C. T.; Campbell, M. N.; Qualls, J. E.; Creamer, T. P. *Proteins: Structure, Function, and Genetics* **2003**, *53*, 68.
(62) Schweitzer-Stenner, R.; Eker, F.; Griebenow, K.; Cao, X.; Nafie, L. A. *Journal of the American Chemical Society* **2004**, *126*, 2768.
(63) Stapley, B. J.; Creamer, T. P. *Protein Sci.* **1999**, *8*, 587.
(64) Asher, S. A.; Mikhonin, A. V.; Bykov, S. V. *J. Am. Chem. Soc.* **2004**, *126*, 8433.
(65) Mezei, M.; Fleming, P. J.; Srinivasan, R.; Rose, G. D. *Proteins: Structure, Function, and Bioinformatics* **2004**, *55*, 502.
(66) Whittington, S. J.; Creamer, T. P. *Biochemistry* **2003**, *42*, 14690.
(67) Fitzkee, N. C.; Rose, G. D. *Proceedings of the National Academy of Sciences of the United States of America* **2004**, *101*, 12497.
(68) Sundaralingam, M.; Sekharudu, Y. C. *Science* **1989**, *244*, 1333.
(69) Kim, D. E.; Yi, Q.; Gladwin, S. T.; Goldberg, J. M.; Baker, D. *J. Mol. Biol.* **1998**, *284*, 807.
(70) Pabit, S. A.; Hagen, S. J. *Biophys J.* **2002**, *83*, 2872.
(71) Shastry, M. C. R.; Luck, S. D.; Roder, H. *Biophys J.* **1998**, *74*, 2714.
(72) Eaton, W. A.; Munoz, V.; Thompson, P. A.; Henry, E. R.; Hofrichter, J. *Acc. Chem. Res.* **1998**, *312*, 745.
(73) Chowdhury, S.; Lee, M. C.; Xiong, G.; Duan, Y. *J. Mol. Biol.* **2003**, *327*, 711.
(74) Gellman, S. H.; Woolfson, D. N. *Nature Structural Biology* **2002**, *9*, 408.

(75) Pascher, T.; Chesick, J. P.; Winkler, J. R.; Gray, H. B. *Science* **1996**, *271*, 628.
(76) Lednev, I. K.; Karnoup, A. S.; Sparrow, M. C.; Asher, S. A. *J. Am. Chem. Soc.* **1999**, *121*, 8074.
(77) Qiu, L.; Pabit, S. A.; Roitberg, A. E.; Hagen, S. J. *Journal of the American Chemical Society* **2002**, *124*, 12952.
(78) Dinner, A. R.; Lazaridis, T.; Karplus, M. *PNAS* **1999**, *96*, 9068.
(79) Blanco, F.; Ramirez-Alvarado, M.; Serrano, L. *Curr. Opin. Struct. Biol.* **1998**, *8*, 107.
(80) Blanco, F. J.; Jimenez, M. A.; Herranz, J.; Rico, M.; Santoro, J.; Nieto, J. L. *JACS* **1993**, *115*, 5887.
(81) Dyer, R. B.; Maness, S. J.; Franzen, S.; Fesinmeyer, R. M.; Olsen, K. A.; Andersen, N. H. *Biochemistry* **2005**, *44*, 10406.
(82) Dyer, R. B.; Maness, S. J.; Peterson, E. S.; Franzen, S.; Fesinmeyer, R. M.; Andersen, N. H. *Biochemistry* **2004**, *43*, 11560.
(83) Pabit, S. A.; Roder, H.; Hagen, S. J. *Biochemistry* **2004**, *43*, 12532.
(84) Creamer, T. P.; Srinivasan, R.; Rose, G. D. *Biochemistry* **1995**, *34*, 16245.
(85) Sankararamakrishnan, R.; Vishveshwara, S. *Biopolymers* **1990**, *30*, 287.

CHAPTER 2

Raman Scattering

2.0 RAMAN SCATTERING

The Raman effect is an inelastic light scattering process where the electromagnetic field and the molecule exchange a quantum of energy. The difference in energy between the incident and scattered photon reports on the quantum energy levels of the molecule. This property of the Raman effect has been widely exploited in vibrational spectroscopy.[1-3]

In both the classical and quantum mechanical treatment of Raman theory the incident photon perturbs the molecule by inducing an oscillating electric dipole moment. In some special cases such as Raman scattering from chiral molecules (Raman optical activity, ROA[4,5]) the magnetic dipole and the electric quadruple moments are required to provide a detailed mathematical description of the phenomenon.[2,4] For the purposes of our present discussion, however, the electric dipole approximation will suffice.

2.1.1 Classical Treatment

When a molecule is placed in an incident electric field $\vec{E}^{\omega}$, a dipole moment ρ_{ind} is induced in the molecule as the nuclei and electron are attracted towards the negative and positive poles of the field, respectively. The induced dipole moment is expressed as:

$$\rho_{ind} = \hat{\alpha}\vec{E}^{\nu} \qquad \ldots(1)$$

Where, $\hat{\alpha}$ is the polarizability tensor of the molecule and $\vec{E}$ is the incident electric field. The polarizability tensor $\hat{\alpha}$ is a function of the nuclear coordinate and hence varies with vibrational motion. We can account for this variability by expanding the polarizability tensor as a Taylor series along the nuclear coordinates:[1,2]

$$\alpha_{\rho\sigma} = (\alpha_{\rho\sigma})_0 + \sum_k (\frac{\partial \alpha_{\rho\sigma}}{\partial Q_k})_0 Q_k + \frac{1}{2}\sum_{k,l} (\frac{\partial^2 \alpha_{\rho\sigma}}{\partial Q_k \partial Q_l})_0 Q_k Q_l + ... \qquad ...(2)$$

The summation is over all normal modes, *k*. Neglecting the higher order terms we can truncate the series at the first derivative:

$$\alpha_{\rho\sigma} = (\alpha_{\rho\sigma})_0 + \sum_k (\frac{\partial \alpha_{\rho\sigma}}{\partial Q_k})_0 Q_k \qquad \ldots(3)$$

Which we re-write as:

$$(\alpha_{\rho\sigma})_k = (\alpha_{\rho\sigma})_0 + (\alpha'_{\rho\sigma})_k Q_k \qquad \ldots(4)$$

Where, $(\alpha_{\rho\sigma})_o$ is the equilibrium polarizability tensor while, $\alpha_{\rho\sigma}$ is the derived polarizability. Assuming mechanical harmonicity, we can express the time-dependence of nuclear coordinate Q_k, as:

$$Q_k = Q_{k_0} \cos(\omega_k t + \delta_k) \qquad \ldots(5)$$

Where, Q_{ko} and δ_k are the normal coordinate amplitude and the phase factor, respectively, while, ω_k, is the natural frequency of the vibration. Substituting equation 5 into equation 4 yields an expression for the time-dependent modulation of polarizability tensor for the k^{th} mode.

$$\alpha_k = \alpha_o + \alpha'_k Q_{k_0} \cos(\omega_k t + \delta_k) \ldots(6)$$

We can express the time-dependent electric field amplitude as:

$$E = E_0 \cos \omega_1 t \qquad \ldots(7)$$

Where, E_o is the scalar amplitude of the electric field while ω_1 is the frequency of the electric field. Substituting eq. 6 and. 7 into eq 1 yields:

$$\rho_{ind} = \alpha_0 E_0 \cos \omega_1 t + \alpha'_k E_0 Q_{k_0} \cos(\omega_k t + \delta) \cos \omega_1 t \quad \ldots(8a)$$

Using the trigonometric function

$$\cos A \cos B = \frac{1}{2}\{\cos(A+B) + \cos(A-B)\} \qquad \ldots(8b)$$

We can re-arrange eq 8b as:

$$\rho_{ind} = \alpha_o E_o \cos(\omega_1 t) + \frac{\alpha'_k E_o}{2}\{\cos(\omega_1 t \pm \omega_k t \pm \delta_k)\} \quad \ldots(9)$$

And re-write eq. 9 as:

$$\rho_{ind} = \rho_o^{Ray} \cos \omega_1 t + \rho_o^{Ram} \cos(\omega_1 t \pm \omega_k t \pm \delta_k) \qquad \ldots(10)$$

Thus, it can be seen from eq. 10 that the interaction of electromagnetic radiation with a molecule results in induced dipole moments that oscillate at three different frequencies. The first dipole ρ_o^{Ray} oscillates at the same frequency as the electric field, therefore, the scattered light radiated by this dipole has the same frequency as the incident photon. This is known as Rayleigh scattering.

The second term in equation 10 describes dipole moments oscillating at beat frequencies between the incident field and the natural frequency of the harmonic oscillator. These dipoles thus radiate photons that differ in energy from the incident photon by a vibrational quantum (Raman Scattering). The additive component gives rise to anti-Stokes Raman scattering, the scattered photon has higher energy than the incident photon ($\omega_s = \omega_1 + \omega_k$). Similarly, in the case of Stokes Raman scattering (subtractive

component) the scattered photon has lower energy than the incident photon ($\omega_s = \omega_1 - \omega_k$).[1,2]

2.1.2 Quantum Mechanical Treatment

While the classical treatment provides a framework to treat Raman scattering, it cannot provide detailed insight into the molecular origins of Raman scattering, in particular the classical theory fails to adequately predict Raman band intensities. A more detailed explanation of the Raman effect requires the use of quantum mechanics (QM). In our QM treatment however, only the molecule is treated in QM detail while, the electromagnetic field (EM) is treated classically. This semi-classical approach is utilized because it greatly simplifies the arithmetic without the loss of generality.[2]

We begin the QM treatment by casting the classical induced dipole moment in QM terms as an induced transition dipole moment:

$$\rho_{ind} = \langle \Psi_f^{'} \mid \rho \mid \Psi_i^{'} \rangle \qquad \ldots(11)$$

Where, Ψ'_f and Ψ'_i are perturbed wavefunctions while ρ is the induced transition dipole moment operator. The perturbed wavefunctions can be expanded as a series:

$$\Psi_f^{'} = \Psi_f^{(o)} + \Psi_f^{(1)} + \Psi_f^{(2)} + .. \qquad \ldots(12a)$$

$$\Psi_i^{'} = \Psi_i^{(o)} + \Psi_i^{(1)} + \Psi_i^{(2)} + .. \qquad (12b)$$

Where $\Psi_i^{(o)}$ represents the unperturbed state, $\Psi_i^{(1)}$ is the first-order correction, $\Psi_i^{(2)}$ is second order correction and so on.[2] The time-dependent perturbation theory allows us to express the perturbed wavefunctions as linear combinations of unperturbed

wavefunctions. Restricting the Hamiltonian to only electric dipole moment terms (H_p) we may therefore write:

$$\Psi_f^{(n)} = \sum_r a_{\rho fr}^{(n)} \Psi_r^{(o)} \qquad \ldots(13a)$$

$$\Psi_i^{(n)} = \sum_r a_{\rho ir}^{(n)} \Psi_r^{(o)} \qquad \ldots(13b)$$

Now introducing the series expansion into equation 12 and collecting terms according to their dependence on the electric field's strength we arrive at:

$$\rho_{fi}^{(o)} = \langle \Psi_f^{(o)} \mid \rho \mid \Psi_i^{(o)} \rangle \qquad \ldots(14a)$$

$$\rho_{fi}^{(1)} = \langle \Psi_f^{(o)} \mid \rho \mid \Psi_i^{(1)} \rangle + \langle \Psi_f^{(1)} \mid \rho \mid \Psi_i^{(o)} \rangle \qquad \ldots(14b)$$

Here, ρ^o_{fi} represent the permanent dipole moment which is independent of incident electric field and does not play a role in the light scattering phenomena.[2] Expanding on the work of Krammers and Heisenberg, Dirac[6] utilized perturbation theory to demonstrate that the induced transition dipole moment (Eq 14b) can be expressed using unperturbed wavefuntions[6] as:

$$\rho^{(1)} = \frac{1}{2}\eta \sum_{r \neq i,f} \{ \frac{\langle f \mid \rho_\rho \mid r \rangle \langle r \mid \rho_\sigma \mid i \rangle}{\omega_{ri} - \omega_1 - i\Gamma_r} + \frac{\langle f \mid \rho_\sigma \mid r \rangle \langle r \mid \rho_\rho \mid i \rangle}{\omega_{ri} + \omega_1 + i\Gamma_r} \} E_{o\sigma} e^{-i\omega_s t} + c.c \qquad \ldots(15)$$

Where, ω_s is frequency of the scattered photon. We now introduce a general transition polarizability $(\alpha)_{fi}$ with component $(\alpha_{\rho\alpha})_{fi}$

$$(\alpha_{\rho\sigma})_{fi} = \frac{1}{\eta} \sum_{r \neq i,f} \{ \frac{\langle f \mid \rho_\rho \mid r \rangle \langle r \mid \rho_\sigma \mid i \rangle}{\omega_{ri} - \omega_1 - i\Gamma_r} + \frac{\langle f \mid \rho_\sigma \mid r \rangle \langle r \mid \rho_\rho \mid i \rangle}{\omega_{ri} + \omega_1 + i\Gamma_r} \} \qquad \ldots(16)$$

2.1.3 Frequency Denominators

An examination of equation 16 reveal that $(\alpha)_{fi}$ changes with $(\omega_{ri}-\omega_1)$ i.e. as the frequency of the incident electric field approaches the natural frequency of the molecule, the polarizability tensor $(\alpha_{\rho\alpha})_{fi}$ changes.

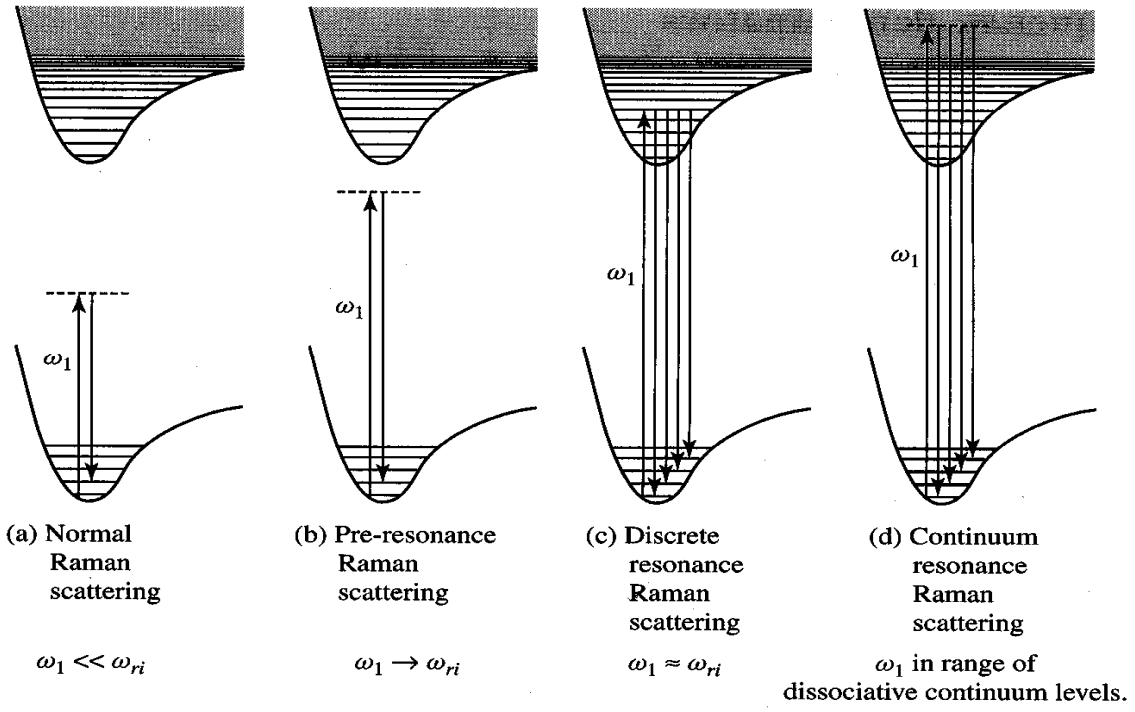

Figure 2.1: Different types of Raman scattering processes and their dependence upon the $\omega_{ri}-\omega_1$ term. Figure adopted from Long.[2]

When $\omega_{ri}>>\omega_1$ such that the incident frequency ω_1 is far from resonance with any molecular transition i.e. ω_1 does not overlap with any absorption bands then ignoring the $i\Gamma_r$ term yields $(\omega_{ri}-\omega_1)\sim \omega_{ri}$. In this case (normal Raman scattering) the system is excited from its initial state to the virtual state (r), from where it transitions to the final state (Fig 1a). The so-called virtual state is not a solution of the Schrödinger equation and hence

does not correspond to a well-defined energy level. These states are described by the time-dependent wavefunctions where the energy and hence the contribution of each state to the wavefunctions evolves with the time evolution of the wavefunction.[2] The polarizability tensor therefore, contains contributions from all the molecular states.

As the ω_l approaches a molecular transition frequency, $\omega_{ri,}$ (Fig 1b) the relative contribution of $-i\Gamma_r$ to the dominator increases which impacts the contribution of the r^{th} state to the sum over state. This process is referred to as pre-resonance Raman scattering. If $\eta\omega_l$ is large enough to reach dissociative states, the resulting scattering is termed continuum resonance Raman scattering (Fig 1d).[2]

When $\omega_l \approx \omega_{ri}$ i.e. the excitation frequency is in resonance with an absorption band, the resultant light scattering process is referred to as "resonance Raman scattering". A quick inspection of equation 16 reveals that the resonance condition greatly simplifies our mathematical treatment since $(\omega_{ri} - \omega_l - i\Gamma) \sim -i\Gamma$. As $i\Gamma$ is very small, the contribution from the first term (Eq 16) to $(\alpha_{\rho\alpha})_{fi}$ increases rapidly as resonance approaches. The contribution of the second term (Eq. 16), however, remains relatively small as the denominator, $(\omega_{ri} + \omega_l + i\Gamma)$, grows linearly. We can therefore ignore its contribution to the transition polarizability tensor.[2] Consequently, in resonance Raman scattering the sum over states is dominated by a few or even a single state corresponding to the resonant electronic transition.

Resonance Raman band intensities thus contain detailed information about the virtual states $|r\rangle$ and their lifetimes which can be exploited to better understand the excited state geometry of the molecule.[2] Meanwhile, the band frequencies report on the

ground state geometry and can be utilized in determining the ground state geometry of the molecule.

2.1.4 Utility of Resonance Raman in the study of protein folding

The principle advantage of resonance Raman is the relative simplicity of its spectrum. In resonance-enhanced Raman, only those vibrations that satisfy the Frank-Condon condition for the dominant |r> state are preferentially enhanced, i.e. a vibration that distorts the local ground state geometry towards that of the excited that geometry is preferentially enhanced.

This unique feature of resonance Raman allows spectroscopists to examine a specific chromophore in a large macromolecule by simply selecting an appropriate excitation wavelength specific to the chromphore of interest. In proteins, e.g. at 229-nm excitation the UV-resonance Raman (UVRR) spectrum of proteins is dominated by the resonance enhanced Tyr and Trp vibrations which are sensitive to the solvent exposure of Tyr and Trp side chains.[7]

At ~204-nm the Raman excitation is in resonance with ~200-nm amide NV_1 absorption band and hence the UVRR spectra dominated by amide vibrations. These vibrations, spanning the region between 1100-1700 cm^{-1} are sensitive to protein's secondary structure.[8] Recent developments indicate the $AmIII_3$ vibration ($C\text{-}N_s$ with NH_b, 1200-1280 cm^{-1}) sinusoidally depends upon the Ψ-dihedral angle. Asher and co-workers[9] have demonstrated the frequency domain $AmIII_3$ spectra can be utilized to

directly calculate the Boltzmann-weighted energy landscape of proteins and peptides during their (un)folding reaction along the Ψ-reaction coordinate.

2.2 REFRENCES

(1) Long, D. A. *Raman Scattering*; McGraw-Hill International Book Company: New York, USA, 1977.
(2) Long, D. A. *The Raman Effect A Unified Treatment of the Theory of Raman Scattering by Molecules*; John Wiley & Sons Ltd.: West Sussex, England, 2002.
(3) Asher, S. A. *Handbook of Vibrational Spectroscopy, John Whiley & Sons, Ltd.* **2001**, *1*, 557.
(4) Barron, L. D. *Nature (London)* **2000**, *405*, 895.
(5) Barron, L. D.; Blanch, E. W.; Hecht, L. *Advances in Protein Chemistry* **2002**, *62*, 51.
(6) Dirac, P. A. M. *Proceeding of the Royal Society of London, Series A, Containing Papers of a Mathematical and Physical Character* **1927**, *114*, 710.
(7) Chi, Z.; Asher, S. A. *Journal of Physical Chemistry B* **1998**, *102*, 9595.
(8) Chi, Z.; Chen, X. G.; Holtz, J. S. W.; Asher, S. A. *Biochemistry* **1998**, *37*, 2854.
(9) Asher, S. A.; Mikhonin, A. V.; Bykov, S. V. *J. Am. Chem. Soc.* **2004**, *126*, 8433.

CHAPTER 3

UV-Resonance Raman Thermal Unfolding Study of Trp-Cage Shows That It Is Not a Simple Two-State Miniprotein

This Chapter was published in *J. Am. Chem. Soc.* 2005 127(31), 10943-10950. The co-authors are Zeeshan Ahmed, Ilir A. Beta, Aleksandr V. Mikhonin, and Sanford A. Asher

3.0 UV-RESONANCE RAMAN THERMAL UNFOLDING STUDY OF TRP-CAGE SHOWS THAT IT IS NOT A SIMPLE TWO-STATE MINIPROTEIN

Trp-cage, a synthetic 20 residue polypeptide, is proposed to be an ultrafast folding synthetic miniprotein which utilizes tertiary contacts to define its native conformation. We utilized UV resonance Raman spectroscopy (UVRS) with 204- and 229-nm excitation to follow its thermal melting. Our results indicate that Trp-cage melting is complex and it is not a simple two state process. Using 204-nm excitation we probe the peptide secondary structure and find the Trp-cage's α-helix shows a broad melting curve where on average four α-helical amide bonds melt upon a temperature increase from 4º to 70 ºC. Using 229-nm excitation we probe the environment of the Trp side chain and find that its immediate environment becomes more compact as the temperature is increased from 4º to 20 ºC; however, further temperature increases lead to exposure of the Trp to water. The χ^2 angle of the Trp side chain remains invariant throughout the entire temperature range. Previous kinetic results indicated a single exponential decay in the 4-70 ºC temperature range, suggesting that Trp-cage behaves as a two-state folder. However, this mini-protein does not show clear two-state behavior in our steady state studies. Rather it shows a continuous distribution of steady state spectral parameters. Only the α-helix melting curve even hint of a cooperative transition. Possibly, the

previous kinetic results monitor only a small region of the Trp-cage which locally appears two-state. This would then argue for spatially decoupled folding even for this small peptide.

3.1 INTRODUCTION

The primary sequence of proteins encodes both the structure of the native and unfolded states, as well as the dynamics of the protein (un)folding processes. [1-16] Over the last 50 years significant efforts have been expended to elucidate the mechanisms of protein folding and unfolding. Part of this effort has examined the thermodynamic and kinetic behavior of small model systems such as the beta hairpins[17-19] and alanine based α-helices (AP). [1-33]

These systems display secondary structure motifs that change with temperature. These simple systems also avoid tertiary structural motifs that could complicate the conformational dynamics of these pure secondary structure motifs. The secondary structure unfolding of these small peptides, such as the alanine based α-helical peptides,[29] involve thermally driven conformational changes of isolated peptide molecules in water, which melt from an α-helical conformation to a PPII conformation.[33] This conformational change is a property of the isolated peptide molecule and does not involve any tertiary type interactions which may dominate (un)folding in larger proteins.

Numerous experimental and computational investigations have probed the thermodynamic and kinetic behavior of these simple model system.[21,24-27] Theoretical

simulations of folding/unfolding have provided the most detailed microscopic understanding of the peptide's folding energy landscape.[24,25] At the same time sophisticated kinetic measurements have examined the earliest steps in the pure secondary structure unfolding process.[21,22,25,31]

To extend our understanding of secondary structure conformational changes to the corresponding phenomena in proteins it is essential to understand the role of tertiary contacts. Obviously we should start this investigation by examining small model protein systems in order to elucidate the impact of defined tertiary contacts such as hydrogen bonding and hydrophobic contacts on the secondary structure evolution.

In this regard, in this study we used UV resonance Raman spectroscopy (UVRS) to study the temperature dependence of the conformation of a 20-residue long mini-protein, Trp-cage synthesized by Neidigh *et al*[30] which has the sequence N_1LYIQWLKDG$_{10}$GPSSGRPPPS. Trp-cage was created during a *de novo* peptide design effort, which resulted from a study of a poorly folded 39 residue long saliva protein of a Gila monster.[30] Using an iterative design effort with selective mutations and truncations, different protein variants were created and their folded states characterized using NMR and circular dichroism spectroscopy (CD). Trp-cage, originally referred to as Tc5b, showed the most structure, displaying a cage of hydrophobic residues surrounding the Trp side chain. Trp-cage was found to be 95% folded under physiological conditions.[30] Trp-cage, which consists entirely of natural amino acids appears to exhibit elements of tertiary structure even though it has no disulfide bridges, metal ion chelation motifs, or stabilization through oligomerization.[34] In addition, Trp-cage possesses a

hydrophobic core, which surrounds the Trp side chain and shields it from the aqueous environment.

The NMR and CD Trp-cage data of Neidigh *et al* suggested a simple two-state unfolding mechanism.[30] Qiu *et al* using the intrinsic fluorescence of Trp determined the folding time to be about 4 μs, which makes Trp-cage the fastest folding polypeptide possessing tertiary contacts.[32]

This is especially noteworthy since the fundamental speed limit on protein folding has been estimated to give rise to a folding time of ~(N/100) μs, where N is number of protein residues.[35-37] This would result in a theoretical folding speed limit for Trp-cage of ~0.2 μs, only 20 times faster than the experimentally determined folding time. This implies an almost optimized energy landscape for this peptide, where folding is largely dominated by free polymer diffusion.[32]

Several groups recently reported theoretical simulations of Trp-cage folding.[33,34,38-40] For example, Simmerling *et al*[33] in their all atom molecular dynamics simulation, presented a detailed molecular picture of Trp-Cage's folding dynamics. Their simulation calculated a native state topology consistent with the NMR structure of Neidigh *et al*[30]. Their simulation at 325 K, which modeled the folding of Trp-cage, found that the extended Trp-cage conformation converges to a native state topology within 20 ns. Snow *et al*[38] carried out stochastic dynamics simulations over a total modeled folding time of 100 μs and found that the unfolded state retains features similar to the native state topology.

In this work we used UV resonance Raman spectroscopy to examine the temperature dependence of the Trp-cage conformation. We studied the protein secondary structure by

exciting within the amide $\pi \rightarrow \pi^*$ transition with 204-nm excitation,[41] and used 229-nm excitation to excite within the aromatic ring $\pi \rightarrow \pi^*$ transitions to study the Trp[42] and Tyr[43,44] aromatic side chains. Our results indicate that Trp-cage's thermal unfolding is much more complex than suggested by previous studies.

3.2 EXPERIMENTAL

The UV resonance Raman (UVRR) spectrometer has been described in detail elsewhere.[45] Briefly, 204-nm UV light was obtained by generating the fifth anti-Stokes Raman harmonic of the 3rd harmonic of a Nd:YAG laser (Coherent, Infinity). The 229-nm excitation was produced by an intracavity frequency doubling of an Ar^+ laser (Coherent, FReD 400). The sample was circulated in a free surface, temperature controlled stream. A ~180° backscattering geometry was used for sampling. The collected light was dispersed by a double monochromator onto a back thinned CCD camera (Princeton Instruments-Spec 10 System).

Polyproline (M.W. 8900) and AcTrpEE (Trp monomer) were acquired from Sigma-Aldrich and used at 12 and 2 μM concentrations, respectively for UV absorption measurements. A solution of 112 μM polyproline, 50 μM Trp monomer, and 0.3 M ClO_4^- was used for the 229 nm excited UVRR temperature dependence measurements. The 21-residue long alanine based helical peptide, AP[25] was obtained from the Pittsburgh Peptide Synthesis Facility (PPSF, >95% purity) and used at 2 mg/ml concentrations for

determining the 204-nm Raman cross sections. 1 mg/ml concentrations of Trp-cage (PPSF, >95% purity) at pH 7 were used for the 204-nm excitation temperature dependence study, while 2 mg/ml concentration was used for the 229-nm excitation temperature dependence study. Previous work indicates there is no significant concentration dependence[30] of Trp-cage's conformation between 1 to 7 mg/ml at pH 7.

Spectra measured at 20 °C subsequent to the elevated temperature measurements were essentially identical to those prior to the temperature increase, indicating no significant sample photo- or thermal degradation or irreversible aggregation. Raman spectra were normalized relative to the peak height of the 932 cm^{-1} ClO_4^- band. 0.1 M perchlorate concentrations were used in the Trp-cage samples, whereas, 0.2 M concentrations were used for the AP peptide samples. The pH was adjusted by adding small aliquots of HCl or NaOH.

3.3 RESULTS AND DISCUSSION

3.3.1 204-nm Excitation Temperature Dependence

We examined the temperature dependence of Trp-Cage's backbone conformation by measuring 204-nm UV resonance Raman spectra between 4º and 70 ºC (Fig 3.1). The spectra show bands mainly arising from amide vibrations, with smaller contributions from the Trp and Tyr aromatic ring vibrations. The Amide I band (AmI) at ~1662 cm^{-1} is predominantly a C=O stretching vibration[46,47] and occurs as a shoulder on the intense

aromatic amino acid band at ~1620 cm^{-1}. The Amide II band (AmII) at 1564 cm^{-1} involves C-N stretching with some N-H bending. [46,47] The AmII' band of proline (AmII'p),[48-53] located at 1474 cm^{-1} is almost a pure C-N stretch, while the C_α-H bending band is located at 1386 cm^{-1}. The presence of the resonance enhanced C_α-H bending band has previously been correlated with the presence of non-helical peptide bond conformations.[54,55]

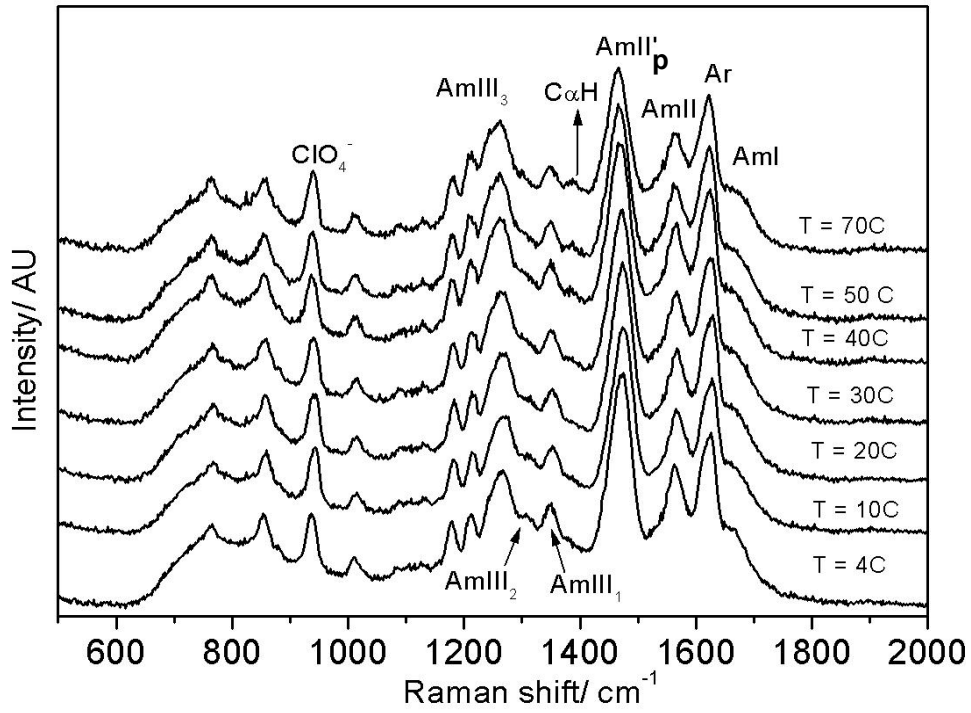

Figure 3.1: 204-nm UV resonance Raman spectra of Trp-Cage measured between 4º and 70 ºC. Three 5 min spectrum were summed and scaled to the intensity of 932 cm^{-1} perchlorate band. The bands arise mainly from amide vibrations except for a few which derive from aromatic side chain vibrations.

The Amide III region has recently been examined and reassigned.[56-60] Trp-cage shows the following bands in this region: the Amide III_3 band at 1264 cm^{-1} (predominantly C-N

stretching and N-H bending[47,54,59]), a shoulder at 1312 cm^{-1} ($AmIII_2$), and an $AmIII_1$ band at 1348 cm^{-1}.

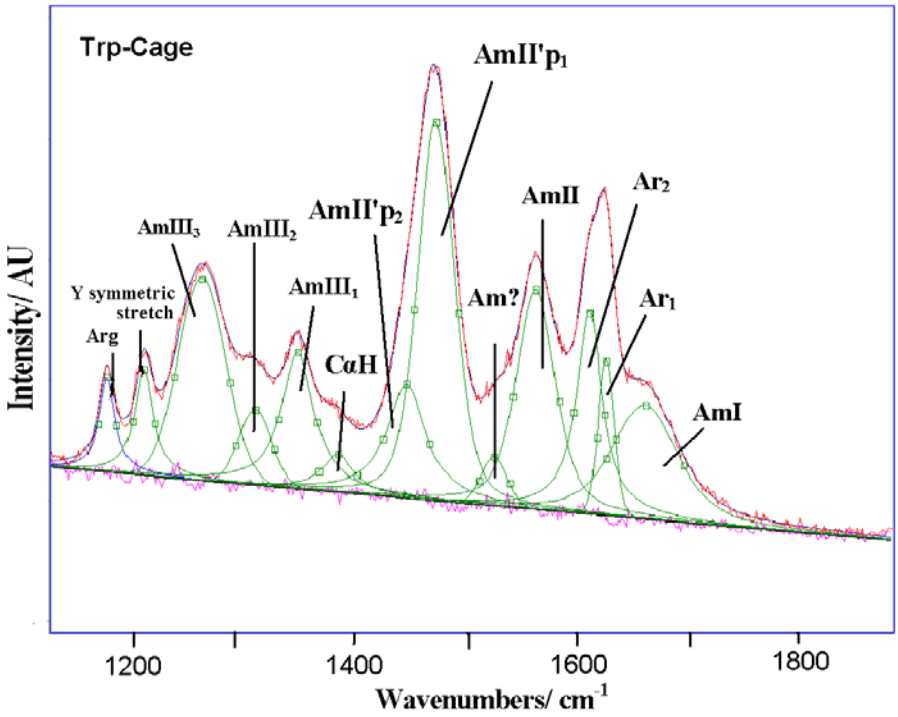

Figure 3.2: Spectral deconvolution of 4 ºC 204-nm UVRR Trp-cage spectra with Voight bands. The excellence of the fit is evident from the flat residual displayed underneath.

We deconvoluted these measured spectra into a sum of a minimum number of Voight bands by using the peak fitting routine in Grams software (Galactic Industries Corporation, Grams version 5). A typical example of such a fit is shown in Fig. 3.2 for the 4 °C 204-nm spectrum. The assignments and frequencies of the deconvoluted bands are listed in Table 3.1.

We observe numerous temperature-induced spectral changes. For example the AmII'p band frequency downshifts from 1474 to 1464 cm^{-1} as the temperature increases from 4

to 70 °C. Furthermore, we find that the $AmIII_3$ band monotonically downshifts from 1264 cm^{-1} at 4 °C to 1256 cm^{-1} at 70 °C. Previously, Lednev *et al*[41] observed a similar temperature dependence of the $AmIII_3$ band in AP peptide.[29,41] As shown in detail by Mikhonin *et al*[59] the $AmIII_3$ band shift results from the weakening of the peptide bond-water hydrogen bonding (N-H····O) at higher temperatures,[29] similar to that observed in *N*-methyl acetamide.[61-63] This is associated with the typical weakening of hydrogen bonding between the protein peptide bonds and the water environment which occurs as the temperature increases.[29]

Table 3.1: Band assignment of Trp-cage's spectra

Band	*Frequency (cm^{-1})*
Amide I	1662
Aromatic I	1627
Aromatic II	1611
Amide II	1564
Amide ?	1526
Amide II'p_1	1474
Amide II'p_2	1447
C_α-H	1386
Amide III_1	1348
Amide III_2	1312
Amide III_3	1264
Tyr (Y) sym stretch	1210
Arg side chain	1178

The difference spectrum between the 4 and 70 °C spectra shown in Fig 3.3 shows a decrease in the intensity of a triplet of bands in the AmIII region centered at ~1300 cm^{-1} which derives from the α-helical conformation.[41,59] The decrease in the intensity of the triplet indicates partial melting of the α-helices as the temperature is increased from 4º to 70 °C. The trough in the $C_\alpha H$[29,41,55] region at ~ 1386 cm^{-1} and the deep trough at ~ 1220 cm^{-1} for the $AmIII_3$ region further confirms the melting of α-helical residues to non-α-helical conformations.[29]

The difference spectra also indicate a 10 cm^{-1} downshift and a significantly decreased Raman intensity for the AmII'p band as the temperature is increased. This suggests either an environmental[64] or conformational[48] change for the proline amide bond(s). The frequency position of AmII'p has been thought to be indicative of *cis-trans* isomerization of the proline. Caswell and Spiro[48] reported that in polyproline, the AmII'p band downshifted from 1465 to 1435 cm^{-1} upon conversion of polyproline from the PPII (*trans*) to PPI (*cis*) conformation. It should, however, be noted that their conclusions were disputed by Harhay and Hudson,[52] who reported that at 200-nm excitation, simple X-Pro dipeptides did not show changes in their AmII'p band frequencies when their *cis* content was increased via a pH increase; furthermore, Harhay and Hudson[52] attributed the decreases in AmII'p band intensities to pH induced bathochromic shifts in the UV absorption.

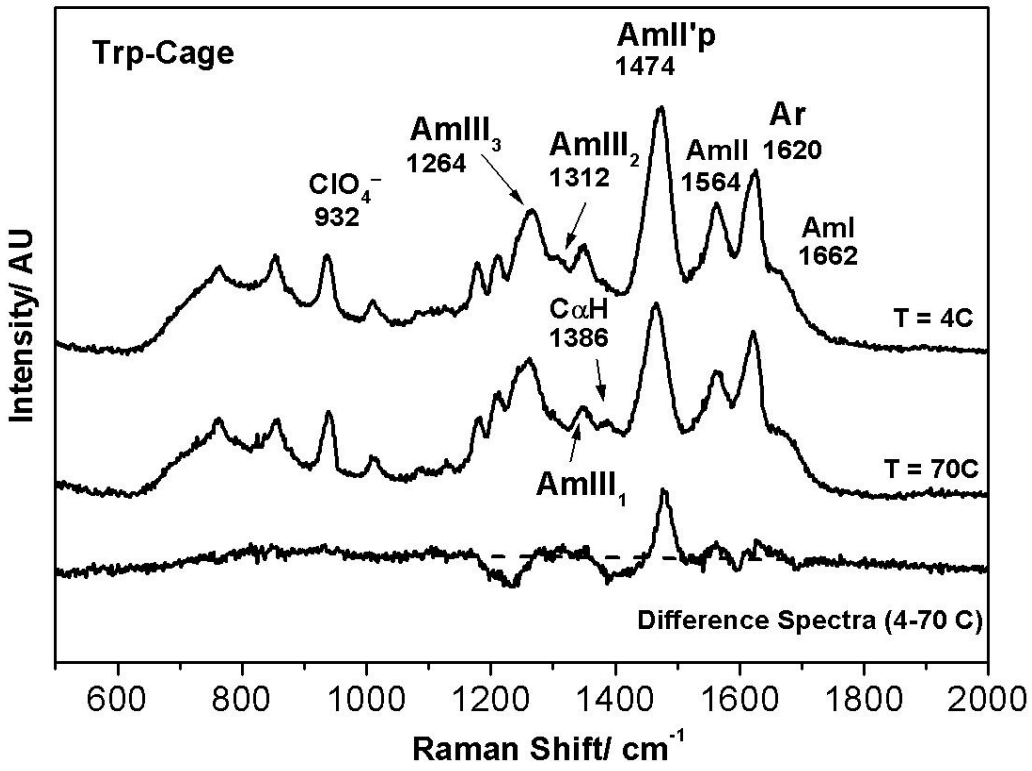

Figure 3.3: 204-nm UV resonance Raman spectra of Trp-cage at 4 and 70 ºC and their difference spectra. The difference spectra show a decrease in the intensity of a triplet in the AmIII frequency region indicating a loss of α-helix with increasing temperature. The intensity of the AmII' of Proline also decreases with increasing temperature.

An alternative interpretation of the AmII'p spectral frequency dependence was suggested by Takeuchi *et al* [64] who proposed that the observed shift in the band position could be due to differences in the hydrogen bonding environment of the proline. The authors reported that in aprotic solvents such as acetonitrile the AmII'p band is downshifted by 25-30 cm^{-1} as compared to aqueous solution, suggesting solvent-amide hydrogen bonding is primarily responsible for the observed changes in band position. In non-hydrogen bonding environments the AmII'p band occurs around 1440 cm^{-1} while

strong hydrogen bonding upshifts the band to 1480 cm^{-1}. [64] Their results would suggest that at 4 ºC the Trp-cage's prolines (1474 cm^{-1}) are strongly hydrogen bonded, while at higher temperatures the amide-water hydrogen bonds are weakened.

3.3.2 Proline-Trp Excitonic Interactions

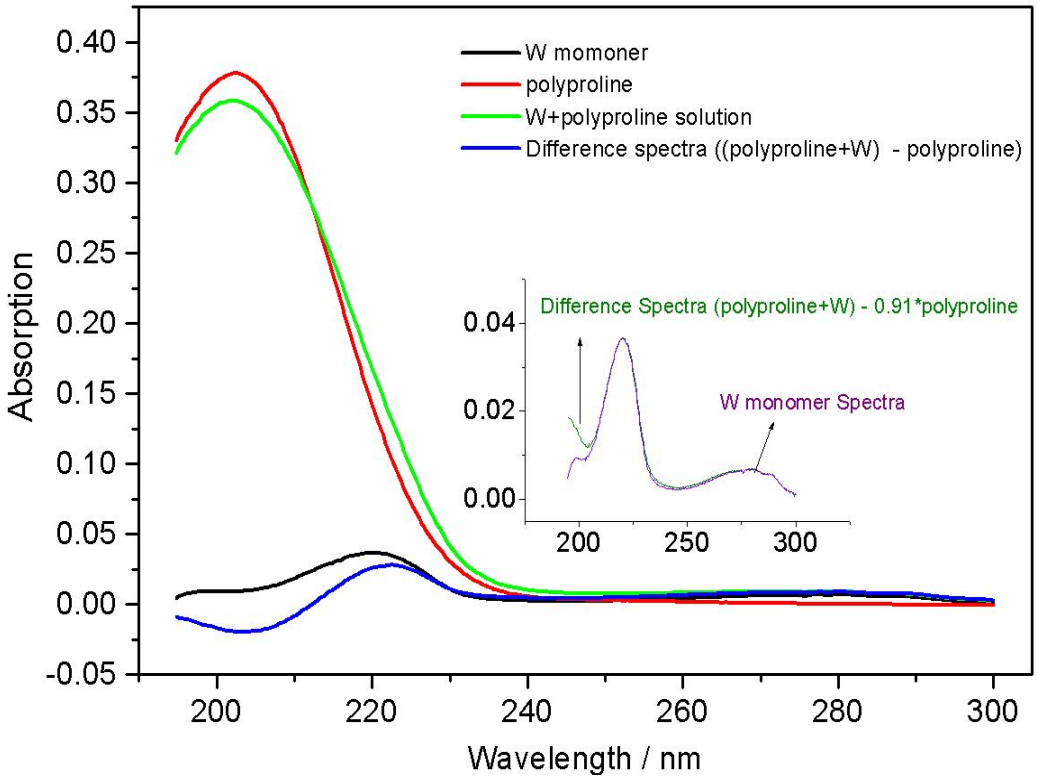

Figure 3.4: UV absorption spectra of Trp monomer (AcTrpEE), polyproline, and a solution of Trp (W) and polyproline, and the (Polyproline + Trp) – Trp difference spectrum. Insert shows Trp monomer spectra and difference spectra of (Polyproline +Trp) minus 0.91* Polyproline.

The decrease in the Raman intensity of the AmII'p appears to result from excitonic interactions between the Trp side chain and proline peptide bond. As shown by the Fig

3.4 absorption spectrum of solutions of polyproline, the addition of Trp monomer decreases the polyproline's 204-nm extinction coefficient by 6%. Presumably this hypochroism results from interactions between the $\pi \rightarrow \pi^*$ transition moments of the proline peptide bond and the $\pi \rightarrow \pi^*$ transition moments of the Trp aromatic ring.

We modeled the Trp-polyproline spectral changes by subtracting the absorption of polyproline from the Trp-polyproline mixture absorption spectrum. As shown in the Fig. 3.4 inset, a scaling of 0.91 for the subtracted polyproline spectrum allows us to recover the B_b absorption curve of Trp between ~204- and 229-nm (see below). The impact of excitonic interactions occurs mainly below 204-nm and appears to involve mainly the polyproline transition. It is clear from the inset difference spectrum that the ~220-nm B_b band of Trp is not affected by the excitonic interactions with proline.

We, thus, expect changes in the excitonic interaction to have no significant impact on the Trp band intensities (to the extent resonance enhancement is dominated by the Trp's B_b transition). The situation, however, is somewhat complex for 204-nm excitation Raman spectra since this excitation occurs on the blue edge of the B_b absorption, between the B_b and B_a electronic transitions.[42] This is a region where a minimum in intensities occurs and the excitation profile dispersion is small.[42] Thus, excitation in this region is expected to be somewhat insensitive to shifts in absorption bands. However, Sweeney and Asher[42] noted evidence for destructive interference for Trp intensities due to the contribution of the higher energy B_a transition. This would then lead to a dependence on absorbance changes for the B_a transition, which could be impacted by excitonic interactions with Pro. Although the situation appears complex, the best overall estimate would be that the Trp intensities excited at 204-nm will show less intensity dependencies

for change in excitonic interactions than would the proline Raman intensities. In addition, the intensities will be relatively insensitive to Trp B_b absorption band shifts.

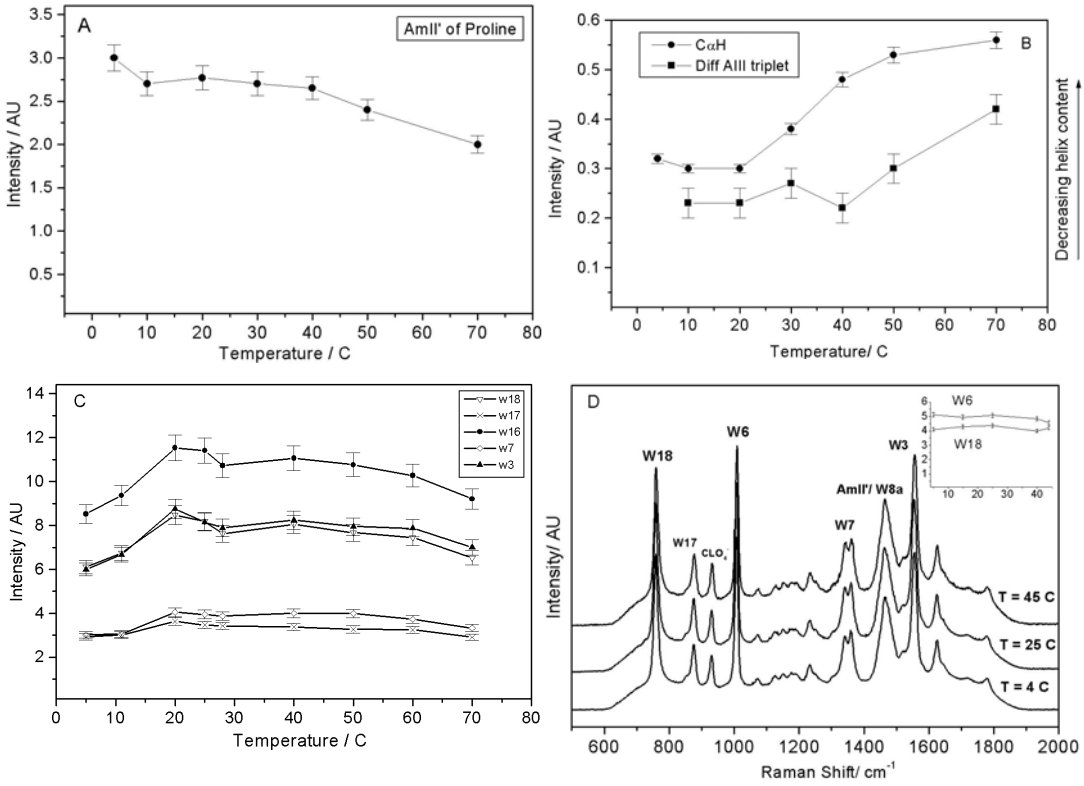

Figure 3.5: A) Temperature dependence of 204-nm excited Raman intensity of proline AmII' band. B) Temperature dependence of the C_α-H symmetric bending band intensity and the α-helical AmIII band triplet intensity. The triplet intensity is extracted from temperature difference spectrum. Increasing C_α-H and AmIII triplet intensities indicate loss of α-helicity at higher temperatures. C) Temperature dependence of the relative Raman intensities of different Trp bands: W18 (▼, 765 cm^{-1}), W17 (x, 884 cm^{-1}), W16 (•, 1014 cm^{-1}), W7 (◊, 1365 cm^{-1}), W3 (▲1558 cm^{-1}). D) 229 nm UV resonance Raman spectra of Trp monomers in polyproline solution at different temperatures. The spectra show bands arising form the resonance enhanced Trp along with AmII' of proline which overlaps with W8a band of Trp. Temperature dependence of W6 and W18 bands of Trp is displayed in the insert.

Fig 3.5A shows that the AmII'p band excited at 204-nm show a monotonic 33% intensity decrease as the temperature increases from 4º to 70 °C. These results indicate that a gradual conformational change occurs that causes hypochromism of the AmII'p band's intensities. This probably results from an increase in Trp-proline excitonic interactions either because the proline(s) and tryptophan become situated closer together or because of a change in the alignments of proline and Trp transition dipole moments.[65] Most likely the packing of prolines about the Trp becomes tighter as the temperature increases. As expected from the discussion above, for 204-nm excitation there are no intensity changes for the Trp Raman bands with temperature (not shown).

3.3.3 α-Helix Melting

Changes in the observed Raman intensity of the C_α-H bending and the $AmIII_3$ band result from decreases in the number of α-helical amide bonds as the temperature increases (Figs. 3.3 and 3.5). We can most easily estimate the change in the number of α-helical amide bonds from the increased intensity of the C_α-H bending band resonance Raman band, which only occurs in non α-helical conformations.[29,55] This band is well isolated in the spectra. A similar analysis using the decreased intensity of the AmIII bands is less reliable due to overlap of the AmIII bands from the folded and unfolded states.[59] Little α-helix melting occurs up until ~25 ºC and the melting curve shows a rough T_M at ~ 40 ºC.

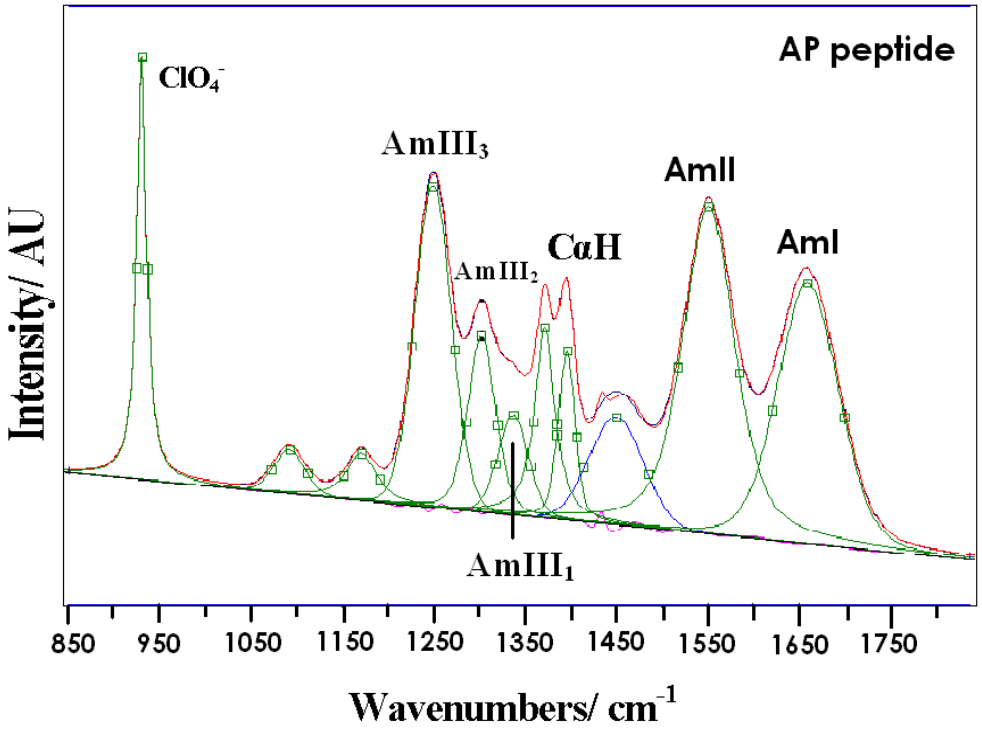

Figure 3.6: 204-nm UV resonance Raman spectrum of AP peptide at 60º C. The measured spectra are deconvoluted into a sum of Voight bands. At 60 ˚C AP is 95% PPII.

We can quantitate the change in the number of α-helical amide bonds by using the Raman cross sections of the C_α-H bending band from a 21-residue, alanine based, mostly α-helical peptide known as AP[41] (Fig 3.6); we are utilizing the assumption that the Trp-cage's unfolded segment C_α-H bending bands have Raman cross sections similar to those of the unfolded PPII conformation of AP.[29] This is a reasonable estimate since C_α-H bending bands have similar cross sections in the PPII and extended β-sheet strand conformations;[29,54,59] we expect similar coupling of C_α-H and N-H for peptide bonds with similar Ψ angles.[66]

AP is ~95% PPII at 60 ºC.[29] Thus, the 204-nm excited 60º C AP spectra are dominated by the PPII conformation, with only small contribution from the α-helical state. The 204 nm AP spectrum in Fig 6 shows a single AmI band at ~ 1660 cm^{-1}. The AmII band is located at ~1555 cm^{-1}, while the C_α-H_b appears as a Fermi doublet at 1370 and 1394 cm^{-1}. The $AmIII_3$ band is located at ~ 1250 cm^{-1}, the $AmIII_2$ band at 1304 cm^{-1}, while the $AmIII_1$ band is found at ~ 1336 cm^{-1}. The origins of the resonance enhanced amide III bands and PPII spectral markers have been extensively described by Mikhonin *et al*[59] and Asher *et al*.[29]

Using Dudik *et al*'s data[67] for the absolute Raman cross section of the 932 cm^{-1} band of perchlorate at 204 nm excitation, we calculated the Raman cross sections for AP:

$$\sigma_A = (I_A N_{ClO4^-} \sigma_{ClO4^-}) / (n_A N_{AP} I_{ClO4^-}) \qquad (1)$$

Where, σ_A and σ_{ClO4^-} are the Raman cross sections of an amide band and the 932 cm^{-1} perchlorate band, respectively. N_{ClO4^-} and N_{AP} are number of perchlorate and AP molecules in the scattering volume, respectively. I_{ClO4^-} is the perchlorate band (932 cm^{-1}) intensity, while I_A is the intensity of the amide band. n_A is the number of amide peptide bonds in AP which contribute to the intensity I_A of the concerned band. The calculated cross sections of AP amide bands are listed in Table 3.2.

Table 3.2: Amide cross sections of AP

Amide Band	*Band assignment of Trp-cage's spectra*
Amide II	17
Amide III_2	10
Amide III_3	20
C_α-H (1370 cm^{-1})	14
C_α-H (1394 cm^{-1})	12

Using the $C_\alpha H$ band cross sections we calculated the number of non-helical amide bonds in Trp-cage as:

$$n_A = (I_{C\alpha H}\, N_{ClO4^-}\, \sigma_{ClO4^-}) / (\sigma_{C\alpha H}\, N_P\, I_{ClO4^-}) \qquad (2)$$

Where, N_P is the number of molecules of Trp-cage in the scattering volume. We estimate that at 4 ºC Trp-cage has six, non-prolyl, non-glycine amide bonds in a non-helical, PPII conformation. Hence there are six non-prolyl, non-glycine amide bonds in an α-helical conformation. From the spectral intensity changes plotted in Fig 3.5B we can calculate the number of α-helix peptide bonds which melt as:

$$\delta n_A = (-\delta I_{C\alpha H}\, N_{ClO4^-}\, \sigma_{ClO4^-}) / (\sigma_{C\alpha H}\, N_P) \qquad (3)$$

Where δn_A is number of α-helical bonds lost or gained and $\delta I_{C\alpha H}$ is the change in normalized C_α-H bending band intensity. The 70% increase in the C_α-H bending band intensity suggests approximately four more amide bonds contribute to the C_α-H bending band intensity at 70 ºC then at temperatures below 30 ºC.

The observed decrease in the helical content is likely associated with a shift in the Trp-cage equilibrium towards non-native, non-helical states, rather then a shortening of the α-helices in their native conformation. We envision that Trp-cage flickers between native and unfolded conformations and that the intensity decrease results from a smaller duty cycle for the native state α-helix length; very short α-helices are inherently unstable.[41]

Our α-helix melting curve appears broader than the melting curve determined by Neidigh *et al*.[30] Their CD and NMR data suggested a cooperative melting of the helix, while our UVRR spectra show a broader α-helix melting curve with little or no helix melting at temperatures below ~25 ºC. The differences probably derive from the fact that their NMR data monitors the melting of both the amide backbone and the side chain conformations. In addition, Neidigh *et al's* CD data are confounded by contributions from the Trp side chain CD signals.[30] In contrast, our 204 nm excitation data reports directly on the melting of the α-helices.

3.3.4 Trp and Tyr water exposure

We examined the environment of the Trp and Tyr residues of Trp-cage by measuring the temperature dependence of the 229-nm UVRR spectra of Trp-cage between 4 and 70 °C (Figs. 3.5 and 3.7). The spectra are dominated by the in-plane aromatic ring vibrations of Trp and Tyr. The Trp bands appear at 766 (W18), 884 (W17), 1014 (W16), 1344 (W7), 1363 (W7) and 1558 cm^{-1} (W3), while those of Tyr are observed at 863 (Y Fermi resonance[49]) 1183 (Y9a), 1212 (Y7a), and 1627 cm^{-1} (Y8a). We do not observe any significant frequency shifts of the Trp and Tyr bands as the temperature increases. We

determined the Trp and Tyr relative Raman cross sections from the ratio of the peak heights of the Trp and Tyr bands relative to that of the 932 cm^{-1} ClO_4^- band.

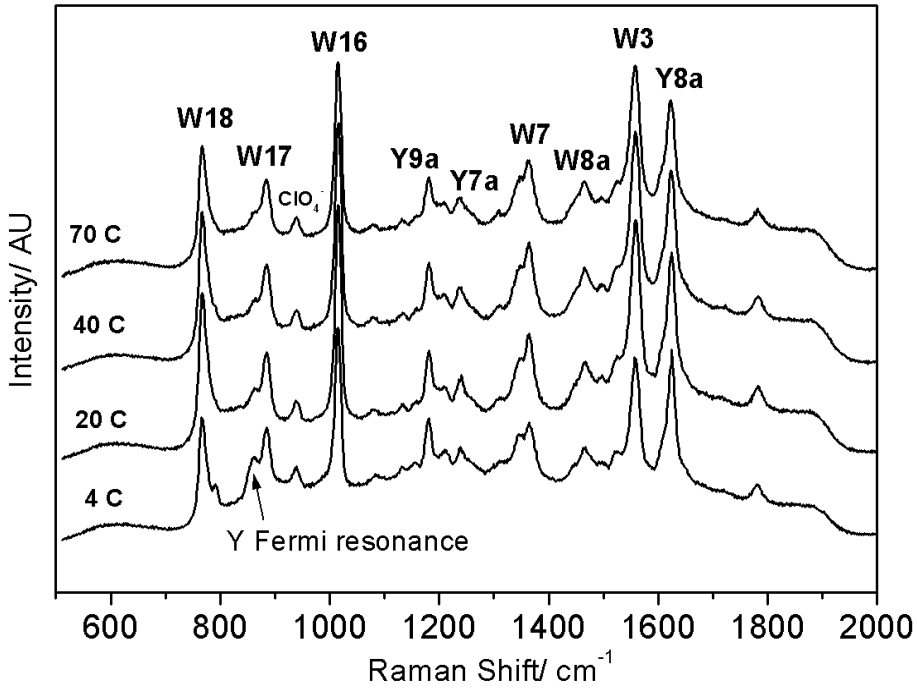

Figure 3.7: 229-nm UV resonance Raman spectra of Trp-Cage at different temperatures. Three spectra accumulated for ten minutes each were summed and normalized to the 932 cm^{-1} perchlorate band intensity. The spectra show bands arising form the resonance enhanced Trp and Tyr ring vibrations.

The Trp-cage Tyr intensities do not vary by more than 5% from 4º to 70 ºC. Boyden *et a* [68] previously reported that Tyr monomers in aqueous solutions show a cross section decrease with increasing temperature due to a temperature induced decrease in the molar absorptivity of the resonant 220-nm absorption band.[74] The lack of an observed monotonic decrease in the Tyr intensities indicates a compensating Trp-cage conformation induced intensity increase. However, we recently demonstrated that

interactions between Tyr and polyproline give rise to blue-shifts in the Tyr resonant 220-nm absorption band.[69] This suggests that these Tyr-proline excitonic interactions decrease as the temperature increases.

As shown in Fig. 5C, the relative Raman intensities of the Trp bands increase by ~35% as the temperature increases from 4 ^{o}C to 20 ^{o}C and then steadily decrease as temperature further increases to 70 ^{o}C. Boyden *et al* [68] showed that the Raman cross sections of monomeric Trp's in pure water do not show any appreciable temperature dependence. In contrast, we earlier demonstrated that the Raman cross sections of the Trp bands depend upon the exposure of the indole ring to water due to the blue shifting of the ~220-nm absorption band upon water exposure.[44] Since 229-nm excitation occurs on the red edge of the Raman excitation profiles, a blue shift in the absorption band decreases the 229 nm Raman cross sections.[44,68] This intensity dependence can thus be used to monitor the solvent exposure of Trp side chain by measuring changes in their relative Raman cross sections.[44,70]

Since, as discussed above, we expect no impact on the B_b transition from proline excitonic interactions we expect that the Trp 229-nm intensity changes primarily result from changes in solvent exposure. This is especially clear from the Fig. 3.5D 229-nm excited UV Raman spectrum of a sample containing Trp and polyproline which demonstrates a negligible Trp band temperature dependence.

The W17 band of Trp has been shown by Miura *et al*[71] to be sensitive to the hydrogen bonding of indole's N-H. If the N-H is free of hydrogen bonding the W17 appears at 883 cm^{-1}, while strong hydrogen bonding of the indole N-H, downshifts the band to 871 cm^{-1}.[71] At 4º C we observe the W17 band at 884 cm^{-1} which remains more or less

invariant as the Trp-cage is heated (Fig. 3.7). The band frequency suggests that the indole does not hydrogen bond within the temperature range examined here. Furthermore, a lack of hydrogen bonding is known to blue shift the Trp excitation profiles, thereby diminishing the 229-nm excited UVRR intensities.[72,73] This is consistent with our measured Trp Raman cross sections at 4 ºC which are lower than what would be expected even for a fully exposed Trp ring.

The temperature induced intensity increases to 20 ºC followed by the decrease suggests that the Trp initially becomes less exposed to water and then as the temperature further increases, its water exposure increases. This occurs in an environment where the Trp's N-H is incapable of hydrogen bonding. These changes are quite gradual with very broad transitions. The loss of exposure to water was also evident in the apparent increased excitonic interactions which resulted in a smaller AmII'p intensity at higher temperatures as discussed above.

The W7 band is a Fermi doublet with bands appearing at ~1360 and 1340 cm^{-1}. The ratio of 1360/1340 cm^{-1} band intensities, the R value is known to be indicative of hydrophobicity of the Trp's immediate environment. R values greater than one suggest a hydrophobic environment akin to that of aliphatic alkanes. A value of about one suggests an aromatic type environment, while values less than one suggest an aqueous environment.[74-78] At 4 ºC the R value is around 1.8 (±0.1) and remains more or less invariant as the temperature is increased, suggesting an invariant hydrophobic environment persists in Trp-cage at all temperatures.

Taken together the R-value analysis and the changes in the Trp band intensities tell us that the Trp ring is always in a hydrophobic environment which has a significant

solvent accessibility. The Trp N-H is not hydrogen bonded at any temperature. The minimum solvent accessibility occurs at ~20 °C. The solvent accessibility at 70 °C is less than that at 4 °C.

We also examined the W3 band of Trp side chain. The position of this band correlates with the absolute value of the χ^2 dihedral angle of the Trp side chain involving C_2-C_3-C_β-C_α linkage.[79] The W3 band is positioned at 1558 cm^{-1} at 4 ºC and does not vary to any significant degree as the temperature is increased. According to the data of Miura *et al* [79] the band position here suggests a $|\chi^2|$ angle of ~110º. The invariance of the χ^2 suggests that Trp's conformation does not vary to any significant extent as the temperature is increased. This demonstrates that the indole's geometry with respect to the linkage to the peptide backbone is constant.

3.4 CONCLUSIONS

Trp-cage was selectively probed using 204-nm and 229-nm UV Raman excitation. We observe a broad melting transition of the α-helix with no significant α-helix melting until ~30 ºC. On the average, four α-helical residues melt between 40–70 ºC. Most likely, at higher temperatures, the Trp-cage conformation flickers between a native and a non-native, non-helical state; The observed change in helicity is probably due to a smaller duty cycle for the native α-helix length.

The decreased proline intensities indicate a strengthening of proline(s)-Trp excitonic interactions with temperature indicating a more compact hydrophobic core. The 229-nm

Trp Raman intensity changes are not monotonic. They show a maximum at ~20 °C, which signals a minimum water exposure at this temperature. Thus, there is a unique structure at ~20 °C which appears to melt at higher and lower temperatures. According to the 229 nm Raman spectra the Trp (indole's N-H group) does not hydrogen bond at any temperature. Furthermore, the C_2-C_3-C_β-C_α (χ^2) dihedral angle appears constant over the 4-70 ºC temperature interval. These results taken together indicate that much of the Trp-cage's native state topology survives to higher temperatures, in agreement with the conclusions of Snow *et al*.[38]

Our results indicate that the thermal unfolding of Trp-cage involves at least two uncoupled steps involving an intermediate state (Fig. 3.8). The sequence of events leading to the unfolded/non-native state of Trp-cage is:

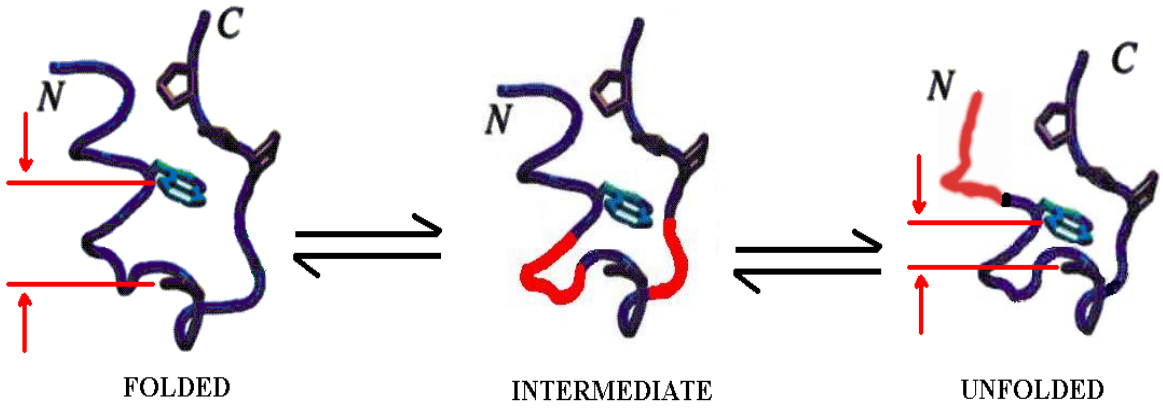

Figure 3.8: A schematic representation of Trp-cage's temperature dependent conformational changes.

- As the temperature is increased from 4-20 ºC, Trp-cage adopts a compact, intermediate conformation that better shields the Trp side chain from water.

- The 204-nm excited C_α-H bending band does not show any significant change in intensity, indicating no change in the α-helical content. The first unfolding step may involve conformational changes around the two, glycine rich, turn/mobile regions: residues 9-10 and 15-17 (shown red in Fig 3.8) to form a tight core around the Trp to better shield it from the aqueous environment.

- As the temperature is further increased from 20º to 70 ºC, the Trp intensities monotonically decrease, indicating an increased solvent exposure of the Trp ring. However, at 70 ºC the Trp intensity is still 6% greater then it was at 4 ºC, signifying that only a partial melting of the compact, intermediate state has occurred.
- The Tyr cross sections do not decrease with temperature. This suggests decreased excitonic interaction induced hypochromic shift, which suggest movement of Tyr away from the proline(s).
- During the same temperature interval the 204-nm excited AmII'p band undergoes a slow, monotonic, decrease in intensity indicating a gradual increase in the Trp-proline excitonic interactions.
- During this temperature increase from ~20-70 °C, the C_α-H bending band intensity increases indicating a loss of helicity with increasing temperature.

Thus, our results in the 30-70 ºC temperature interval indicate a more global conformational change which partially melts the α-helix, while the proline amide bond(s) of polyproline and/or the 3_{10} helix either align and/or brought closer to the Trp. The

partial melting of the α-helix may allow the proline-Trp complex to open more easily to the solvent.

It should be noted that at higher temperatures, Neidigh *et al*[30] noted increasingly negative chemical shift deviations for the δ3 proton of Pro_{12} and α3 of Gly_{11}. This result was rationalized by arguing that the residual high temperature hydrophobic cluster between Trp_6 and Pro_{12} placed these two protons further into the shielding region than their location in the native state.[30] This indicates that the Gly_{11}-, Pro_{12}-Trp_6 distances decrease with increasing temperature. The conclusion drawn from the NMR study agrees with our UV Raman study.

The UVRR data indicate that temperature dependence of the Trp-cage conformation involves a continuous conformational evolution with only partial helix melting at temperatures even as high as 70 ºC. A straightforward interpretation of these data is that Trp-cage melts from a 20 ºC maximally compact state to molten globule-like states at both higher and lower temperatures. Thus, we invoke cold denaturation of a maximally compact 20 ºC state.[80-82] These changes apparently derive from changes in the protein-water interactions.[81,83]

Qiu *et al*'s kinetic results found single exponential decay in the 4-70 ºC temperature range suggesting that Trp-cage behaves as a two-state folder.[35] However, this miniprotein does not show a clear two-state behavior in our steady state studies. Rather it shows a continuous distribution of steady state spectral parameters. Only the α-helix melting curve even hint of a cooperative transition. Possibly the previous kinetic results monitor only a small region of the Trp-cage which locally appears two-state. This would then argue for spatially decoupled folding even for this small peptide.

ACKNOWLEDGMENTS: The authors would like to thank Dr. Ivat Bahar, Dr. John Vires, Prof. A. E. Roitberg, and Prof. S. J. Hagen for helpful discussions and NIH grant 8 RO1 EB002053021 for financial support.

3.5 REFERENCES

(1) Anfinsen, C. B. *Science* **1973**, *181*, 223.
(2) Chan, H. S.; Dill, K. A. *Proteins: Struct. Funct. Genet.* **1998**, *30*, 2.
(3) Dill, K. A. *Biochemistry* **1990**, *29*, 7133.
(4) Jewett, A. I.; Pande, V. S.; Plaxco, K. W. *J. Mol. Biol.* **2003**, *326*, 247.
(5) Hardin, C.; Eastwood, M. P.; Prentiss, M.; Luthey-Schulten, Z.; Wolynes, P. G. *J. Comp. Chem.* **2002**, *23*, 138.
(6) Cleland, J. *Protein folding: in vivo and in vitro*; American Chemical Society: Washingon D. C., 1993.
(7) Dill, K. A.; Alonso, D. O. V.; Hutchinson, K. *Biochemistry* **1989**, *28*, 5439.
(8) Glaser, R. *Biophysics*; Springer: New York, 2000.
(9) Alm, E.; Baker, D. *Proc. Nat. Acad. Sci. U.S.A.* **1999**, *96*, 11305.
(10) Wolynes, P. G.; Onuchic, J. N.; Thirumalai, D. *Science* **1995**, *267*, 1619.
(11) Pappu, R. V.; Srinivasan, R.; Rose, G. D. *Proc. Natl. Acad. Sci. U.S.A.* **2000**, *97*, 12565.
(12) Myers, J. K.; Oas, T. G. *Annu. Rev. Biochem.* **2002**, *71*, 783.
(13) Shortle, D. *Curr. Opin. Struct. Biol.* **1993**, *3*, 66.
(14) Bryngelson, J. D.; Wolynes, P. G. *J. Phys. Chem.* **1989**, *93*, 6902.
(15) Hao, M.-H.; Scheraga Harold, A. *J. Phys. Chem.* **1994**, *98*, 9882.
(16) Dobson, C. M.; Salij, A.; Karplus, M. *Angew. Chem. Int. Ed. Engl.* **1998**, *37*, 868.
(17) Eaton, W. A.; Munoz, V.; Thompson, P. A.; Henry, E. R.; Hofrichter, J. *Acc. Chem. Res.* **1998**, *31*, 745.
(18) Munoz, V.; Henry, E. R.; Hofrichter, J.; Eaton, W. A. *PNAS* **1998**, *95*, 5872.
(19) Dinner, A. R.; Lazaridis, T.; Karplus, M. *PNAS* **1999**, *96*, 9068.
(20) Munoz, V.; Thompson, P. A.; Hofrichter, J.; Eaton, W. A. *Nature* **1997**, *390*, 196.
(21) Thompson, P. A.; Eaton, W. A.; Hofrichter, J. *Biochemistry* **1997**, *30*, 9200.
(22) Bolin, K. A.; Pitkeathly, M.; Miranker, A.; Smith, L. J.; Dobson, C. M. *J. Mol. Biol.* **1996**, *261*, 443.
(23) Garcia, A. E.; Sanbonmatsu, K. Y. *Proc. Nat. Acad. Sci. U.S.A.* **2002**, *99*, 2782.
(24) Andrew, C. D.; Warwicker, J.; Jones, G. R.; Doig, A. J. *Biochemistry* **2002**, *41*, 1897.
(25) Lednev, I. K.; Karnoup, A. S.; Sparrow, M. C.; Asher, S. A. *J. Am. Chem. Soc.* **2001**, *123*, 2388.
(26) Woutersen, S.; Hamm, P. *J. Chem. Phys.* **2001**, *114*, 2727.
(27) Clarke, D. T.; Doig, A. J.; Stapley, B. J.; Jones, G. R. *Proc. Nat. Acad. Sci. U.S.A.* **1999**, *96*, 7232.
(28) Williams, S.; Causgrove, T. P.; Gilmanshin, R.; Fang, K. S.; Callender, R. H.; Woodruff, W. H.; Dyer, R. B. *Biochemistry* **1996**, *35*, 691.

(29) Asher, S. A.; Mikhonin, A. V.; Bykov, S. V. *J. Am. Chem. Soc.* **2004**, *126*, 8433.
(30) Neidigh, J. W.; Fesinmeyer, R. M.; Andersen, N. H. *Nature Structural Biology* **2002**, *9*, 425.
(31) Gellman, S. H.; Woolfson, D. N. *Nature Structural Biology* **2002**, *9*, 408.
(32) Qiu, L.; Pabit, S. A.; Roitberg, A. E.; Hagen, S. J. *Journal of the American Chemical Society* **2002**, *124*, 12952.
(33) Simmerling, C.; Strockbine, B.; Roitberg, A. E. *Journal of the American Chemical Society* **2002**, *124*, 11258.
(34) Chowdhury, S.; Lee, M. C.; Xiong, G.; Duan, Y. *J. Mol. Biol.* **2003**, *327*, 711.
(35) Hagen, S. J.; Hofrichter, L.; Szabo, A.; Eaton, W. A. *Proc. Nat. Acad. Sci. U.S.A.* **1996**, *93*, 11615.
(36) Pascher, T.; Chesick, J. P.; Winkler, J. R.; Gray, H. B. *Science* **1996**, *27*, 1558.
(37) Kubelka, J.; Hofrichter, J.; Eaton, W. A. *Current Opinion in Structural Biology* **2004**, *14*, 76.
(38) Snow, C. D.; Zagrovic, B.; Pande, V. S. *J. Am. Chem. Soc.* **2002**, *124*, 14548.
(39) Zhou, R. *Proceedings of the National Academy of Sciences of the United States of America* **2003**, *100*, 13280.
(40) Chowdhury, S.; Lee, M. C.; Xiong, G.; Duan, Y. *J. Phys. Chem. B* **2004**, *108*, 13855.
(41) Lednev, I. K.; Karnoup, A. S.; Sparrow, M. C.; Asher, S. A. *J. Am. Chem. Soc.* **1999**, *121*, 8074.
(42) Sweeney, J. A.; Asher, S. A. *Journal of Physical Chemistry* **1990**, *94*, 4784.
(43) Ludwig, M.; Asher, S. A. *Journal of the American Chemical Society* **1988**, *110*, 1005.
(44) Chi, Z.; Asher, S. A. *Journal of Physical Chemistry B* **1998**, *102*, 9595.
(45) Bykov, S. B.; Lednev, I. K.; Ianoul, A.; Mikhonin, A. V.; Asher, S. A. *Appl. Spectrosc.* **2005**, *59*, 1541.
(46) Chi, Z.; Asher, S. A. *Biochemistry* **1998**, *37*, 2865.

(47) Mirkin, N. G.; Krimm, S. *Journal of Molecular Structure* **1996**, *377*, 219.
(48) Caswell, D. S.; Spiro, T. G. *Journal of the American Chemical Society* **1987**, *109*, 2796.
(49) Rippon, W. B.; Koeing, J. L.; Walton, A. G. *J. Am. Chem. Soc.* **1970**, *92*, 7455.
(50) Mayne, L.; Hudson, B. *J. Phys. Chem.* **1987**, *91*, 4438.
(51) Dorman, D. E.; Torchia, D. A.; Bovey, F. A. *Macromolecules* **1973**, *6*, 80.
(52) Harhay, G. P.; Hudson, B. S. *J. Phys. Chem.* **1991**, *95*, 3511.
(53) Swenson, C. A. *Biopolymers* **1971**, *10*, 2591.
(54) Chi, Z.; Chen, X. G.; Holtz, J. S. W.; Asher, S. A. *Biochemistry* **1998**, *37*, 2854.
(55) Wang, Y.; Purrello, R.; Jordan, T.; Spiro, T. G. *Journal of the American Chemical Society* **1991**, *113*, 6359.
(56) Diem, M.; Lee, O.; Roberts, G. M. *J. Phys. Chem.* **1992**, *96*, 548.
(57) Lee, S.-H.; Krimm, S. *Biopolymers* **1998**, *46*, 283.
(58) Lee, S.-H.; Krimm, S. *J. Raman Spectrosc.* **1998**, *29*, 73.
(59) Mikhonin, A. V.; Ahmed, Z.; Ianoul, A.; Asher., S. A. *J. Phys. Chem. B* **2004**, *108*, 19020.

(60) Overman, S. A.; Thomas, G. J., Jr. *Biochemistry* **1998**, *37*, 5654.
(61) Torri, H. *J. Phys. Chem. A* **2004**, *108*, 7272.
(62) Besley, N. A.; Oakley, M. T.; Cowan, A. J.; Hirst, J. D. *J. Am. Chem. Soc.* **2004**, *126*, 13502.
(63) Triggs, N. E.; Valentini, J. J. *J. Phys. Chem* **1992**, *96*, 6922.
(64) Takeuchi, H.; Harada, I. *Journal of Raman Spectroscopy* **1990**, *21*, 509.
(65) Cantor, C. R.; R., S. P. *Biophysical Chemistry*; Freeman and Company: San Francisco, USA, 1980; Vol. 1.
(66) Asher, S. A.; Ianoul, A.; Mix, G.; Boyden, M. N.; Karnoup, A.; Diem, M.; Schweitzer-Stenner, R. *J. Am. Chem. Soc.* **2001**, *123*, 11775.
(67) Dudik, J. M.; Johnson, C. R.; Asher, S. A. *Journal of Chemical Physics* **1985**, *82*, 1732.
(68) Boyden, M. N.; Asher, S. A. *Biochemistry* **2001**, *40*, 13723.
(69) Ahmed, Z.; Myshakina, N. S.; Asher, S. A. *In Preparation* **2006**.
(70) Chi, Z.; Asher, S. A. *Biochemistry* **1999**, *38*, 8196.
(71) Miura, T.; Thomas, G. J., Jr. *Subcell. Biochem.* **1995**, *24*, 55.
(72) Rodgers, K. R.; Su, C.; Subramaniam, S.; Spiro, T. G. *J. Am. Chem. Soc.* **1992**, *114*, 3697.
(73) Mukerji, I.; Spiro, T. G. *Biochemistry* **1994**, *33*, 13132.
(74) Harada, I.; Miura, T.; Takeuchi, H. *Spectrochim. Acta A: Mol. Spectrosc.* **1986**, *42A*, 307.
(75) Hideo, I.; Nemoto, Y.; Harada, I. *Biochemistry* **1990**, *29*, 1572.
(76) Kochendoerfer, G. G.; Kaminaka, S.; Mathies, R. A. *Biochemistry* **1997**, *36*, 13153.
(77) Hashimoto, S.; Obata, K.; Takeuchi, H.; Needleman, R.; Lanyi, J. K. *Biochemistry* **1997**, *36*, 11583.
(78) Miura, T.; Takeuchi, H.; Harada, I. *Biochemistry* **1988**, *27*, 88.
(79) Miura, T.; Takeuchi, H.; Harada, I. *J. Raman Spectrosc.* **1989**, *20*, 667.
(80) Andersen, N. H.; Cort, J. R.; Liu, Z.; Sjoberg, S. J.; Tong, H. *Journal of the American Chemical Society* **1996**, *118*, 10309.
(81) Privalov, P. L. *Critical Reviews in Biochemistry and Molecular Biology* **1990**, *25*, 281.
(82) Privalov, P. L.; Griko, Y. V.; Venyaminov, S. Y.; Kutyshenko, V. P. *Journal of Molecular Biology* **1986**, *190*, 487.
(83) Urry, D. W. *Journal of Physical Chemistry B* **1997**, *101*, 11007.

CHAPTER 4

UV-Resonance Raman Investigation of a 3_{10} Helical Peptide Reveals a Rough Energy Landscape

This Chapter was published in *Biochemistry* 2006, 45(30), 9068-9073. The co-authors are Zeeshan Ahmed and Sanford A. Asher

4.0 UV-RESONANCE RAMAN INVESTIGATION OF A 3_{10} HELICAL PEPTIDE REVEALS A ROUGH ENERGY LANDSCAPE

We used UVRRS at 194- and 204-nm excitation to examine the backbone conformation of a 13-residue polypeptide ($gp41_{659-671}$) that has been shown by NMR to predominantly fold into a 3_{10}-helix. Examination of the conformation sensitive $AmIII_3$ region indicates the peptide has significant populations of β-turn, PPII, 3_{10}-, and π-helix like conformations but little α-helix. We estimate that at 1 ºC on average six of the twelve peptide bonds are in folded conformations (predominantly 3_{10}-, and π-helix) while the other six are in unfolded (β-turn/PPII) conformations. The folded and unfolded populations do not change significantly as the temperature is increased from 1 ºC to 60 ºC, suggesting a unique energy landscape where the folded and unfolded conformations are essentially degenerate in energy and show identical temperature dependence.

4.1 INTRODUCTION

An understanding of the mechanisms of protein folding will enable the *de novo* design of proteins with profound commercial and medical applications.[1-19] Over the last 50 years, significant efforts have been expended to elucidate protein folding and unfolding mechanisms. Part of this effort has examined the thermodynamic and kinetics of small model systems such as beta hairpins [20-22] and alanine based α-helices. [23-33] These studies have provided detailed microscopic knowledge of the folding energy landscape of these isolated motifs. Theoretical simulations have suggested that 3_{10}-helices and/or type III β-turns may serve as intermediates in the α-helix folding pathway.[34-39] The formation of kinetic intermediates such as β-turn or 3_{10} helix lowers the entropic cost of nucleating the first helical residue, thus facilitating the helix folding transition.[34,40,41]

The 3_{10}-helix is the fourth most common secondary structural motif in proteins.[34-59] On average, in proteins, three to four percent of peptide residues occur in a 3_{10}-helix conformation.[48] The 3_{10}-helix differs from an α-helix in that the tighter packing of the backbone forces the C=O···H-N hydrogen bonds to point outwards, away from the helical axis resulting in decreased stability of the 3_{10}-helix as compared to the α-helix.[25,48]

Recent ESR [39,42] and NMR [43] work by Millhauser *et al* [41] suggests the presence of 3_{10}-helix at the terminus of short alanine based helical peptides. The authors proposed that 3_{10} helices are a relic of the folding process. They reasoned that nascent helices contain mixtures of unfolded and turn conformations, specifically type III turns. As folding

conditions begin to favor helical structures, the type III turn conformation (a single 3_{10}-helix unit) propagates i.e. the chain adopts a 3_{10}-helix conformation. As the helical domain lengthens the α-helix conformation competes with the 3_{10}-helix conformation. Finally, at longer helical lengths the α-helix conformation dominates. Some 3_{10}-helix/type III turn like conformations may survive at the termini.[41]

It should be noted that Millhauser's results have been disputed by Smythe *et al* [44] who argued that the rotational diffusion of the flexible labels used in Milhauser *et al*'s [41] ESR study confounded spectral interpretation. Using Toac residues as ESR labels, Smythe et al found no evidence for a significant 3_{10}-helix population in a 17-residue, alanine based helical peptide.[44]

The inability to characterize simple monomeric 3_{10}-helices is a major stumbling block in advancing our understanding of the α-helix (un)folding process; furthermore, the lack of such a model system has made unambiguous identification of a 3_{10}-helix spectroscopic markers difficult. Schievano *et al* [45] recently reported the first water soluble 3_{10}-helix; however, this particular peptide consisted of unnatural amino acids. Unfortunately, the conformation dynamics of peptides with unnatural amino acids may be irrelevant to the study of biological problems. In this context, Biron *et al*'s recent discovery of an all natural amino acid tridecapeptide, $gp41_{659\text{-}671}$ [48] that folds into a 3_{10}-helix is of great significance since it enables the study of 3_{10} helices.

$gp41_{659\text{-}671}$ is a thirteen-residue peptide of the sequence E_{659}LLELDKWAS$_{669}$LWN extracted from the glycoprotein gp41 of HIV-1 virus, corresponding to residues 659-671. NOE constraints indicate that in water at 277 K, the monomeric form of the peptide folds into a nine residue long 3_{10}-helix.[48] Biron *et al* proposed that the 3_{10}-helix is stabilized by

favorable hydrophobic stacking interactions between L663, W666, L669 and W670.[48] Residues E662, K665, S668, and N671 form the polar face where E662 and K665 may engage in weak electrostatic interactions. Burial of considerable hydrophobic surface area is proposed to favor the 3_{10} helix over the α-helix conformation.[48]

In this work, we used UV resonance Raman spectroscopy to examine $gp41_{659\text{-}671}$'s conformation. We studied the peptide secondary structure by exciting within the amide $\pi \rightarrow \pi^*$ transition with 204 nm and 194 nm excitation. Our results indicate that the 3_{10} helix is in equilibrium with multiple secondary structures, namely the π-helix, β-turns and PPII conformation, creating an energy landscape where the folded and unfolded conformations are essentially degenerate in energy and show identical temperature dependence.

4.2 EXPERIMENTAL

The UV resonance Raman spectrometer has been described in detail elsewhere.[60] Briefly, 204 nm UV light was generated by generation of the fifth anti-Stokes Raman harmonic of the 3rd harmonic of a Nd:YAG laser (Coherent, Infinity). The 194 nm deep UV light was generated as the (3ω+ω) fourth harmonic of a diode pumped Ti:Sapphire laser (Positive Light, Indigo-S). The sample was circulated in a free surface, temperature controlled stream. A 135° backscattering geometry was used for sampling. The collected light was dispersed by a subtractive double monochromator onto a back thinned CCD camera (Princeton Instruments-Spec 10).

The $gp41_{659-671}$ peptide was obtained from the Pittsburgh Peptide Synthesis Facility (>95% purity) and used at 1 mg/ml concentrations, at pH 7. UVRR spectra measured at 20 °C during and after the Raman measurements were essentially identical, indicating the lack of significant photo and/or thermal degradation. Raman spectra were normalized relative to the peak height of the 932 cm^{-1} ClO_4^- band. 0.05 and 0.1 M concentrations of ClO_4^- were used for the 204- and 194-nm excited UVRR measurements. Helix promoter TFE was acquired form Aldrich. Solution pH was adjusted by adding small aliquots of dilute HCl or NaOH. CD measurements were carried out on a JASCO 710 spectrometer using 0.3 mg/ml peptide concentration.

4.3 RESULTS AND DISCUSSION

4.3.1 204 nm excitation temperature dependence

The 204 nm excitation Raman spectra (Fig 4.1) show bands arising from amide and to a lesser extent Trp vibrations. In order to facilitate spectral interpretation we subtracted the Trp contribution from the temperature dependent 204-nm excited $gp41_{659-671}$ spectra (Fig 4.2). The band intensities of the resulting spectra were normalized with respect to the AmI band intensity. The spectra show an AmI vibration at 1668 cm^{-1} which is predominantly a C=O stretching vibration.[61,62] The 1556 cm^{-1} molecular oxygen stretching band [32,63] overlaps with the 1558 cm^{-1} AmII band. The AmII vibration involves C-N stretching with some N-H bending.[61,62] The trough in the 1420-1500 cm^{-1}

region is due to the 1483 cm^{-1} COO^- stretching band from the Trp monomer which was subtracted from the original peptide spectra.[64,65]

A weak 1355 cm^{-1} band ($AmIII_1$/residual W7) appears as a shoulder on the 1390 cm^{-1} C_α-H bending band. The C_α-H bending band intensity derives from non α-helical peptide bond conformations.[61,66]

A weak $AmIII_2$ band is located at ~1320 cm^{-1}. A broad $AmIII_3$ band (predominantly C-N_s and N-H_b mode [61,66-69]) at 1257 cm^{-1} shows additional features at 1293 and 1226 cm^{-1}. Mikhonin *et al* [70] recently demonstrated that the "pure" α-helix UVRR spectra show a narrow $AmIII_3$ band centered at 1260 cm^{-1} (Fig 4.2). The presence of a broad $AmIII_3$ band here indicates the existence of multiple conformations in $gp41_{659-671}$.

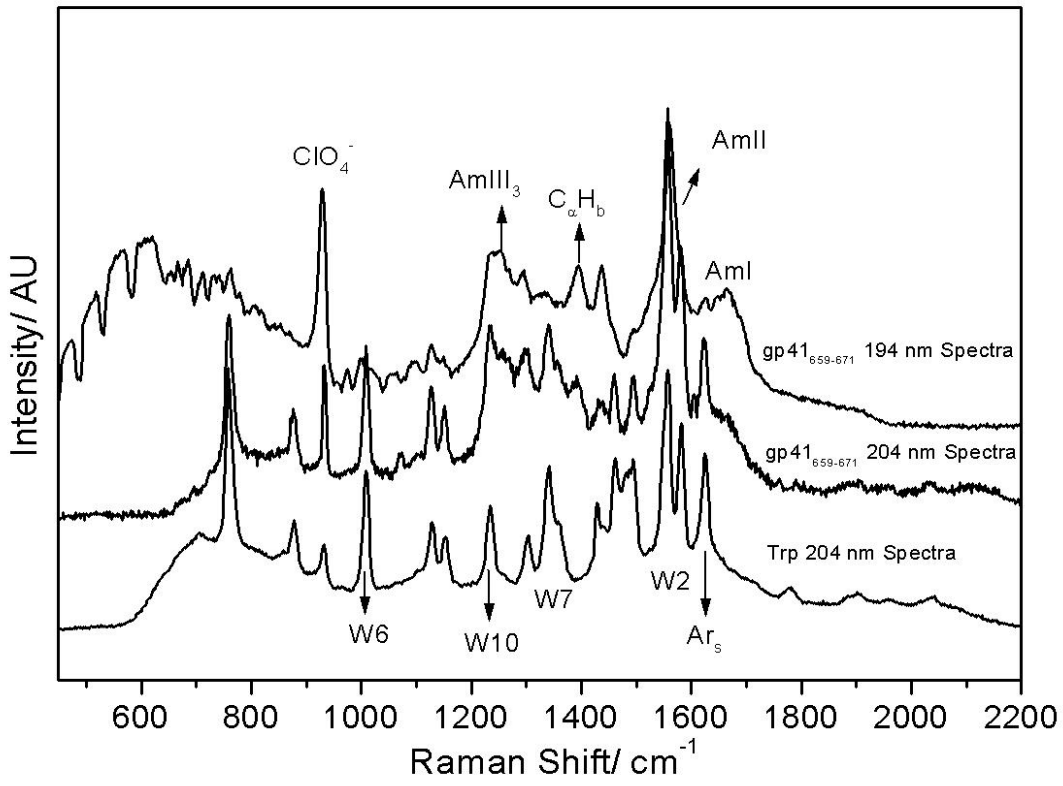

Figure 4.1: 204- and 194-nm UV resonance Raman spectra of $gp41_{659-671}$ measured at 1 ºC. Also displayed are the 204-nm excitation UVRR spectra of Trp monomer, where the 1483 cm^{-1} carboxylate stretching band overlaps with the W4 and W5 bands of Trp. As compared to 204-nm, the 194-nm excited $gp41_{659-671}$ spectra shows considerably less Trp spectral contribution. The decreased Trp contribution allows us to resolve amide bands from overlapping Trp bands.

As the solution temperature is increased from 1 ºC to 30 ºC, the 1390 cm^{-1} C_α-H_b and the $AmIII_3$ bands show a slight decrease in intensity (Fig 4.2). A similar temperature induced intensity decrease was previously observed for a water exposed, PPII peptide whose conformation was temperature independent.[24,67] The lack of conformation induced changes in the $AmIII_3$ and C_α-H_b region suggest that $gp41_{659\text{-}671}$ does not undergo a thermally induced helix melting transition between 1 ºC and 30 ºC.

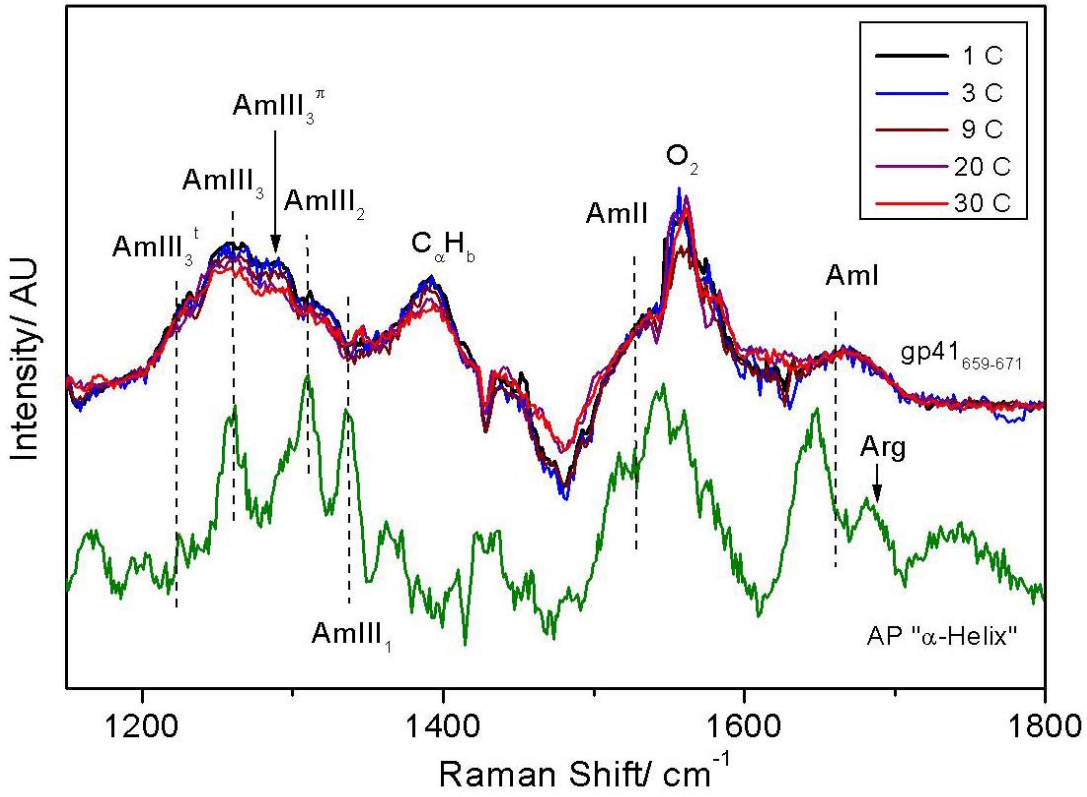

Figure 4.2: Upper traces are 204-nm UV-resonance Raman spectra of $gp41_{659\text{-}671}$ measured between 1 ºC and 30 ºC. In order to facilitate spectral interpretation the Trp contribution was subtracted. The resulting spectra show resonance enhanced amide vibrations. Below, the green trace shows the 204-nm excited pure α-helix spectra of AP peptide (adapted from ref 70) which shows its characteristic narrow $AmIII_3$ band at 1260 cm^{-1}.

We can quantitate the number of helical amide bonds by using the Raman cross section of the C_α-H bending band from a 21-residue, alanine based, mostly α-helical peptide known as AP [24]; we are utilizing the assumption that the $gp41_{659\text{-}671}$'s unfolded segment C_α-H bending bands have Raman cross sections similar to those of the unfolded/PPII conformation of AP. This is a reasonable estimate since C_α-H_b bands have similar cross sections in the PPII and extended β-sheet strand conformations [61]; we expect similar coupling between C_α-H_b and N-H_b for peptide bonds with similar Ψ angles,[69] Since the α-helix and the 3_{10}-helix conformations have similar Ψ angles, [45] we assume that as in the α-helix, the putative 3_{10}-helix will show a negligible C_α-H band intensity. Thus we use the C_α-H band intensity to estimate the number of bonds in PPII conformation. Based on the C_α-H band cross sections of the alanine based, mainly α-helical peptide AP (see ref 19), we calculate the number of non helical amide bonds in $gp41_{659\text{-}671}$ as:

$$n_A = (I_{C\alpha H}\, N_{ClO4^-} - \sigma_{ClO4^-}) / (\sigma_{C\alpha H}\, N_P\, I_{ClO4^-}) \qquad (1)$$

Where, $\sigma_{C\alpha H}$ and σ_{ClO4^-} are the Raman cross sections of the C_α-H band and the 932 cm^{-1} perchlorate band, respectively. N_{ClO4^-} and N_P are number of perchlorate and $gp41_{659\text{-}671}$ molecules in the scattering volume, respectively. I_{ClO4^-} is the perchlorate band (932 cm^{-1}) intensity, while $I_{C\alpha H}$ is the intensity of the C_α-H band. n_A is the number of amide peptide bonds in $gp41_{659\text{-}671}$ which contribute to the intensity $I_{C\alpha H.}$ We calculate that at 1 ºC six of 12 peptide bonds are in a PPII-like conformation while six peptide bonds adopt α-helix like conformations.

As noted above, $gp41_{659\text{-}671}$ does not show a temperature dependent decrease in helicity. The observed behavior can be rationalized by requiring the folded and unfolded

state ensembles to be nearly degenerate in energy and equally disordered i.e. the number of conformations comprising the folded and unfolded state are nearly equal. Under such circumstances the peptide has an equal probability of populating either helix or unfolded state, and as such their relative population distribution would not be impacted by increasing temperature. These results are consistent with Biron *et al*'s study that reported a lack of 3_{10}-helix melting with increasing temperature.[48]

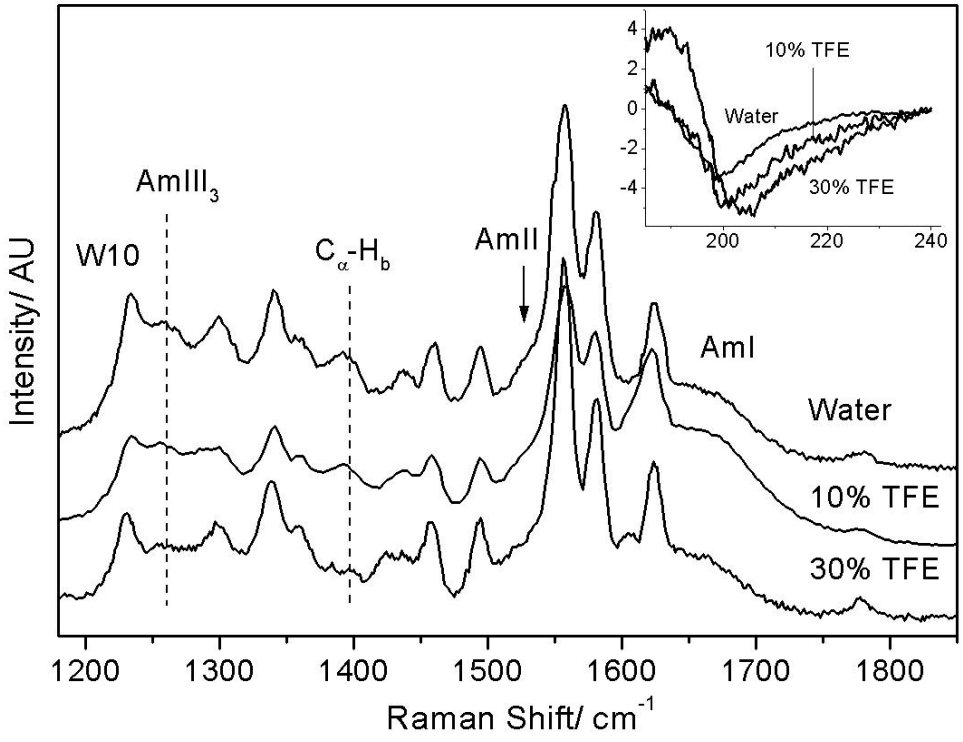

Figure 4.3: 204-nm UV-resonance Raman spectra of $gp41_{659-671}$ in pure water, 10 % and 30% v/v TFE concentration at 1 ºC. The TFE contribution has been subtracted from the spectra. The resulting spectra show bands arising from amide and Trp vibrations. In 10% TFE the presence of C_α-H_b band indicates ~55% helicity, whereas in 30% TFE the C_α-H_b band shows negligible band intensity indicating a 92% helical content. Insert shows CD spectra of $gp41_{659-671}$ in water, 10% and 30% v/v TFE solutions. As discussed in the text these CD spectra show the peptide's 3_{10}-helix content increases with TFE concentration.

The $gp41_{659-671}$ peptide, however, does show a conformation change in TFE-water solutions (Fig 3). Manning and Woody [71] proposed that the CD spectra of 3_{10}- and α-helix should show different values of $R = \Theta_{222}/\Theta_{207}$. The 3_{10}-helix is expected to show a lower R-value (R~0.3) as compared to the α-helix (R ~1). Additionally, the 3_{10}-helix is expected to show a weak positive band at ~195-nm, while the α-helix shows a relatively strong positive band at ~195-nm.[59,71] As shown in Fig 4.3 (inset), the CD spectra show an R-value of ~0.3 in water and water-TFE solutions indicating the presence of 3_{10}-helices. In water we observe a negative maximum at 200-nm without a trough at 222-nm. This suggests a significant population of unfolded conformations; UVRR indicates only 50% helicity in water. Our CD spectra of $gp41_{659-671}$ differs from Biron et al's in that their peptide spectra in pure water shows greater 3_{10}-helix content. We do not know the reason for differences in the two measurements. Addition of 10% TFE does not impact the position of the 200-nm negative band, but 30% TFE red shifts the band maxima to 205-nm, indicating increased 3_{10}-helix content. These results are confirmed by our UVRR measurements where the peptide spectra in 10% TFE show ~55% helicity, whereas, in 30% TFE the peptide shows negligible C_α-H_b band intensity, indicating ~ 92% helicity (Fig 4.3). The TFE stabilized helix does not show any appreciable melting with increasing temperature (not shown).

It should be noted that our UVRR results do not necessarily suggest that a single, continuous 3_{10}-helix of six-peptide bonds exists in water. Recently, Mikhonin and Asher[72] demonstrated that the resonance enhanced AmIII and C_α-H_b bands scatter

independently i.e. there is negligible coupling between adjacent peptide bonds. Hence, the UVRR spectra in the AmIII and C_α-H_b region can be regarded as a linear sum of individual peptide bonds. We therefore envision a scenario where in water the peptide is flickering between folded and unfolded conformations; the observed C_α-H band intensity is therefore, a measure of the peptide's residence time in extended PPII like conformations. Hence, the observed 50% helical content could indicate that during the measurement period a peptide bond has an equal probability of being in the folded or unfolded/extended conformation regions of the Ramachandran space.

4.4 CONFORMATION ANALYSIS

The conformational space sampled by $gp41_{659\text{-}671}$ peptide in water can be quantitatively analyzed by an examination of the $AmIII_3$ region. The subtraction of the Trp contribution, however, results in a noisy spectrum which complicates assignment of the $AmIII_3$ bands. Previously, Fodor *et al*[73] reported that Trp cross sections weaken at shorter excitation wavelengths. Thus by exciting at 194-nm we are able to selectively enhance the amide vibrations relative to Trp vibrations and acquire spectra dominated by amide vibrations.

We deconvoluted the measured 194-nm excitation spectrum into a sum of a minimum number of Voight bands by using the peak fitting routine in Grams software (Galactic Industries Corporation, Grams version 5, Fig 4.4). The 194 nm excitation UVRR spectra show an AmI band at 1664 cm^{-1} with a weak aromatic stretching band at 1665 cm^{-1}. The

decreased aromatic stretching band intensity allows us to resolve the AmI band. Increased contribution from diatomic oxygen interferes with the AmII band located at ~1556 cm^{-1}. The W4 and W5 Trp bands are located at 1491 and 1437 cm^{-1}. An intense C_α-H bending band located at 1394 cm^{-1} shows only a negligible temperature induced decrease in intensity (Fig 4.5). A small $AmIII_1$ band at 1340 cm^{-1} overlaps the W7 band of Trp, while a weak $AmIII_2$ band is observed at ~1300 cm^{-1}. As with 204 nm excitation we observe $AmIII_3$ bands at 1293, 1254, and 1224 cm^{-1}. As the temperature is increased from 1 to 60 ºC, the AmII band intensity decreases while the band position downshifts from 1560 to 1557 cm^{-1} (Fig 4.5). The $AmIII_1$, $AmIII_2$, and the 1293 cm^{-1} $AmIII_3$ band remain more or less invariant with increasing temperature. The broad 1254 cm^{-1} $AmIII_3$ band downshifts, while the 1224 cm^{-1} $AmIII_3$ band shows increased band intensity with increasing temperature.

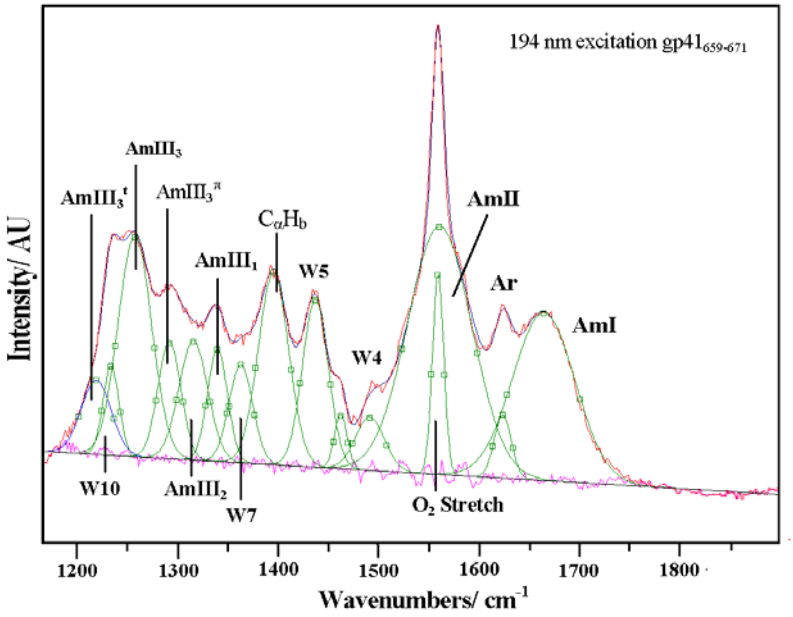

Figure 4.4: Spectral deconvolution of 1 ºC 194-nm UVRR $gp41_{659-671}$ spectra with Voight bands. The excellence of the fit is evident from the flat residual displayed underneath

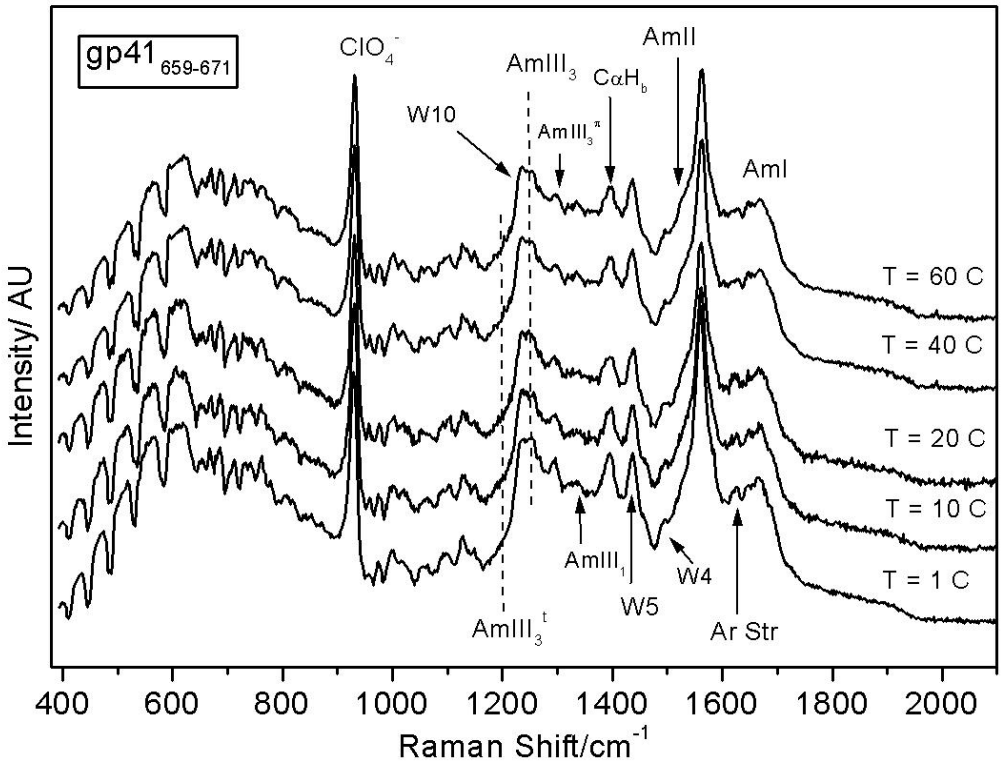

Figure 4.5: 194-nm UV resonance Raman spectra of $gp41_{659-671}$ measured between 1 ºC and 60 ºC. Three 10 min spectra were summed and scaled to the intensity of 932 cm^{-1} perchlorate band. The bands arise mainly from amide vibrations except for those that derive from Trp ring vibrations.

Recently, Mikhonin *et al* [74] quantitatively demonstrated that the $AmIII_3$ band frequency depends upon the ψ dihedral angle and the hydrogen bonding state of the amide bond ψ.[67,74] Using their methodology for correlating the ψ dihedral angle with the $AmIII_3$ band position, we determine that the 1224 cm^{-1} band could originate from either the distorted β-sheet (ψ = +40º) or β-turn like (ψ = -3º) conformations.

In the 277 to 302 K temperature interval, Biron *et al* [48] using analytical ultra centrifugation did not observe any significant aggregation or dimerization products of $gp41_{659-671}$. We therefore conclude that the 1224 cm^{-1} band originates from β-turn

conformations and assign the 1224 cm^{-1} band as the β-turn amide III_3 ($AmIII_3^t$). The ψ dihedral angle of -3º indicated by the $AmIII_3^t$ band position suggests the presence of type I turns.

The 1293 cm^{-1} $AmIII_3$ band does not show any significant temperature dependent shift in band position indicating a conformation dominated by intra-peptide hydrogen bonds. According to the data of Mikhonin *et al* [74] the band position likely correlates to ψ = -75º, suggesting the presence of a π-helix like conformation. Previous studies of peptides with significant 3_{10} helix populations found appreciable π-helix populations in equilibrium with the native helix[38,46] MD simulations suggest that the π-helix may serve as an intermediate in the α-helix folding pathway.[38] Alternatively, Cartailler and Luecke suggest π-helices exist as defects in α-helices where the presence of a π-helix like 1→5 hydrogen bond (π-bulge) introduces a kink in the α-helix.[75]

The broad 1254 cm^{-1} $AmIII_3$ band is composed of overlapping helical and PPII conformations. The 1254 cm^{-1} band maximum indicates a dominant 3_{10}-helix conformation, though it should be noted that the type III turn conformation (a single 3_{10} helix unit) is expected to contribute in this frequency region as it populates similar dihedral angles.[41] Typical α-helical peptides show an $AmIII_3$ band maximum at 1263 cm^{-1}. The 9 cm^{-1} shift in the $AmIII_3$ band position of $gp41_{659\text{-}671}$ as compared to typical α-helical peptides such as the AP peptide [24] indicates the average ψ angle of $gp41_{659\text{-}671}$ deviates from the typical α-helix conformation by +10º. This result demonstrates that UVRR can discriminate between conformationally similar α- and 3_{10}-helicies.

Recent MD simulations have suggested that distorted α-helices exist in a rapid equilibrium with the 3_{10}-helix conformations.[76] While we do not find any definitive evidence for significant concentration of α-helix conformation, the broad width of the $AmIII_3$ band suggests that a small α-helix population may exist (see Fig. 4.2).

4.5 CONCLUSIONS

We examined the secondary structure of $gp41_{659\text{-}671}$ by exciting the backbone at 204 and 194 nm. Our results indicate that six of the 12 peptide bonds adopt helical conformations (predominantly 3_{10}- or π-helix). An examination of the conformation sensitive $AmIII_3$ region indicates $gp41_{659\text{-}671}$ shows a broad distribution of conformations that includes PPII, β-turn, 3_{10}-, and π-helix conformations but little α-helix; furthermore, we demonstrate that the $AmIII_3$ band position can be used to distinguish a 3_{10}-helix from an α-helix conformation. A lack of temperature induced change in the $AmIII_3$ band intensities indicates an energy landscape where the helical and unfolded conformations occupy degenerate energy levels with similar entropies. This allows for nearly equal population of both the helical and unfolded conformations, as evidenced by the C_α-H band intensity which indicates a 50% helical content, independent of temperature.

ACKNOWLEDGMENTS: The authors would like to thank Prof. J. Anglister, Prof. C. Toniolo, Prof. A. Ozdemir, A. V. Mikhonin, and Dr. N. Myshakina for helpful discussions, and Prof. C. Schafmeister for donating the TFE sample.

4.6 REFERENCES

(1) Anfinsen, C. B. *Science* **1973**, *181*, 223.
(2) Chan, H. S.; Dill, K. A. *Proteins: Struct. Funct. Genet.* **1998**, *30*, 2.
(3) Dill, K. A. *Biochemistry* **1990**, *29*, 7133.
(4) Jewett, A. I.; Pande, V. S.; Plaxco, K. W. *J. Mol. Biol.* **2003**, *326*, 247.
(5) Hardin, C.; Eastwood, M. P.; Prentiss, M.; Luthey-Schulten, Z.; Wolynes, P. G. *J. Comp. Chem.* **2002**, *23*, 138.
(6) Cleland, J. *Protein folding: in vivo and in vitro*; American Chemical Society: Washingon D. C., 1993.
(7) Dill, K. A.; Alonso, D. O. V.; Hutchinson, K. *Biochemistry* **1989**, *28*, 5439.
(8) Glaser, R. *Biophysics*; Springer: New York, 2000.
(9) Alm, E.; Baker, D. *Proc. Nat. Acad. Sci. U.S.A.* **1999**, *96*, 11305.
(10) Wolynes, P. G.; Onuchic, J. N.; Thirumalai, D. *Science* **1995**, *267*, 1619.
(11) Pappu, R. V.; Srinivasan, R.; Rose, G. D. *Proc. Natl. Acad. Sci. U.S.A.* **2000**, *97*, 12565.
(12) Myers, J. K.; Oas, T. G. *Annu. Rev. Biochem.* **2002**, *71*, 783.
(13) Shortle, D. *Curr. Opin. Struct. Biol.* **1993**, *3*, 66.
(14) Bryngelson, J. D.; Wolynes, P. G. *J. Phys. Chem.* **1989**, *93*, 6902.
(15) Hao, M.-H.; Scheraga Harold, A. *J. Phys. Chem.* **1994**, *98*, 9882.
(16) Dobson, C. M.; Salij, A.; Karplus, M. *Angew. Chem. Int. Ed. Engl.* **1998**, *37*, 868.
(17) Munoz, V.; Thompson, P. A.; Hofrichter, J.; Eaton, W. A. *Nature* **1997**, *390*, 196.
(18) Urry, D. W. *Journal of Physical Chemistry B* **1997**, *101*, 11007.
(19) Ahmed, Z.; Illir, A. B.; Mikhonin, A. V.; Asher, S. A. *J. Am. Chem. soc.* **2005**, *127*, 10943.
(20) Eaton, W. A.; Munoz, V.; Thompson, P. A.; Henry, E. R.; Hofrichter, J. *Acc. Chem. Res.* **1998**, *31*, 745.
(21) Munoz, V.; Henry, E. R.; Hofrichter, J.; Eaton, W. A. *PNAS* **1998**, *95*, 5872.
(22) Dinner, A. R.; Lazaridis, T.; Karplus, M. *PNAS* **1999**, *96*, 9068.
(23) Thompson, P. A.; Eaton, W. A.; Hofrichter, J. *Biochemistry* **1997**, *30*, 9200.
(24) Lednev, I. K.; Karnoup, A. S.; Sparrow, M. C.; Asher, S. A. *J. Am. Chem. Soc.* **1999**, *121*, 8074.
(25) Bolin, K. A.; Pitkeathly, M.; Miranker, A.; Smith, L. J.; Dobson, C. M. *J. Mol. Biol.* **1996**, *261*, 443.
(26) Garcia, A. E.; Sanbonmatsu, K. Y. *Proc. Nat. Acad. Sci. U.S.A.* **2002**, *99*, 2782.
(27) Andrew, C. D.; Warwicker, J.; Jones, G. R.; Doig, A. J. *Biochemistry* **2002**, *41*, 1897.
(28) Lednev, I. K.; Karnoup, A. S.; Sparrow, M. C.; Asher, S. A. *J. Am. Chem. Soc.* **2001**, *123*, 2388.
(29) Woutersen, S.; Hamm, P. *J. Chem. Phys.* **2001**, *114*, 2727.

(30) Clarke, D. T.; Doig, A. J.; Stapley, B. J.; Jones, G. R. *Proc. Nat. Acad. Sci. U.S.A.* **1999**, *96*, 7232.
(31) Williams, S.; Causgrove, T. P.; Gilmanshin, R.; Fang, K. S.; Callender, R. H.; Woodruff, W. H.; Dyer, R. B. *Biochemistry* **1996**, *35*, 691.
(32) Ianoul, A.; Mikhonin, A.; Lednev, I. K.; Asher, S. A. *Journal of Physical Chemistry A* **2002**, *106*, 3621.
(33) Asher, S. A.; Mikhonin, A. V.; Bykov, S. V. *J. Am. Chem. Soc.* **2004**, *126*, 8433.
(34) Sheinerman, F. B.; Brooks Charles, L., 3rd. *J. Am. Chem. Soc.* **1995**, *117*, 10098.
(35) Sung, S.-S. *Biophys J.* **1995**, *68*, 826.
(36) Tobias, D. J.; Brooks Charles, L., 3rd. *Biochemistry* **1991**, *30*, 6059.
(37) Young, W. S.; Brooks Charles, L., 3rd. *Biochemistry* **1995**, *34*, 7614.
(38) Armen, R.; Alonso, D. O. V.; Daggett, V. *Protein Sci.* **2003**, *12*, 1145.
(39) Fiori, W. R.; Miick, S. M.; Millhauser, G. L. *Biochemistry* **1993**, *32*, 11957.
(40) Sundaralingam, M.; Sekharudu, Y. C. *Science* **1989**, *244*, 1333.
(41) Millhauser, G. L. *Biochemistry* **1995**, *34*, 3873.
(42) Miick, S. M.; Martinez, G. V.; Fiori, W. R.; Todd, A. P.; Millhauser, G. L. *Nature* **1992**, *359*, 653.
(43) Millhauser, G. L.; Stenland, C. J.; Hanson, P.; Bolin, K. A.; van de Ven, F. J. M. *J. Mol. Biol.* **1997**, *267*, 963.
(44) Smythe, M. L.; Huston, S. E.; Marshall, G. R. *JACS* **1995**, *117*, 5445.
(45) Schievano, E.; Bisello, A.; Chorev, M.; Bisol, A.; Mammi, S.; Peggion, E. *JACS* **2001**, *123*, 2743.
(46) Kim, S. W.; Cross, T. A. *Journal of Magnetic Resonance* **2004**, *168*, 187.
(47) Toniolo, C.; Formaggio, F.; Tognon, S.; Broxterman, Q. B.; Kaptein, B.; Huang, R.; Setnicka, V.; Keiderling, T. A.; McColl, I. H.; Hecht, L.; Barron, L. D. *Biopolymers* **2004**, *75*, 32.
(48) Biron, Z.; Khare, S.; Samson, A. O.; Hayek, Y.; Naider, f.; Anglister, J. *Biochemistry* **2002**, *41*, 12687.
(49) Andersen, N. H.; Liu, Z.; Prickett, K. S. *FEBS Letters* **1996**, *399*, 47.
(50) Hanson, P.; Anderson, D. J.; Martinez, G.; Millhauser, G. L.; Formaggio, F.; Crisma, M.; Toniolo, C.; Vita, C. *Molecular Physics* **1998**, *95*, 957.
(51) Basu, G.; Kitao, A.; Hirata, F.; Go, N. *JACS* **1994**, *116*, 6307.
(52) Gratias, R.; Konat, R.; Kessler, H.; Crisma, M.; Valle, G.; Polese, A.; Formaggio, F.; Toniolo, C.; Broxterman, Q. B.; Kamphuis, J. *JACS* **1998**, *120*, 4763.
(53) Yasui, S. C.; Keiderling, T. A.; Formaggio, F.; Bonora, G. M.; Toniolo, C. *JACS* **1986**, *108*, 4988.
(54) Wieczorek, R.; Dannenberg, J. J. *Journal of the American Chemical Society* **2003**, *125*, 14065.
(55) Kennedy, D. F.; Crisma, M.; Toniolo, C.; Chapman, D. *Biochemistry* **1991**, *30*, 6541.
(56) Zhang, L.; Hermans, J. *JACS* **1994**, *116*, 11915.
(57) Kubelka, J.; Silva, G. D.; Keiderling, T. A. *JACS* **2002**, *124*, 5325.
(58) Toniolo, C.; Bonora, G. M.; Bavoso, A.; Benedetti, E.; Di Blasio, B.; Pavone, V.; Pedone, C. *Macromolecules* **1986**, *19*, 472.

(59) Toniolo, C.; Polese, A.; Formaggio, F.; Crisma, M.; Kamphuis, J. *JACS* **1996**, *118*, 2744.
(60) Bykov, S. B.; Lednev, I. K.; Ianoul, A.; Mikhonin, A. V.; Asher, S. A. *Appl. Spectrosc.* **2005**, *59*, 1541.
(61) Chi, Z.; Chen, X. G.; Holtz, J. S. W.; Asher, S. A. *Biochemistry* **1998**, *37*, 2854.
(62) Mirkin, N. G.; Krimm, S. *Journal of Molecular Structure* **1996**, *377*, 219.
(63) Matsui, T.; Chenung, A. S.-C.; Leung, K. W.-S.; Yoshino, K.; Parkinson, W. H.; Thorne, A. P.; Murray, J. E.; Ito, K.; Imajo, T. *Journal of Molecular Spectroscopy* **2003**, *219*, 45.
(64) Pajcini, V.; Chen, X. G.; Bormett, R. W.; Geib, S. J.; Li, P.; Asher, S. A.; Lidiak, E. G. *Journal of the American Chemical Society* **1996**, *118*, 9705.
(65) Chen, X. G.; Li, P.; Holtz, J. S. W.; Chi, Z.; Pajcini, V.; Asher, S. A.; Kelly, L. A. *Journal of the American Chemical Society* **1996**, *118*, 9716.
(66) Wang, Y.; Purrello, R.; Jordan, T.; Spiro, T. G. *Journal of the American Chemical Society* **1991**, *113*, 6359.
(67) Mikhonin, A. V.; Ahmed, Z.; Ianoul, A.; Asher., S. A. *J. Phys. Chem. B* **2004**, *108*, 19020.
(68) Mikhonin, A. V.; Myshakina, N. S.; Bykov, S. V.; Asher, S. A. *JACS* **2005**, *127*, 7712.
(69) Asher, S. A.; Ianoul, A.; Mix, G.; Boyden, M. N.; Karnoup, A.; Diem, M.; Schweitzer-Stenner, R. *J. Am. Chem. Soc.* **2001**, *123*, 11775.
(70) Mikhonin, A. V.; Asher, S. A. *JACS* **2006**, *128*, 13789.
(71) Manning, M. C.; Woody, R. W. *Biopolymers* **1991**, *31*, 569.
(72) Mikhonin, A. V.; Asher, S. A. *Journal of Physical Chemistry B* **2005**, *109*, 3047.
(73) Fodor, S. P.; Copeland, R. A.; Gryogon, C. A.; Spiro, T. G. *JACS* **1989**, *111*, 5509.
(74) Mikhonin, A. V.; Bykov, S. V.; Myshakina, N. S.; Asher, S. A. *J. Phys. Chem. B* **2006**, *110*, 5509.
(75) Cartailler, J.-P.; Luecke, H. *Structure* **2004**, *12*, 133.
(76) Higo, J.; N., I.; Kuroda, M.; Ono, S.; Nakajima, N.; Nakamura, H. K. *Prot. Science* **2001**, *10*, 1160.

CHAPTER 5

Circular Dichroism and UV-Resonance Raman Investigation of the Temperature Dependence of the Conformations of Linear and Cyclic

This chapter was published in *Biopolymers*, in press. The co-authors are Zeeshan Ahmed, Jonathan Scaffidi and Sanford A. Asher

5.0 CIRCULAR DICHROISM AND UV-RESONANCE RAMAN INVESTIGATION OF THE TEMPERATURE DEPENDENCE OF THE CONFORMATIONS OF LINEAR AND CYCLIC ELASTIN

We used electronic circular dichroism (CD) and UV resonance Raman (UVRR) spectroscopy at 204-nm excitation to examine the temperature dependence of conformational changes in cyclic and linear elastin peptides. We utilize CD spectroscopy to study global conformation changes in elastin peptides, while UVRR is utilized to probe the local conformation and hydrogen bonding of Val and Pro peptide bonds. The UVRR amide spectral features of Gly are conformation insensitive. Our results indicate that at 20 ºC cyclic elastin predominantly populates distorted β-strand, β-type II and β-type III turn conformations. At 60 ºC, the β-type II turn population increases while the distorted β-strand population decreases. Linear elastin predominantly adopts distorted β-strand and β-type III turn conformations with some β-type II turn population at 20 ˚C. Increasing temperature to 60 ˚C, results in a small increase in the turn population. Our UVRR results suggest that the higher turn content likely arises due to conformation/hydration changes at the proline peptide bonds.

5.1 INTRODUCTION

In recent years the unique elasticity and resilience of elastin-based peptides has drawn interest from both the biophysics and material science communities.[1-16] Elastin is an important structural peptide that enables elastic deformations of biological assemblies. Biological motion, for example, is enabled by elastin's unique ability to repetitively and reversibly deform upon stress. We each benefit from the elastic properties of elastin, where, hopefully, our aorta reversibly contracts and expands 10^9 times during our lives. Biochemical, genetic and structural analysis of elastin fibers has demonstrated that the elastin found in skin, blood vessel walls and lung tissue is a composite of an amorphous component (elastin) and a microfibrillar component (fibrillin). Elastin mimetic peptide $(VPGXG)_n$-where n is the number of repeat pentamers, is widely used as a model system for studying elastin's remarkable viscoelastic properties.

Over the years, considerable effort have been expended to elucidate the mechanism of elastin's unique elasticity.[3-13,17-26] The elastic properties are thought to be associated with or a consequence of elastin's unusual phase transition behavior, which closely resembles that of the thermal volume phase transition behavior of poly(*N*-isopropylacryamide) (PNIPAM).[27-39] PNIPAM polymers contain both hydrophilic and hydrophobic regions whose exposure to the aqueous medium may change as the polymer collapses at high temperature. The transition temperature of PNIPAM polymers is determined by a

delicate balance between amide-water hydrogen bonding, isopropyl group-water interaction, and van der Waals interactions between the hydrophobic groups.[30]

Elastin exists as a highly mobile expanded chain below a certain characteristic temperature that the elastin literature refers to as the "critical temperature, T_c". Above T_c, the peptide chain adopts a compact conformation resulting in a significantly decreased radius of gyration and reduced chain mobility.[24] The elastin literature calls this thermal behavior an "inverse temperature transition".[20,40] Just as for PNIPAM,[29,30] the transition temperature of elastin peptides can be tuned by changing the hydrophobicity of the polymer. In the $(VPGXG)_n$ system we can substitute at the X residue.[41]

The remarkable viscoelastic properties of elastin peptides are thought to arise from weakening of peptide-water interactions at elevated temperatures which results in a hydrophobic collapse of the peptide [15,24,40] The balance between enthalpy and entropy determines the critical temperature. Below T_c, the favorable enthalpic contribution from amide-water hydrogen bonds and/or charged side chain-water interactions compensate for the unfavorable entropy arising from solvation of hydrophobic groups.[24] The relative importance of this enthalpy advantage is decreased at higher temperatures. Part of this loss results from increased thermal fluctuations which weaken peptide-water hydrogen bonds. The loss of water-peptide hydrogen bonding-derived stabilization forces the extended peptide chains to contract to minimize the impact of the unfavorable entropy.[24] Increased librational entropy [42-45] of the released water molecules reduces the entropic cost of hydrophobic solvation and compensates for the loss of configuration entropy incurred upon elastin's transition. [3,4,22,23]

Unfortunately, there are no high resolution NMR or X-ray structures of elastin because of the high mobility of the peptide's backbone.[40] This lack of detailed knowledge regarding conformational transitions in elastin has significantly impeded efforts for establishing a clear link between structure and function of elastin peptides. Based on spectroscopic studies, Venkatachalam and Urry [23] proposed that that upon an increase in temperature, the highly mobile peptide chains adopt a rigid, well ordered β-spiral conformation. A β-spiral is composed of repetitive β-type II turns, which form a helix-like structure without inter-turn (i – i + 4) hydrogen bonds.[17,22,23,46] This model is supported by NMR and Raman studies.[47] These spectroscopic studies found that the collapsed state of the polymer resembles the structure of cyclic $(VPGVG)_3$ peptide crystallized from a mixed water/D_2O-methanol solvent.[17,18,22,23]

Below T_c, the cyclic peptide exists in a β-type II turn conformation which at high concentrations precipitates at elevated temperatures, presumably into an ordered β-spiral-like conformation.[23] Reiersen *et al* [40] used CD spectroscopy to demonstrate that the transition is independent of chain length. The smallest cooperative unit appears to be the pentamer (VPGXG), indicating that long range interactions do not play a significant role in elastin's inverse transition. The authors demonstrate that small elastin peptides show a broad transition between 1 and 77 ºC where the CD global minimum (200 nm) decreases with increasing temperature. The temperature-dependent behavior of (VPGVG)-repeat elastin peptides appears to be pH-independent.[40]

While Venkatachalam and Urry's β-spiral model is consistent with some of the spectroscopic studies, it does not agree with studies of tissue-derived, water-swollen elastin fibers, which indicate that elastin collapses to a random coil-like conformation.[48-

[51] Recent molecular dynamics simulations by Li *et al* [3,4] suggest that the collapsed state of elastin is best described as a "compact amorphous structure". The MD study found that when starting from an idealized β-spiral conformation at low temperatures, the expanded peptide chain retained significant β-spiral population. At high temperatures, however, β-turns and β-strand-like conformations dominate. These results suggest that the collapsed state of elastin may be best described as a molten globule where the peptide chain locally adopts a short-range β-spiral-like conformation.[3,4]

In this work we used CD and UVRR to examine temperature-dependent conformation changes in cyclic and linear elastin. Our results indicate that the cyclic peptide predominantly populates distorted β-strand, β-type II and type III turn conformations. In contrast, linear elastin predominantly populates β-type III turn and distorted β-strand conformations, with a minor β-type II turn population, as well.

5.2 EXPERIMENTAL

The UV resonance Raman spectrometer has been described in detail elsewhere.[52] Briefly, 2 mw of 204 nm UV light was generated by Raman-shifting the 355 nm 3rd harmonic output of an Nd:YAG laser (Coherent, Infinity) in H_2 gas. These UV pulses were then focused at ~45 degrees from the normal to produce a sub-mm spot near the interior surface of a rotating fused silica NMR tube (Wilmad) filled with ~1 mL of the sample solution. A 135^{o} backscattering geometry was used for collecting the Raman scattered light, which was then dispersed by a custom-made subtractive double

monochromator onto a back thinned CCD camera (Princeton Instruments-Spec 10 System).[52]

The 15-residue long cyclic $(VPGVG)_3$ and linear elastin $GVG(VPGVG)_2VP$ were obtained from the Pittsburgh Peptide Synthesis Facility (PPSF, >95% purity) and used at 1 mg/ml concentrations at pH 7. The cyclic peptide was prepared by cyclization of the linear variant (PPSF, >95% purity). Raman spectra (average of three five-minute spectra) were normalized relative to the peak height of the 0.1 M perchlorate's 932 cm^{-1} band. Three replicate measurements of separately prepared elastin solutions were recorded to ensure measurement reproducibility. Solution pH was adjusted by adding small aliquots of HCl or NaOH. Temperature-dependent CD spectra (average of 10 spectral accumulations) of similarly prepared solutions (pH ~5) at 1 mg/ml were measured on a Jasco-715 spectropolarimeter using a 200 μm path length quartz cell. CD and Raman spectra of linear elastin measured at 20 °C subsequent to the elevated temperature measurements were similar to those measured prior to the temperature increase, indicating the absence of significant photo- or thermal degradation or irreversible aggregation. The CD spectrum of cyclic elastin shows a slight overall decrease in amplitude after heating. This change likely derives from temperature-induced degassing/bubble formation on cell walls at high temperatures.

5.3 RESULTS AND DISCUSSION

5.3.1 Cyclic Elastin

We examined the temperature dependence of cyclic elastin's conformation by measuring the circular dichroism (CD) spectra between 0 and 50 ºC (Fig 5.1). At 0 ºC the cyclic elastin spectrum shows a negative maxima at ~222 nm, a maximum at ~207-nm and a global minimum below 200 nm. Previous studies indicate that in elastin peptides the presence of a relatively weak negative maxima at ~222 nm is indicative of the presence of β-type I/III turn conformation, while the maximum at ~207 nm is indicative of a β-type II turn conformation.[24,40,53] It should be noted that typically a negative maxima at 222 nm is associated with either an α-helix- or 3_{10}-helix-like conformation. However, in such cases the global minimum is located above 200 nm, typically around 205-207-nm.[53-55] In cyclic elastin the global minimum is located below 200 nm, which indicates a significant random coil population, thus excluding the possibility that the feature at 222 nm arises from either α-helix or 3_{10} helix-like conformations. These results indicate the global conformation of cyclic elastin contains significant random coil and β type II and β-type III turn conformations. As the solution temperature is increased, the global minimum value becomes less negative (Fig 5.2). A decreased global minimum is regarded as a hallmark of elastin's inverse temperature transition.[24,56,57] No significant changes are observed in either the 222- or 207-nm region (Fig 5.1).

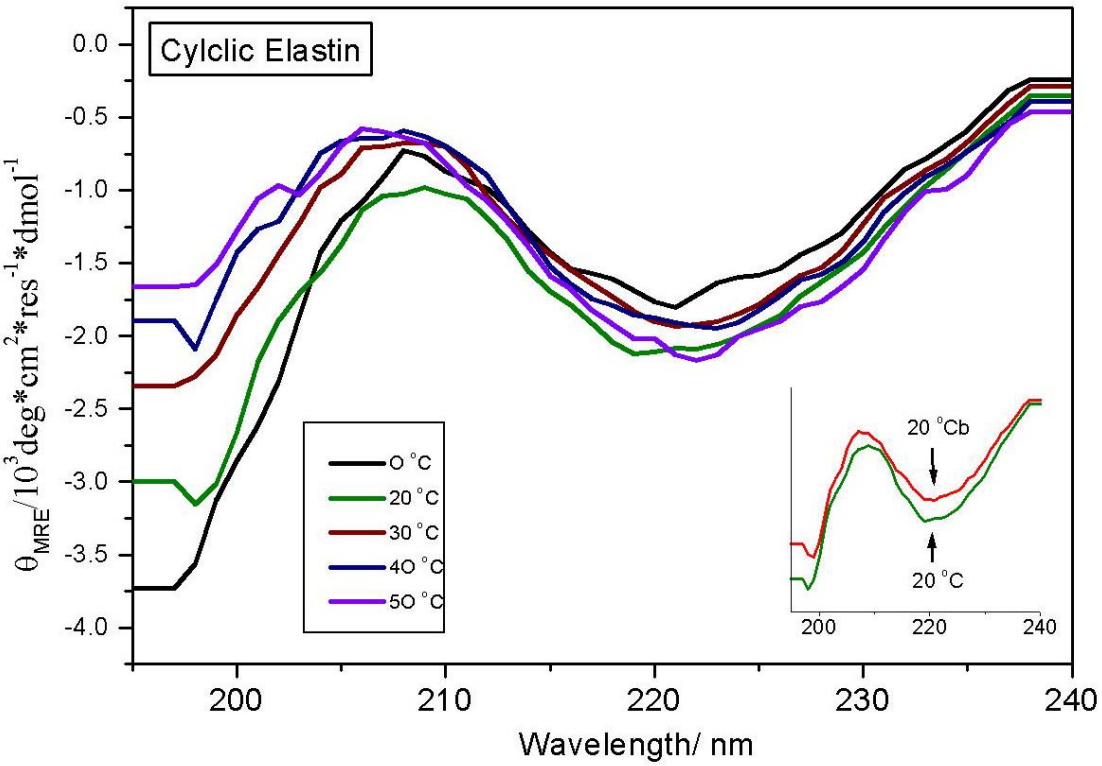

Figure 5.1: Temperature dependent CD spectra of cyclic elastin. The insert shows the 20 ºC CD spectra of cyclic elastin during and subsequent to heating. The CD spectrum subsequent to heating (20 ºCb) shows a slight overall decrease in spectral intensity after heating. This change likely derives from temperature induced degassing/bubble formation on cell walls at high temperatures.

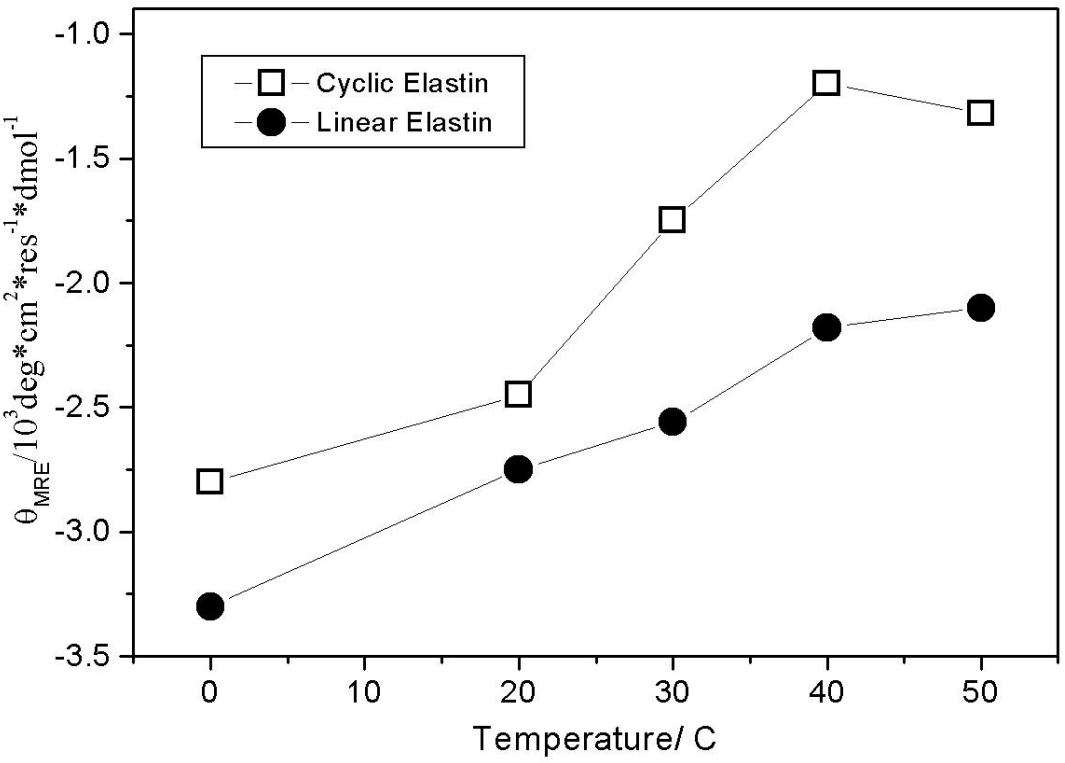

Figure 5.2: Temperature dependent changes in the mean residue ellipticities of cyclic and linear elastin at 200 nm

We further probed the temperature dependence of cyclic elastin's backbone conformation by measuring the 204-nm-excited UV resonance Raman spectra at 20 ºC and 60 ºC (Fig 5.3). There are only three unique types of peptide bonds in elastin, those involving Gly, Pro and Val. The Raman amide bands significantly differ for these peptide bonds such that they are easily differentiated.

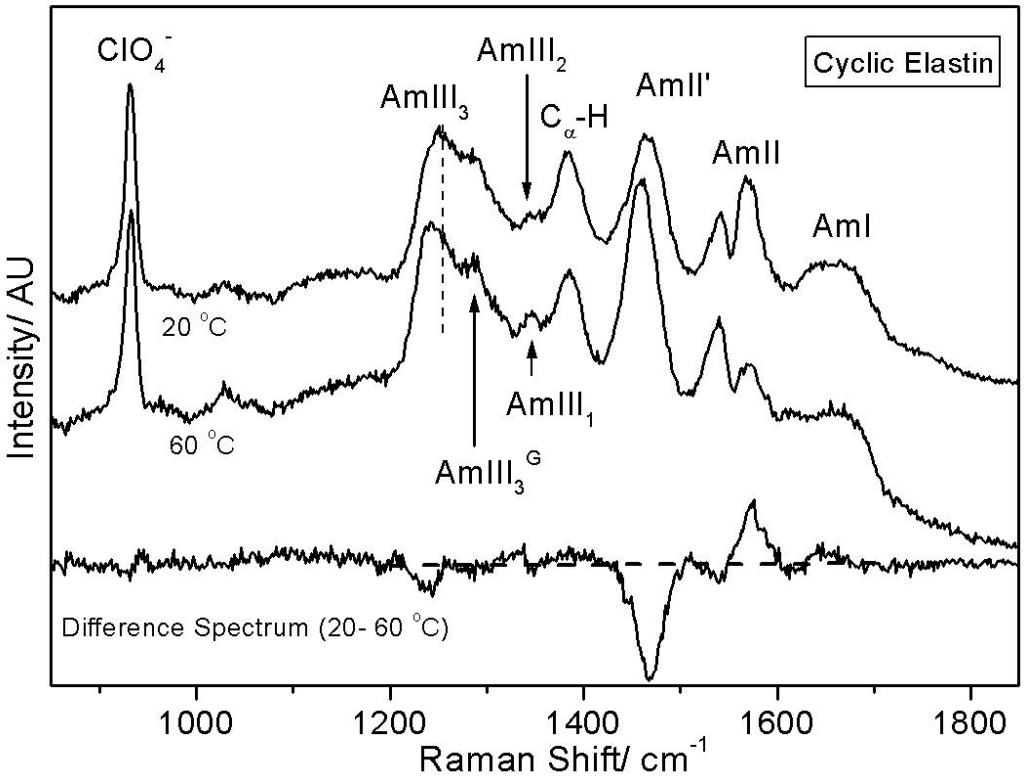

Figure 5.3: 204-nm UV resonance Raman spectra of cyclic elastin measured at 20 and 60 ºC normalized to the intensity of 932 cm^{-1} perchlorate band. The difference spectrum shows temperature dependent changes in the conformation-sensitive $AmIII_3$ region, as well as intensity changes in the C_α-H_b region. The AmII'p narrows at 60 ˚C suggesting the proline peptide bonds adopt a more well-defined conformation at higher temperatures. The trough in the AmII region is an artifact that derives from over-subtraction of the interfering O_2-stretching vibration at 1560 cm^{-1} when the NMR tube contribution was subtracted from the measured spectrum.

Proline forms a tertiary amide where the pyrrolidine ring side chain loops back onto the backbone. Consequently, Pro peptide bond lacks the amide hydrogen (NH) [58,59] and all the C-N stretching motion is concentrated in a single Raman band labeled AmII'p (amide

II' of proline).[60] The AmII'p band is thought to be sensitive to local conformation and/or hydrogen bonding of the Pro peptide bond.[61-63]

In secondary amides such as those formed by Val and Gly, the amide hydrogen's bending motion (NH_b) couples with the C-N_s and $C_\alpha H_b$ motion, resulting in a complex spectrum that shows multiple bands, namely the AmII (C-N_s with some NH_b at ~1550 cm^{-1}), $C_\alpha H_b$ (1380 cm^{-1}), and various AmIII bands (predominantly C-N_s and NH_b, between ~1200 cm^{-1} and 1280 cm^{-1}).

The Gly peptide bond spectrum spectroscopically differs from other non-prolyl peptide bonds due to its two low mass hydrogen atom side chains. The Gly peptide bonds show a single AmIII band at 1284 cm^{-1} ($AmIII^G$) in the amide III region.[64,65] In contrast the Val peptide bonds show typical Raman spectra in the AmIII region comprising of the $AmIII_1$, and $AmIII_2$ bands along with the conformationally sensitive $AmIII_3$ band. The conformation sensitivity of the $AmIII_3$ band arises due to Ψ-angle-dependent coupling between NH_b and $C_\alpha H_b$ motions.[66] In extended PPII-like conformations the NH and $C_\alpha H$ hydrogens are cis allowing for a maximum coupling between NH_b and $C_\alpha H_b$ motions. However, in α-helical conformations the NH and $C_\alpha H$ hydrogens are trans which results in insignificant coupling.[67] In Gly, this conformation sensitivity may be lost or decreased due to the presence of two C_α hydrogens ($C_\alpha H_2$) which allows for some coupling with $C_\alpha H$ for all accessible Ψ angles.

Thus, for elastin peptides we use the AmII'p and the Val $AmIII_3$ bands to probe the conformation and/or hydrogen bonding state of Pro and Val peptide bonds. We utilize

CD spectroscopy along with the UVRR information on the Val and Pro peptide bonds to infer Gly peptide bond conformation.

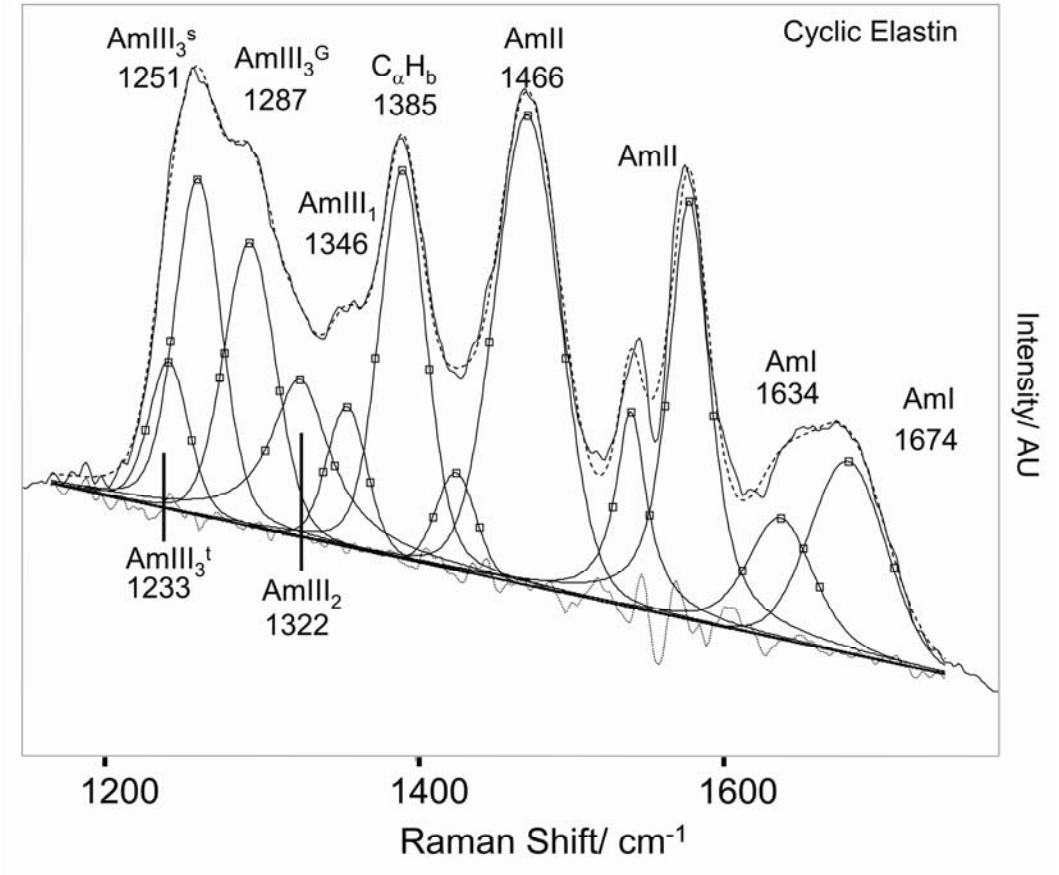

Figure 5.4: Spectral deconvolution of 20 ºC 204 nm UV resonance Raman spectra of cyclic elastin with mixed Gaussian and Lorentzian bands. The quality of the fit is evident from the flat residual displayed underneath.

As shown in Fig 5.4, we deconvoluted the measured 204-nm excited UVRR spectrum into a sum of a minimum number of mixed Gaussian and Lorentzian bands by using the peak fitting routine in Grams (Galactic Industries Corporation, Grams version 5). The broad ~1660 cm^{-1}AmI band (predominantly C=Os) is composed of two overlapping bands centered at 1674 and 1635 cm^{-1}. Thomas *et at* have reported that the amide I

region of crystalline cyclic elastin suspended in its mother liquor shows two prominent AmI bands at ~1652 and 1676 cm^{-1}. These authors suggest that both the 1652 and 1676 cm^{-1} AmI bands likely derive from β-type II turn conformations.[47] However, the origin of the frequency difference between these two AmI bands was not discussed.

The two underlying AmI components (1674 and 1635 cm^{-1}) do not result from intrinsically different frequencies for the amide I bands of the Val, Gly and Pro peptide bonds. Polyproline peptides show AmI bands in the region between 1640 cm^{-1} and 1650 cm^{-1}, while polyglycine peptides show AmI bands at ~1650 cm^{-1}.[65,68,69] The typical non-prolyl, non-glycyl peptide bonds in unfolded peptide conformations typically show a single broad amide I band at 1665 cm^{-1}.[70,71] This frequency spread would not typically result in two overlapping AmI bands at 1635 and 1674 cm^{-1}.

The frequency differences observed for the amide I band either results from significantly different amide bond conformations or from different carbonyl hydrogen bonding. Lazarev *et al*[68] reported that the IR absorption spectra of Z-$(Gly_1$-Pro_2-$Gly_3)_4$-OMe peptide in D_2O shows a broad AmI band that appears to be composed of three different AmI components located at 1632 cm^{-1}, 1650 cm^{-1} and 1669 cm^{-1}. These authors attributed the high frequency 1669 cm^{-1} AmI component to the dehydrated/weakly hydrogen-bonded carbonyl of Gly_3.[68] Recently Spiro and coworkers reported observing a similar high frequency UVRR AmI band in the PPII (1677 cm^{-1}) and β-sheet (1670 cm^{-1}) conformation of polyK peptide.[72] Boury and coworkers[73] suggest that a similar high-frequency AmI component in Gliadin and Globulin proteins derives from random coil and/or β-turn conformations.

Our CD results indicate that the cyclic elastin peptide predominantly adopts an extended β-strand-like conformation with some β-turn character, discounting the possibility that the high frequency AmI component derives from β-sheet-like conformations. We therefore, conclude that the broad 1635 cm^{-1} AmI component of elastin likely derives from hydrogen-bonded peptide bonds, whereas the 1674 cm^{-1} component of elastin derives from dehydrated or weakly hydrogen bonded peptide bonds.

The peptide bond dehydration may correlate with weak amide-amide hydrogen bonding in β–turn-like conformations. X-ray studies of cyclic elastin peptide $(VPGVG)_3$ indicate three β-type II turns. The β-turn spans the VPGV unit and includes a hydrogen bond between the two Val peptide bonds. The other Gly residue appears to serve as a bridge between adjacent turns.[47,74] It is likely that in aqueous solutions, the weakly hydrogen-bonded turn conformation is stabilized against strong peptide-water hydrogen bonding by the bulky β-branched side chains of Val which are known to restrict water access to the peptide backbone.[75] A lack of significant change in elastin's AmI region at high temperatures (Fig 5.2) suggests minimal changes in elastin's hydrogen bonding state. Similar results were reported by Thomas *et al.* who did not observe any significant change in the amide spectra upon the phase transition.[47] A lack of significant change in the AmI region at high temperatures suggests the inverse temperature transition of elastin does not significantly impact the hydrogen bonding state of the peptide backbone.

The AmII band at ~1558 cm^{-1} involves C-N stretching with some N-H bending.[71] The trough in the AmII region (Fig 5.3) is an artifact from over-subtraction of the interfering molecular oxygen vibration at 1560 cm^{-1}.

The AmII' band of Pro (AmII'p)[60] located at 1466 cm^{-1} is predominantly a C-N stretch which is thought to be sensitive to local conformation and/or hydrogen bonding of Pro's peptide bond. The AmII'p downshifts from 1466 to 1460 cm^{-1} and its band width (FWHM) appears to narrow from 50 cm^{-1} to 47 cm^{-1} as the solution temperature is increased from 20 to 60 ˚C (Fig 5.3). We recently demonstrated that the AmII'p band frequency is sensitive to the peptide backbone conformation of proline.[61] The narrowing of the AmII'p band at high temperatures indicates a narrower conformational distribution of the proline peptide bond at 60 ºC.

Takeuchi *et al*[62] suggested that the AmII'p frequency depends on the hydrogen bonding state of Pro.[62,76] If that were true then the observed changes in the AmII'p frequency would suggest weakening of amide-water hydrogen bonds at high temperature. However, we see little evidence from the AmI band for peptide bond dehydration.

The $C_\alpha H_b$ band is located at 1385 cm^{-1}. The presence of the resonance-enhanced $C_\alpha H_b$ band is correlated with the presence of non α-helical conformations.[70,77] In elastin peptides the $C_\alpha H_b$ intensity derives only from the Val and Gly peptide bonds, although as discussed above, we expect that the impact of Val peptide bond conformational changes on the $C_\alpha H_b$ band intensity would be more than what would occur for the Gly peptide bond.

The Amide III region has recently been examined and reassigned.[78-82] The $AmIII_1$ band is located at 1346 cm^{-1}, while a weak $AmIII_2$ band is located at ~1322 cm^{-1}. In cyclic elastin these bands derive only from Val peptide bonds. The 1287 cm^{-1} AmIII band likely derives from glycine peptide bonds. The broad $AmIII_3$ band located at ~1246

cm^{-1} is composed of two overlapping bands at ~1251 and ~1233 cm^{-1} (Fig 5.3) which derive from the Val peptide bonds.

Recently, Mikhonin *et al* [83] quantitatively demonstrated that the $AmIII_3$ band frequency depends upon the ψ dihedral angle and the hydrogen bonding state of the amide bond.[78,83] Furthermore, Mikhonin and Asher [84] demonstrated that the resonance enhanced AmIII and $C_\alpha H_b$ bands each scatter independently i.e. there is negligible coupling between adjacent peptide bonds. The UVRR spectra in the AmIII and $C_\alpha H_b$ region can therefore be regarded as a linear sum of individual peptide bonds. Hence, the $AmIII_3$ spectra represent the time-averaged conformation distribution of the peptide bonds.[54,85]

Using Mikhonin *et al's*[83] methodology for correlating the ψ dihedral angle with the $AmIII_3$ band position, we find that the 1251 cm^{-1} band could originate from either a β-type III turn-like conformation (ψ ~ -35º) or a distorted β-strand-like conformation (ψ ~ +165º, see Table 5.1). The presence of a strong $C_\alpha H_b$ band indicates the existence of significant non-α-helical conformations. As discussed above, the presence of a minimum at 222 nm along with a global minimum below 200 nm in the CD spectra (Fig 1) indicates that some fraction of cyclic elastin exists in a β-type III turn conformation with a significant content of random-coil like conformation. We therefore conclude that the 1251 cm^{-1} Raman band of cyclic elastin likely contains contributions from both the distorted β-strand and type-III turn like conformations. Similarly, Mikhonin *et al's* data suggest the 1233 cm^{-1} $AmIII_3$ band could originate from either anti-parallel β-sheet (ψ = +135º) or β-turn (ψ = 0º) conformations. Taking our cue from previous elastin studies [23] we assign the 1233 cm^{-1} $AmIII_3$ band to β-type II turn conformations of the Val peptide bonds.

Table 5.1: Conformation Distribution of Linear and Cyclic Elastin

Band Position (cm^{-1})	Ψ Angle (degree)	Conformation
Cyclic Elastin		
1251	-35º	β-Type III turn
	+165º	Distorted β-strand
1233	0º	β-Type II turn
Linear Elastin		
1250	-35º	β-Type III turn
	+165º	Distorted β-strand
1230	0º	β-Type II turn

The spectra in the $C_\alpha H_b$ and $AmIII_3$ region show some changes in band intensities and position as the temperature is increased from 20 to 60 ˚C. The frequency of the $C_\alpha H_b$ band is temperature independent.[54,78,86] The $C_\alpha H_b$ band region in the difference spectrum shows a small positive peak; decrease in the $C_\alpha H_b$ band intensity at high temperatures indicates a decrease in the extended state (distorted β-strand) population (Fig 5.3). The $AmIII_3$ band appears to show increased band intensity at 60 ˚C, as indicated by a trough in the difference spectrum at ~1235 cm^{-1}, which suggests an increased β-type II turn population.

5.3.2 Linear Elastin

At 20 ºC, the 204-nm UVRR spectrum of linear elastin (Fig. 5.5A) resembles the 20 ºC cyclic elastin spectrum—suggesting that the ensemble conformations of linear elastin's Val and Pro peptide bonds are similar to their counterparts in cyclic elastin. The cyclic and linear elastin peptides have similar sequences, although the cyclic peptide has an extra peptide bond (P-G) due to cyclization of the linear variant and has no charged groups.

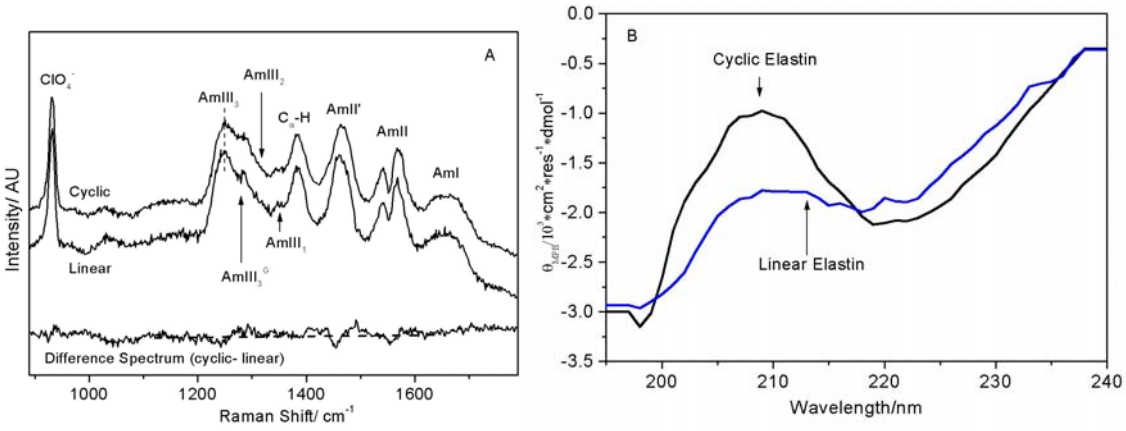

Figure 5.5: A) 204-nm UV resonance Raman spectra of linear and cyclic elastin at 20 ºC and their difference spectra. The featureless difference spectrum indicates that the cyclic and linear peptides have similar conformations. B) CD spectra of linear and cyclic elastin at 20 ºC. Cyclic elastin shows a more prominent positive feature at ~207 nm, indicating a greater population of β-type II turns in the cyclic peptide.

The CD spectrum shows a smaller β-type II turn population for linear elastin than for cyclic peptide as indicated by a less prominent band maximum at ~207-nm (Fig 5.5B).[12,24,40] A lack of significant difference in the UVRR spectra of linear elastin versus

cyclic elastin suggests that the increased turn population is localized in conformational changes at the Gly peptide bonds. Previous studies suggested that linear elastin's Gly residues are highly mobile.[87]

The CD spectra of linear elastin show little temperature dependence at 222- and 207-nm (Fig 5.6), whereas the global minimum below 200 nm becomes less negative with increasing temperature (Fig 5.2 and 5.6). The linear slope of the melting curve indicates a non-cooperative transition (Fig 5.2). The presence of a negative maxima at ~222 nm indicates the presence of β-type III turn conformation, while a weak maximum at ~207-nm is indicative of some β-type II turn conformation.[40] Presence of the global minimum below 200 nm indicates a significant random coil population.[40,53]

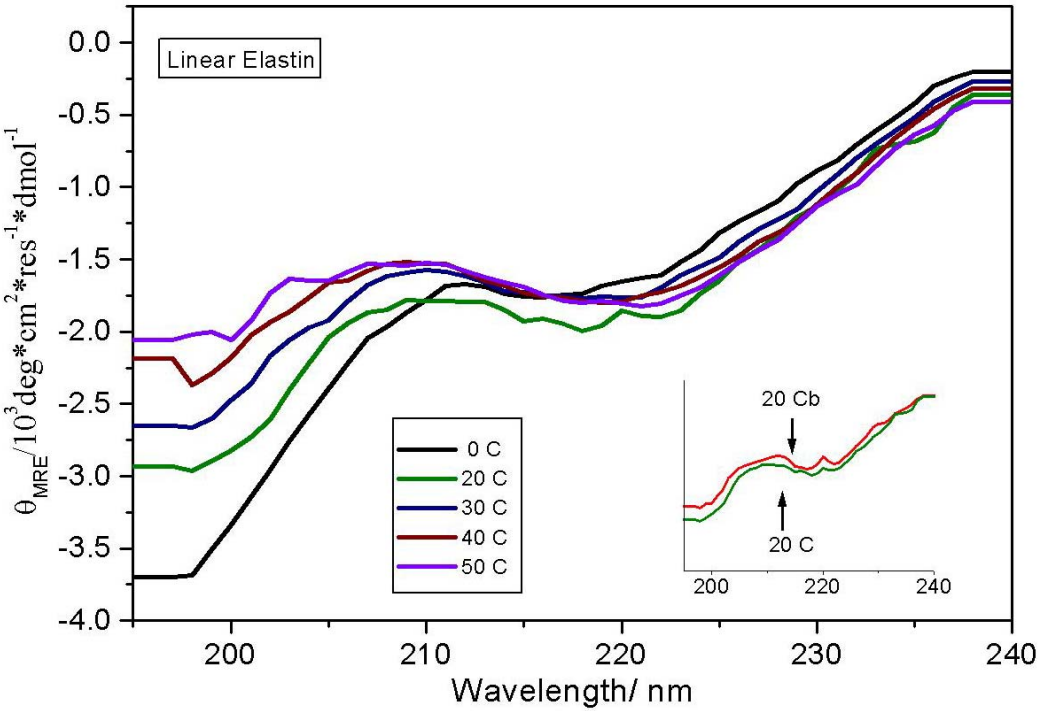

Figure 5.6: Temperature dependent CD spectra of linear elastin. The insert shows the 20 ºC CD spectra of cyclic elastin during and subsequent (20 ºC) to heating.

The mean residual ellipticity (MRE) of linear elastin at 198 nm of ~4000 deg*cm^2*residue^{-1}*dmol^{-1} at 0 ºC is significantly smaller than the values reported by Reiersen *et al* [40] for short elastin-like peptides. Although, the sequence of peptides in the two studies differs (our peptides have extra Val and Pro residues at the N-terminus) both Reiersen *et al*'s and our study show similar spectral features. The relatively small MRE indicates greater β-turn character [40] for our peptide, which likely arises due to the presence of hydrophobic terminal Val and Pro residues. Our CD results indicate that the linear elastin peptide predominantly populates random coil and β-type III turn-like conformations along with a small population of β-type II turns.

As shown in Fig. 5.7, spectral deconvolution of the UVRR spectrum of linear elastin at 20 ºC reveals a similar AmI region as cyclic elastin's with AmI bands at ~1635 cm^{-1} and 1672 cm^{-1}. The trough in the AmII region is an artifact arising due to over-subtraction of the 1560 cm^{-1} molecular oxygen contribution. The AmII'p is located at 1463 cm^{-1}, while the resonance-enhanced $C_\alpha H_b$ [70,77] is located at 1383 cm^{-1}. The $AmIII_1$ band is located at 1348 cm^{-1} while a weak $AmIII_2$ band is located at 1318 cm^{-1}. The $AmIII^G$ is located at ~1285 cm^{-1}. The conformation-sensitive $AmIII_3$ region (deriving from Val) shows a broad band at ~ 1247 cm^{-1} that is likely composed of two overlapping bands located at ~1250 and ~1232 cm^{-1} (Fig 5.7). According to Mikhonin *et al* [83] the 1232 cm^{-1} band likely derives from β-type II turn like conformations (ψ ~ 0º), while the 1250 cm^{-1} band likely derives from distorted β-strand (ψ ~ +165º) and β-type III turn-like conformations (ψ ~ -35º, see table 1).

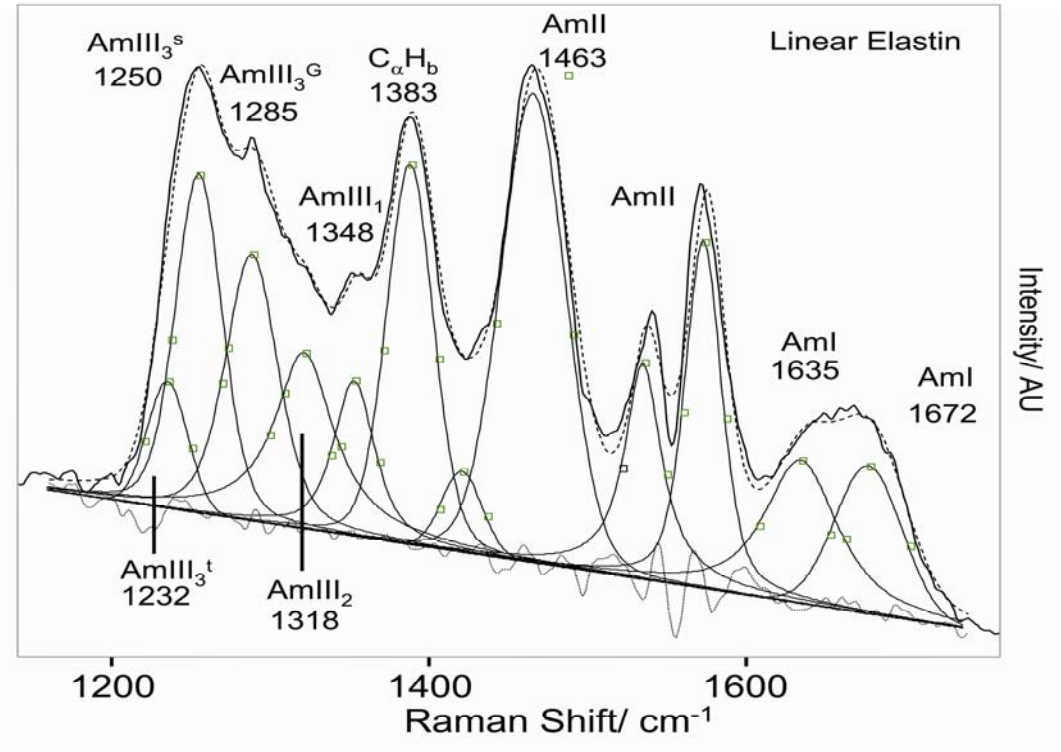

Figure 5.7: Spectral deconvolution of 20 ºC 204 nm UV resonance Raman spectra of linear elastin with Gaussian and Lorentzian bands. The quality of the fit is evident from the flat residual.

Recently, Ohgo *et al* [88] utilized solid-state NMR techniques in conjunction with a statistical analysis of Brookhaven Protein Databank (PDB) to estimate the angular distribution of the two central Val peptide bonds (Val 14 and 16) in an isotope-labeled $(VPGVG)_6$ lyophilized peptide. The authors found that Val-14 shows a bimodal distribution of (Φ,Ψ) values at: (-110 ± 20º, 130 ± 20º) and (-75 ± 15º, -15 ± 15º) which constitutes 70% and 30% of total population, respectively. Val-16 residue adopts the (Φ,Ψ) values of (-90 ± 15 º, 120 ± 15º). A bimodal distribution was also observed for the central Gly and Pro peptide bonds suggesting that elastin conformation is an ensemble of multiple conformations with some minor β-spiral contribution. Ohgo *et al*'s [88] calculated

Ψ angle values for Val are similar to our UVRR-derived Ψ angles. The slight differences in Ψ angle values likely derive from increased peptide backbone mobility in our aqueous phase experiment. This suggests that the aqueous conformations observed in our UVRR experiment also occur in the lyophilized solid-state samples of Ohgo *et al*. [88]

As the solution temperature is increased from 20 to 60 ˚C, the $AmIII_3$ band shows a small increase in band intensity as indicated by a trough in the difference spectrum at ~1237 cm^{-1}, suggesting an increased β-type II turn population (Fig 5.8). The AmII'p band narrows (ΔFWHM = 2 cm^{-1}) as the solution temperature is increased from 20 to 60 ˚C, suggesting a narrower conformation distribution at 60 ºC, although the narrowing in linear elastin (ΔFWHM = 2 cm^{-1}, Fig 5.8) is just a little less than in cyclic elastin (ΔFWHM = 3 cm^{-1}, Fig. 5.2). Furthermore, unlike in cyclic elastin, the band position of the AmII'p band in linear elastin remains invariant with temperature. This suggests that unlike the prolines of cyclic elastin, linear elastin's prolines do not undergo a significant conformation change with increasing temperature.

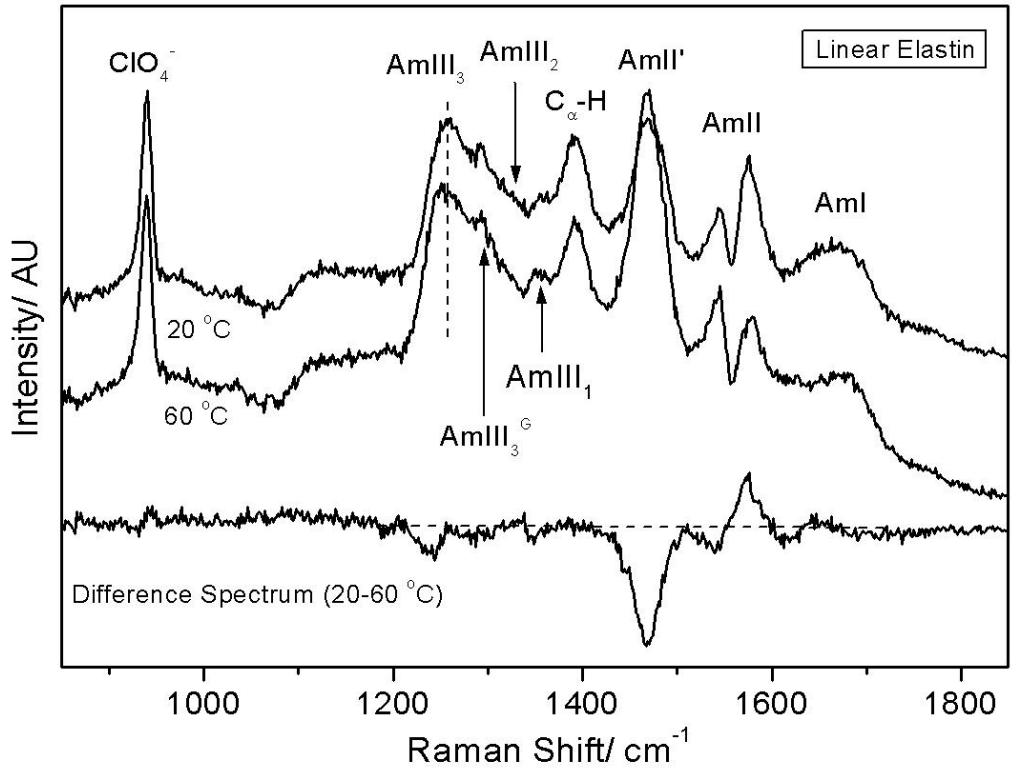

Figure 5.8: 204-nm UV resonance Raman spectra of linear elastin measured at 20 and 60 ºC. The difference spectrum shows narrowing of the AmII' band width at 60 ºC which is indicative of a transition to a relatively well-defined conformation. The trough in the AmII region is an artifact that derives from over-subtraction of the interfering O_2 stretching vibration at 1560 cm^{-1} when the NMR tube contribution was subtracted from the measured spectra

5.4 CONCLUSION

We utilize electronic circular dichroism (CD) and UV resonance Raman spectroscopy at 204-nm excitation to examine the temperature dependence of conformational changes in cyclic and linear elastin peptides. We use CD spectroscopy to examine global conformation changes in elastin peptides, while UVRR probes the local conformation and

hydrogen bonding of Val and Pro peptide bonds. Our results indicate that the cyclic peptide predominantly populates distorted β-strand, β-type II and β-type III turn conformations at 20 ºC. At 60 ºC, the β-type II turn population increases somewhat while the distorted β-strand population decreases as indicated by changes in the $AmIII_3$ and $C_\alpha H_b$ regions.

The ensemble population of linear elastin is predominantly β-type III turn and distorted β-strand with some β-type II turn population regardless of solution temperature. Increasing temperature results in a small increase in the β-type II turn population; furthermore, we observe narrowing of the AmII'p band with increasing temperature which suggests a narrowed conformation distribution at high temperatures.

Our CD spectra of linear elastin vs. cyclic elastin indicate a greater β-type II-turn population for cyclic elastin. However, the UVRR of cyclic and linear elastin do not show any significant differences. This result suggest that the increased type II turn content of cyclic elastin is likely due to cyclization induced conformation changes at Gly peptide bonds.

Our results demonstrate that for both cyclic and linear elastin the global conformation changes are predominantly driven by conformation changes at the proline and glycine peptide bonds, whereas the Val peptide bonds show relatively little conformation changes with increasing temperature. However, the Val peptide bonds are probably not mere spectators; they likely play a pivotal role in the inverse temperature transition of elastin peptides.

We find that both the cyclic and linear elastin peptide show a broad AmI band which is likely composed of two overlapping bands at ~1674 and 1635 cm^{-1}. The 1635 cm^{-1}

component derives from hydrogen-bonded peptide bonds, whereas the ~1674 cm^{-1} component likely derives from dehydrated/weakly hydrogen-bonded peptide bonds that are likely engaged in weak intra-molecular hydrogen bonding as part of a local β-turn conformation.[47] The weakly hydrogen-bonded β-turn is likely protected against amide-water hydrogen bonds by the bulky β-branched side chains of Val, which are known to shield the peptide backbone from water molecules.[75] The absence of some peptide-water hydrogen bonds in the extended conformation of elastin as compared to typical unfolded peptides such as the XAO peptide which predominantly adopts a PPII conformation,[71,89-91] reduces the enthalpic advantage of the elastin's extended state over its entropically unfavorable collapsed state and narrows the free energy gap between the extended and collapsed states such that a temperature increase induces the inverse transition.

A lack of significant change in the AmI region at high temperature suggests the inverse temperature transition of elastin does not significantly impact the hydrogen bonding state of the peptide backbone. Furthermore, small intensity changes in the AmIII and $C_\alpha H_b$ band region indicate that elastin's phase transition is accompanied by only a small conformation change resulting in increased β-turn population. The increased β-turn content does not appear to impact the hydrogen bonding state of elastin. It is likely that the phase transition in elastin peptides is primarily driven by changes in conformation and/or hydration of the alkyl side chains.

ACKNOWLEDGMENTS: The authors would like to thank Prof. D. W. Urry and Konstantin V. Pimenov for helpful discussions and NIH grant RO1 EB002053 for financial support.

5.5 REFERENCES

(1) Alonso, M.; Reboto, V.; Guiscardo, L.; San Martin, A.; Rodriguez-Cabello, J. C. *Macromolecules* **2000**, *33*, 9480.
(2) Urry, D. W.; Parker, T. M. *Journal of Muscle Research and Cell Motility* **2002**, *23*, 543.
(3) Li, B.; Alonso, D. O. V.; Bennion, B. J.; Daggett, V. *Journal of the American Chemical Society* **2001**, *123*, 11991.
(4) Li, B.; Alonso, D. O. V.; Daggett, V. *Journal of Molecular Biology* **2001**, *305*, 581.
(5) Debelle, L.; Alix, A. J. P.; Wei, S. M.; Jacob, M.-P. *Eur. J. Biochem.* **1998**, *258*, 533.
(6) Fernandes, R. J.; Eyre, D. R. *Biochemical and Biophysical Research Communications* **1999**, *261*, 635.
(7) Herrera, B.; Eisenberg, G.; Holberndt, O.; Desco, M. M.; Rábano, A.; García-Barreno, P.; Del Cañizo, J. F. *Cryobiology* **2000**, *41*, 43.
(8) Kim, B.-S.; Nikolovski, J.; Bonadio, J.; Smiley, E.; Mooney, D. J. *Experimental Cell Research* **1999**, *251*, 318.
(9) Lapis, K.; Tímár, J. *seminar in Cancer Biology* **2002**, *12*, 209.
(10) Lindholt, J. S.; Heickendorff, L.; Vammen, S.; Fasting, H.; Henneberg, E. W. *Eur. J. Vasc Endovasc. Surg.* **2001**, *21*, 235.
(11) Nakamura, F.; Suyama, K. *Archives of Biochemistry and Biophysics* **1996**, *325*, 167.
(12) Reiersen, H.; Rees, A. R. *Biochemical and Biophysical Research Communications* **2000**, *276*, 899.
(13) Robert, L. *seminar in Cancer Biology* **2002**, *12*, 157.
(14) Krukau, A.; Brovchenko, I.; Geiger, A. *Biomacromolecules* **2007**, *8*, 2196.
(15) Tamura, T.; Yamaoka, T.; Kunugi, S.; Panitch, A.; Tirrell, D. A. *Biomacromolecules* **2000**, *1*, 552.
(16) Bressan, G.; Prockop, D. J. *Biochemistry* **1977**, *16*, 1406.
(17) Khaled, M. A.; Prasad, K. U.; Venkatachalam, C. M.; Urry, D. W. *Journal of the American Chemical Society* **1985**, *107*, 7139.
(18) Urry, D. W.; Chang, D. K.; Krishna, N. R.; Huang, D. H.; Trapane, T. L.; Prasad, K. U. *Biopolymers* **1989**, *28*, 819.
(19) Urry, D. W.; Harris, R. D.; Prasad, K. U. *Journal of the American Chemical Society* **1988**, *110*, 3303.
(20) Urry, D. W.; Haynes, B.; Zhang, H.; Harris, R. D.; Prasad, K. U. *Proceedings of the National Academy of Sciences of the United States of America* **1988**, *85*, 3407.
(21) Urry, D. W.; Peng, S.; Parker, T. *Journal of the American Chemical Society* **1993**, *115*, 7509.
(22) Venkatachalam, C. M.; Khaled, M. A.; Sugano, H.; Urry, D. W. *Journal of the American Chemical Society* **1981**, *103*, 2372.
(23) Venkatachalam, C. M.; Urry, D. W. *Macromolecules* **1981**, *14*, 1225.

(24) Urry, D. W. *Journal of Physical Chemistry B* **1997**, *101*, 11007.
(25) Urry, D. W.; Peng, S.; Xu, J.; McPherson, D. T. *Journal of the American Chemical Society* **1997**, *119*, 1161.
(26) Bressan, G.; Prockop, D. J. *Biochemisty* **1977**, *16*, 1406.
(27) Debord, S. B.; Lyon, L. A. *Journal of Physical Chemistry B* **2003**, *107*, 2927.
(28) Ding, Y.; Ye, X.; Zhang, G. *Macromolecules* **2005**, *38*, 904.
(29) Reese, C. E.; Mikhonin, A. V.; Kamenjicki, M.; Tikhonov, A.; Asher, S. A. *Journal of the American Chemical Society* **2004**, *126*, 1493.
(30) Wang, J.; Gan, D.; Lyon, L. A.; El-Sayed, M. A. *Journal of the American Chemical Society* **2001**, *123*, 11284.
(31) Wang, X.; Wu, C. *Macromolecules* **1999**, *32*, 4299.
(32) Hoare, T.; Pelton, R. *Langmuir* **2004**, *20*, 2123.
(33) Hu, T.; You, Y.; Pan, C.; Wu, C. *Journal of Physical Chemistry B* **2002**, *106*, 6659.
(34) Jones, C. D.; Lyon, L. A. *Macromolecules* **2003**, *36*, 1988.
(35) Kunugi, S.; Kameyama, K.; Tada, T.; Tanaka, N.; Shibayama, M.; Akashi, M. *Brazilian Journal of Medical and Biological Research* **2005**, *38*, 1233.
(36) Li, C.; Bergbreiter, D. E. *Chemical Industries (Dekker)* **2003**, *89*, 545.
(37) Zhu, P. W.; Napper, D. H. *Journal of Colloid and Interface Science* **1996**, *177*, 343.
(38) Zhu, P. W.; Napper, D. H. *Journal of Physical Chemistry B* **1997**, *101*, 3155.
(39) Zhu, P. W.; Napper, D. H. *Physical Review E: Statistical Physics, Plasmas, Fluids, and Related Interdisciplinary Topics* **2000**, *61*, 6866.
(40) Reiersen, H.; Clarke, A. R.; Rees, A. R. *J. Mol. Biol.* **1998**, *283*, 255.
(41) Luan, C. H.; Parker, T. M.; Gowda, D. C.; Urry, D. W. *Biopolymers* **1992**, *32*, 1251.
(42) Frank, H. S. *Journal of Chemcial Physics* **1945**, *13*, 478.
(43) Searle, M. S.; Williams, D. H. *J. Am. Chem. Soc.* **1992**, *114*, 10690.
(44) Searle, M. S.; Williams, D. H.; Gerhard, U. *J. Am. Chem. Soc.* **1992**, *114*, 10697.
(45) Tanford, C. *The hydrophobic effect: formation of micelles and biological membranes*; Wiley: New York, 1973.
(46) Chang, D. K.; Venkatachalam, C. M.; Prasad, K. U.; Urry, D. W. *Journal of Biomolecular Structure & Dynamics* **1989**, *6*, 851.
(47) Thomas, G. J., Jr.; Prescott, B.; Urry, D. W. *Biopolymers* **1987**, *26*, 921.
(48) Gosline, J. M. *Biopolymers* **1978**, *17*, 697.
(49) Gosline, J. M.; French, C. J. *Biopolymers* **1979**, *18*, 2091.
(50) Gosline, J. M.; Yew, F. F.; Weis-Fogh, T. *Biopolymers* **1975**, *14*, 1811.
(51) Hoeve, C. A. J.; Flory, P. J. *Biopolymers* **1974**, *13*, 677.
(52) Bykov, S. B.; Lednev, I. K.; Ianoul, A.; Mikhonin, A. V.; Asher, S. A. *Appl. Spectrosc.* **2005**, *59*, 1541.
(53) Manning, M. C.; Woody, R. W. *Biopolymers* **1991**, *31*, 569.
(54) Ahmed, Z.; Asher, S. A. *Biochemistry* **2006**, *45*, 9068.
(55) Biron, Z.; Khare, S.; Samson, A. O.; Hayek, Y.; Naider, f.; Anglister, J. *Biochemistry* **2002**, *41*, 12687.

(56) Foster, J. A.; Bruenger, E.; Rubin, L.; Imberman, M.; Kagan, H.; Mecham, R.; Franzblau, C. *Biopolymers* **1975**, *15*, 833.
(57) Tamburro, A. M.; Guantieri, V.; Daga-Gordini, D.; Abatangelo, G. *J. Biol. Chem.* **1978**, *253*, 2893.
(58) Dorman, D. E.; Torchia, D. A.; Bovey, F. A. *Macromolecules* **1973**, *6*, 80.
(59) Garrett, R. H. G., Charles M.; *Biochemistry*, Second ed.; Saunders College Publishing: Philadelphia, Pa, 1999.
(60) Caswell, D. S.; Spiro, T. G. *Journal of the American Chemical Society* **1987**, *109*, 2796.
(61) Ahmed, Z.; Myshakina, N. S.; Asher, S. A. *manuscript in press* **2007**.
(62) Takeuchi, H.; Harada, I. *Journal of Raman Spectroscopy* **1990**, *21*, 509.
(63) Jordan, T.; Mukerji, I.; Wang, Y.; Spiro, T. G. *J. Mol. Struct.* **1996**, *379*, 51.
(64) Chen, X. G.; Li, P.; Holtz, J. S. W.; Chi, Z.; Pajcini, V.; Asher, S. A.; Kelly, L. A. *Journal of the American Chemical Society* **1996**, *118*, 9716.
(65) Pajcini, V.; Asher, S. A. *Journal of the American Chemical Society* **1999**, *121*, 10942.
(66) Asher, S. A.; Ianoul, A.; Mix, G.; Boyden, M. N.; Karnoup, A.; Diem, M.; Schweitzer-Stenner, R. *Journal of the American Chemical Society* **2001**, *123*, 11775.
(67) Asher, S. A.; Ianoul, A.; Mix, G.; Boyden, M. N.; Karnoup, A.; Diem, M.; Schweitzer-Stenner, R. *J. Am. Chem. Soc.* **2001**, *123*, 11775.
(68) Lazarev, Y. A.; Grishkovsky, B. A.; Khromova, T. B. *Biopolymers* **1985**, *24*, 1449.
(69) Li, P.; Chen, X. G.; Shulin, E.; Asher, S. A. *Journal of the American Chemical Society* **1997**, *119*, 1116.
(70) Chi, Z.; Chen, X. G.; Holtz, J. S. W.; Asher, S. A. *Biochemistry* **1998**, *37*, 2854.
(71) Mikhonin, A. V.; Ahmed, Z.; Ianoul, A.; Asher, S. A. *Journal of Physical Chemistry B* **2004**, *108*, 19020.
(72) JiJi, R. D.; Balakrishnan, G.; Hu, Y.; Spiro, T. G. *Biochemistry* **2006**, *45*, 34.
(73) Chourpa, I.; Ducel, V.; Richard, J.; Dubois, P.; Boury, F. *Biomacromolecules* **2006**, *7*, 2616.
(74) Cook, W. J.; Einspahr, H.; Trapane, T. L.; Urry, D. W.; Bugg, C. E. *J. Am. Chem. Soc* **1980**, *102*, 5502.
(75) Avbelj, F.; Baldwin, R. L. *Proc. Nat. Acad. Sci. U.S.A.* **2003**, *100*, 5742.
(76) Jordon, T.; Mukerji, I.; Yang, W.; Spiro, T. G. *J. Biol. Chem.* **1996**, *379*, 51.
(77) Wang, Y.; Purrello, R.; Jordan, T.; Spiro, T. G. *Journal of the American Chemical Society* **1991**, *113*, 6359.
(78) Mikhonin, A. V.; Ahmed, Z.; Ianoul, A.; Asher., S. A. *J. Phys. Chem. B* **2004**, *108*, 19020.
(79) Lee, S.-H.; Krimm, S. *Biopolymers* **1998**, *46*, 283.
(80) Overman, S. A.; Thomas, G. J., Jr. *Biochemistry* **1995**, *34*, 5440.
(81) Overman, S. A.; Thomas, G. J., Jr. *Biochemistry* **1998**, *37*, 5654.
(82) Overman, S. A.; Thomas, G. J., Jr. *J. Raman Spectrosc.* **1998**, *29*, 23.
(83) Mikhonin, A. V.; Bykov, S. V.; Myshakina, N. S.; Asher, S. A. *J. Phys. Chem. B* **2006**, *110*, 5509.

(84) Mikhonin, A. V.; Asher, S. A. *Journal of Physical Chemistry B* **2005**, *109*, 3047.
(85) Ahmed, Z.; Illir, A. B.; Mikhonin, A. V.; Asher, S. A. *J. Am. Chem. soc.* **2005**, *127*, 10943.
(86) Lednev, I. K.; Karnoup, A. S.; Sparrow, M. C.; Asher, S. A. *J. Am. Chem. Soc.* **1999**, *121*, 8074.
(87) Perry, A.; Stypa, M. P.; Foster, J. A.; Kumashiro, K. K. *J. Am. Chem. Soc.* **2002**, *124*, 6832.
(88) Ohgo, K.; Ashida, J.; Kumashiro, K. K.; Asakura, T. *Macromolecules* **2005**, *38*, 6038.
(89) Shi, Z.; Olson, C. A.; Rose, G. D.; Baldwin, R. L.; Kallenbach, N. R. *Proceedings of the National Academy of Sciences of the United States of America* **2002**, *99*, 9190.
(90) Schweitzer-Stenner, R.; Eker, F.; Griebenow, K.; Cao, X.; Nafie, L. A. *Journal of the American Chemical Society* **2004**, *126*, 2768.
(91) Stapley, B. J.; Creamer, T. P. *Protein Sci.* **1999**, *8*, 587.

CHAPTER 6

UV-Resonance Raman Reveals Temperature-Induced Hydrophobic Collapse in Polyproline Peptide

This chapter has submitted for publication**.** The co-authors are Zeeshan Ahmed, Nataliya S. Myshakina and Sanford A. Asher.

6.0 UV-RESONANCE RAMAN REVEALS TEMPERATURE-INDUCED HYDROPHOBIC COLLAPSE IN POLYPROLINE PEPTIDE

We utilized UV-resonance Raman (UVRR) measurements and density functional theory (DFT) calculations to relate that the AmII'p frequency to the Ψ-angle. The AmII'p frequency shifts by ~ 25 cm^{-1} as the Ψ-angle is varied over allowed angles of the pro peptide bond. The AmII'p frequency does not show any significant dependence on the Φ-dihedral angle. We use this AmII'p frequency dependence on the Ψ-angle to demonstrate that the polyproline peptide undergoes a temperature-induced hydrophobic collapse. The temperature-induced 7 cm^{-1} downshift in the AmII'p frequency of the polyproline peptide results from a 45º rotation of the Ψ dihedral angle from Ψ = 145º (ideal PPII conformation) to Ψ = 100º (collapsed PPII conformation). The resulting hydrophobic collapse of polyproline is driven by changes in peptide-water interactions. The collapsed polyproline peptide is ~26% shorter in length, which results in a ~25% decrease in its solvent accessible surface area

6.1 INTRODUCTION

The unique pyrrolidine ring side chain of the proline amino acid loops back onto itself to form a tertiary amide that imposes significant restrictions on the N-C_α (Φ) bond rotation.[1-5] The reduced conformational freedom of pro residues enforces local order in proteins and peptides which is often utilized in the nucleation and control of secondary structure motifs.[1-10] Lacking an amide hydrogen, pro residues cannot engage in more than one inter-peptide hydrogen bond.[8,9,11-14] Consequently, pro residues are typically found at the start of α-helices, the edges of β-sheets, and most frequently, loops, unordered, and turn regions[1]. When located in the middle of stable helices, such as in trans-membrane proteins, pro residues induce a kink along the α-helical axis.[15,16]

The pro peptide bond's *cis-trans* isomerization can influence protein conformation during folding, as it often controls the rate limiting step.[17,18] For example, in refolding of ribonuclease T_1, the pro *cis-trans* isomerization rate constant is estimated to be $1x10^3$ s^{-1}.[19] In contrast, a typical protein such as cytochrome b_{562} has a refolding rate of 2×10^5 s^{-1}.[20-22]

Given the important impact of pro peptide bond isomerization on folding kinetics, it is important to identify spectroscopic markers that can differentiate between *cis* and *trans* isomers of the pro peptide bond. While, it is possible to differentiate isomeric states of pro by ^{13}C-NMR spectroscopy,[23-26] no such clear-cut quantitative markers yet exist in IR[27] or Raman spectroscopy.[28,29] Recent Raman studies have investigated the AmII' band of pro (AmII'p) as a possible marker for pro isomerization.[29-34]

The AmII'p vibration is similar to the AmII' vibration of deuterated amide bonds in that it involves significant C-N stretching.[35-38] The Raman AmII'p frequency and intensity has been experimentally observed to depend upon protein conformation.[31-33] In addition, the band frequency appears to depend on the identity of the neighboring (*i*-1) residue.[34] These studies also led to the suggestion that the AmII'p frequency was sensitive to the isomeric state of the pro peptide bond. However, significant disagreements exist in the literature over the quantitative interpretation of the AmII'p band frequency dependence.[31-34]

Caswell and Spiro reported that in polyproline the AmII' band downshifts from 1465 to 1435 cm^{-1} upon conversion of polyproline from the PPII (*trans*) to the PPI (*cis*) conformation.[31] However, Harhay and Hudson[30] reported that at 200-nm excitation, simple X-Pro dipeptides did not show any changes in the AmII'p band frequencies when their *cis* content was increased via pH increases. These authors also attributed the observed decrease in the AmII'p band intensity to a pH induced bathochromic shift of the UV absorption.[30]

An alternative interpretation of the AmII'p spectral frequency dependence was suggested by Takeuchi and Harada[34] who proposed that the shift in the band position observed during denaturation of proteins could be due to changes in the hydrogen bonding of the pro peptide bond. The authors reported that in aprotic solvents such as acetonitrile, the AmII'p downshifts by ~25 cm^{-1} as compared to aqueous solution, suggesting that solvent-amide hydrogen bonding is primarily responsible for the observed changes in band position.[34]

Takeuchi and Harada's[34] hydrogen bonding mechanism, however, fails to reconcile the frequency differences observed in small, solvent accessible, X-Pro dipeptides where the band positions are known to differ by as much as 10 cm^{-1} depending upon the identity of the neighboring residue (*i*-1). Jordon *et al*[39] suggested that the side chain modes of the *i*-1 residue likely couple with the $C\text{-}N_s$ vibration of the pro peptide bond.

A more recent study by Triggs and Valentini however, directly contradicts Takeuchi and Harada's[34] interpretation of the AmII'p frequency shift.[40] In their UV-Raman study, utilizing pre-resonance enhancement, Triggs and Valentini systematically examined the impact of solvation and hydrogen bonding by using model peptide bonds of ε-caprolactam, *N,N*-dimethylacetamide (DMA) and *N*-methylacetamide (NMA) in the liquid, aqueous and gaseous phases.[40] Their results demonstrate that the AmI ($C{=}O_s$) frequency is sensitive to hydrogen bonding. However, the frequency of the AmII'-like vibrations of DMA (a tertiary amide) and ε-caprolactam (a *cis* amide) show no significant dependence on hydrogen bonding.[40]

In a recent theoretical study of NMA and NMA-water complexes (and their deuteratred isotopomers) we recently demonstrated that the AmII and AmII' like vibrations of NMA and *d*-NMA lack significant dependence on C=O hydrogen bonding because the $C\text{-}N_s$ motion makes a relatively small contribution to the AmII (~25%) and AmII' like vibrations (~8%).[41] In contrast the hydrogen bond dependent AmI C=O's vibration is > 75% $C{=}O_s$. The hydrogen bond dependence of the AmII ($C\text{-}N_s$ and NH_b) vibration of NMA derives from its $N\text{-}H_b$ component which makes up to 50% of the AmII normal mode composition.[41]

The apparent lack of an AmII'p hydrogen bonding frequency dependence obscures our understanding of AmII'p frequency shifts. In particular, it frustrates our understanding of conformation/hydration changes in pro rich peptides such as the pro rich elastin peptides. These biologically important peptides undergo a large volume-change in response to specific stimuli such as temperature or ionic strength.[42]

Here we systematically examine the conformation, isomerization and hydrogen bond dependence of the AmII'p frequency of various pro derivatives using a combination of UV resonance Raman (UVRR) measurements and density functional theory (DFT) calculations. Our results indicate that the AmII'p band position is insensitive to changes in amide-water hydrogen bond strength.

The frequency of the *cis* and *trans* conformers differs by ~8 cm^{-1}. We find that the AmII'p band position is very sensitive to non-planarity of the pro peptide bond as measured by its Θ-dihedral angle. The peptide bond non-planarity is modulated by conformation changes that alter the Ψ-angle such that the amide nitrogen is pushed out of the peptide bond plane. This result allows us to correlate the AmII'p Raman band frequency to the local conformation of the pro peptide bond.

We correlate a temperature-induced 7 cm^{-1} downshift in the AmII'p frequency of the polyproline peptide to conformational changes deriving from a 45º rotation of the Ψ-dihedral angle from Ψ = 145º (extended PPII conformation) to Ψ = 100º (collapsed PPII conformation). The collapsed polyproline peptide is ~26% shorter in length, which reduces its solvent accessible surface area by ~25%.

6.2 EXPERIMENTAL

The UV resonance Raman (UVRR) spectrometer has been described in detail elsewhere.[43] Briefly, 204 nm UV light was obtained by generating the fifth anti-Stokes Raman harmonic of the 3rd harmonic of a Nd:YAG laser (Coherent, Infinity) in H_2 gas. The sample was circulated in a free surface, temperature controlled stream. A 165° backscattering geometry was used for sampling. The collected light was dispersed by a subtractive double monochromator onto a back thinned CCD camera (Princeton Instruments-Spec 10 System).[43]

Ac-Pro and X-Pro dipeptides (X = Trp, Ala, Gly, Val, Leu, Ser, and Phe) were acquired from Bachem, while polyproline (m.w. = 5800), sodium perchlorate and D_2O were acquired from Sigma-Aldrich. The chemicals were used as received. 1 mg/ml of peptide concentration in 0.2 M sodium perchlorate solution were used for UVRR measurements.

6.2.1 Computational details

All calculations were performed using the Gaussian'03[44] calculation package at the DFT[45-47] level of theory employing the B3LYP[48-50] combinational functional and 6-311+G* basis set. Calculated frequencies were scaled by a 0.98 scaling factor.[51,52] The Polarizable Continuum Model (PCM) as implemented in Gaussian'03 was utilized to account for solvent effects. We optimized the geometry and calculated the harmonic vibrational frequencies of the following species:

1. The c*is* and *trans* isomers of Ac-Pro-Me, where the *cis* and *trans* isomers were defined by the ω torsional angle C'-N-C-C". During geometry optimization this torsional angle was fixed at 180° for the *trans* conformer and 0° for the *cis*-conformer.

2. The frequencies of the optimized *trans* zwitterionic ala-pro molecule (Φ = -90º, Ψ = 145º) were calculated in vacuum (ε = 1.00) and in water (ε = 78.39), acetonitrile (ε = 36.64), and heptane (ε = 1.92) to probe the impact of the dielectric constant on the AmII'p vibrational frequency. Similarly, we calculated the frequency of *trans* zwitterionic ala-pro in water (PCM) hydrogen bonded to an explicit water molecule at the C=O site. The angle between the water molecule and the C=O group was fixed at 180º during optimization.

3. A series of zwitterionic ala-pro conformers with the Φ-dihedral angle fixed at -80° and Ψ = -90°, -70°, -60°, -50°, -45°, 60°, 90°, 120°, 140°, 145°, 150° were calculated in water. In heptane (PCM) only Ψ = -90°, -60°, -45°, 60°, 120°, 145°, 160° values were calculated. In gas phase calculations ala-pro conformers were calculated for Φ = -80° and Ψ = -90°, -60°, -45°, 60°, 120°, 145°.

4. A series of zwitterionic ala-pro conformers with Ψ = 145° and Φ = -60°, -90°, -100° and -120° were calculated for ala-pro in water and in the gas phase. In heptane and acetonitrile, we calculated conformers with Φ = -60°, -90° and -120°. To prevent any impact from possible charge transfer/electrostatic interactions between the C=O and the N-termini, we froze the NH_3^+ rotation during the geometry optimization.

The structures of a 10-mer collapsed polyproline (Φ = -80º, Ψ = 100º) and canonical PPII polyproline (Φ = -80º, Ψ = 145º) were calculated by utilizing the *protein* utility in Tinker[53] and visualized using VMD software.[54] End-to-end distance and radii of the two polymers were estimated using CAChe™ (Fujitsu). Solvent accessible surface area of both polymers was calculated using the Spacefill utility of Tinker utilizing a 1.4 Å radius probe to calculate the accessible and excluded volumes.

6.3 RESULTS AND DISCUSSION

6.3.1 Impact of *cis-trans* isomerization

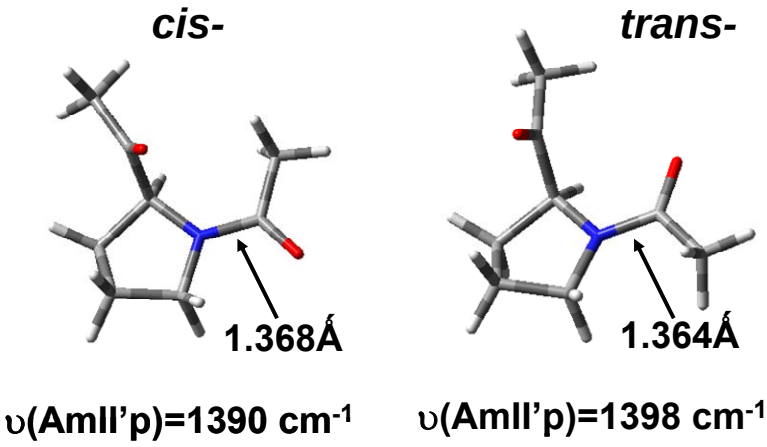

Figure 6.1: The calculated structures of cis and trans isomers of Ac-Pro-Me. The C-N bond length elongates (0.004 Å) in the cis conformation resulting in an 8 cm^{-1} downshift of the AmII'p vibration. The C=O bond length contracts by 0.003 Å which results in a 13 cm^{-1} upshift of the AmI' vibration.

We examined the impact of *cis-trans* isomerization on the AmII'p frequency by calculating the vibrational spectra of the *cis* and *trans* conformers of methylated Ac-Pro (Fig. 6.1). Our calculations show that *trans*→ *cis* isomerization results in a slight elongation of the C-N bond length (~ 0.004 Å) and a nearly equal contraction of C=O bond length (0.003 Å). The elongation of the C-N bond length results in an 8 cm^{-1} downshift of the *cis*-AmII'p vibration, while the *cis*-AmI' vibration upshifts by 13 cm^{-1}.

Changes in the calculated peptide bond geometry likely derive from differences in electron distribution between the *cis* and *trans* conformers. According to Hinderaker and Raines,[56] the PPII conformation of proline peptides is stabilized by n→ π* interactions which result in delocalization of a nonbonding pair of electrons from the amide oxygen's n orbital to the neighboring amide oxygen's π* orbital.[56] The authors suggest that significant $n\rightarrow\pi^*$ interactions occurs when the $O_{i-1}\ldots C_i$ distance is ≤3.2 Å and the $O_{i-1}\ldots C_i{=}O_i$ angle falls between 99° and 119°.[56] As shown in Table 6.1 only the calculated *trans* proline geometry satisfies these criteria.

Table 6.1: Calculated geometric parameters of *cis*- and *trans*-conformer of Ac-Pro-Me

	Trans-Proline	*Cis-Proline*
d(C-N), Å	1.364	1.368
d(C=O), Å	1.227	1.223
$d(O_{i-1}\ldots C_i)$, Å	3.045	4.393
$\angle (O_{i-1}\ldots C_i{=}O_i)$, °	102.51	78.27
$d(C_{i-1}{=}O_{i-1})$,Å	1.211	1.209

The $n \rightarrow \pi^*$ interaction results in re-distribution of electronic density away from the oxygen's lone pair orbital.[56] Therefore, in the *trans* PPII conformer, the C=O double bond character decreases, while the C-N bond order increases. Lacking this $n \rightarrow \pi^*$ charge transfer *cis*-proline has a lower C-N bond order, which gives rise to the calculated 8 cm^{-1} downshift of the AmII'p vibration upon *trans* → *cis* isomerization.

6.3.2 The impact of hydrogen bonding

As discussed above, the work of Triggs and Valentini[40] contradicts Takeuchi and Harada's[34] suggestion that the AmII'p frequency is sensitive to the hydrogen bonding state of the pro peptide bond. The frequencies of the AmII'-like vibrations of tertiary (DMA) and cis (ε-caprolactum) amides do not a show significant sensitivity to hydrogen bonding.[40]

Here we re-examine the impact of water-peptide hydrogen bonds by examining the temperature dependence of the Raman spectra of Ac-Pro, Ala-Pro, Gly-Pro, Phe-Pro, Ser-Pro and Val-Pro dipeptides.[57-60] The AmII' vibration of *N*-deuterated NMA (*d*-NMA) in D_2O shows a significant temperature dependence (-0.07 $cm^{-1}/^oC$).[57] If the observed frequency shift of the AmII' band of *N*-deutertated-NMA (*d*-NMA) primarily derives from hydrogen bonding changes at the carbonyl then the AmII'p should show a similar temperature dependence (~4 cm^{-1} shift over a 60 ˚C interval). However, if the temperature dependence of the AmII' band of *d*-NMA derives from its small N-D_b component (5%),[40,61,62] as suggested by Triggs and Valentini[40] then the AmII'p, which

altogether lacks the N-H bond, will not be significantly impacted by changes in carbonyl hydrogen bonding.

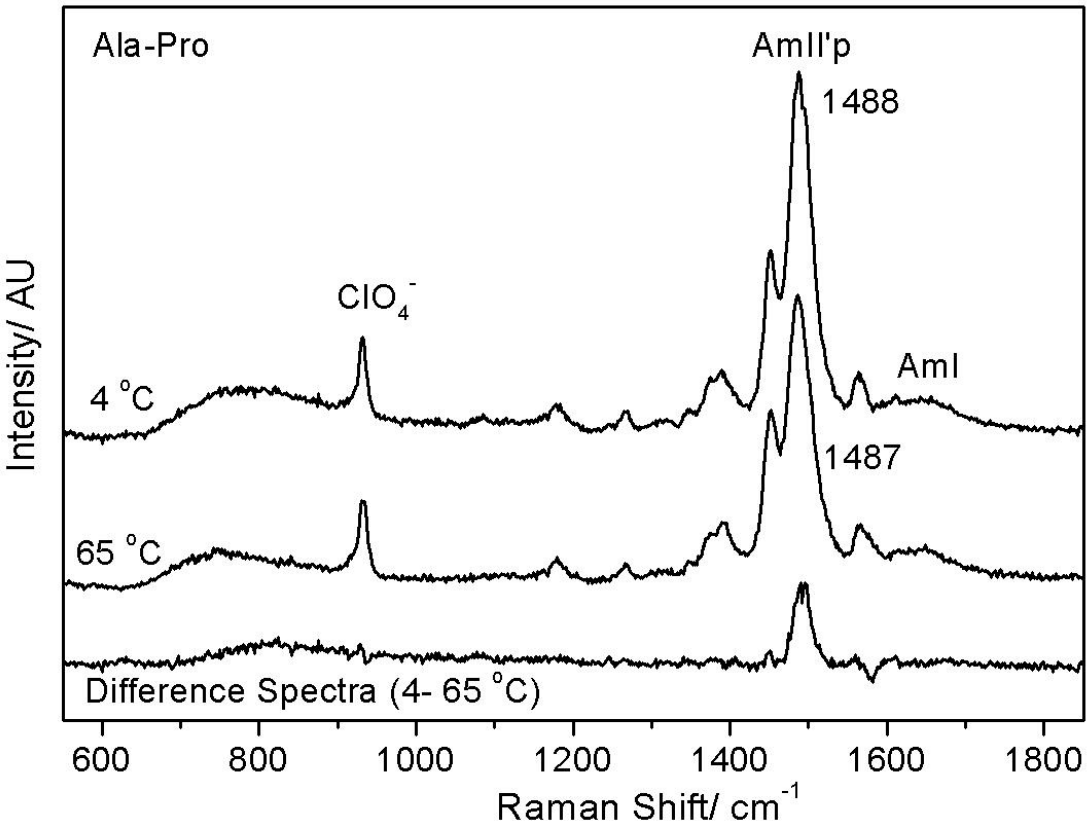

Figure 6.2: The 204-nm excited AmII'p band of Ala-Pro (1mg/ml) shows an insignificant change in frequency ($\Delta\nu$ = 1 cm^{-1}) as the temperature is increased from 4 to 65 ºC. The band intensity however, shows a 22% decrease with increasing temperature.

As shown in Fig 6.2, the frequency of the AmII'p of ala-pro barely downshifts from 1488 cm^{-1} to 1487 cm^{-1} as the solution temperature increases from 4 to 65 ºC. The band intensity however, shows a ~22% decrease. We observe similarly insignificant temperature-induced frequency shifts in other pro dipeptides (Table 6.2). These results

clearly indicate that changes in hydrogen bond strength do not significantly impact the AmII'p frequency.

Table 6.2: Temperature dependence of AmII'p frequency

Peptide	AmII'p frequency 4 ºC (cm^{-1})	AmII'p frequency 65 ºC (cm^{-1})	$\Delta\nu$/ ºC (cm^{-1}/ºC)
Ala-Pro	1488	1487	-.017
Gly-Pro	1486	1485	-.017
Ser-Pro	1482	1480	-0.03
Val-Pro	1476	1475	-0.017

Our recent theoretical study of NMA-water complexes demonstrated that C=O-water hydrogen bonding impacts the peptide bond geometry resulting in the elongation of the C=O bond and contraction of the C-N bond.[41] The AmII and AmII'-like vibrations of NMA and *d*-NMA however, lack significant dependence on C=O hydrogen bonding because C-N_s motion makes a relatively small contribution to the AmII (~25%) and the AmII' like vibrations (~8%).[41] In contrast, the C=O hydrogen bond sensitive AmI vibration is 75% C=O_s.

A lack of significant hydrogen bond strength dependence of the AmII'p frequency in small, water accessible pro dipeptides suggests that the normal mode composition of the AmII'p vibration contains relatively little C-N_s. Indeed our theoretical calculations of Ala-Pro immersed in PCM water indicate that the AmII'p normal mode composition

contains only ~26-28 % C-N_s motion (Table 6.3). A relatively small C-N_s contribution minimizes the impact of hydrogen bond induced peptide bond geometry changes.

The ~25 cm^{-1} downshift in the AmII'p frequency observed by Takeuchi and Harada[34] in acetonitrile cannot mainly result form *cis-trans* isomerization of the proline peptide bond. As discussed above we calculate that the *cis* conformer downshifts 8 cm^{-1} from that of the trans conformer. Takeuchi and Harada's[34] 25 cm^{-1} downshift of AmII'p frequency could derive from conformational alterations about the Φ,Ψ angles. Alternatively, the AmII'p frequency downshift may derive from differences in the solvent dielectric constant.[63] For the AmI vibration, previous studies indicate that the hydration induced frequency downshift requires both the solvent dielectric constant increase (bulk water) and explicit hydrogen bonding of the peptide bond.[63-65] The frequency downshifts of the AmI vibration in NMA observed in protic solvents (explicit hydrogen bonding) are far larger those observed in aprotic solvents with similar dielectric constants.[63,64]

Table 6.3: Calculated normal mode composition of ala-pro (Ψ = 145º).

Conformation	Gas Phase υ(AmII'p)	PED (>5%)	Water υ(AmII'p)	PED(>5%)
Φ = -60º	1442	CH_3 sym def (25) -C-N s (21) -C=O s (10) C-C s (8) CH_3 asym def' (6) –C=O inp b (6)	1470	C-N s (28) -CH_3 asym def' (23) - C-C s (8) C=O s (7) C=O inp b (6)
Φ = -90º	1457	C=O s (20) C-N s (19) -CH_3 asym def' (8) - C-C s (8) -CH_3 sym def (7) C=O	1471	CH_3 asym def' (26) -C-N s (26) C-C s (7) -C=O s (7) - C=O inp b (6)

inp b (6)

Our temperature dependent UVRR experiment (Fig 6.2) directly probes the impact of hydrogen bond strength on the AmII'p frequency. Dielectric constant changes are relatively minor. In contrast, Takeuchi and Harada's[34] experiment replaces water with acetonitrile as the solvent media, incurring large changes in the both the dielectric constant and the hydrogen bonding state of the peptide bond. Such large changes in the environment may impact the peptide bond geometry and/or the normal mode composition of the AmII'p vibration.

We evaluated the impact of the dielectric constant changes on AmII'p frequency of ala-pro by using DFT calculations in PCM water ($\varepsilon = 78.39$), acetonitrile ($\varepsilon = 36.64$), heptane ($\varepsilon = 1.92$) and vacuum ($\varepsilon = 1.00$). Our results indicate that the AmII'p frequency downshifts by 5 cm^{-1}, whereas, the AmI' frequency upshifts by 42 cm^{-1} as the dielectric constant decreases from 78.39 (water) to 1.92 (heptane, Table 6.4). The calculated 9 cm^{-1} difference in the AmII'p frequency between the gas phase and heptane derives from the PCM perturbation to the AmII'p mode composition. The relative change in the AmII'p frequency between water and acetonitrile is negligible, which suggests that the 25 cm^{-1} downshift in the AmII'p frequency observed by Takeuchi and Harada[34] does not derive from differences in the solvent dielectric constant.

Table 6.4: Ala-Pro (Φ = -90°, Ψ = 145°) AmII'p frequency dependence on solvent dielectric effect and hydrogen bonding

Solvent media	Dielectric constant	AmII'p frequency/ cm^{-1}	AmI' frequency/ cm^{-1}
Water	78.39	1471	1661
Water+H_2O [a]	78.39	1470	1648
Acetonitrile	36.64	1472	1664
Heptane	1.92	1466	1703
Vacuum	1.00	1457	1715

[a] Ala-Pro hydrogen bonded to an explicit water molecule, immersed in PCM water.

We examined the impact of local hydrogen bonding on the AmII'p frequency by calculating the frequency of the AmII'p vibration of Ala-Pro in PCM water (ε = 78.39), versus ala-pro in PCM water but hydrogen bonded to an explicit water molecule. The presence of an explicit water molecule has a negligible impact on the AmII'p frequency indicating that the AmII'p vibration does not show any significant dependence on water-C=O hydrogen bonding (Table 6.4). This result is in agreement with our UVRR results (Fig 2) which indicate the frequency of AmII'p is insensitive to C=O hydrogen bonding.

Our results, thus, indicate that hydrogen bond strength and solvent dielectric effect have a negligible impact on the AmII'p frequency. We therefore conclude that the 25 cm^{-1} downshift in the AmII'p frequency observed by Takeuchi and Harada[34] likely derives from (Φ,Ψ) conformational changes in the pro peptide bond.

6.3.3 Ψ-angle dependence

We explore the impact of Ψ-angle rotation on the AmII'p frequency by calculating vibrational frequencies for a series of zwitterionic ala-pro conformers spanning the allowed Ψ-angles at a fixed Φ = -80° (Fig 6.3). To simplify the discussion, we divide all calculated conformers into two groups: helical conformers (Ψ ≤ 0˚) and extended conformers (Ψ > 0˚).

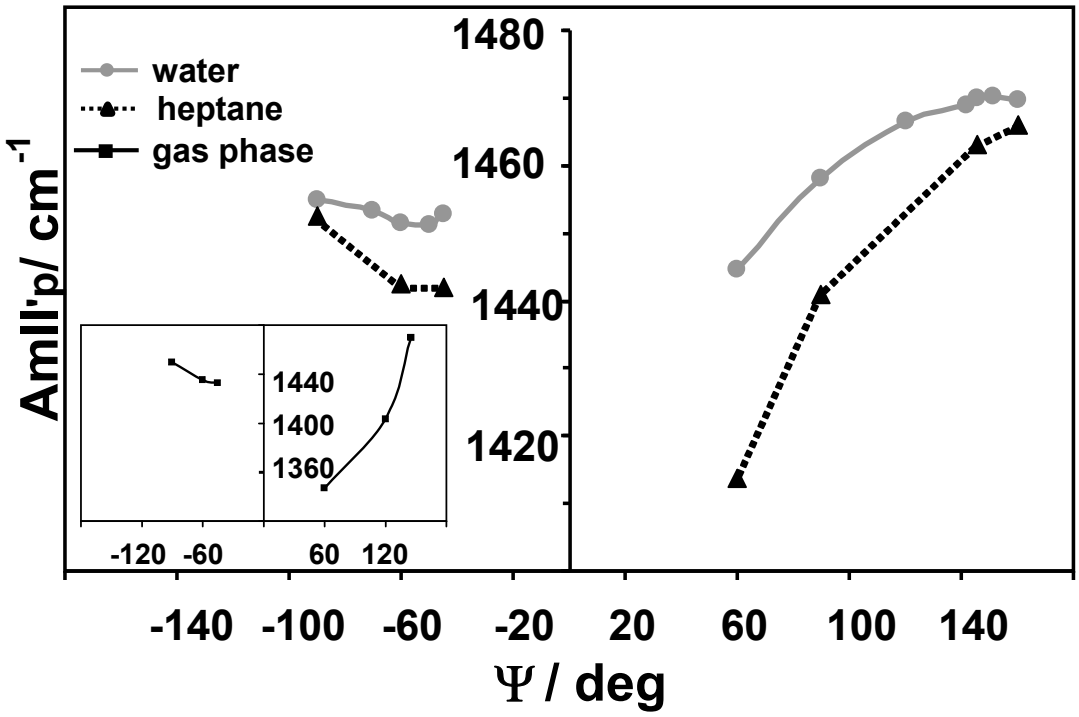

Figure 6.3: Calculated conformational dependence of AmII'p frequency of ala-pro on Ψ-dihedral angle in water, heptane and gas phase (insert).

Analysis of the zwitterionic ala-pro reveals that the calculated AmII'p frequencies of extended conformers upshift by ~25 cm^{-1} when the Ψ-angle is varied from 60º to 150º. In contrast, the AmII'p frequency of *helical* conformers shows a weak Ψ-angle

dependence. The AmII'p frequency downshifts by 4 cm^{-1} as the Ψ-angle is varied from -90° to -45° (Fig. 6.3). The AmII'p frequency shift in both the helical and extended conformation linearly correlates with changes in C-N bond length (Fig. 6.4).

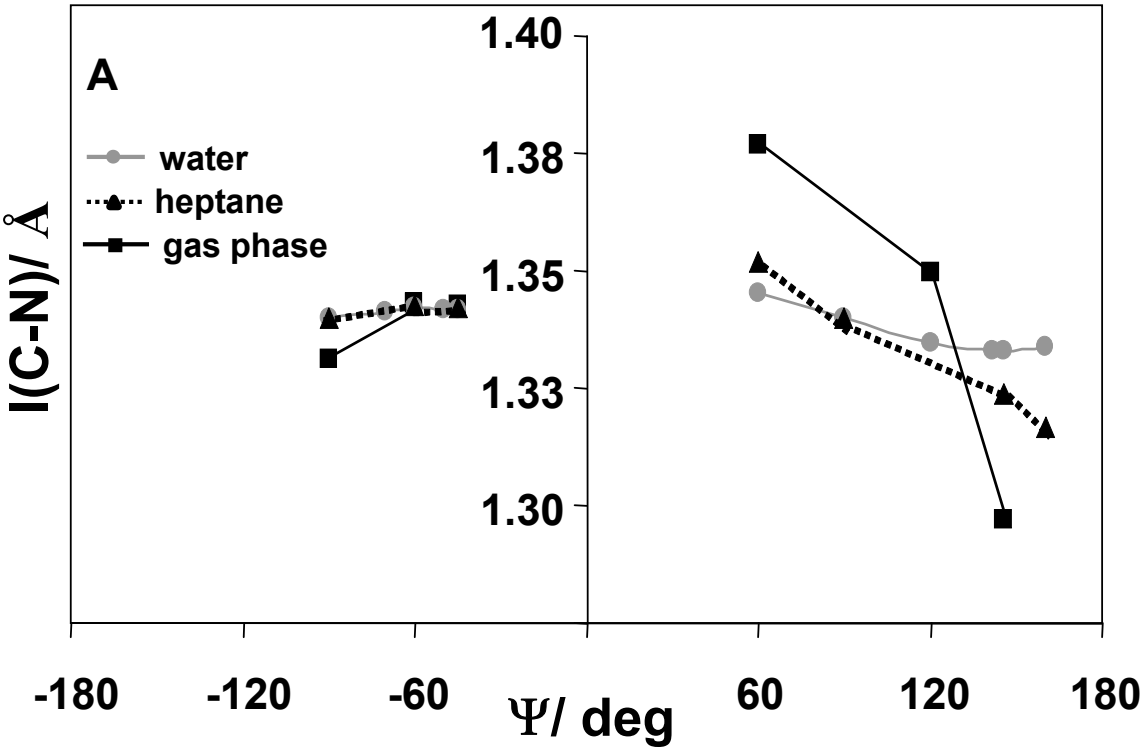

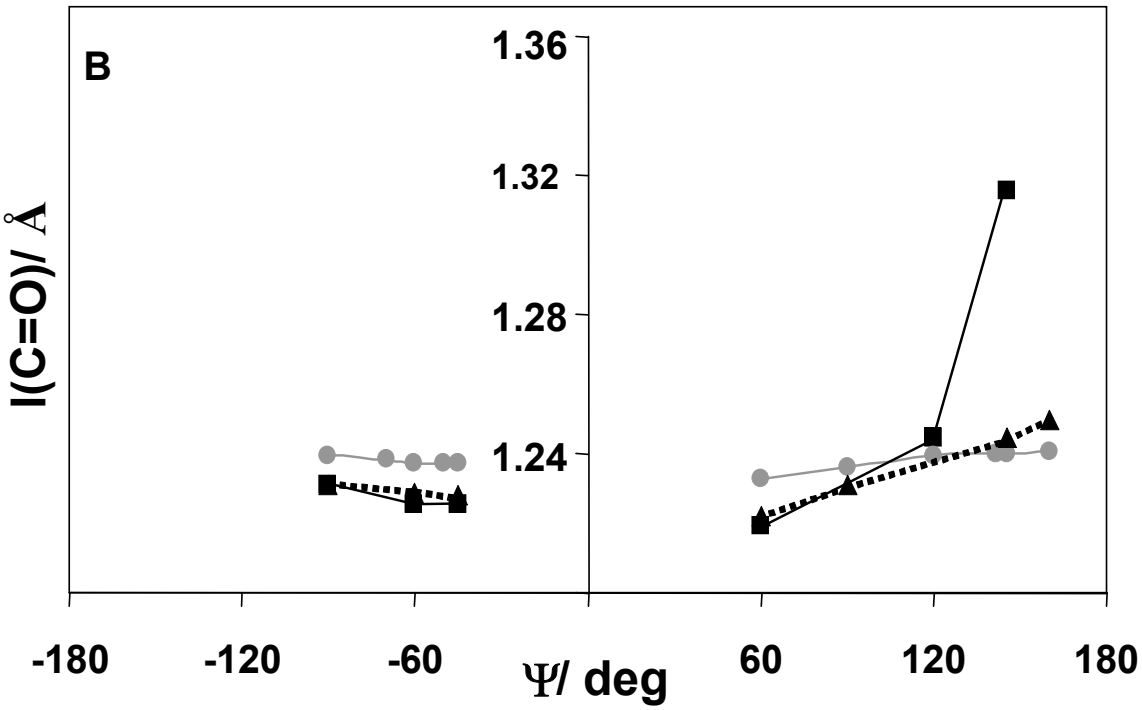
B
1.36
1.32
1.28
1.24
l(C=O)/ Å
-180
-120
-60
Ψ/ deg
60
120
180

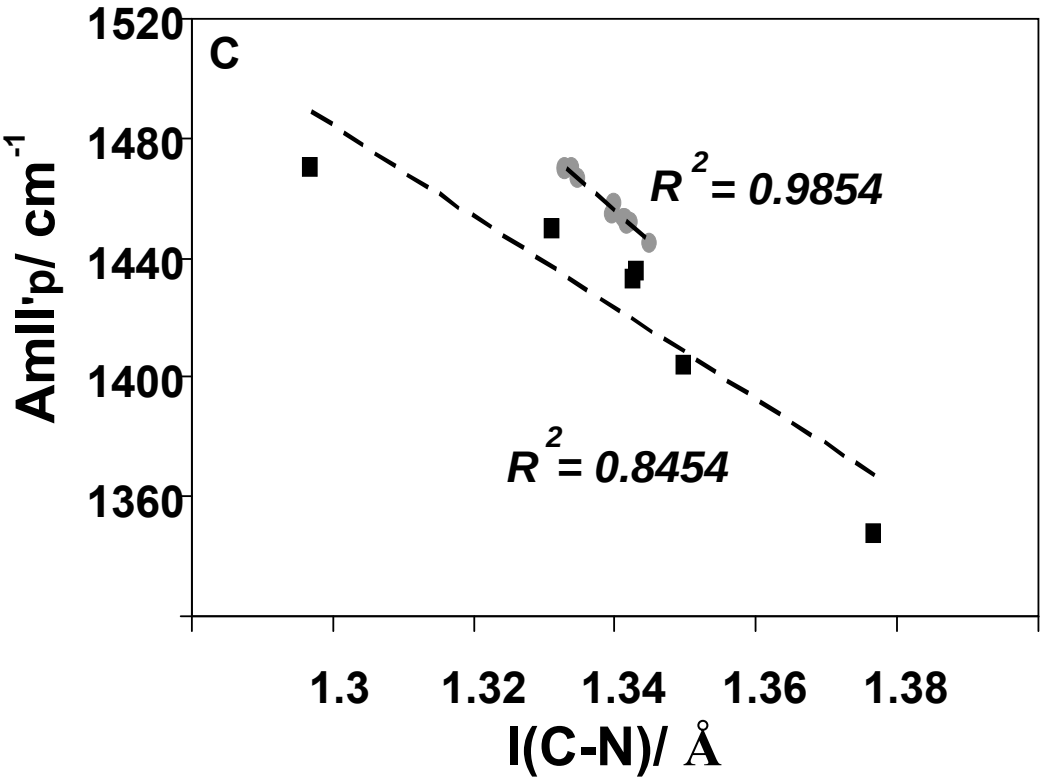
C
1520
1480
1440
1400
1360
AmII'p/ cm-1
R2 = 0.9854
R2 = 0.8454
1.3
1.32
1.34
1.36
1.38
l(C-N)/ Å

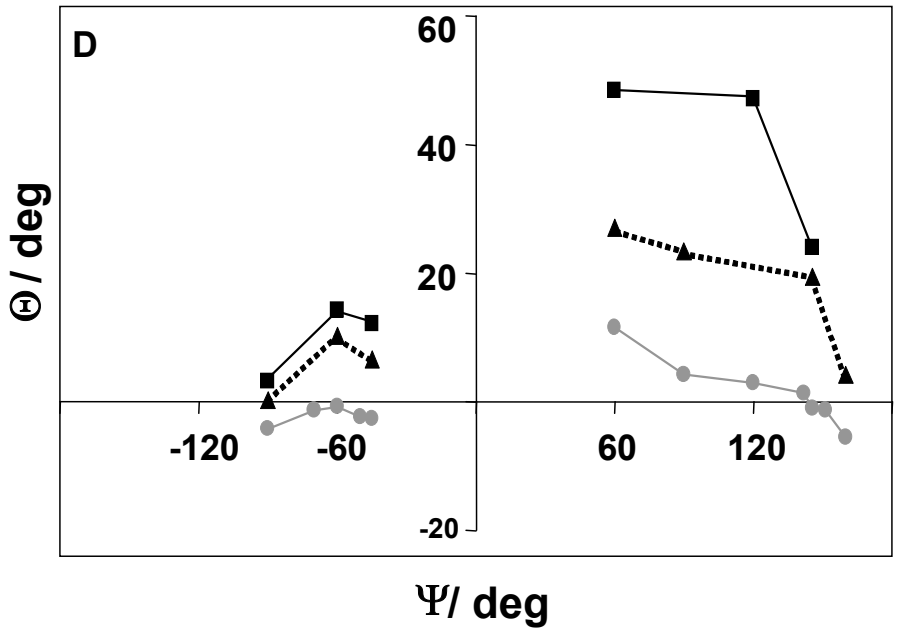

Figure 6.4: Calculated Ψ-dependence of the (A) C-N bond length (B) and C=O bond length of ala-pro in water, heptane and gas phase. C) Calculated dependence of ala-pro AmII'p frequency and C-N bond length in water (grey circles) and gas phase (black squares). D) Calculated Ψ-dependence of the peptide bond planarity angle (Θ) in water, heptane and gas phase

Our calculations reveal that the C-N bond length changes derive from changes in planarity of the peptide bond which can be monitored by the torsional angle Θ.[66,67]

$$\Theta = -\omega + \omega^1 + \pi$$

where the ω^1 torsional angle in the pro peptide bond is defined by atoms C_α, C, N, and C^*, where C^* is the carbon atom of the pyrrolidine ring (Fig. 6.5). The magnitude of Θ correlates with the extent of peptide bond nitrogen pyramidalization. Large Θ values indicate more extensive pyramidalization due to rehybridization of the amide nitrogen.[66-75]

The pyramidal nitrogen is sp^3 hybridized, while the planar nitrogen corresponds to sp^2 hybridization. Rehybridization directly impacts the C-N bond length. Structures with more sp^3

hybridization have longer C-N bond lengths then the shorter C-N bond lengths of sp^2–like structures.[66-75] Figure 6.4d displays the dependence of Θ upon Ψ rotation. As the Ψ-angle is varied, Θ changes, indicating that the Ψ conformation changes directly impact the non-planarity of the peptide bond. The C-N bond length change deriving from increased non-planarity of the peptide bond correlates with changes in the AmII'p band frequency (Fig 6.4).

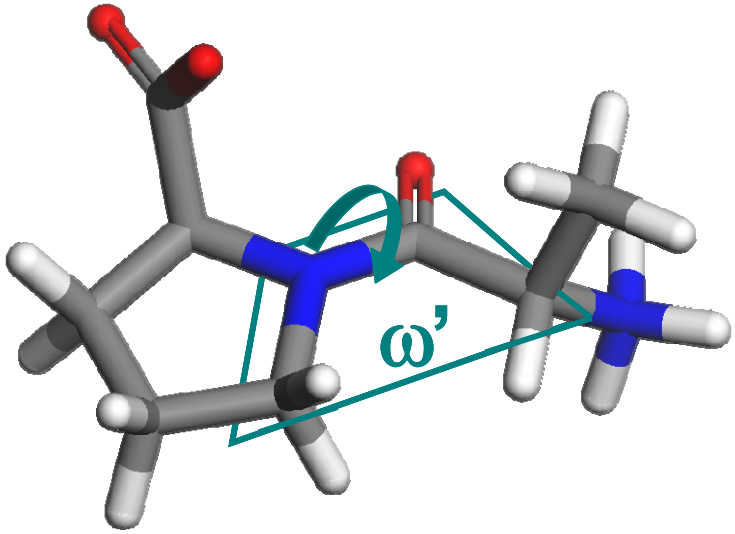

Figure 6.5: The torsional angle ω' of ala-pro is defined as a rotation around C-N bond in the dihedral plane defined by the C-C(O)-N-C* atoms.

Our results are in agreement with recent statistical analyses of protein conformation and its correlation with the ω-angle. Previously, MacArthur and Thornton's[70] statistical analysis of 85 high resolution x-ray structures of proteins from the protein databank (PDB) indicated a systematic dependence of the ω-angle on the (Φ,Ψ) angles. Recently, Esposito *et al's*[76] statistical analysis of 163 high resolution protein x-ray structures from the PDB suggested that the ω-angle values are strongly correlated with the Ψ-dihedral angle. In contrast, the ω-angle values shows an insignificant dependence on the Φ-dihedral angle.[76]

It should be noted that *ab initio* calculations of Asher *et al*[77] indicate that the frequency of the $AmIII_3$ vibration (C-N_s with in-phase NH_b) sinusoidally depends on the Ψ-dihedral angle. Recently, Mirkin and Krimm's[78] DFT calculations indicate that the N-H_s (amide A) frequency is also conformation sensitive. These authors attribute the conformation sensitivity of the N-H_s vibration to conformation-induced pyramidalization of the amide nitrogen.[78]

The conformational sensitivity of the various amide vibrations all appear to derive from the pyramidalization of the amide nitrogen, which directly impacts the amide bond geometry, resulting in significant changes in the amide vibrational frequencies. The general trend relating vibrational frequencies to (Φ,Ψ) conformation changes however, shows differences between the different amide vibrations. A lack of uniform conformation sensitivity amongst the various amide vibrations is due to differences in normal mode composition, e. g. the $AmIII_3$ frequency sinusoidally depends on the Ψ-dihedral angle, while the AmII'p frequency does not show such a simple Ψ-dependence. Normal mode composition analysis of non-pro, non-gly peptide bonds indicate that in addition to amide nitrogen pyramidization, Ψ-angle changes impact the coupling of C_α-H_b to N-H_b which significantly impact the $AmIII_3$ frequency.[77] The AmII'p vibration lacks the amide NH.

We probe the impact of solvent dielectric effect on the calculated Ψ-angle dependence of the AmII'p frequency by computing the AmII'p frequency of various ala-pro conformers in vacuum, water, heptane, and acetonitrile utilizing the PCM model. Our results indicate that changes in the dielectric constant of the surrounding media do not significantly impact the general trend relating the Ψ-angle to the AmII'p frequency (Fig 6.3 and 6.4). However, the frequency shifts are larger in low dielectric environments like heptane (fig 6.3). This effect

derives from stabilization of the non-planar peptide bond in low dielectric environments. Consequently, the deviations from peptide bond planarity are larger in low dielectric environments.

The stabilization of the non-planar peptide bond in low dielectric environments can be understood from the solvent's impact on the peptide bond's resonance structure. In polar solvents, the high dielectric environment stabilizes the charged form of the peptide bond [$^{-}$O(C)N^{+}H].[41,79] In this charged state, the carbonyl bond is elongated whereas, the C-N bond contracts as its double bond character increases. The increased sp^2 character of the C-N bond in the charged state results in a more planar peptide bond.[41] Thus, in polar solvents the non-planar peptide bond is energetically unfavorable.

In the gas phase the general trend relating the Ψ-angle changes to the AmII'p frequency, however appears to deviate at Ψ >120º. This deviation in the AmII'p frequency derives from the terminal NH_3^+ group's attempt to donate a proton to the peptide bond C=O. Enol formation is unfavorable in aqueous solutions.

Our investigation of the conformation and solvent-dependence of the AmII'p frequency indicate that the Ψ-angle and environment-dependence of various amide vibrations derive from pyramidalization of the amide nitrogen. Deviations from planarity whether induced via Ψ-angle conformation changes or changes in solvent dielectric constant, impact the planarity of the peptide bond. Consequently, as the sp^2 character of the amide nitrogen decreases, the C-N bond elongates whereas the C=O bond contracts. Consequently, those amide vibrations containing significant contributions from the nitrogen stretching (AmII, AmII', AmII'p, AmIII and N-H_s vibrations) show a frequency downshift, while the C=O_s (AmI) show frequency upshifts.

6.3.4 Φ-angle dependence

We calculated the Φ-dependence of the AmII'p frequency for zwitterionic ala-pro conformers in water, spanning the Φ-angle from -60˚ to -120˚ with Ψ = 145˚. Within this range of Φ, the AmII'p frequency varies by ~2 cm^{-1} (Fig 6.6), indicating the AmII'p frequency does not show any significant dependence on the Φ dihedral angles. We calculate similar results for ala-pro conformers in acetonitrile. This result is not surprising. As discussed above, Esposito *et al*'s[76] statistical analysis of 163 high resolution protein x-ray structures from the PDB indicates the variations in the ω angle do not show a significant correlation with the Φ-dihedral angle.

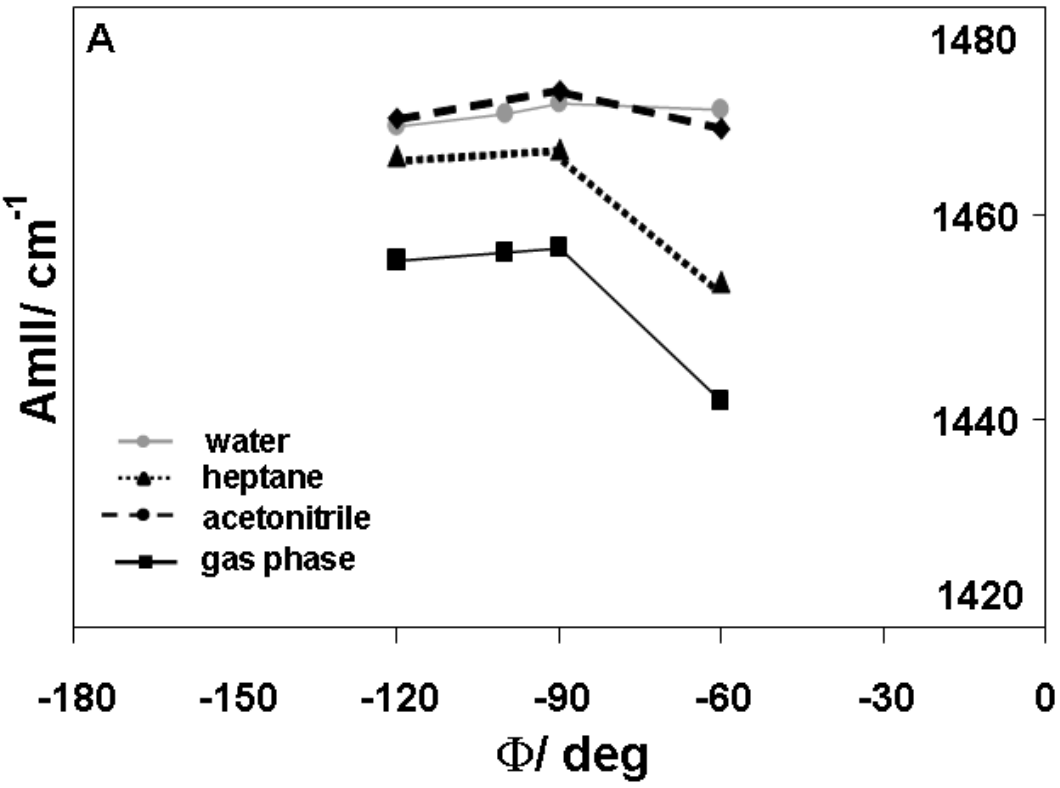
A
1480
1460
1440
1420
AmII/ cm-1
water
heptane
acetonitrile
gas phase
-180
-150
-120
-90
-60
-30
0
Φ/ deg

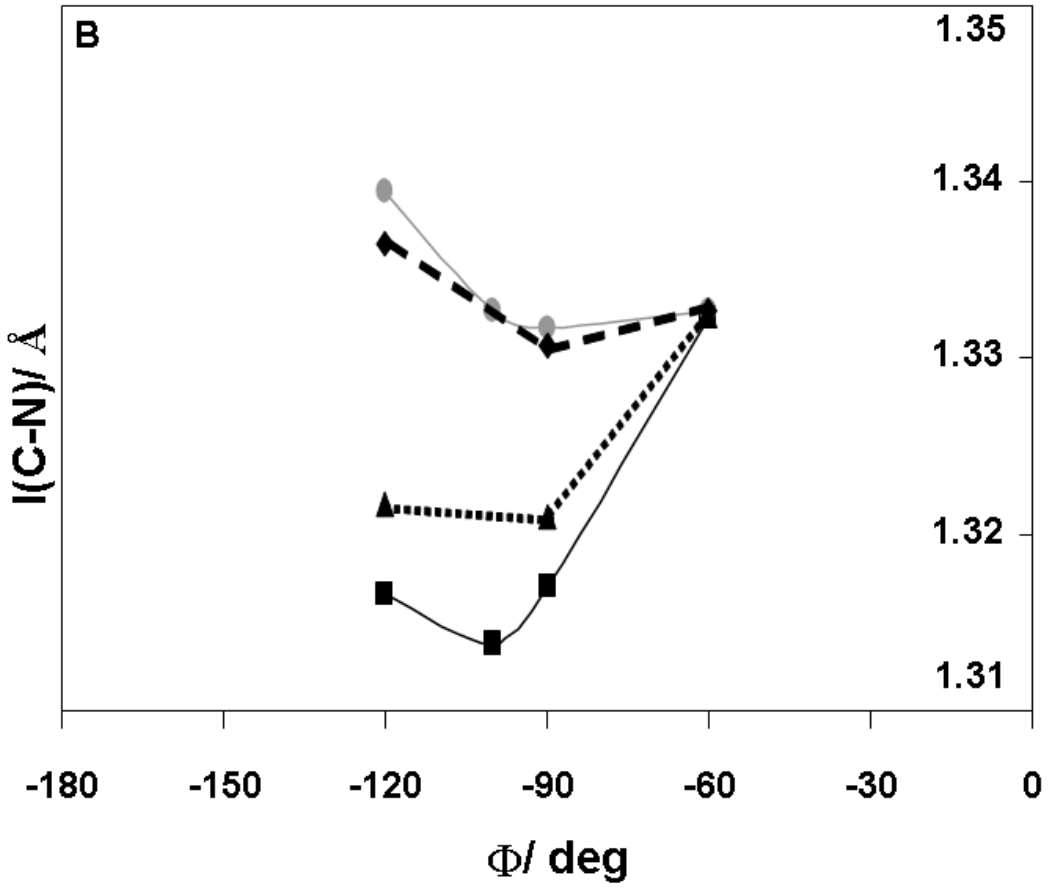
B
1.35
1.34
1.33
1.32
1.31
l(C-N)/ Å
-180
-150
-120
-90
-60
-30
0
Φ/ deg

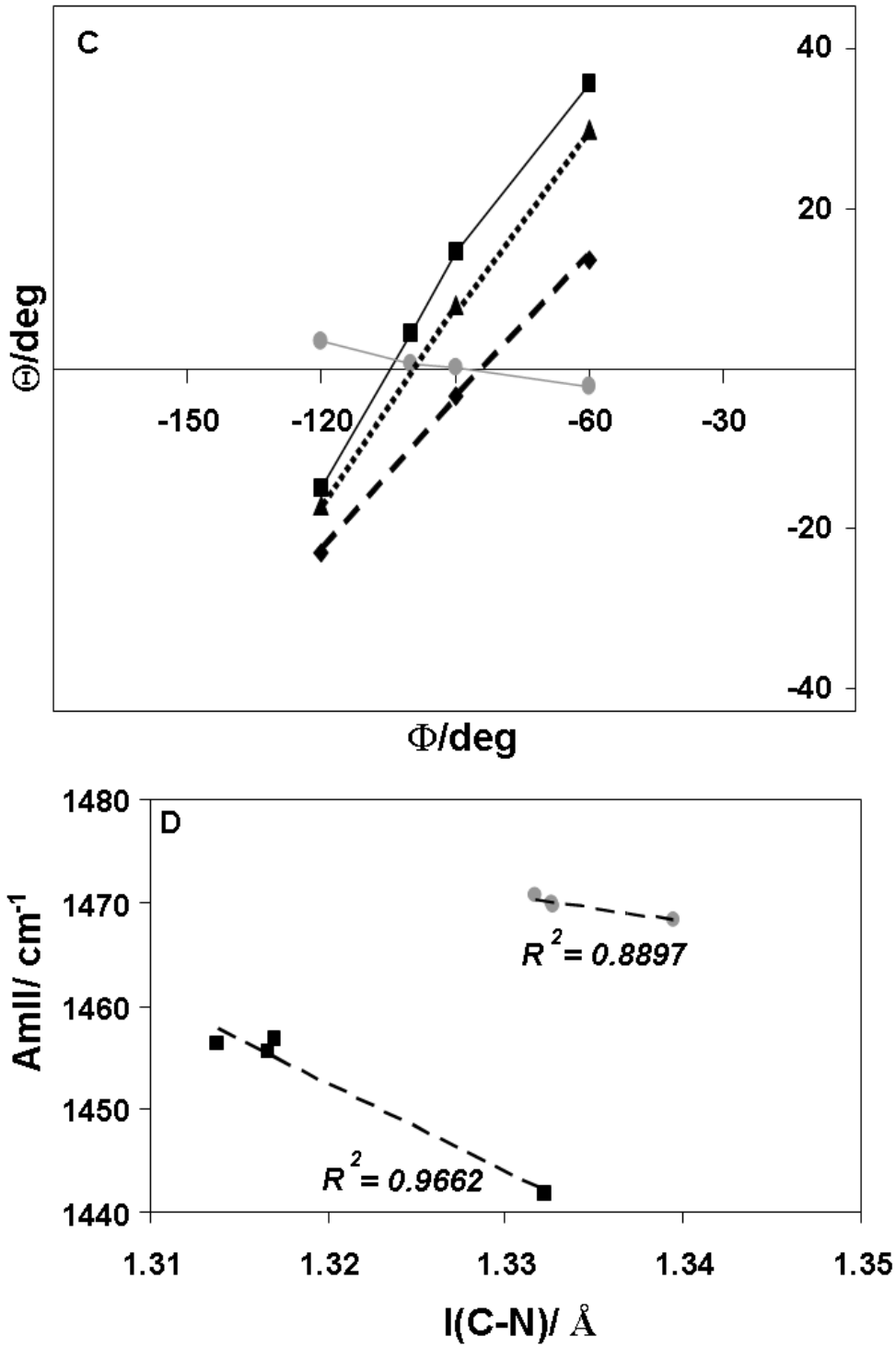

Figure 6.6: Calculated Φ-dependence of ala-pro (A) AmII'p frequency (B) C-N bond length (C) and the Θ planarity angle in water, heptane, acetonitrile and gas phase. (D) The calculated ala-pro AmII'p frequencies and C-N bond lengths in water (grey circles) and gas phase (black squares) are linearly correlated.

In low dielectric constant media like heptane and vacuum the calculated AmII'p frequency shows a small dependence on the Φ-dihedral angle. In particular, the AmII'p frequency dramatically decreases as the Φ-dihedral angle decreases from -90º to -60º (Fig 6.6). However, at high dielectric constant as in water or acetonitrile, there is no change in the AmII'p frequency over this range of Φ-angles. This can be explained by the normal mode composition analysis (Table 6.3). In the gas phase, the normal mode composition of the AmII'p vibration of the Φ = -60˚conformer contains significant amounts (25%) of methyl symmetric deformation. At higher dielectric constant the AmII'p normal mode composition changes because methyl symmetric deformation is replaced by methyl asymmetric deformation. This normal mode composition change results in an increase in the AmII'p frequency of the Φ = -60˚ ala-pro conformer in water as compared to ala-pro in heptane or gas phase.

6.3.5 Temperature Dependent Spectra of Polyproline

As shown in Fig 6.7, the AmII'p band of polyproline downshifts from 1472 to 1465 cm^{-1} as the solution temperature is increased from 5 to 65 ºC. The 7 cm^{-1} downshift derives from either a nearly 100% conversion from the *trans* to *cis* conformation or a conformation change along the Ψ-dihedral angle.

As shown in Fig 6.7 (insert) the CD spectra of polyproline at both 5 and 50 ºC show a small positive peak at 225 nm and a global minima at ~205 nm indicating a predominantly *trans* (PPII) conformation[80-84] at both temperatures. We do not observe any spectral features corresponding to the *cis* (PPI) conformation, which is known to show a medium intensity negative band at 198-200 nm, a strong positive band at ~214 nm and a weak negative band at

~231 nm.[84] These features are clearly lacking in the polyproline spectra at either temperature (Fig 6.7, insert).

Our CD results demonstrate that the temperature induced downshift in the Raman AmII'p frequency of polyproline (Fig 6.7) does not derive from isomerization of the pro peptide bond. Furthermore, the AmI' of polyproline does not show any significant change in band position with increasing temperature. As discussed above a *trans*→ *cis* isomerization is expected to upshift the AmI' band by ~13 cm^{-1}.

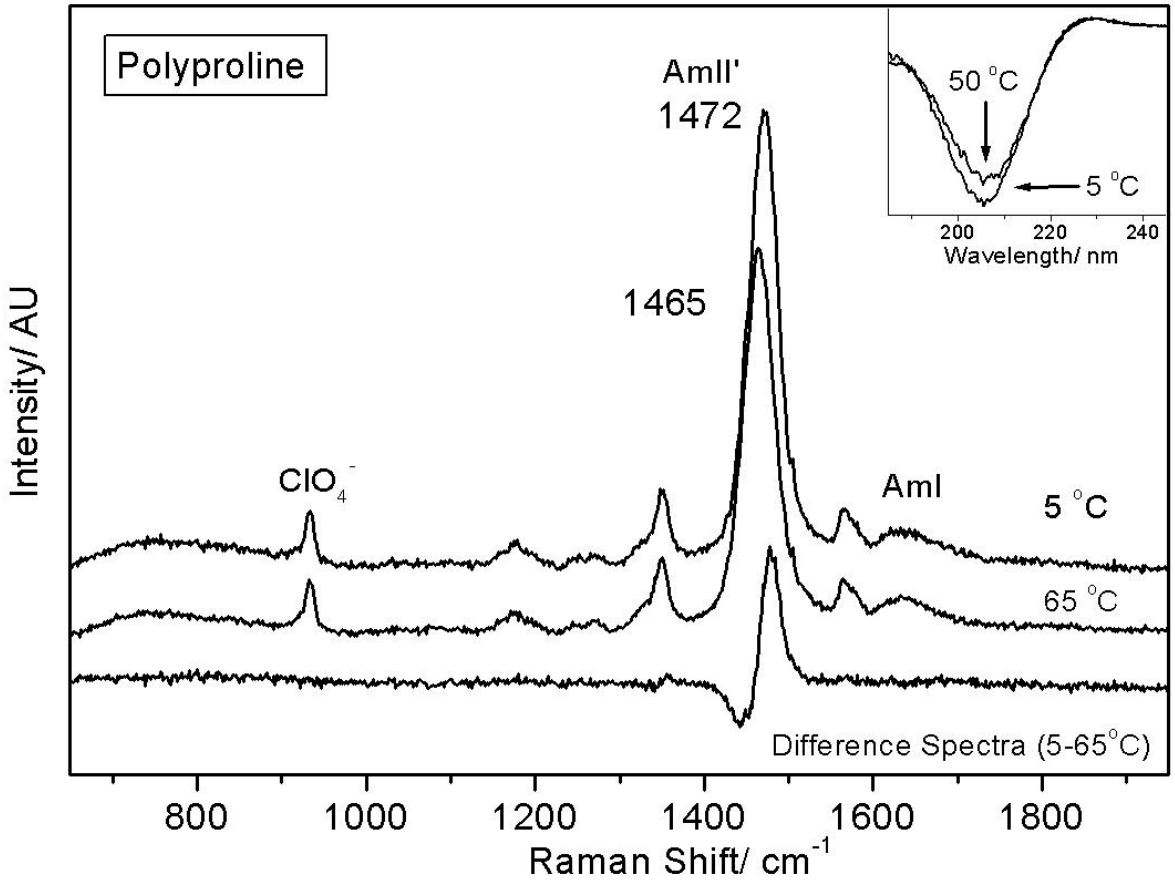

Figure 6.7: Polyproline shows a 7 cm^{-1} downshift in the AmII'p band frequency as the temperature increases from 5 to 65 ºC. The CD spectra (insert) of polyproline at 5 and 50 ºC shows characteristic features of the PPII conformation, indicating a lack of significant *trans* to *cis* isomerization with increasing temperature.

Our theoretical results, discussed above, indicate that the observed temperature induced downshift in the AmII'p frequency of polyproline is due to a small conformation change that distorts the native PPII conformation. As shown in Fig 6.3, starting from an ideal PPII conformation (Φ = -80º, Ψ = 145º) the observed 7 cm^{-1} shift could result from a 45º rotation of the Ψ angle from Ψ = 145º to Ψ = 100º. Previously, Swenson and Formanek[85] had suggested that the temperature-induced upshift in the AmI' frequency of polyproline may derive from slight changes in the Ψ-angle. These authors attributed the observed changes in polyproline to a temperature-induced disruption of pro-water interactions.[85]

Our results suggest that at high temperatures polyproline adopts a distorted PPII-like conformation that is more compact than the low temperature ideal PPII-like conformation (Fig 6.8). Our modeling of polyproline suggests that the distorted or compact PPII conformation should be ~26 % shorter than the ideal PPII conformation, which results in a ~25% decrease in the solvent accessible surface area of the collapsed polymer.

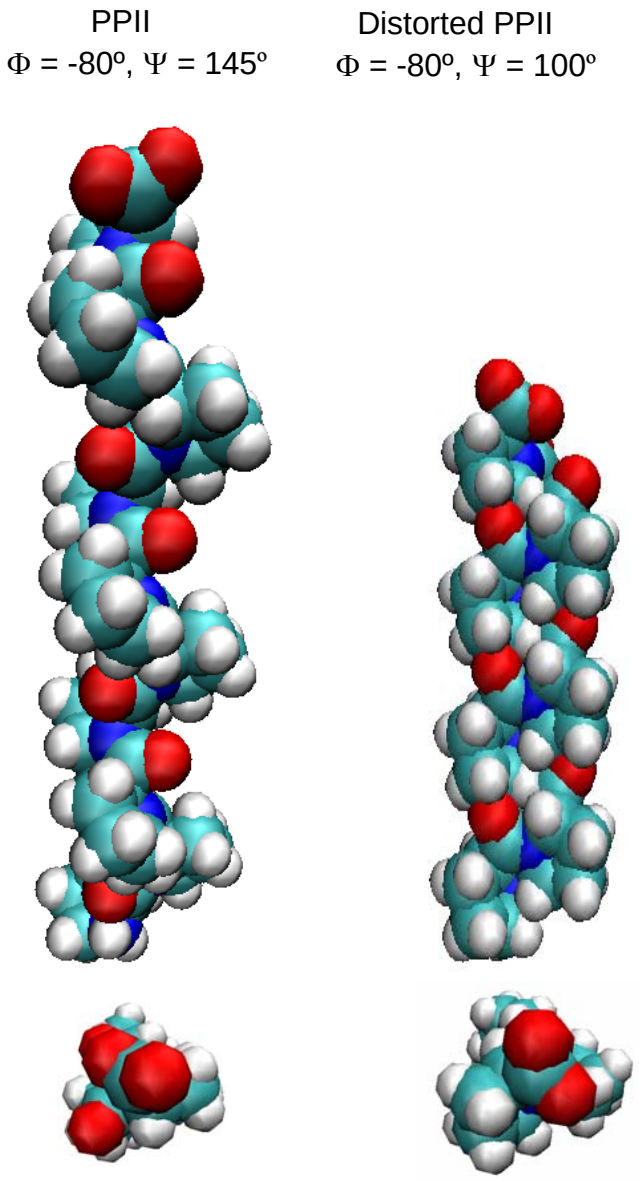

Figure 6.8: The structure of ideal PPII pro peptide (left) and the proposed structure of collapsed polyproline (right).

Fig 6.8 shows that the C=O bonds in the PPII conformation all line-up along the helical axis in an extended, water-exposed conformation. Water molecules can, thus, form an extensive hydrogen bonded network giving rise to an extended solvation shell. Explicit solvent Monte

Carlo simulations of Rose and co-workers[86] indicate that the more negative peptide-water stabilization interaction energy favors the PPII conformation over the β-strand conformation.[86]

Higher temperatures disrupt the favorable peptide-water/solvation shell interactions. Consequently, the polyproline peptide adopts a more compact conformation that significantly reduces its solvent accessible surface area. In the collapsed state of the polyproline peptide the amide C=O's are buried in hydrophobic crevices which cannot stabilize bridging water clusters or shells.[86] The attendant decrease in well-ordered water molecules in the solvation shell about pro's hydrophobic side chains results in increased entropy of the system, thus, stabilizing the peptide in its collapsed state.

6.4 CONCLUSIONS

Utilizing UVRR experiments and DFT calculations we systematically examined the dependence of the AmII'p frequency on hydrogen bonding, *cis-trans* isomerization, and conformation changes. Our UVRR results show that the AmII'p does not show any significant change in frequency with increasing temperature. These results indicate that the frequency of the AmII'p is not sensitive to changes in carbonyl-water hydrogen bonding.[40] Our theoretical calculations, indicate the AmII'p band frequency shows an 8 cm^{-1} downshift upon *trans* to *cis* isomerization of the peptide bond. This frequency dependence arises due to a slight elongation of the C-N bond in the *cis* conformer.

Our results indicate the AmII'p frequency is most sensitive to the planarity of the pro peptide bond as measured by its Θ dihedral angle. The peptide bond non-planarity can be modulated by

Ψ angle changes that push the amide nitrogen out of the peptide bond plane. The non-planar amide bond has a larger sp^3 character at the amide nitrogen and hence shows a larger C-N bond length as compared to the planar amide bond. The change in C-N bond length directly correlates with changes in the AmII'p frequency.

Our calculations indicate that in the allowed region of the Ramachandran space, the AmII'p frequency shows the largest variation in the extended state (PPII/β-strand) region, whereas the AmII'p frequency shows only a weak conformational dependence when it occurs within the α-helical region. Conformational changes causing alterations of the Φ-dihedral angle do not significantly impact the AmII'p frequency.

These results allow us to correlate changes in AmII'p frequency with conformation changes at the pro peptide bond. We calculate that the ~25 cm^{-1} downshift in the AmII'p frequency of pro-pro dipeptide between water and acetonitrile observed by Takeuchi and Harada[34] likely derives from a ~85º rotation of the Ψ-dihedral angle from Ψ ~ 60º to Ψ~145º.

We correlate the 7 cm^{-1} downshift in the AmII'p frequency of polyproline to a temperature-induced distortion of the native PPII structure (Ψ = 145º). At high temperatures the polyproline peptide adopts a compact PPII structure with Ψ = 100º, which results in a 25% decrease in its solvent accessible surface area, while its end-to-end distance decreases by ~26%. The hydrophobic collapse in polyproline is driven by a temperature-induced loss of favorable interactions between pro and its solvation shell.

ACKNOWLEDGMENTS: The authors would like to thank Dr. Sasmita Das for helpful discussions and NIH grant RO1 EB002053 for financial support.

6.5 REFERENCES

(1) Reiersen, H.; Rees, A. R. *Trends in Biochemical Sciences* **2001**, *26*, 679.
(2) Madison, V. *Biopolymers* **1977**, *16*, 2671.
(3) Venkatachalam, C. M.; Price, B. J.; Krimm, S. *Biopolymers* **1975**, *14*, 1121.
(4) Johnston, N.; Krimm, S. *Biopolymers* **1971**, *10*, 2597.
(5) Dorman, D. E.; Torchia, D. A.; Bovey, F. A. *Macromolecules* **1973**, *6*, 80.
(6) Tamburro, A. M.; Guantieri, V.; Pandolfo, L.; Scopa, A. *Biopolymers* **1990**, *29*, 855.
(7) Chiu, C. H.; Bersohn, R. *Biopolymers* **1977**, *16*, 277.
(8) Mclachlan, A. D. *Biopolymers* **1977**, *16*, 1271.
(9) Nemethy, G.; Scheraga Harold, A. *Biopolymers* **1984**, *32*, 2781.
(10) Harper, E. T.; Rose, G. D. *Biochemistry* **1993**, *32*, 7605.
(11) Tamaki, M.; Akabori, S.; Muramatsu, I. *Biopolymers* **1996**, *39*, 129.
(12) Garrett, R. H. G., Charles M.; *Biochemistry*, Second ed.; Saunders College Publishing: Philadelphia, Pa, 1999.
(13) Glaser, R. *Biophysics*; Springer: New York, 2000.
(14) Piela, L.; Nemethy, G.; Scheraga Harold, A. *Biopolymers* **1987**, *26*, 1587.
(15) Sankararamakrishnan, R.; Vishveshwara, S. *Biopolymers* **1990**, *30*, 287.
(16) Deber, C. M.; Glibowicka, M.; Woolley, G. A. *Biopolymers* **1990**, *29*, 149.
(17) Seshadri, S.; Oberg, K. A.; Fink, A. L. *Biochemistry* **1994**, *33*, 1351.
(18) Houry, W. A.; Scheraga Harold, A. *Biochemistry* **1996**, *35*, 11719.
(19) Mayr, L. M.; Odefey, C.; Schutkowski, M.; Schmid, F. X. *Biochemistry* **1996**, *35*, 5550.
(20) Pascher, T.; Chesick, J. P.; Winkler, J. R.; Gray, H. B. *Science* **1996**, *27*, 1558.
(21) Hagen, S. J.; Hofrichter, L.; Szabo, A.; Eaton, W. A. *Proc. Nat. Acad. Sci. U.S.A.* **1996**, *93*, 11615.
(22) Kubelka, J.; Hofrichter, J.; Eaton, W. A. *Current Opinion in Structural Biology* **2004**, *14*, 76.
(23) Lyubovitsky, J. G.; Gray, H. B.; Winkler, J. R. *J. Am. Chem. Soc.* **2002**, *124*, 5481.
(24) Reimer, U.; Scherer, G.; Drewello, M.; Kruber, S.; Schutkowski, M.; Fischer, G. *Journal of Molecular Biology* **1998**, *279*, 449.
(25) Grathwohl, C.; Wuthrich, K. *Biopolymers* **1976**, *15*, 2043.
(26) Grathwohl, C.; Wuthrich, K. *Biopolymers* **1976**, *15*, 2025.
(27) Swenson, C. A. *Biopolymers* **1971**, *10*, 2591.
(28) Rippon, W. B.; Koeing, J. L.; Walton, A. G. *J. Am. Chem. Soc.* **1970**, *92*, 7455.
(29) Harhay, G. P.; Hudson, B. *J. Phys. Chem* **1993**, *97*, 8158.
(30) Harhay, G. P.; Hudson, B. S. *J. Phys. Chem.* **1991**, *95*, 3511.
(31) Caswell, D. S.; Spiro, T. G. *Journal of the American Chemical Society* **1987**, *109*, 2796.
(32) Mayne, L.; Hudson, B. *J. Phys. Chem.* **1987**, *91*, 4438.
(33) Mayne, L.; Hudson, B. *Methods Enzymol.* **1986**, *130*, 331.

(34) Takeuchi, H.; Harada, I. *Journal of Raman Spectroscopy* **1990**, *21*, 509.
(35) Song, S.; Asher, S. A.; Krimm, S. *J. Am. Chem. Soc.* **1991**, *113*, 1155.
(36) Qian, W.; Mirkin N, G.; Krimm, S. *Chemical Physics Letters* **1999**, *315*, 125.
(37) Mirkin, N. G.; Krimm, S. *Journal of Molecular Structure* **1996**, *377*, 219.
(38) Cheam, T. C.; Krimm, S. *Spectrochimica Acta Part A: Molecular Spectroscopy* **1984**, *40*, 481.
(39) Jordon, T.; Mukerji, I.; Yang, W.; Spiro, T. G. *J. Biol. Chem.* **1996**, *379*, 51.
(40) Triggs, N. E.; Valentini, J. J. *J. Phys. Chem* **1992**, *96*, 6922.
(41) Myshakina, N. S.; Ahmed, Z.; Asher, S. A. *J. Phys. Chem. B, in press* **2008**.
(42) Urry, D. W. *Journal of Physical Chemistry B* **1997**, *101*, 11007.
(43) Ahmed, Z.; Scaffidi, J.; Asher, S. A. *Biopolymers* **2008**, *in press*.
(44) Bykov, S. B.; Lednev, I. K.; Ianoul, A.; Mikhonin, A. V.; Asher, S. A. *Appl. Spectrosc.* **2005**, *59*, 1541.
(45) Frisch, M. J. T., G. W.; Schlegel, H. B.; Scuseria, G. E.; Robb, M. A.; Cheeseman, J. R.; Montgomery, Jr., J. A.; Vreven, T.; Kudin, K. N.; Burant, J. C.; Millam, J. M.; Iyengar, S. S.; Tomasi, J.; Barone, V.; Mennucci, B.; Cossi, M.; Scalmani, G.; Rega, N.; Petersson, G. A.; Nakatsuji, H.; Hada, M.; Ehara, M.; Toyota, K.; Fukuda, R.; Hasegawa, J.; Ishida, M.; Nakajima, T.; Honda, Y.; Kitao, O.; Nakai, H.; Klene, M.; Li, X.; Knox, J. E.; Hratchian, H. P.; Cross, J. B.; Bakken, V.; Adamo, C.; Jaramillo, J.; Gomperts, R.; Stratmann, R. E.; Yazyev, O.; Austin, A. J.; Cammi, R.; Pomelli, C.; Ochterski, J. W.; Ayala, P. Y.; Morokuma, K.; Voth, G. A.; Salvador, P.; Dannenberg, J. J.; Zakrzewski, V. G.; Dapprich, S.; Daniels, A. D.; Strain, M. C.; Farkas, O.; Malick, D. K.; Rabuck, A. D.; Raghavachari, K.; Foresman, J. B.; Ortiz, J. V.; Cui, Q.; Baboul, A. G.; Clifford, S.; Cioslowski, J.; Stefanov, B. B.; Liu, G.; Liashenko, A.; Piskorz, P.; Komaromi, I.; Martin, R. L.; Fox, D. J.; Keith, T.; Al-Laham, M. A.; Peng, C. Y.; Nanayakkara, A.; Challacombe, M.; Gill, P. M. W.; Johnson, B.; Chen, W.; Wong, M. W.; Gonzalez, C.; and Pople, J. A. Gaussian 03; Revision C.01 ed.; Gaussian, Inc.: Wallingford CT., 2004.
(46) Kohn, W.; Sham, L. J. *Physical Review* **1965**, *137*, 1697.
(47) Parr, R. G.; Yang, W. *Density-functional theory of atoms and molecules*; Oxford Univ. Press: Oxford, 1989.
(48) Hohenberg, P.; Kohn, W. *Phys. Rev.* **1964**, *136*, B864.
(49) Becke, A. D. *Journal of Chemical Physics* **1993**, *98*, 5648.
(50) Lee, C.; Yang, W.; Parr, R. G. *Physical Review B: Condensed Matter and Materials Physics* **1988**, *37*, 785.
(51) Miehlich, B.; Savin, A.; Stoll, H.; Preuss, H. *Chemical Physics Letters* **1989**, *157*, 200.
(52) Irikura, K. K.; Johnson, R. D., III; Kacker, R. N. *Journal of Physical Chemistry A* **2005**, *109*, 8430.
(53) Halls, M. D.; Velkovski, J.; Schlegel, H. B. *Theoretical Chemistry Accounts* **2001**, *105*, 413.
(54) Ponder, J. W. TINKER, Software Tools for Molecular Design. In *http://dasher. wustl. edu/tinker.*
(55) Humphrey, W.; Dalke, A.; Schulten, K. *J. Molec. Graphics* **1996**, *14*, 33.
(56) Hinderaker, M. P.; Raines, R. T. *Prot. Sci.* **2003**, *12*, 1188.
(57) Mikhonin, A. V.; Ahmed, Z.; Ianoul, A.; Asher, S. A. *Journal of Physical Chemistry B* **2004**, *108*, 19020.

(58) Lednev, I. K.; Karnoup, A. S.; Sparrow, M. C.; Asher, S. A. *J. Am. Chem. Soc.* **1999**, *121*, 8074.
(59) Manas, E. S.; Getahun, Z.; Wright, W. W.; DeGrado, W. F.; Vanderkooi, J. M. *J. Am. Chem. Soc.* **2000**, *122*, 9883.
(60) Neidigh, J. W.; Fesinmeyer, R. M.; Andersen, N. H. *Nature Structural Biology* **2002**, *9*, 425.
(61) Chen, X. G.; Asher, S. A.; Schweitzer-Stenner, R.; Mirkin, N. G.; Krimm, S. *Journal of the American Chemical Society* **1995**, *117*, 2884.
(62) Torii, H.; Tasumi, M. *Journal of Raman Spectroscopy* **1998**, *29*, 81.
(63) Torii, H.; Tatsumi, T.; Tasumi, M. *J. Raman Spectrosc.* **1998**, *29*, 537.
(64) Eaton, G.; Symons, C. R.; Rastogi, P. P. *J. Chem. Soc., Faraday Trans.1* **1989**, *85*, 3257.
(65) Ham, S.; Kim, J.-H.; Lee, H.; Cho, M. *Journal of Chemical Physics* **2003**, *118*, 3491.
(66) Ramachandran, G. N.; Lakshminarayanan, A. V.; Kolaskar, A. S. *Biochimica et Biophysica Acta, Protein Structure and Molecular Enzymology* **1973**, *303*, 8.
(67) Ramek, M.; Yu, C.-H.; Sakon, J.; Schafer, L. *J. Phys. Chem. A.* **2000**, *104*, 9636.
(68) Selvarengan, P.; Kolandaivel, P. *Bioorganic Chemistry* **2005**, *33*, 253.
(69) Ramachandran, G. N. *Biopolymers* **1968**, *6*, 1494.
(70) MacArthur, M. W.; Thornton, J. M. *J. Mol. Biol.* **1996**, *264*, 1180.
(71) Otani, Y.; Nagae, O.; Naruse, Y.; Inagaki, S.; Ohno, M.; Yamaguchi, K.; Yamada, G.; Uchiyama, M.; Ohwada, T. *J. Am. Chem. Soc* **2003**, *125*, 15191.
(72) Krimm, S.; Mirkin N, G. *J. Phys. Chem. A.* **2004**, *108*, 5438.
(73) Lopez-Garriga, J. J.; Hanton, S.; Babcock, G. T.; Harrison, J. F. *J. Am. Chem. Soc.* **1986**, *108*, 7251.
(74) Lopez, X.; Mujika, J. I.; Blackburn, G. M.; Karplus, M. *J. Phys. Chem. A.* **2003**, *107*, 2304.
(75) Alkorta, I.; Cativiela, C.; Elguero, J.; Gil, A. M.; Jimenez, A. I. *New J. Chem.* **2005**, *29*, 1450.
(76) Esposito, L.; De Simone, A.; Zagari, A.; Vitagliano, L. *J. Mol. Struct.* **2005**, *347*, 483.
(77) Asher, S. A.; Ianoul, A.; Mix, G.; Boyden, M. N.; Karnoup, A.; Diem, M.; Schweitzer-Stenner, R. *Journal of the American Chemical Society* **2001**, *123*, 11775.
(78) Mirkin, N. G.; Krimm, S. *Journal of Physical Chemistry A* **2004**, *108*, 5438.
(79) Milner-White, E. J. *Protein Sci.* **1997**, *6*, 2477.
(80) Creamer, T. P. *Proteins: Structure, Function, and Genetics* **1998**, *33*, 218.
(81) Tiffany, M. L.; Krimm, S. *Biopolymers* **1968**, *6*, 1379.
(82) Tiffany, M. L.; Krimm, S. *Biopolymers* **1969**, *8*, 347.
(83) Tiffany, M. L.; Krimm, S. *Biopolymers* **1972**, *11*, 2309.
(84) Kakinoki, S.; Hirano, Y.; Oka, M. *Polymer Bulletin* **2005**, *53*, 109.
(85) Swenson, C. A.; Formanek, R. *The Journal of Physical Chemistry* **1967**, *71*, 4073.
(86) Mezei, M.; Fleming, P. J.; Srinivasan, R.; Rose, G. D. *Proteins: Structure, Function, and Bioinformatics* **2004**, *55*, 502.
(87) Li, B.; Alonso, D. O. V.; Bennion, B. J.; Daggett, V. *Journal of the American Chemical Society* **2001**, *123*, 11991.
(88) Gosline, J. M. *Biopolymers* **1978**, *17*, 697.
(89) Ohgo, K.; Ashida, J.; Kumashiro, K. K.; Asakura, T. *Macromolecules* **2005**, *38*, 6038.
(90) Reiersen, H.; Clarke, A. R.; Rees, A. R. *J. Mol. Biol.* **1998**, *283*, 255.

CHAPTER 7

UV-resonance Raman Determination of Molecular Mechanism of Poly(*N*-Isopropylacrylamide) Volume Phase Transition Hydrophobic Collapse

This chapter is being prepared for submittal for publication. The co-authors are Zeeshan Ahmed, Edward A. Gooding, Konstantin V. Pimenov, Luling Wang, Sanford A. Asher

7.0 UV-RESONANCE RAMAN DETERMINATION OF MOLECULAR MECHANISM OF POLY(*N*-ISOPROPYLACRYLAMIDE) VOLUME PHASE TRANSITION HYDROPHOBIC COLLAPSE

Poly(N-isopropylacrylamide) (PNIPAM) is the premier example of a macromolecule that undergoes a hydrophobic collapse when heated above its lower critical solution temperature (LCST). Here we utilize, dynamic light scattering, H-NMR, steady-state and time-resolved UVRR measurements to determine the molecular mechanism of PNIPAM's hydrophobic collapse. Our steady-state results indicate that in the collapsed state the amide bonds of PNIPAM do not engage in inter-amide hydrogen bonding, but are hydrogen bonded to water molecules. At low temperatures, the amide bonds of PNIPAM are predominantly fully water hydrogen bonded, whereas, in the collapsed state one of the two normal C=O hydrogen bonds is lost. The NH-water hydrogen bonding, however, remains unperturbed by the PNIPAM collapse. Our kinetic results indicate a mono-exponential collapse with τ~360 ($\pm$85) ns. The collapse rate indicates a persistence length of n~10. At lengths shorter than the persistence length the polymer acts as an elastic rod, whereas, at lengths longer than the persistence length the polymer backbone conformation forms a random coil. Based on these results we propose that at low temperatures PNIPAM adopts an extended, water-exposed conformation that is stabilized by

favorable NIPAM-water solvation shell interactions which stabilize large clusters of water molecules. At elevated temperatures, thermal agitation disrupts these interactions. The PNIPAM+water polymer undergoes a volume phase transition, expels water and shrinks to a compact conformation that reduces its hydrophobic solvent accessible surface area. In this compact state, PNIPAM forms small hydrophobic nano-pockets where the (*i*, *i* +3) isopropyl groups make hydrophobic contacts. A persistent length of n~10 suggests a cooperative collapse where hydrophobic interactions between adjacent hydrophobic pockets stabilize the collapsed PNIPAM.

7.1 INTRODUCTION

Poly(N-isopropylacrylamide) (PNIPAM) is the premier example of a macromolecule that undergoes a hydrophobic collapse when heated above its lower critical solution temperature (LCST).[1-17] Below its LCST, PNIPAM exists in a swollen, well-hydrated state that is nearly refractive index matched to water; the polymer weakly scatters light.[1-6,18,19] At the transition temperature (T_t~32-35 ˚C) the polymer undergoes a hydrophobic collapse, expels water and adopts a compact state[3,5,6] and shows a dramatic increase in turbidity.

This temperature dependent PNIPAM collapse, which in the physics community is called a "volume phase transition" (VPT) [1-6,19] gives rise to very large volume changes for cross-linked PNIPAM, which can be used to actuate chemical and physical phenomena. This VPT has been utilized in drug delivery,[20,21] synthesis[22,23] (where PNIPAM serves as a nanoreactor) and sensor

development.[3,24,25] For these applications, PNIPAM nanogels are functionalized such that environmental changes induce PNIPAM chemical changes (e.g. deprotonation of a carboxylic acids) that shift the PNIPAM's critical transition temperature. The PNIPAM hydrophobic collapse can thus be designed to occur in response to a specific chemical stimulus such as pH changes.[26-29]

The PNIPAM hydrophobic collapse results from the temperature dependence of PNIPAM-water interactions.[27,28,30-33] Presumably, at low temperatures the favorable enthalpy of amide-water hydrogen bonding stabilizes the swollen state of PNIPAM by overcoming the unfavorable entropy of water solvation of the isopropyl hydrophobic groups.[34] As the temperature increases towards the VPT the unfavorable hydrophobic solvation entropy eventually dominates, forcing the PNIPAM collapse, releasing water into the bulk. Recent dielectric relaxation studies suggest that the average number of hydrating water molecules per NIPAM group falls from 11 to ~ 2 upon the hydrophobic collapse.[35,36]

The temperature dependence of the entropy-enthalpy balance determines the critical VPT temperature. This VPT is similar to the "inverse temperature transition" of elastin-like peptides that undergo well-known transitions from an extended, highly mobile conformation to a collapsed molten globule-like conformation at higher temperatures.[37-41] This VPT of PNIPAM and elastin-like peptides is related to the cold-denaturation[42-48] phenomenon observed in proteins such as myoglobin. Proteins typically undergo a transition from a native compact state to disordered, expanded state as the solution temperature *decreases*.[49,50] Protein cold denaturation appears also to be driven by the temperature dependence of the free energy of solvation of the hydrophobic groups.[50] At higher physiological temperatures, the low hydrophobic solvation entropy favors compact or folded protein conformations where hydrophobic groups are protected

from water. At lower temperatures expanded conformations with hydrophobic groups exposed to water become stabilized over the folded, compact conformations.[42-50]

There is intense interest in developing a molecular understanding of the molecular mechanism of PNIPAM's VPT. In the work here, we probe this VPT using monodisperse, highly charged PNIPAM nanogels which undergo the VPT.[3,51] This simple homogeneous system can be straight-forwardly studied and the VPT here is not confounded by processes such as polymer aggregation.

Kinetic studies of macroscopic PNIPAM hydrogels find that the rate of polymer collapse should scale as l^{-2}, where l is the smallest dimension of the material.[52,53] Thus, PNIPAM nanogels are expected to show relatively fast collapse kinetics, as compared to macroscopic gels that take hours or days.[3] Indeed, Wang *et al*'s[1] T-jump kinetic turbidity measurements of ~400 nm diameter PNIPAM nanoparticles showed a single exponential collapse with an apparent time constant of ~390 ns. In addition, Reese *et al*[3] utilized kinetic turbidity measurements following a laser induced T-jump to examine the collapse of ~350 nm diameter PNIPAM nanogels and observed a multi-exponential process with a major component occurring in less than 1 μs.[3] Reese *et al*[3] also showed that individual PNIPAM nanoparticles show an apparent single exponential collapse with $\tau \sim 120$ ns.

To date most spectroscopic studies of the PNIPAM's hydrophobic collapse have focused on its steady state behavior. Utilizing FTIR,[34,54-59] ATR/FTIR[60] and Raman spectroscopy[27,28,30,31,33] several groups independently determined that PNIPAM's hydrophobic collapse disrupts the hydration of both hydrophobic and hydrophilic groups. In particular, FTIR[34,54-59] and ATR/IR[60] studies focusing on the AmI region (C=O stretch) showed that hydrogen bonding of the amide carbonyl changes with temperature. The consensus appears to be

that the hydrogen bonds present at low temperatures are disrupted upon the higher temperature PNIPAM hydrophobic collapse.

In this study we utilize steady-state and time-resolved UV resonance Raman (UVRR) spectroscopy to directly examine the equilibrium and kinetics of amide dehydration during the PNIPAM's hydrophobic collapse. Our results indicate that the amide dehydration is complete within ~1 μs.

7.2 EXPERIMENTAL

The ~170 nm diameter PNIPAM nanoparticles (T_t ~33 ºC) were synthesized using previously published techniques.[51] Briefly, the PNIPAM particles were synthesized by dispersion polymerization. 1.40 g NIPAM (Aldrich, used after recrystallization), 0.0242 g 2-acrylamido-2-methyl-1-propanesulfonic acid (ionic co-monomer, Aldrich), 0.0659 g N, N′-methylenebisacrylamide (cross-linker, Fluka), 0.036 g sodium dodecyl sulfate (surfactant, Aldrich) and 0.088 g ammonium persulfate (initiator, Sigma-Aldrich) were added to 100 mL 18 MΩ deionied water and reacted at 70 ˚C for 4 hr under stirring. The crude product was filtered by glass wool and dialysized against DI water by using a Snakeskin™ dialysis tube (10,000 MWCO) for 2 weeks to remove impurities such as unreacted NIPAM monomers, dodecyl sulfate and single chains. Deuterium labeled d_7-PNIPAM monomers (the isopropyl group hydrogens are deuterated) were acquired from Cambridge Isotopes and used to synthesize ~100 nm diameter d_7-PNIPAM particles. Temperature dependent changes in particle size were measured by dynamic light scattering (ZetaPALS, Brookhaven Instruments Corporation).

The solid sample of dried PNIPAM nanoparticles was prepared by allowing a sample of PNIPAM particles to slowly dehydrate at room temperature under a steady flow of dry nitrogen gas.

The hydrogen-deuterium exchange (HDX) studies were carried out on a 300 MHz H-NMR instrument (Bruker). A 100 μl solution of 0.73% wt/vol of PNIPAM in water at 20º and 55 ºC was diluted with D_2O (at 20º and 55 ºC, respectively) to a final volume of 1 ml. All H-NMR spectra were immediately acquired following solution preparation at 20º and 55 ºC, except for one room temperature H-NMR spectra which was allowed to sit for 24 hr to rule-out any slow exchange. The time between solution preparation and spectral acquisition was less then 5 min. The 20 ºC NMR spectra of PNIPAM in H_2O only was acquired utilizing 850 μl of stock PNIPAM solution with 50 μl of CD_3CN for deuterium locking.

A home built UV resonance Raman (UVRR) spectrometer was used for both steady-state and kinetic measurements.[61] The T-jump results were obtained with a home-built nanosecond pump-probe setup. The probe laser was a 1 kHz repetition rate Photonics Industries Ti:Sapphire laser which produced ~204-nm laser light with an average energy of 2.4 μJ per pulse and a pulse width (FWHM) of 14 ns. The output beam was collimated and focused to a spot size of ~ 100 μm at the sample.

The pump laser was a 1 kHz repetition rate Photonics Industries YLF-pumped OPO, which produced 1.9 μm pulses with an average energy of 1 mJ per pulse and a pulse width of 13 ns. The IR beam was collimated, made collinear with the UV beam and focused to a spot size of ~165 μm at the sample. The pump and probe lasers were synchronized and a variable delay was obtained by using a digital pulse generator (DG535, Stanford Research systems, Inc). These

delay times were confirmed by measuring reflections of the pump and probe pulses with fast photodiodes by using an oscilloscope (TDS 3054B, Tektronix).

A 10 ml solution of 0.73% wt/vol PNIPAM nanoparticles was circulated in a free surface, temperature controlled stream. The concentration of PNIPAM was chosen to match the sample absorption for both the UV probe ($OD_{204\ nm}$ = 156) and IR pump laser. This ensures that during the T-jump experiment, the UV laser probes the heated volume of the sample stream.[62]

A ~165^{o} laser excitation backscattering geometry was used for sampling. The collected light was dispersed by a subtractive double monochromator onto a back thinned CCD camera (400 B Princeton Instruments-Spec 10 System).[61] Four 2 min. spectra were averaged.

The magnitude of the T-jump was determined from the UVRR water O-H stretching region which is highly temperature dependent.[62,63] T-jump spectra were compared to equilibrium spectra taken at different temperatures (data not shown), demonstrating a ~15 °C T-jump from the initial equilibrium temperature of 30 ºC to a final temperature of 45 ºC.

The steady-state UVRR spectra were acquired on the same spectrometer by using only the probe laser. The UVRR PNIPAM spectra in the amide region taken with and without T-jumps were normalized to the intensity of the isopropyl group's CH_3 deformation band at ~1460 cm^{-1} and subtracted from the equilibrium 30 °C spectrum.

The transient difference feature in the AmI region was fitted to the convolution of a Gaussian instrument function with the sum of a step function and an exponential rise. The step function accounts for the essentially instantaneous spectral changes due to the T-jump which were not associated with PNIPAM structural changes, while the exponential rise time derives from the dynamics of the polymer structural collapse. The 22 ns width of the Gaussian instrument function is due to the pump and probe laser pulse widths and the 15 ns timing jitter.

The instrument function was determined by fitting the difference Raman signal in the water O-H stretching region around 3300 cm^{-1}. The T-jump gives rise to an essentially instantaneous temperature change, since thermalization of near-IR laser excitation in water is known to occur on the psec timescale.[63]

7.3 RESULTS AND DISCUSSION:

7.3.1 DLS measurements

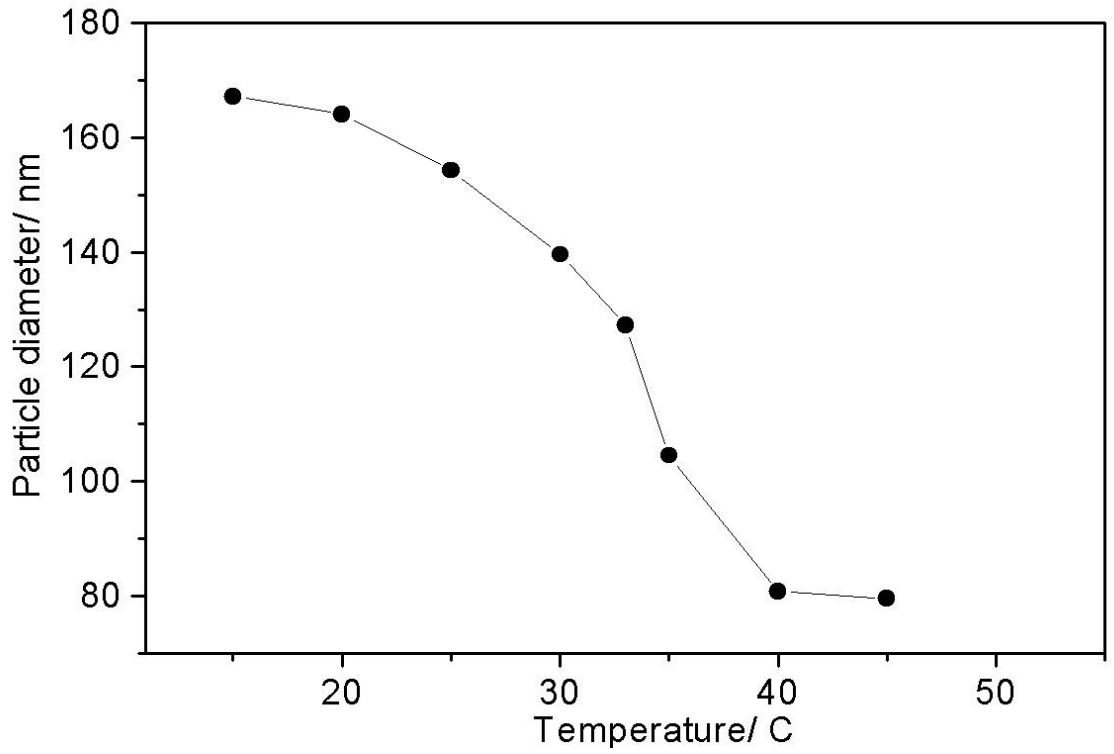

Figure 7.1: Temperature dependent DLS measurements show that PNIPAM particles collapse between 20 ºC and 40 ºC with a transition temperature of ~33 ºC

The Fig 7.1 temperature dependent DLS measurements indicate that between 4 ºC and 45 ˚C the particle size collapses from 167 nm to 80 nm, with a transition temperature T_t ~ 33 ºC. The PNIPAM particles undergo a hydrophobic collapse from a high-volume water-swollen state to a 9-fold smaller volume, compact state.[3,5,6] The volume change suggests an ~88% reduction in water molecules inside the PNIPAM particles, which represents a loss of ~$8.7*10^7$ water molecules for the ~$2.4*10^6$ amide bonds in the nanogel particles, a ratio similar to the 81% loss in water hydration estimated by Ono *et al*.[36]

7.3.2 UVRR spectral band assignments

The 204-nm excited UVRR spectra of PNIPAM (Fig 7.2) resemble the typical amide spectra seen for proteins. We observe a broad AmI band (predominantly C=Os)[64-66] at 1625 cm^{-1} while, the AmII band (predominantly C-N_s with NH_b)[66,67] is located at 1565 cm^{-1}. The resonance enhanced $C_\alpha H_b$ band[68-70] is located at 1387 cm^{-1}. Two weak AmIII bands are observed at 1345 and 1321 cm^{-1}, whereas, a strong AmIII band (C-N_s with NH_b)[66,67] located at 1258 cm^{-1} shows shoulders at 1284 cm^{-1} and ~1230 cm^{-1}. It should be noted that a similar molecule, *N*-methylacetamide shows only a single intense AmIII band at 1315 cm^{-1}.[66,67,71] Likely, the multiple AmIII bands in PNIPAM arise due to coupling between the AmIII vibration (C-N_s with NH_b) and isopropyl group vibrations.

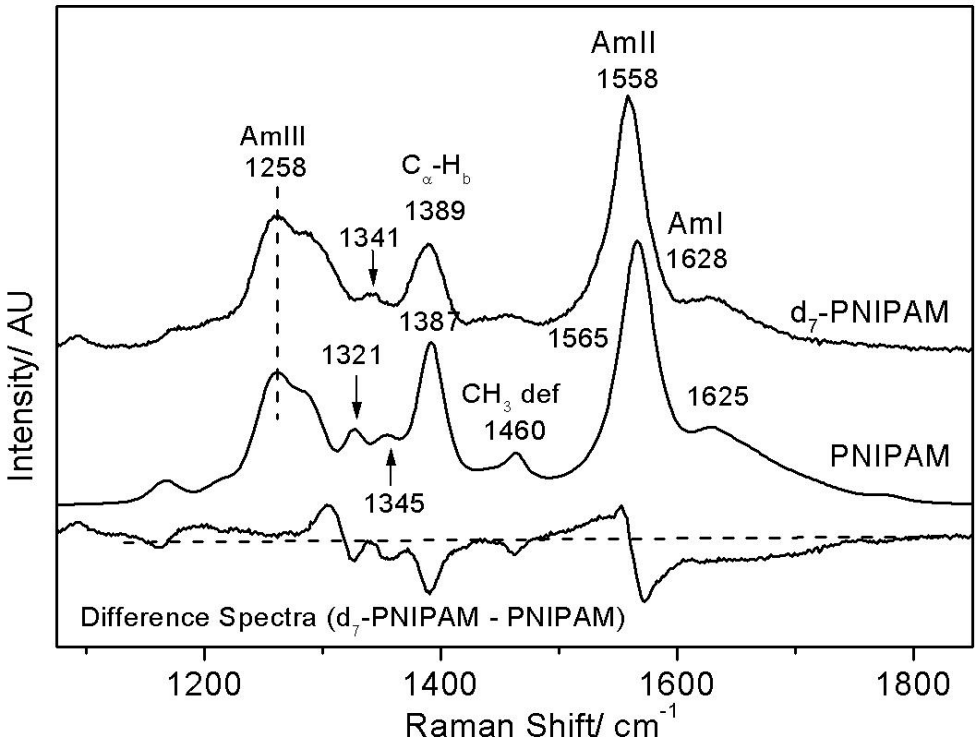

Figure 7.2: 204 nm excited UV Raman spectra of PNIPAM and d_7-PNIPAM at 5 ºC. Both spectra were normalized to the peak intensity of their AmIII bands. The difference spectrum was obtained by subtracting the PNIPAM spectra from that of d_7-PNIPAM.

In order to ascertain the impact of the pendent isopropyl group on amide vibrations we examined the 204-nm excited UVRR spectra of deuterium labeled d_7-PNIPAM. In d_7-PNIPAM the seven hydrogen atoms of the isopropyl group have been replaced with deuterium atoms (Fig 7.3). The largest impact of deuterium labeling is observed in the AmII region (Fig 7.2) where deuterium labeling broadens and downshifts the AmII band (ΔFWHM = 2 cm^{-1}, $\Delta\nu$ = 7 cm^{-1}). This result indicates that the normal mode composition of the AmII vibration in PNIPAM contains significant contribution from the isopropyl group motion.

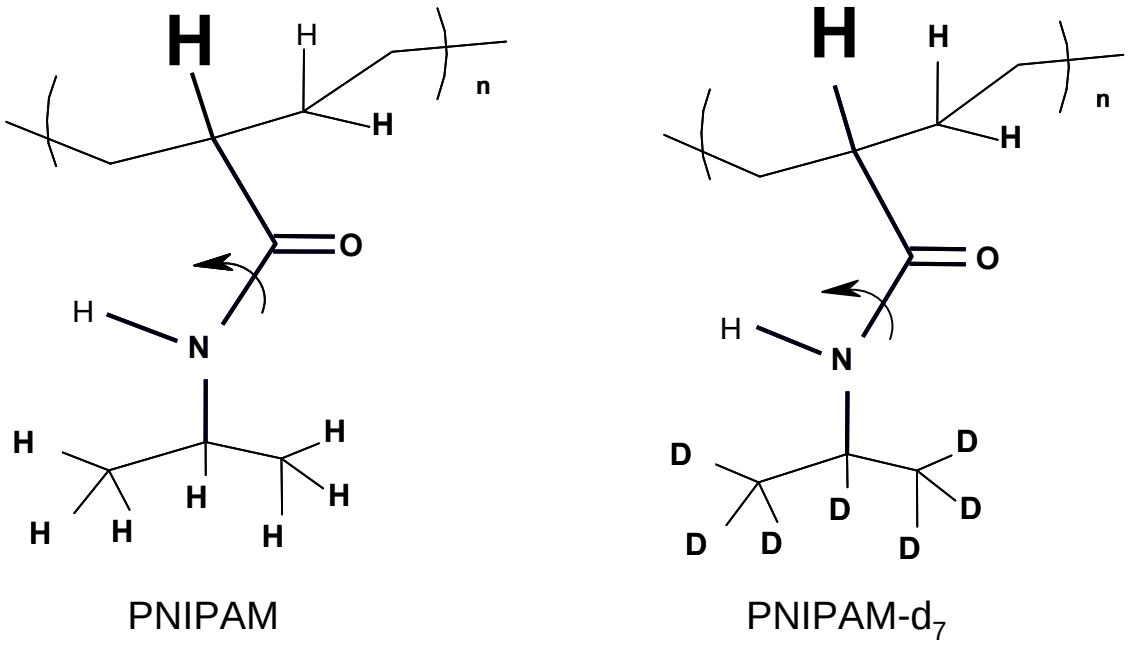

Figure 7.3: The structure of PNIPAM and its deuterated isotopomers, d_7-PNIPAM. The C_α-hydrogen that gives rise to the resonance enhanced $C_\alpha H_b$ band at ~1387 cm^{-1} is highlighted. The curved arrow highlights the Ψ dihedral angle rotation around the C_α-C(O) bond. The AmIII band frequency is sensitive to the Ramachandran Ψ angle rotation around the C_α-C(O) bond.

Upon deuteration, the weak ~1460 cm^{-1} band of PNIPAM is replaced by a broad low intensity feature centered around ~1445 cm^{-1} (d_7-PNIPAM, Fig 7.2). The 1460 cm^{-1} band of PNIPAM derives from a non-resonant enhanced CH_3 deformation mode of the isopropyl group.[72]

Deuterium labeling decreases the 1387 cm^{-1} $C_\alpha H_b$ band intensity but does not significantly impact the band frequency. The 1387 cm^{-1} band in the natural abundance NIPAM has a ~50% contribution from isopropyl CH_3 umbrella motion. The d_7- PNIPAM completely derives from the amide $C_\alpha H$ bending vibration (Fig 7.3).

In the AmIII region deuterium labeling appears to only impact the AmIII bands at 1300 cm^{-1}, 1345 cm^{-1} and 1321 cm^{-1}. The frequencies of the strong AmIII band centered at 1258 cm^{-1} and its shoulders at ~1284 cm^{-1} and 1230 cm^{-1} are not impacted by isopropyl group deuteration (Fig 7.2). Upon deuteration both the 1345 cm^{-1} and 1321 cm^{-1} AmIII bands of PNIPAM appear to have been replaced by a single band located at ~1341 cm^{-1} (Fig 7.2). The difference spectrum between d_7-PNIPAM and PNIPAM shows a positive peak at ~1300 cm^{-1}.

This result indicates that the 1345 cm^{-1}, 1321 cm^{-1} and 1300 cm^{-1} AmIII bands contain significant contribution from isopropyl vibrations. We, therefore, conclude that the 1345 cm^{-1} and 1321 cm^{-1} AmIII bands of PNIPAM are not the same vibrations as the $AmIII_1$ and $AmIII_2$ vibrations observed in peptides which derive from coupling between the AmIII vibration and the heavy atom vibrations of the peptide backbone.[67]

As noted above the frequencies of the AmIII bands located in the region of 1200-~1290 cm^{-1} are not impacted by deuterium labeling of PNIPAM's isopropyl group (Fig 7.2). This result indicates that the AmIII bands located in this region do not contain a significant contribution from the isopropyl group, and, thus, derive from the "classical AmIII" vibration[67] which is predominantly a C-N_s stretching coupled with in-phase NH_b motion.[66,67] Extensive Raman studies indicate that the "classical" AmIII vibration is sensitive to hydrogen bonding and dihedral angle changes around the C_α-C bond length (see Fig 7.3).[67,69,73] In peptides this vibration is referred to as the $AmIII_3$ vibration.[67] In subsequent discussion, we refer to this band as simply the AmIII band.

7.3.3 Temperature dependence of PNIPAM

As the temperature is increased from 4 to 65 ˚C the AmI band of PNIPAM shows a ~28 cm^{-1} upshift from 1623 to 1651 cm^{-1} and its intensity increases by ~15% (Fig 7.4) suggesting a $T_t \sim 37$ ºC. We can model the spectral changes in the AmI region by using three Gaussian bands located at 1624 cm^{-1}, 1655 cm^{-1} and 1700 cm^{-1} (Fig 7.5). The low intensity 1700 cm^{-1} AmI feature likely derives from dehydrated amides, while the 1624 cm^{-1} band derives from fully hydrogen bonded amides at least 2 waters hydrogen bonded at the C=O (hydrogen bonded at sites A and C, Fig 7.5A) and one water hydrogen bonded at the N-H site (hydrogen bonded at the B site).[74,75] The 1655 cm^{-1} AmI band, which occurs ~30 cm^{-1} to higher frequency from the fully hydrogen bonded AmI band, probably derives from an intermediate hydrogen bonded state, with only two hydrogen bonded waters, one each at the C=O and N-H sites[74,75] (hydrogen bonded at the A and B sites).

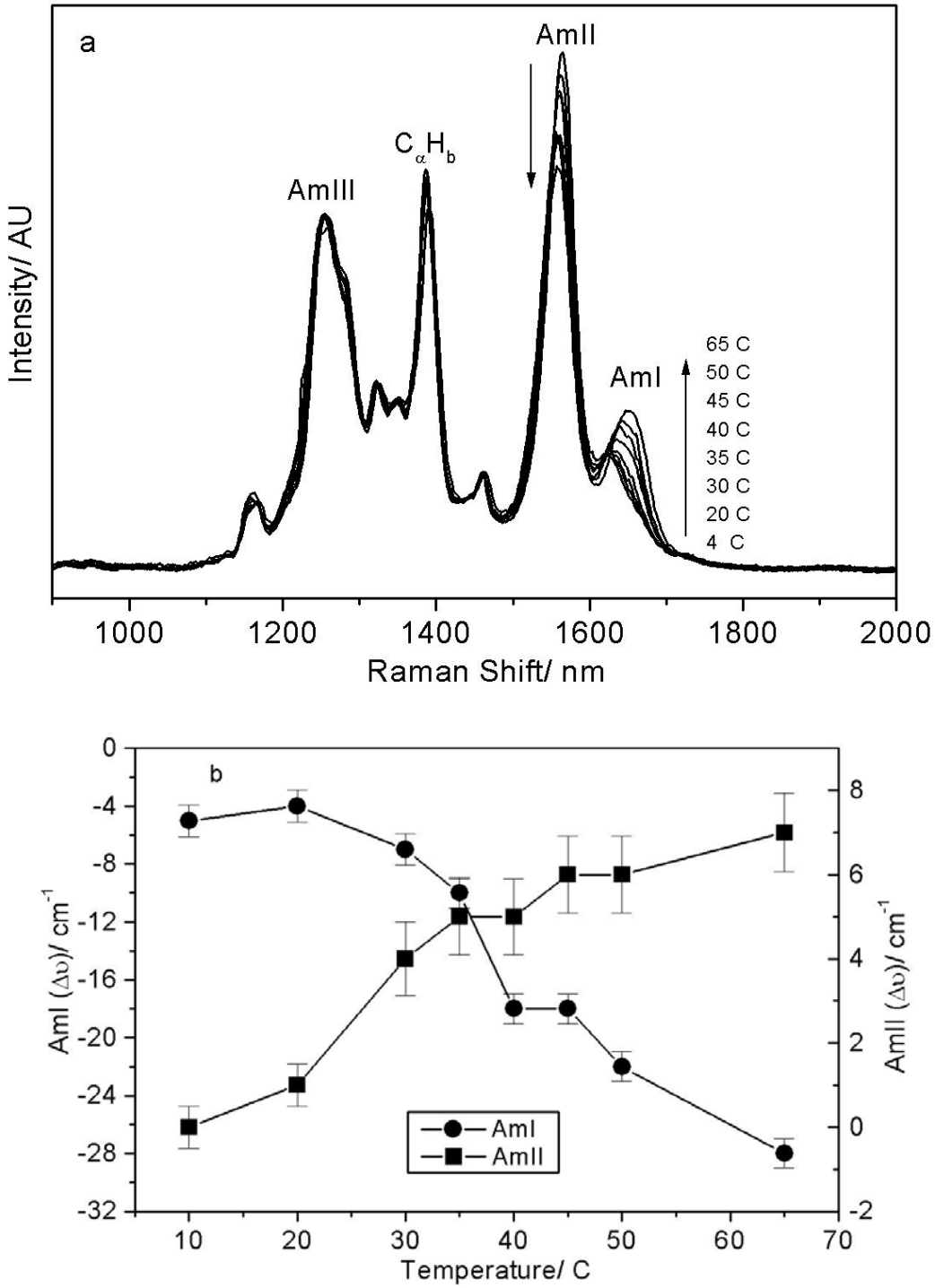

Figure 7.4: Temperature dependence of the 204 nm excited UVRR spectra of PNIPAM. The AmI band intensity increases and upshifts with temperature, while the AmII band intensity decreases. and downshifts with temperature.

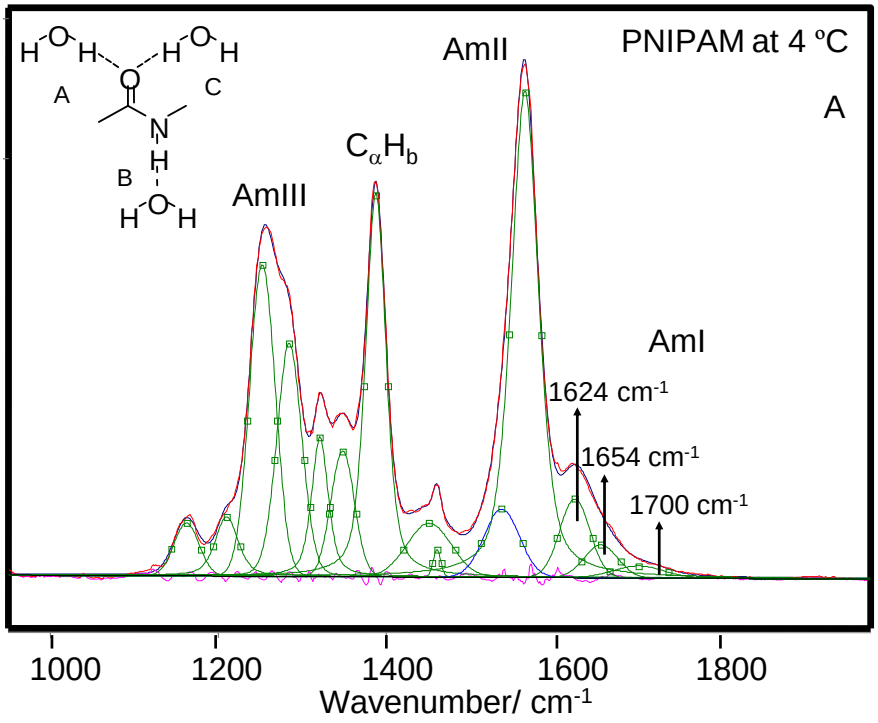
PNIPAM at 4 ºC
A
AmII
AmIII
$C_\alpha H_b$
AmI
1624 cm-1
1654 cm-1
1700 cm-1
A
B
C
1000
1200
1400
1600
1800
Wavenumber/ cm-1

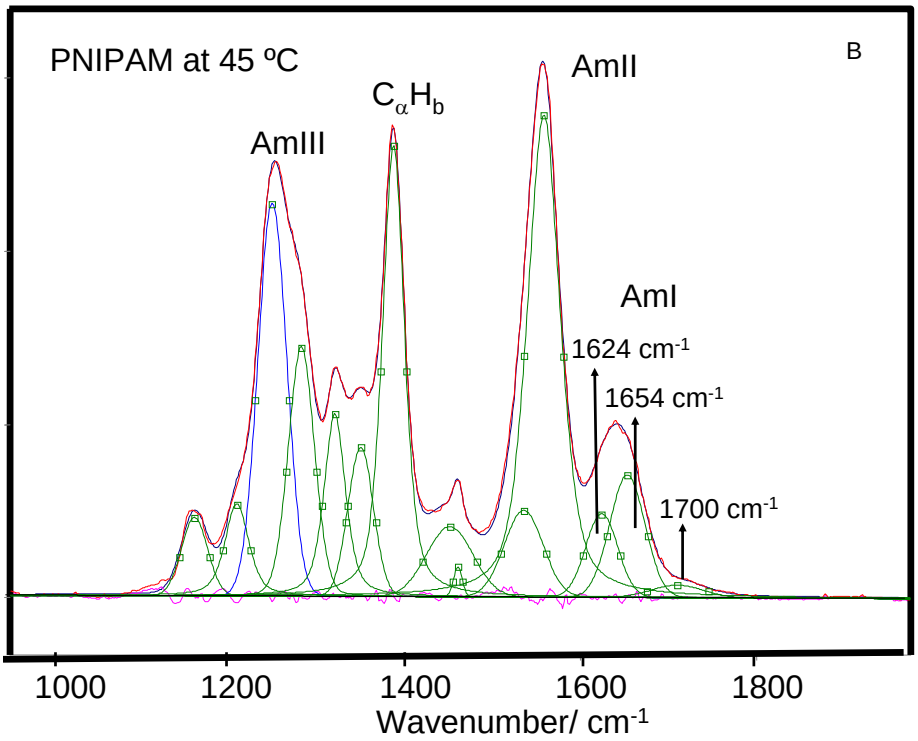

Figure 7.5: 204-nm excited UVRR spectra of PNIPAM at (A) 4 ºC and (B) 45 ºC the spectra were decomposed into a minimum sum of mixed Lorentzian and Gaussian bands. The AmI region was fit to Gaussian bands. The measured and modeled spectra overlap almost completely. The different amide-hydrogen bonding sites are shown in the Fig 5A insert.

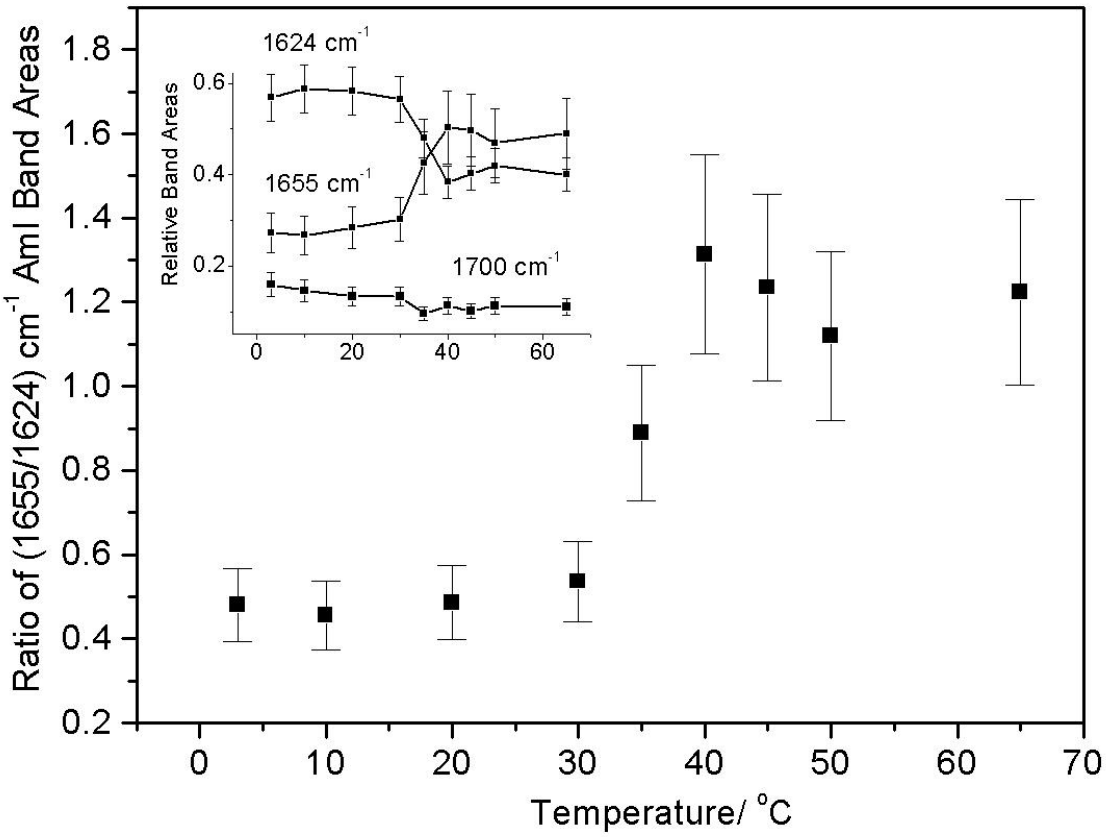

Figure 7.6: The intensity ratio of the 1655 cm^{-1}/1624 cm^{-1} AmI bands shows an abrupt increase between 30 ºC and 40 ºC.

The AmI spectral changes result from changes in the intensity ratio of the 1624 cm^{-1} and 1654 cm^{-1} AmI bands over the 30-40 ºC temperature range (Fig 7.6). Obviously, the PNIPAM's hydrophobic collapse decreases the hydration of the pendent amide bonds increasing the intensity of the higher frequency 1654 cm^{-1} AmI band. At low temperature the 1624 cm^{-1} band dominates indicating that most of the amide bonds are fully hydrogen bonded at all three sites (A, B, and C), while above 30 ºC the amides predominantly show A and B hydrogen bonding. Our spectral modeling suggests (assuming similar Raman cross sections) that the PNIPAM collapse results in a hydration change, where at low temperature fully hydrated amides, which

constitute ~60 % of the population decreases to ~40 % of the population at the higher temperature. The less hydrated A and B site hydrogen bonded amide population increases from ~ 30 % to 50 % of the population. The fully dehydrated amide population decreases only slightly. The presence of multiple AmI bands-representing various degrees of amide hydrogen bonding even at low temperatures, indicates that pockets of collapsed polymer, hydrophobic domains are present at all temperatures.

The intensity ratio of the (1655/1624) cm^{-1} AmI bands does not show any significant change until the solution temperature increases above 30 ºC. Light scattering (Fig 7.1), in contrast, shows a ~24% decrease in particle diameter (and a 56% volume decrease) between 15 ºC and 30 ºC. This indicates that a large particle volume decrease occurs due to the temperature increase to 30 ºC, in the absence of any obvious Raman changes in the amide hydration level.

Previously, Manas *et al*[76] utilizing IR spectroscopy demonstrated that burial of an amide bond inside protein's hydrophobic core upshifts the AmI band by ~26 cm^{-1} as compared to a water-exposed amide.[76] This upshift in the AmI band frequency derives from a weakening/loss of hydrogen bonding[64,76-78] and a decrease in the dielectric constant of the surrounding media.[78,79] Theoretical studies suggest that the dielectric constant in the protein's hydrophobic interior is $\varepsilon \sim$ 4-20.[80-82]

Recently, Iwai *et al*[25] utilized a florescent dye, 9,-(4-N, N-dimethylaminophenyl)phenanthrene to probe the local dielectric constant in a PNIPAM hydrogel. These authors interpreted the temperature induced shift in λ_{max} of the fluorescence as arising due to a change in the dielectric constant of the surrounding media. They suggest that at 40 ºC (above the LCST) the local dielectric constant in the collapsed state of PNIPAM is ~17, while at 15 ºC the local dielectric constant is ~ 63, close to that of pure water.[25] The relatively

high dielectric constant of the high temperature PNIPAM nanoparticles indicates significant water penetration of the collapsed particle's interior.

Recently, Ono *et al*[36] utilized dielectric relaxation methods to estimate that in the collapsed state of PNIPAM the number of hydrating water molecules is ≤ 2 per NIPAM group. In contrast, the low temperature hydrated state boasts ~11 water molecules per amide group.[36]

The loss/weakening of amide hydrogen bonding observed in the AmI region is confirmed by spectral changes in the AmII and AmIII region. The AmII band systematically loses 10% of its intensity while the AmI band intensity shows a ~15% increase as the temperature increases from 4 to 65 ºC. Previously, Triggs and Valentini[83] observed that upon water hydrogen bonding, the AmI band intensity of *N*-methylacetamide (NMA), a model amide bond, decreases while the AmII band intensity increases. The ratio of the AmI to AmII intensity also increases as the solvent polarity increases.[70,83,84] These authors suggest that hydrogen bonding stabilizes the charged resonance form of the amide bond [$^{-}$O(C)=NH^{+}]. This makes the ground state geometry more like that of the excited state along the C=O coordinate and less like that of the excited state along the C-N coordinate, thus diminishing the displacement along the C=O bond and increasing the displacement along the C-N bond. Consequently, hydrogen bonding results in a relatively smaller resonance enhancement of the AmI vibration and a greater enhancement of the AmII vibration.[83]

The AmII and AmIII band frequencies downshift with increasing temperature. The AmII band downshifts from 1565 to 1558 cm^{-1} while the AmIII band downshifts from 1258 to 1252 cm^{-1} as the temperature increases from 4 to 65 ºC (Fig 7.4). Similar temperature-dependent changes in the AmII and AmIII frequencies have been observed for water-exposed peptide

bonds[67,85,86] and attributed to temperature induced weakening and/or loss of amide-water hydrogen bonding.[62,67,76]

It should be noted that changes in AmII and AmIII frequencies are ~5 times smaller then the upshift in the AmI frequency. This result is highly unusual. Typically, the temperature induced frequency shifts are largest for the AmII vibration (-0.11 $cm^{-1}/ºC$), followed by the AmIII vibration (-0.09 $cm^{-1}/ºC$) with the AmI vibration showing a smaller upshift.[67]

Utilizing high level density functional theory calculations of NMA and NMA-water complexes we recently demonstrated that the AmI vibration is predominantly sensitive to changes in hydrogen bonding at the C=O, while the AmII vibration is almost exclusively sensitive to hydrogen bonding at the N-H site.

Assuming the amide vibrations in PNIPAM and NMA have similar normal mode compositions we can conclude that the AmI frequency shift indicates an increase in the A (C=O) and B (N-H) site water hydrogen bonded amide population. A lack of significant change in the AmII frequency indicates little or no change in hydrogen bonding at the B site. The results drawn from both the AmI and AmII frequency shifts indicate little or no change in N-H hydrogen bonding, while a decrease in hydrogen bonding occurs at the C=O.

We also examined the exposure of the amide groups by measuring their hydrogen-deuterium exchange rates at room temperature and 55 ºC. We found that all the amide N-H were exchanged within the ~5 min it took to prepare and measure the H-NMR spectra (data not shown). This result clearly indicates that the collapsed PNIPAM does not significantly hinder diffusion of D_2O into the collapsed particle. This result, thus, indicates that in the collapsed state of PNIPAM, the amide bonds are hydrogen bonded to water and not to each other.

The 1387 cm^{-1} $C_\alpha H_b$ bending band shows no significant temperature-induced frequency or intensity change. Previous studies indicate that the $C_\alpha H_b$ band intensity is greatest when the $C_\alpha H$ and amide N-H bonds are *cis,* which allows for maximum coupling.[69,87] However, in the *trans* conformation the two bonds lie far from each other giving minimal coupling. In proteins, the *cis* C_α-H bond conformation corresponds to an extended β-strand while the *trans* conformation corresponds to α-helix-like conformation.[69] The lack of change in the $C_\alpha H_b$ band during PNIPAM's hydrophobic collapse thus indicates essentially identical Ramachandran Ψ angles for the collapsed and fully hydrated PNIPAM conformations. Further, the AmII and AmIII features at both low and high temperatures demonstrate that the amide bond conformation remains in the trans amide form throughout the VPT.

We compared the collapsed form of PNIPAM in water to that of fully dried PNIPAM prepared by flowing dry nitrogen over the sample. As compared to the collapsed particles in water (45 ºC), the dry, solid PNIPAM at room temperature AmI band intensity is dramatically increased and its frequency is upshifted by 7 cm^{-1}, while its band width (ΔFWHM = 5 cm^{-1}) significantly narrows (Fig 7.7). The solid PNIPAM AmII vibration shows a 7 cm^{-1} downshift in the dry, solid state whereas, the AmIII vibration downshifts by only ~4 cm^{-1}. The magnitude of the AmII frequency downshift between the dry, solid and the collapsed 45 °C aqueous PNIPAM nanogel is similar to the temperature induced frequency shift observed for the AmII vibration between 4º and 45 ºC ($\Delta\nu$ = 6 cm^{-1}), indicating weakening of NH-water hydrogen bonding. The impact of particle dehydration on the AmI frequency is relatively small as compared to the large upshift observed in the PNIPAM nanogel in water between 4º and 45 ºC. Spectral modeling of the AmI region with three Gaussians indicates that the 7 cm^{-1} upshift in the AmI region derives

from a ~49% increase in the A and B hydrogen bonded amides (1654 cm^{-1} peak) as compared to the collapsed 45 ºC aqueous state (Fig 7.7).

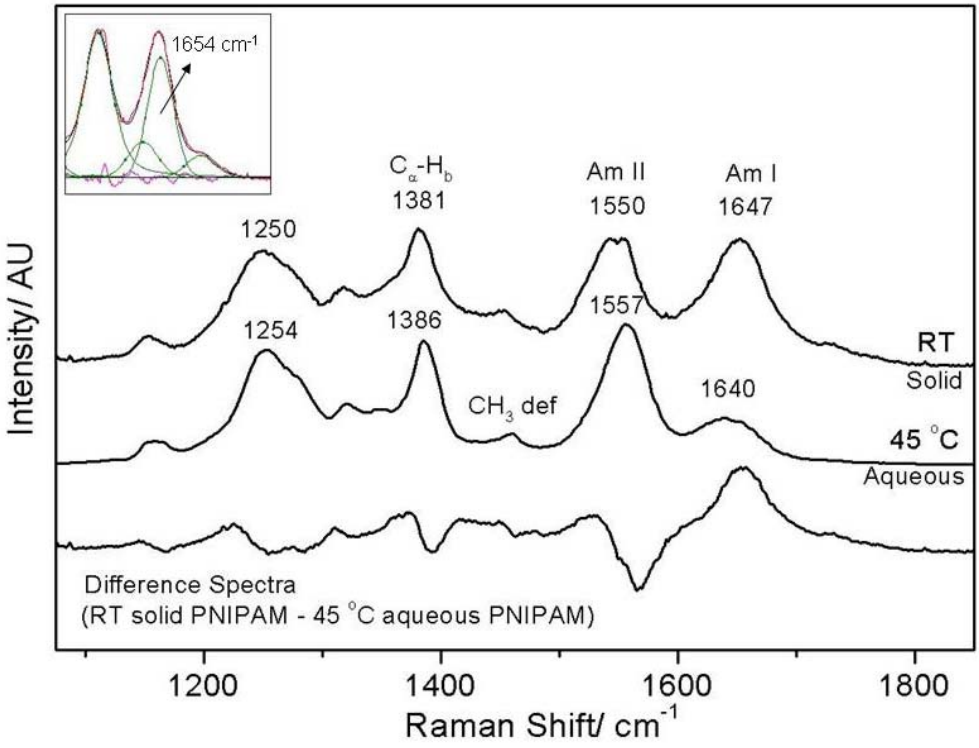

Figure 7.7: PNIPAM spectra in water (45 ºC) and in the solid dehydrated state normalized to the peak intensity of the AmIII bands show significant differences in the amide band frequencies. In particular, the AmI vibration upshifts while, the AmII vibration downshifts by 7 cm^{-1} upon PNIPAM dehydration. The insert shows the results of spectral decomposition in the AmI and AmII region of the dry, solid PNIPAM which show increased band intensity for the 1654 cm^{-1} AmI region.

The $C_\alpha H_b$ band intensity is slightly greater in the solid state as compared to the collapsed aqueous phase (Fig 7.7). The $C_\alpha H_b$ band intensity is sensitive to changes in coupling between the $C_\alpha H$ and N-H_b motions. The strength of coupling between the two motions in inversely correlated with the distance between the two hydrogens.[88] Thus, the increased $C_\alpha H_b$ band intensity indicates that the conformation of the amide bonds in the solid, dry state differs

somewhat from their aqueous counterparts in that its ensemble structure favors a more extended conformations. There are also changes in the AmIII band shape which also indicates some Ψ-conformation alterations for some of the pendent amides.

The presence in dry PNIPAM of 1654 cm^{-1} AmI band which we observed for A and B hydrogen bonded peptide bonds in water probably derives from inter-chain hydrogen bonding between pendent amides. The formation of hydrogen bonded inter-chain aggregates is likely responsible for conformation changes at the amide bond as indicated by increased $C_\alpha H_b$ band intensity in the dry solid.

7.3.4 A Model of PNIPAM Collapse

In PNIPAM, our results indicate that at low temperatures the amide bonds are predominantly water-exposed. Likely at low temperatures the amides of PNIPAM are in an extended, trans amide conformation, as indicated by a strong $C_\alpha H_b$ band (Fig 7.4), that allows for favorable interactions between the amide and a surrounding hydration shell.[89] In the extended state the exposed amide bonds provide three hydrogen bonding sites where three water molecules localize and serve as nucleating sites for formation of large water clusters i.e. the hydration shells. The formation of these water cluster is highly cooperative, e.g. cooperative effects in a water pentamer cluster result in hydrogen bonds energies that are almost twice as large as the linear hydrogen bonded dimmer.[90] Presumably, by providing a nucleation site the amide bond lowers the free energy barrier to formation of large water clusters. The free energy gained via formation of large water-clusters stabilizes the well-hydrated extended PNIPAM conformation.

At elevated temperatures, increased thermal agitation disrupts the extensive hydrogen bonding network that stabilizes these large water clusters. The loss of favorable interactions destabilizes the exposed PNIPAM conformation with its significantly exposed hydrophobic surface area. PNIPAM then collapses to a compact conformation that reduces its hydrophobic solvent accessible surface area. Such a compact state may be formed by pushing the *i*, *i*+3 isopropyl groups closer together to form local hydrophobic pockets where the C=O groups are located inside the hydrophobic core (Fig 7.8) which results in a large upshift of the AmI band. Nearer-neighbor interactions are sterically forbidden.

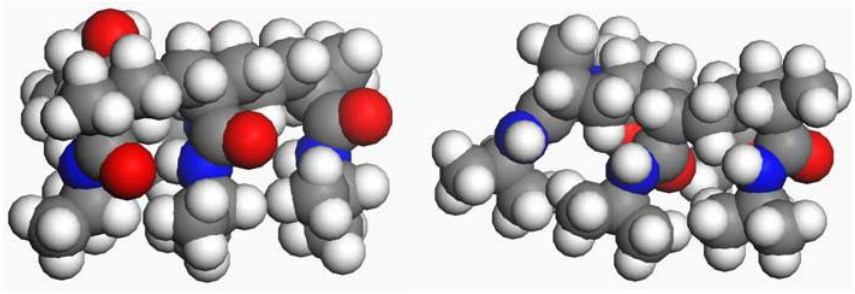

Figure 7.8: A cartoon of collapsed and extended conformation of PNIPAM (side-view) as drawn in Material Studio software. Note that the carbonyl groups are fully exposed in the extended conformation but are located inside the hydrophobic pocket in the collapsed state. The carbonyl oxygens are colored red while, the nitrogens are blue.

The formation of a collapsed hydrophobic cluster or a nano-pocket reduces PNIPAM's exposed hydrophobic surface area. The loss of well-ordered water molecules from the hydrophobic group's solvation shell into the bulk increases the system entropy, thus stabilizing the compact PNIPAM conformation. Previously, Okada and Tanaka's numerical simulations of PNIPAM in water indicate the temperature of LCST depends upon the hydration cooperativity.[91]

Daggett and co-workers[91b] found that the hydrophobic collapse of elastin peptides is also driven by changes in water's orientation entropy.

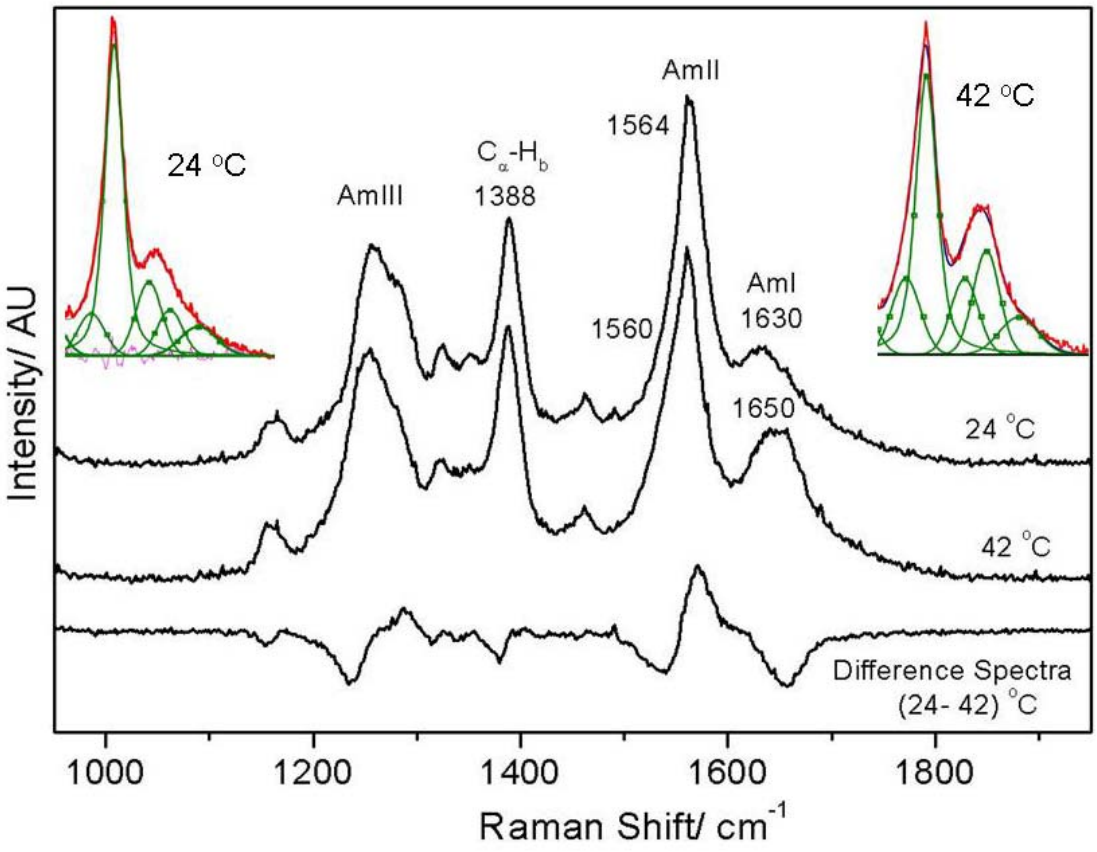

Figure 7.9: Single chain PNIPAM shows a ~20 cm^{-1} upshift in the AmI vibrational frequency upon PNIPAM collapse. Spectral decomposition of the AmI and AmII regions at 24 and 42 ºC are shown in inserts.

As shown in Fig 7.9, we observe similar temperature-induced spectral changes for single PNIPAM polymer chains (m.w. ~25, 000) as observed for cross-linked PNIPAM nanoparticles. Utilizing the same band decomposition routine used for PNIPAM nanogels (Fig 7.5) we find that a temperature increase form 24 ºC to 42 ºC results in an A and B hydrogen bonded population increase from ~33% to 47%, while the fully hydrated population shows an equivalent decrease.

This result indicates that the VPT evident for PNIPAM nanoparticles also occurs in single PNIPAM polymer chains.

7.3.5 Kinetics of PNIPAM's hydrophobic collapse

We examined the dynamics of the VPT to see if the dynamics would give insight into the VPT reaction coordinate. As shown in Fig 7.10A, a 15 ˚C T-jump results in prompt changes in the PNIPAM amide UVRR spectra which occur at the shortest delay times resolved. As in the equilibrium spectra the spectral changes are most prominent for the AmI band. The difference spectra at longer times resemble the equilibrium difference spectrum (Fig 7.10A). The kinetic changes in the AmI region can be accurately modeled as a single exponential process which yields a time constant of 360 ± 85 ns (Fig 7.10B).

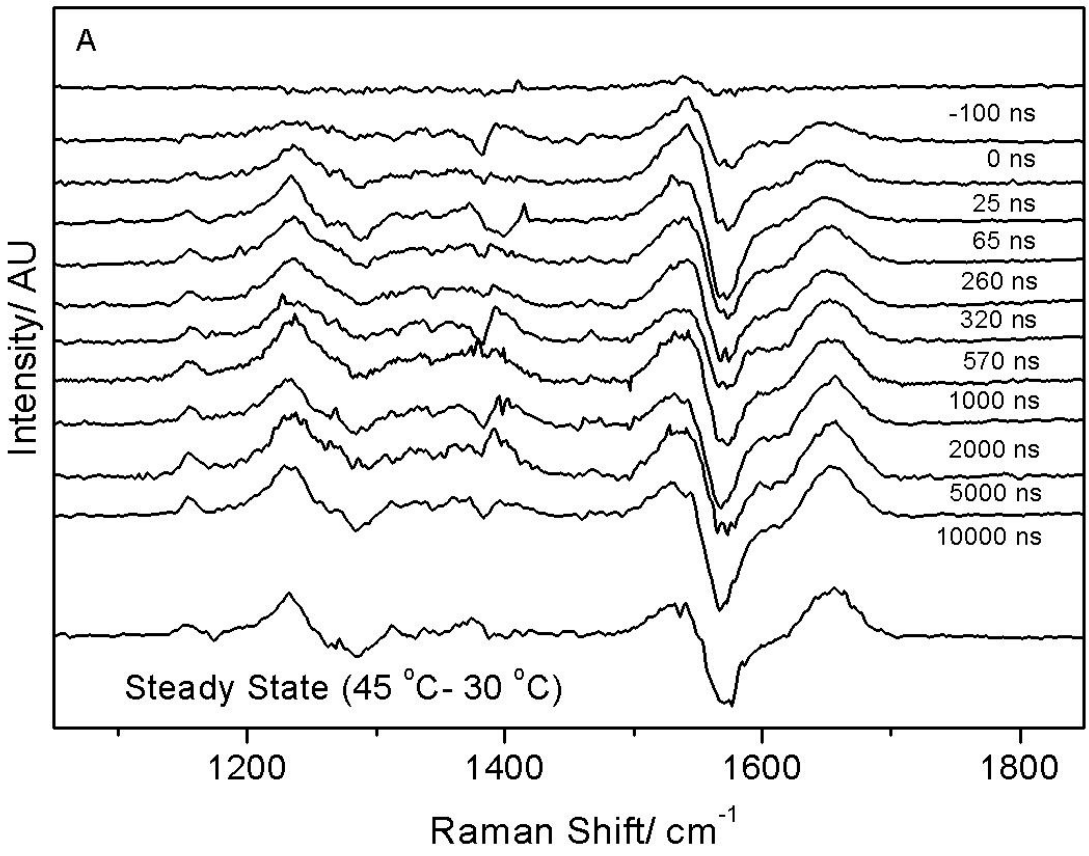
A
-100 ns
0 ns
25 ns
65 ns
260 ns
320 ns
570 ns
1000 ns
2000 ns
5000 ns
10000 ns
Steady State (45 °C- 30 °C)
Intensity/ AU
1200
1400
1600
1800
Raman Shift/ cm-1

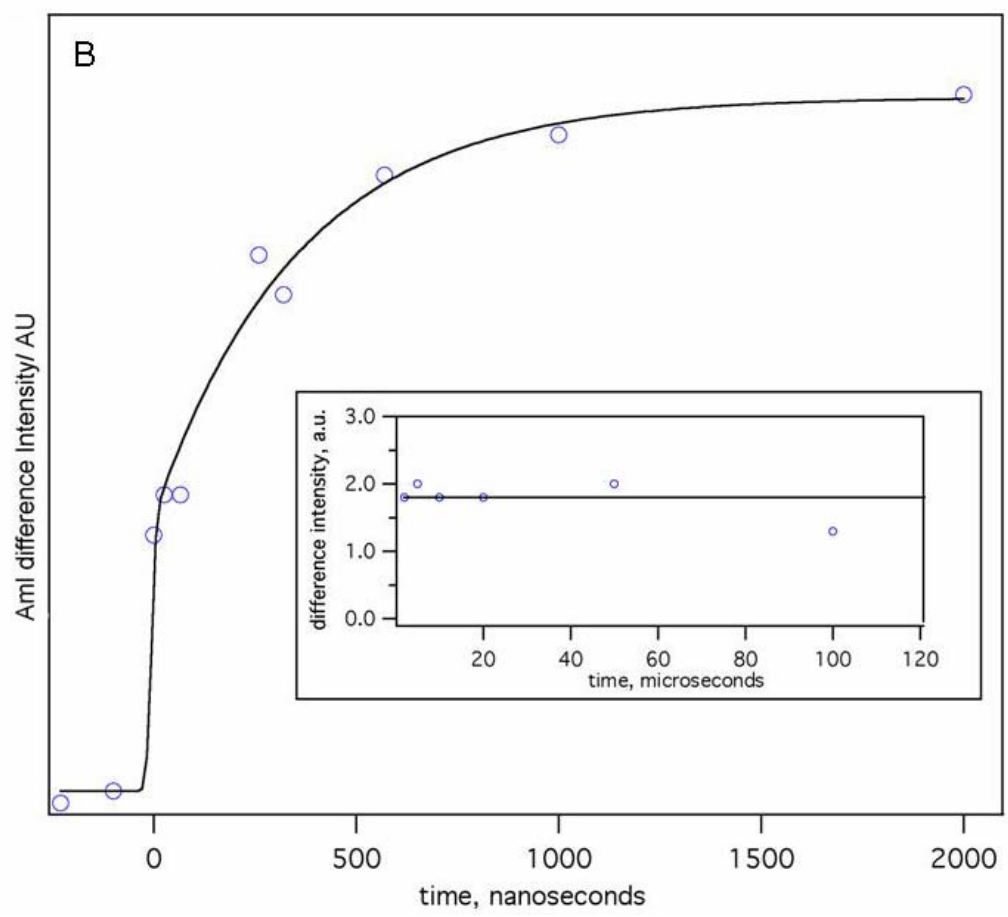

Figure 7.10: Time resolved 204-nm UVRR (hot – 30 ºC) difference spectra at different delay times. The AmI band shows the largest spectral shift. B) The peak-to-peak AmI band amplitude in the (hot – 30 ºC) transient difference spectra at different delay time is used to model the kinetics of the PNIPAM's hydrophobic collapse. All changes in the AmI region are complete within 1 μs; we do not observe any significant changes in the AmI region at longer timescales (insert). The amide band intensity in the difference spectra shows a small decrease at 100 μs which indicates sample volume cooling due to equilibration.

The PNIPAM amide dehydration appears complete within 1 μs; we do not observe any significant change in the AmI region at longer time scales (Fig 7.10B insert). The prompt spectral changes in the AmII and AmIII regions are very similar to features observed by Lednev *et al*[62] in T-jump Raman measurements of an α-helical polyala peptide. They demonstrated that

these changes derived from the temperature-induced frequency shifts independent of peptide structural changes.[62]

Our success in modeling the transient spectral changes as a single exponential indicates that at least kinetically the PNIPAM collapse occurs as a two-state process with no significant intermediates observed. Previous steady-state light scattering studies of single PNIPAM chains indicate the polymer collapse involves at-least two-intermediate states as suggested by small but significant temperature-dependent changes in $<R_g/R_h>$.[92] Our steady-state (Fig 7.6) and kinetic (Fig 7.10) results indicate that these intermediates do not significantly impact PNIPAM hydration during the polymer collapse.

Our results are consistent with previous kinetic studies of Wang *et al*[1] and Reese *et al*[3] that indicate a single exponential collapse of free PNIPAM particles with relaxation times of ~390 ns and ~120 ns, respectively. The observed time for the PNIPAM's hydrophobic collapse is similar to the folding time observed for small α-helical peptides[62] and some designed ultra-fast folding mini-proteins,[86,93,94] where folding is regarded as being essentially limited by solvent friction.[93,95-102] The rate of collapse in PNIPAM may also be limited by polymer and water diffusion.

Polymer collapse is likely limited by the rate at which distant part of the polymer can form contacts.[103-106] The rate of intra-chain contact formation or the rate of loop formation has been extensively studied in the context of protein folding.[103-106] These studies indicate that the rate of loop formation is limited by solvent viscosity and chain stiffness. For short peptide chains (<10 mers) in water the rate of loop formation appears to be $\sim 10^7$ s^{-1}.[104,106] The rate of loop formation decreases with increasing chain length but due to chain stiffness which limits the

conformation space available to the polymer chain, the rate of loop formation levels off at ~10^5 s^{-1} for n> 20.[106]

Assuming amide dehydration in PNIPAM is limited by the rate of polymer collapse, the observed collapse rate in PNIPAM (10^6 s^{-1}) suggests an average persistence length in PNIPAM of n~10.[104,106] At lengths shorter than the persistence length the polymer acts as an elastic rod, whereas, at lengths longer than the persistence length the polymer backbone conformation forms a random coil. The estimated persistent length is roughly three times longer than the smallest possible PNIPAM length required to form a local hydrophobic nano-pocket. This suggests that probably the adjacent hydrophobic pockets coalesce via hydrophobic interactions to stabilize the collapsed particle.

PNIPAM chains as small as a 10-mer is thus expected to show a temperature induced hydrophobic collapse. It should be noted that a 10-mer is also the minimum length required for a polypeptide to fold into a stable α-helix conformation

7.4 CONCLUSIONS

PNIPAM has long been utilized as a model system for understanding temperature-induced polymer hydrophobic collapse. Here we utilize DLS, H-NMR, and steady-state UVRR measurements to determine that in the collapsed state the amide bonds of PNIPAM do not engage in inter-amide hydrogen bonding. Our measurements clearly indicate that above T_t the amide bonds of PNIPAM are predominantly hydrogen bonded on average to two water

molecules each, with one water-peptide hydrogen bond at the C=O and N-H site each. In contrast, at low temperatures the C=O is hydrogen bonded to two water molecules.

Based on our spectroscopic data we propose that at low temperatures the PNIPAM-water interactions stabilize an extended water-exposed conformation. At elevated temperatures, thermal agitation disrupts the solvation shell around *N*-isopropylacrylamide (NIPAM). The loss of favorable NIPAM-water solvation shell interactions forces the PNIPAM chain to adopt a compact conformation, forming local hydrophobic pockets that significantly reduce the solvent exposure of its pendent NIPAM amide groups. The resulting decrease in hydrophobic solvation increases the system entropy which stabilizes the compact/dehydrated state of PNIPAM.

Steric constraints prevent hydrophobic contacts between nearest neighbors. The (*i*, *i*+3) is the nearest neighbor pair that can form hydrophobic contacts free of steric clashes (Fig 8). The formation of local hydrophobic clusters results in a loss on average of one C=O-water hydrogen bond, which results in a 28 cm^{-1} upshift in the average AmI frequency. This provides a convenient marker for examining the temporal evolution of the PNIPAM collapse.

Our time-resolved UVRR measurements indicate that the changes in C=O-water hydrogen bonding can be modeled as a mono-exponential collapse with a time constant of 360 (± 80) ns. Changes in the AmII region are complete within 60 ns, indicating the AmII frequency shifts derive from temperature induced weakening of NH-water hydrogen bonds. Similar temperature induced changes in the amide band frequencies were observed by Lednev et al[1] in their T-jump study of a mainly α-helical peptide. Thus, the NH hydrogen bonding does not appear to significantly change.

Assuming the PNIPAM collapse is diffusion limited, the rate of collapse (10^6 s^{-1}) suggests a persistence length of n~10. The estimated persistence length is ~3-times longer than

the shortest polymer length that is sterically allowed to form a hydrophobic cluster. This suggests that the hydrophobic collapse is a cooperative process where probably adjacent hydrophobic pockets coalesce via hydrophobic interactions to stabilize the collapsed particle.

The hydrophobic collapse of PNIPAM is driven by changes in polymer-water interactions. In the extended state, favorable interactions between the amide and a surrounding hydration shell. At high temperatures, increased thermal agitation disrupts the NIPAM-water solvation shell interactions, reducing the favorable free energy of the system. Aqueous PNIPAM compensates for the loss of favorable amide-water interactions by adopting a compact conformation which reduces its solvent accessible surface, resulting in the loss of well-ordered water molecules solvating the hydrophobic isopropyl groups. This results in a significant increase in the entropy, thus, favoring the compact state of PNIPAM.

Previously, Daggett and co-workers[2] found that the hydrophobic collapse of elastin peptides is also driven by changes in water's orientation entropy. Our results here suggest that PNIPAM hydrophobic collapse is driven by temperature induced changes in water hydrogen bonding.

ACKNOWLEDGMENTS: The authors would like to thank Prof. David Earl Prof. Ken Jordan and Dr. Adam Hixson for helpful discussions, Dr. Damodaran Krishnan for help with H-NMR measurements and NIH grant RO1 EB002053 for financial support.

7.5 REFERENCES

(1) Wang, J.; Gan, D.; Lyon, L. A.; El-Sayed, M. A. *Journal of the American Chemical Society* **2001**, *123*, 11284.
(2) Wang, X.; Wu, C. *Macromolecules* **1999**, *32*, 4299.
(3) Reese, C. E.; Mikhonin, A. V.; Kamenjicki, M.; Tikhonov, A.; Asher, S. A. *Journal of the American Chemical Society* **2004**, *126*, 1493.
(4) Tiktopulo, E. I.; Uversky, V. N.; Lushchik, V. B.; Klenin, S. I.; Bychkova, V. E.; Ptitsyn, O. B. *Macromolecules* **1995**, *28*, 7519.
(5) Katsumoto, Y.; Tanaka, T.; Ozaki, Y. *Macromolecular Symposia* **2004**, *205*, 209.
(6) Katsumoto, Y.; Tanaka, T.; Sato, H.; Ozaki, Y. *Journal of Physical Chemistry A* **2002**, *106*, 3429.
(7) Saunders, B. R.; Crowther, H. M.; Morris, G. E.; Mears, S. J.; Cosgrove, T.; Vincent, B. *Colloids and Surfaces, A: Physicochemical and Engineering Aspects* **1999**, *149*, 57.
(8) Saunders, B. R.; Vincent, B. *Advances in Colloid and Interface Science* **1999**, *80*, 1.
(9) Yi, Y.; Oh, K. S.; Bae, Y. H. *Polymer* **1997**, *38*, 3471.
(10) Cimen, E. K.; Rzaev, Z. M. O.; Piskin, E. *Journal of Applied Polymer Science* **2005**, *95*, 573.
(11) Crowther, H. M.; Saunders, B. R.; Mears, S. J.; Cosgrove, T.; Vincent, B.; King, S. M.; Yu, G.-E. *Colloids and Surfaces, A: Physicochemical and Engineering Aspects* **1999**, *152*, 327.
(12) Ding, Z.; Chen, G.; Hoffman, A. S. *Journal of Biomedical Materials Research* **1998**, *39*, 498.
(13) Harmon, M. E.; Frank, C. W. *ACS Symposium Series* **2003**, *833*, 2.
(14) Inoue, T.; Chen, G.; Nakamae, K.; Hoffman, A. S. *Polymer Gels and Networks* **1998**, *5*, 561.
(15) Mendez, S.; Curro, J. G.; McCoy, J. D.; Lopez, G. P. *Macromolecules* **2005**, *38*, 174.
(16) Zeng, F.; Tong, Z.; Feng, H. *Polymer* **1997**, *38*, 5539.
(17) Zhao, Y.; Cao, Y.; Yang, Y.; Wu, C. *Macromolecules* **2003**, *36*, 855.
(18) Mao, H.; Li, C.; Zhang, Y.; Furyk, S.; Cremer, P. S.; Bergbreiter, D. E. *Macromolecules* **2004**, *37*, 1031.
(19) Gan, D.; Lyon, L. A. *Journal of the American Chemical Society* **2001**, *123*, 7511.
(20) Hoare, T.; Pelton, R. *Langmuir* **2004**, *20*, 2123.
(21) Dufresnea, M.-H.; Garreca, D. L.; Santa, V.; Lerouxa, J.-C.; Range, M. *International Journal of Pharmaceutics* **2004**, *277*, 81.
(22) Bergbreiter, D. E.; Case, B. L.; Liu, Y.-S.; Caraway, J. W. *Macromolecules* **1998**, *31*, 6053.
(23) Jiang, X.; Xiong, D.; Zheng, P.; Zhang, W.; Shi, L. *Journal of Polymer Science Part A: Polymer Chemistry* **2007**, *45*, 2812.
(24) Zhang, Y.; Guan, Y.; Zhou, S. *Biomacromolecules* **2006**, *7*, 3196.

(25) Iwai, K.; Matsumura, Y.; Uchiyama, S.; de Silva, A. P. *Journal of Materials Chemistry* **2005**, *15*, 2796.
(26) Barker, I. C.; Cowie, J. M. G.; Huckerby, T. N.; Shaw, D. A.; Soutar, I.; Swanson, L. *Macromolecules* **2003**, *20*, 7765.
(27) Annaka, M.; Motokawa, K.; Sasaki, S.; Nakahira, T.; Kawasaki, H.; Maeda, H.; Amo, Y.; Tominaga, Y. *Journal of Chemical Physics* **2000**, *113*, 5980.
(28) Annaka, M.; Amo, Y.; Sasaki, S.; Tominaga, Y.; Motokawa, K.; Nakahira, T. *Physical Review E: Statistical, Nonlinear, and Soft Matter Physics* **2002**, *65*, 031805/1.
(29) Annaka, M.; Tanaka, C.; Nakahira, T.; Sugiyama, M.; Aoyagi, T.; Okano, T. *Macromolecules* **2002**, *35*, 8173.
(30) Suzuki, Y.; Suzuki, N.; Takasu, Y.; Nishio, I. *Journal of Chemical Physics* **1997**, *107*, 5890.
(31) Terada, T.; Inaba, T.; Kitano, H.; Maeda, Y.; Tsukida, N. *Macromolecular Chemistry and Physics* **1994**, *195*, 3261.
(32) Appel, R.; Zerda, T. W.; Wang, C.; Hu, Z. *Polymer* **2000**, *42*, 1561.
(33) Appel, R.; Xu, W.; Zerda, T. W.; Hu, Z. *Macromolecules* **1998**, *31*, 5071.
(34) Meersman, F.; Wang, J.; Wu, Y.; K., H. *Macromolecules* **2005**, *38*, 8923.
(35) Ono, O.; Shikata, T. *J. Am. Chem. Soc.* **2006**, *128*, 10030.
(36) Ono, Y.; Shikata, T. *J. Phys. Chem. B.* **2007**, *111*, 1511.
(37) Ahmed, Z.; Scaffidi, J.; Asher, S. A. *Biopolymers* **2008**, *in press*.
(38) Urry, D. W.; Parker, T. M. *Journal of Muscle Research and Cell Motility* **2002**, *23*, 543.
(39) Tamburro, A. M.; Bochicchio, B.; Pepe, a. *Biochemistry* **2003**, *42*, 13347.
(40) Rodriguez-Cabello, J. C.; Alonso, M.; Diez, M. I.; Caballero, M. I.; Herguedas, M. M. *Macromolecular Chemistry and Physics* **1999**, *200*, 1831.
(41) Alonso, M.; Reboto, V.; Guiscardo, L.; San Martin, A.; Rodriguez-Cabello, J. C. *Macromolecules* **2000**, *33*, 9480.
(42) Tsai, C.-J.; Maizel, J. V., Jr.; Nussinov, R. *Critical Reviews in Biochemistry and Molecular Biology* **2002**, *37*, 55.
(43) Tauc, P.; Fusi, P.; Tortora, P.; Lange, R.; Brochon, J. C. *Advances in High Pressure Bioscience and Biotechnology, Proceedings of the International Conference -- Heidelberg, Aug. 30-Sept. 3, 1998* **1999**, 191.
(44) Tang Xiaolin, C.; Pikal Michael, J. *Pharmaceutical research* **2005**, *22*, 1167.
(45) Tamura, A. *Netsu Sokutei* **1995**, *22*, 186.
(46) Graziano, G.; Catanzano, F.; Riccio, A.; Barone, G. *Journal of Biochemistry (Tokyo)* **1997**, *122*, 395.
(47) Goto, Y. *Baiosaiensu to Indasutori* **2002**, *60*, 235.
(48) Andersen, N. H.; Cort, J. R.; Liu, Z.; Sjoberg, S. J.; Tong, H. *Journal of the American Chemical Society* **1996**, *118*, 10309.
(49) Privalov, P. L.; Griko, Y. V.; Venyaminov, S. Y.; Kutyshenko, V. P. *Journal of Molecular Biology* **1986**, *190*, 487.
(50) Privalov, P. L. *Critical Reviews in Biochemistry and Molecular Biology* **1990**, *25*, 281.
(51) Weissman, J. M.; Sunkara, H. B.; Tse, A. S.; Asher, S. A. *Science* **1996**, *274*, 959.
(52) Tanaka, T.; Fillmore, D. J. *Journal of Chemical Physics* **1979**, *70*, 1214.
(53) Tanaka, T.; Hocker, L. O.; Benedek, G. B. *Journal of Chemcial Physics* **1973**, *59*, 5151.
(54) Maeda, Y.; Higuchi, T.; Ikeda, I. *Langmuir* **2000**, *16*, 7503.

(55) Maeda, Y.; Nakamura, T.; Ikeda, I. *Macromolecules* **2001**, *34*, 1391.
(56) Maeda, Y.; Nakamura, T.; Ikeda, I. *Macromolecules* **2001**, *34*, 8246.
(57) Maeda, Y.; Taniguchi, N.; Ikeda, I. *Macromolecular Rapid Communications* **2001**, *22*, 1390.
(58) Maeda, Y.; Yamamoto, H.; Ikeda, I. *Macromolecules* **2003**, *36*, 5055.
(59) Maeda, Y.; Yamamoto, H.; Ikeda, I. *Colloid and Polymer Science* **2004**, *282*, 1268.
(60) Lin, S.-Y.; Chen, K.-S.; Run-Chu, L. *Polymer* **1999**, *40*, 2619.
(61) Bykov, S. B.; Lednev, I. K.; Ianoul, A.; Mikhonin, A. V.; Asher, S. A. *Appl. Spectrosc.* **2005**, *59*, 1541.
(62) Lednev, I. K.; Karnoup, A. S.; Sparrow, M. C.; Asher, S. A. *J. Am. Chem. Soc.* **1999**, *121*, 8074.
(63) Williams, S.; Causgrove, T. P.; Gilmanshin, R.; Fang, K. S.; Callender, R. H.; Woodruff, W. H.; Dyer, R. B. *Biochemistry* **1996**, *35*, 691.
(64) Torii, H.; Tasumi, M. *Journal of Raman Spectroscopy* **1998**, *29*, 81.
(65) Torii, H.; Tasumi, M. *International Journal of Quantum Chemistry* **1998**, *70*, 241.
(66) Chen, X. G.; Schweitzer-Stenner, R.; Asher, S. A.; Mirkin, N. G.; Krimm, S. *J. Phys. Chem.* **1995**, *99*, 3074.
(67) Mikhonin, A. V.; Ahmed, Z.; Ianoul, A.; Asher, S. A. *Journal of Physical Chemistry B* **2004**, *108*, 19020.
(68) Chi, Z.; Chen, X. G.; Holtz, J. S. W.; Asher, S. A. *Biochemistry* **1998**, *37*, 2854.
(69) Asher, S. A.; Ianoul, A.; Mix, G.; Boyden, M. N.; Karnoup, A.; Diem, M.; Schweitzer-Stenner, R. *J. Am. Chem. Soc.* **2001**, *123*, 11775.
(70) Wang, Y.; Purrello, R.; Jordan, T.; Spiro, T. G. *Journal of the American Chemical Society* **1991**, *113*, 6359.
(71) Wang, Y.; Purrello, R.; Spiro, T. G. *Journal of the American Chemical Society* **1989**, *111*, 8274.
(72) Pan, Y. V.; Wesley, R. A.; Luginbuhl, R.; Denton, D. D.; Ratner, B. D. *Biomacromolecules* **2001**, *2*, 32.
(73) Mikhonin, A. V.; Bykov, S. V.; Myshakina, N. S.; Asher, S. A. *J. Phys. Chem. B* **2006**, *110*, 5509.
(74) Myshakina, N. S.; Ahmed, Z.; Asher, S. A. *J. Phys. Chem. B,* **2008**, *112*, 11873.
(75) Torii, H.; Tatsumi, T.; Tasumi, M. *J. Raman Spectrosc.* **1998**, *29*, 537.
(76) Manas, E. S.; Getahun, Z.; Wright, W. W.; DeGrado, W. F.; Vanderkooi, J. M. *J. Am. Chem. Soc.* **2000**, *122*, 9883.
(77) Torii, H.; Tatsumi, T.; Kanazawa, T.; Tasumi, M. *Journal of Physical Chemistry B* **1998**, *102*, 309.
(78) Torii, H.; Tatsumi, T.; Tasumi, M. *Mikrochimica Acta, Supplement* **1997**, *14*, 531.
(79) Dioumaev, A. K.; Brainman, M. S. *J. Am. Chem. Soc.* **1995**, *117*, 10572.
(80) Simonson, T.; Brooks III, C. L. *J. Am. Chem. Soc* **1996**, *118*, 8452.
(81) Simonson, T.; Perahia, D. *Proc. Nat. Acad. Sci. U.S.A.* **1995**, *92*, 1082.
(82) Dwyer, J. J.; Gittis, A. G.; Karp, D. A.; Lattman, E. E.; Spencer, D. S.; Stites, W. E.; Garcia-Moreno E., B. *Biophys J.* **2000**, *79*, 1610.
(83) Triggs, N. E.; Valentini, J. J. *J. Phys. Chem* **1992**, *96*, 6922.
(84) Mayne, L. C.; Hudson, B. *J. Phys. Chem* **1991**, *95*, 2962.
(85) Ahmed, Z.; Asher, S. A. *Biochemistry* **2006**, *45*, 9068.

(86) Ahmed, Z.; Illir, A. B.; Mikhonin, A. V.; Asher, S. A. *J. Am. Chem. soc.* **2005**, *127*, 10943.
(87) Wang, Y.; Purrello, R.; Georgiou, S.; Spiro, T. G. *Journal of the American Chemical Society* **1991**, *113*, 6368.
(88) Asher, S. A.; Ianoul, A.; Mix, G.; Boyden, M. N.; Karnoup, A.; Diem, M.; Schweitzer-Stenner, R. *Journal of the American Chemical Society* **2001**, *123*, 11775.
(89) Mezei, M.; Fleming, P. J.; Srinivasan, R.; Rose, G. D. *Proteins: Structure, Function, and Bioinformatics* **2004**, *55*, 502.
(90) Ludwig, R. *Angew. Chem. Int. Ed.* **2001**, *40*, 1808.
(91) Okada, Y.; Tanaka, F.; Kujawa, P.; Winnik, F. M. *Journal of Chemcial Physics* **2006**, *125*, 244902.(91b)Li, B.; Alonso, D. O. V.; Bennion, B. J.; Daggett, V. *Journal of the American Chemical Society* **2001**, *123*, 11991.
(92) Wu, C.; Wang, X. *Physical review letters* **1998**, *80*, 4092.
(93) Qiu, L.; Pabit, S. A.; Roitberg, A. E.; Hagen, S. J. *Journal of the American Chemical Society* **2002**, *124*, 12952.
(94) Dyer, R. B.; Gai, F.; Woodruff, W. H. *Acc. Chem. Res.* **1998**, *31*, 709.
(95) Bieri, O.; Wirz, J.; Hellrung, B.; Schutkowski, M.; Drewello, M.; Kiefhaber, T. *Proceedings of the National Academy of Sciences of the United States of America* **1999**, *96*, 9597.
(96) Hagen, S. J.; Qiu, L.; Pabit, S. A. *Journal of Physics: Condensed Matter* **2005**, *17*, S1503.
(97) Kubelka, J.; Buscaglia, M.; Hofrichter, J.; Eaton, W. A. *NATO Science Series, Series I: Life and Behavioural Sciences* **2005**, *364*, 1.
(98) Kubelka, J.; Hofrichter, J.; Eaton, W. A. *Current Opinion in Structural Biology* **2004**, *14*, 76.
(99) McCammon, J. A. *Proceedings of the National Academy of Sciences of the United States of America* **1996**, *93*, 11426.
(100) Nguyen, H.; Jaeger, M.; Kelly, J. W.; Gruebele, M. *Journal of Physical Chemistry B* **2005**, *109*, 15182.
(101) Pabit, S. A.; Roder, H.; Hagen, S. J. *Biochemistry* **2004**, *43*, 12532.
(102) Qiu, L.; Hagen, S. J. *Journal of the American Chemical Society* **2004**, *126*, 3398.
(103) Fierz, B.; Kiefhaber, T. *J. Am. Chem. Soc* **2007**, *129*, 672.
(104) Krieger, F.; Moeglich, A.; Kiefhaber, T. *Journal of the American Chemical Society* **2005**, *127*, 3346.
(105) Lapidus, L. J.; Steinbach, P. J.; Eaton, W. A.; Szabo, A.; Hofrichter, J. *J. Phys. Chem. B.* **2002**, *106*, 11628.
(106) Lee, J. C.; Lai, B. T.; Kozak, J. J.; Gray, H. B.; Winkler, J. R. *J. Phys. Chem. B* **2007**, *111*, 2107.

8.0 CONCLUSIONS

Our initial work with the Trp-cage peptide (chapter 3) and elastin-based peptides (chapter 5) highlighted the dearth of knowledge about pro peptide bonds and 3_{10}-helix. In chapter 3 we assumed that 3_{10}-helix being conformationally similar to an α-helix would show similar spectral features in the $AmIII_3$ and $C_\alpha H_b$ regions. This assumption was based on previous theoretical work by Asher and co-workers[1] that relates the resonance $C_\alpha H_b$ intensity to coupling between the $C_\alpha H_b$ and NH_b motions. In non-α-helical conformations like the PPII conformation, the $C_\alpha H$ and the NH hydrogens are in *cis* position, which allows for maximum coupling. In α-helix like conformations the two hydrogens are in *trans* position and hence do not couple strongly.[1] We therefore assumed that being conformationally similar the α-helix and 3_{10}-helix should show similar spectral features. The significance of any spectral differences between the α- and 3_{10}-helix deriving from a small Ψ-angle difference between the two conformations was however, not clear.

Similarly, in chapter 3 we note that the AmII'p downshifts by 10 cm^{-1} as the Trp-cage peptide undergoes thermal denaturation over the temperature range 4-70 ºC. The pro literature, fraught with disagreements suggested that the AmII'p frequency shifts may be attributed to either *cis-trans* isomerization or peptide bond hydrogen bonding.

We therefore initiated a focused research effort to fill in these gaps in our knowledge. In specific we focused our efforts to a) identify UVRR spectroscopic markers of 3_{10}-helix and b) understand the significance of pro peptide bond's most prominent spectroscopic signature the AmII'p.

We examined the temperature-dependent conformation of a model 3_{10}-helix peptide $gp41_{659\text{-}671}$ (chapter 4). Our results clearly indicate that UVRR spectroscopy can discriminate between the conformationally similar 3_{10}- and α-helix. Our temperature-dependent UVRR measurements indicate that $gp41_{659\text{-}671}$ peptide has a rough energy landscape where the folded and unfolded conformations are equally populated at all temperatures.

Having determined the spectroscopic markers for 3_{10}-helicies we turned our attention to pro peptides. Utilizing DFT calculations and UVRR measurements we developed a methodology that allows us to correlate changes in AmII'p frequency to changes in Ψ-dihedral angle at the pro peptide bond (chapter 6). Using this methodology we correlate a 7 cm^{-1} downshift in the AmII'p frequency of polyproline peptide to a 45º rotation in the Ψ-angle from Ψ = 145º to Ψ = 100º. Molecular modeling reveals that the Ψ = 100º conformation corresponds to a more compact, less water-accessible PPII structure. This result indicates that polyproline peptides undergo a temperature-induced hydrophobic collapse that results in a significant decrease in its end-to-end distance and solvent exposure.

Recent Monte Carlo work from Rose lab[2] indicates the extended water-exposed PPII conformation is stabilized by favorable interactions between the peptide and its first water-solvation shell. Our results suggest that the temperature-induced hydrophobic collapse in polyproline peptide is driven by temperature-induced disruption of the pro-water interactions. At elevated temperatures increased thermal agitation disrupts the extensive hydrogen bonding

network between the pro peptides and surrounding water molecules. The system (peptide + water) attains equilibrium by increasing its entropy which compensates for the loss of favorable peptide-water solvation shell interactions. This is accomplished when the peptide chain adopts a more compact conformation that significantly reduces its solvent accessible surface area (SASA), thus reducing the number of well-ordered water molecules in the solvation shell around hydrophobic groups. The release of water molecules from the well-ordered solvation shell of hydrophobic groups results in an increase in the overall entropy of the system which stabilizes the peptide's compact conformation. We therefore conclude that entropy changes in water solvation shell are responsible for pro hydrophobic collapse.

We further investigate the role of solute-water interactions in driving polymer collapse by examining the temperature-induced hydrophobic collapse of PNIPAM nanogels (chapter 7). PNIPAM has long been utilized as a model system for understanding temperature-induced polymer hydrophobic collapse. We utilize steady-state UVRR, DLS and H-NMR measurements to determine that in the collapsed state the amide bonds of PNIPAM do not engage in inter-molecular hydrogen bonding. Our measurements clearly indicate that above T_t the amide bonds of PNIPAM are predominantly hydrogen bonded to two water molecules each, with one water-peptide hydrogen bond at the C=O and N-H site each. At low temperatures the amide bond is fully hydrogen bonded with two C=O-water hydrogen bonds and one NH-water hydrogen bond.

Based on our results we propose that at low temperatures the PNIPAM-water interactions stabilize an extended water-exposed conformation. At elevated temperatures, thermal agitation disrupts the solvation shell around the *N*-isopropylacrylamide (NIPAM). The loss of favorable NIPAM-water solvation shell interactions forces the PNIPAM chain to adopt a compact conformation, forming local hydrophobic pockets that significantly reduce the solvent exposure

of its pendent NIPAM group. Decrease in hydrophobic solvation increases system entropy and stabilizes the compact/dehydrated state of PNIPAM. The formation of local hydrophobic pockets between the (*i,i*+3) groups results in the dehydration of the C=O group which results in a loss of one C=O-water hydrogen bond.

The loss of C=O-water hydrogen bond in the collapsed PNIPAM results in a 28 cm^{-1} upshift in the AmI frequency. This provides a convenient marker for examining the temporal evolution PNIPAM collapse.

Our time-resolved UVRR measurements indicate the amide dehydration is complete within 1 μs. Spectral modeling indicates that changes in C=O-water hydrogen bonding can be modeled as mono-exponential collapse with a time constant of 360 (± 80) ns. Changes in the AmII region are complete within 60 ns, indicating the AmII frequency shifts derive from temperature-induced weakening of NH-water hydrogen bonds.

The rate of collapse of PNIPAM (10^6 s^{-1}) suggests a persistent length of ~10 for PNIPAM polymers. This suggests the PNIPAM collapse is a cooperative process where hydrophobic interactions between the adjacent hydrophobic pockets are needed to stabilize the collapsed PNIPAM. It should be noted that a 10-mer is also the minimum length required for a polypeptide to fold into a stable α-helix conformation.

Our results in chapter 6 and 7 have highlighted the role, changes in water solvation shell play in driving protein hydrophobic collapse. These results indicate that in order to obtain a more complete understanding of protein folding we need to understand the role of water during protein folding. Up till now the role of water molecules as been largely ignored, in favor of the solute i.e. the peptide chain. Research efforts have almost exclusively (and rightly so) focused

on developing novel spectroscopic tools for determining protein conformation. These efforts have greatly improved our understanding of some of the earliest events in protein folding.

Our results, however, indicate that a similar effort is now needed to understand the structure of water in response to protein conformation changes. The developments of new spectroscopic tools and methodologies that allow us to correlate changes in vibrational spectra to structural/entropy changes in water will greatly enhance our understanding of the basic physics underlying protein folding.

Our UVRR and DFT results in chapter 5 indicate the changes in AmII'p frequency are correlated to Ψ-angle changes. In future work we need to further refine this relationship to allow experimentalist to directly correlate the AmII'p frequency to the Ψ-angle of the pro peptide bond. This will be accomplished by growing x-ray quality crystals where a single pro peptide bond is limited to a specific Ψ-angle. By examining an extensive series of crystal structures with varying Ψ-angles we can quantitatively establish a direct correlation between the AmII'p frequency and its Ψ-angle. Similar approaches have been successfully utilized in correlating the W3 band frequency to the Trp χ^2 angle[3] and the $AmIII_3$ band frequency to the Ψ-angle[1] of non-pro, non-gly peptide bonds. This will allow future workers to directly and quantitatively track conformation changes in the pro peptide bond during protein folding and/or protein-protein and protein-ligand interactions.

8.1 REFERENCES

(1) Asher, S. A.; Ianoul, A.; Mix, G.; Boyden, M. N.; Karnoup, A.; Diem, M.; Schweitzer-Stenner, R. *Journal of the American Chemical Society* **2001**, *123*, 11775.

(2) Mezei, M.; Fleming, P. J.; Srinivasan, R.; Rose, G. D. *Proteins: Structure, Function, and Bioinformatics* **2004**, *55*, 502.

(3) Miura, T.; Takeuchi, H.; Harada, I. *J. Raman Spectrosc.* **1989**, *20*, 667.